Summer 2024

A 3D Co-culture Model of Senescent Cell Burden and Salivary Gland Fibrosis

Stephen Rose
University at Albany, State University of New York, esoar2000@yahoo.com

A 3D CO-CULTURE MODEL OF SENESCENT CELL BURDEN AND SALIVARY GLAND FIBROSIS

by

Stephen C. Rose

A Dissertation

Submitted to the University at Albany, State University of New York

In Partial Fulfillment of

the Requirements for the Degree of

Doctor of Philosophy

College of Nanotechnology, Science, and Engineering

Department of Nanoscale Science and Engineering

August 2024

ABSTRACT

Patients with head and neck cancer often suffer collateral radiation damage to the salivary glands, leading to fibrosis. Histological examinations indicate that radiation encourages fibrosis by promoting cellular changes leading to both senescent and myofibroblast phenotypes, coupled with a significant loss of regenerative and acinar cells. Chronic hypofunction remains a primary concern, even with modified radiation approaches to sparing salivary glands. Current treatments primarily offer symptomatic relief without rectifying irreversible glandular tissue damage. This limitation arises, in part, from a deficiency in predictive preclinical models to study this multifaceted problem.

We introduce a 3D in vitro microtissue model to address this limitation, employing a scaffold-free co-culture of stromal cells, such as NIH-3T3 fibroblasts and salivary epithelial cells, such as SCA-9 cells. Our methods prioritize generating salivary gland spheroids less than 200 μm in diameter, ensuring optimal nutrient diffusion and preventing necrotic core development. The formation process involves precise controls on parameters such as initial cell count, cell solution volume, culture duration, and spheroid formation technique (e.g., hanging drops, non-adhesive microwells). We have also devised assays tailored for 3D spheroids, encompassing various staining techniques for cell viability, apoptosis, senescence, fibrosis, and immunocytochemistry analysis of specific markers.

When exposed to clinically relevant X-ray radiation doses, these microtissues showed cell death and apoptosis, especially on the spheroid's surface, and manifested changes in collagen type I fibers and α-smooth muscle actin (α-SMA) within a sixteen-day frame.

Further, we sought to examine the effects of a preexisting senescent cell burden on our 3D microtissue model by exposing it to senescence-conditioned media before radiation exposure. This experiment incorporated additional assays, including 3D assays of cell viability, apoptosis, DNA damage, and senescence and additional assays such as immunocytochemistry analysis of fibrosis markers and picrosirius red staining of collagen fibrils to evaluate fibrosis-related ECM changes.

In conclusion, we have made considerable progress in creating a 3D in vitro model to study radiation-induced salivary gland fibrosis and the role that senescent cell burden plays in its development. This novel tool promises to enhance our comprehension of salivary gland fibrosis mechanisms and pave the way for more effective therapeutic interventions, drug evaluations, and exploration of new treatment approaches.

ACKNOWLEDGEMENTS

My time pursuing a Ph.D. at the College of Nanoscale Science and Engineering (CNSE), SUNY Polytechnic Institute has been immensely fulfilling, which is now the Department of Nanoscale Science and Engineering after being re-united with the University at Albany, State University of New York (SUNY). I am deeply grateful to individuals who have consistently encouraged, guided, and fueled my passions. They've been instrumental in helping me navigate the challenges of the Ph.D. process and life in general, especially during the hardships of the COVID-19 pandemic. My progress stands as a testament to your incredible support system.

I extend my heartfelt gratitude to Dr. Susan Sharfstein for initially offering me the chance to acquire invaluable lab experience before I embarked on my Ph.D. journey at SUNY Albany. Furthermore, her continued trust in providing me with diverse project opportunities and graciously incorporating me and my thesis project midway through my Ph.D. speaks volumes of her generosity. I sincerely appreciate her dedication to nurturing my interests, even when it meant embracing an extra project alongside her research endeavors. Dr. Sharfstein's expert guidance on producing meaningful research and her adeptness at data analysis have not just been pivotal but also influential in framing my thesis. Her pragmatic methods for overcoming obstacles have consistently motivated me to tackle both professional and personal challenges with a positive perspective. My most profound appreciation goes out to her for always prioritizing my best interests, even when it may not have been advantageous for her.

Dr. Yubing Xie has been a significant influence on my Ph.D. journey. Her inventive approaches to enhancing research productivity have consistently elevated my work. Her accessibility, kind heart, and encouragement have helped me navigate the many twists and turns of my Ph.D.

pursuit. Her unwavering belief in me and her generosity has been a constant source of strength during tough times. I am deeply grateful for her impact on my research productivity and her belief in my potential.

I owe a debt of gratitude to Dr. James Castracane, Dr. Nathaniel Cady, and Dr. Andres Melendez for their insightful questions and unwavering guidance throughout my Ph.D. journey. While initially hesitant, I'm thankful for the chance to delve into the salivary gland regeneration project. It was an ideal platform to explore my fascination with aging and disease. I sincerely appreciate the autonomy I experienced under his mentorship. The responsibilities paired with that freedom became a vibrant learning environment, shaping the core of my Ph.D. experience.

I thank Dr. Melinda Larsen for allowing me to collaborate with her lab at the University of Albany. Her expertise and profound understanding of salivary gland biology have been indispensable. Her astute feedback and mentorship have consistently elevated the quality of my work. Additionally, I'd like to thank Dr. Deirdre Nelson for her candid and constructive input, which greatly refined my thesis—a special thanks to Raphael Pena for his help at the Larsen Lab. I'm deeply thankful for these invaluable opportunities.

My most profound appreciation goes to Dr. Pujhitha Ramesh for her invaluable lab mentorship, troubleshooting prowess, and unwavering accessibility, kindness, and encouragement. Her support has undoubtedly saved countless hours, and I'm grateful for her assistance.

Equally, I'm indebted to Dr. Xulang Zhang for her gentle guidance and unwavering support, particularly in mastering qPCR analysis.

I want to acknowledge my past and present colleagues and fellow graduate students at CNSE, including Dr. Sujith Kollampally, Dr. Tristen Head, Dr. Michael Dolan, and Tia Swenty.

This would not be possible without the CNSE, and I am grateful for its existence.

Maryanne Calkins deserves a special mention. On the home front, she has been an unyielding pillar, offering tireless support around the clock and an unwavering belief in my capabilities and dreams.

My profound gratitude goes out to my Grandmother, Elsie Isabel Rose. Her boundless love during my early years instilled a relentless drive, pushing me to contribute something meaningful to the world, hoping that it would mirror the depth of her affection.

Lastly, I owe an immeasurable debt to my friends and family. Their emotional sustenance has been irreplaceable throughout my Ph.D. journey. Words truly cannot capture the breadth and depth of my gratitude.

TABLE OF CONTENTS

.

LIST OF FIGURES

*** Tables and figures have their own numbering schemes and are listed here in order of appearance in the text.**

LIST OF TABLES

Chapter 1: Introduction and background: radiation, fibrosis, senescence, and 3D microtissue models in salivary gland research

1.1 Introduction

While small and often overlooked, the salivary glands play an essential role in our daily lives. From aiding digestion to maintaining oral health and facilitating speech, their importance cannot be overstated [1]. Yet, like all tissues, they are susceptible to various insults and damage, one of the most potent being radiation [2]. The increasing application of radiation in the medical field, particularly in oncology treatments, underscores the need to understand its repercussions on these delicate tissues.

Traditional 2D cell culture systems have driven our cellular and molecular biology understanding. However, they often fail to capture the complex three-dimensional (3D) interactions and microenvironments in vivo [3]. This discrepancy between 2D cultures and the in vivo microenvironment can lead to misrepresentations and limit the applicability of findings. Hence, recent years have witnessed a rising interest in 3D microtissue models, which promise to bridge this gap.

3D microtissue models, particularly spheroids, have emerged as powerful tools in biomedical research. They offer a more physiologically relevant representation of in vivo tissues, encapsulating essential cellular interactions, extracellular matrix (ECM) compositions, and gradient-driven behaviors [4]. This has rendered them particularly invaluable in studying tissue-specific responses.

Cellular senescence, a state of irreversible cell cycle arrest, adds another layer of complexity to understanding tissue responses, especially post-radiation. Senescence has garnered attention for its implications in aging and various pathological contexts, including fibrosis and cancer [5–7].

As cells transition into senescence, they undergo significant morphological, physiological, and secretory changes that can profoundly impact the surrounding microenvironment and, by extension, tissue functionality [8,9].

This dissertation seeks to link these threads of inquiry: the utility of 3D microtissue models, the intricacies of salivary gland biology, the overarching shadow of radiation, and the nuanced role of cellular senescence. By juxtaposing these elements, we aim to shed light on the delicate interplay between senescent cells and radiation-induced damage in salivary gland tissues, using the 3D spheroid model as our lens. The journey will progress from model development and validation to probing cellular mechanisms and exploring potential therapeutic avenues.

This inaugural chapter will lay down the foundational knowledge required to navigate the subsequent explorations. Through a brief overview of salivary gland fibrosis, cellular senescence, 3D models in research, and the effects of radiation on salivary glands, we aim to equip the reader with a holistic understanding of the current landscape, setting the stage for the deeper investigations that follow.

1.2 Current understanding of salivary gland fibrosis

Salivary gland fibrosis is a debilitating condition marked by the excessive accumulation of extracellular matrix (ECM) components, primarily collagen, leading to the scarring and functional decline of the gland. This pathological remodeling is a simple aftermath of tissue injury and a multifaceted response involving various cell types, signaling pathways, and intricate molecular cascades [10].

The etiology of salivary gland fibrosis spans a spectrum of causes. Chronic inflammation, autoimmune conditions like Sjögren's syndrome [11], radiation therapy for head and neck

cancers[12], and even some pharmacological agents have been recognized as potential triggers, which are associated with salivary gland fibrosis [12]. These factors can instigate an intricate cascade of events that ultimately converge on fibrosis.

At the cellular level, fibroblasts are central to the fibrotic process. Upon activation by various stimuli, such as transforming growth factor-beta (TGF-β), these quiescent cells transdifferentiate into myofibroblasts [13]. Characterized by the expression of alpha-smooth muscle actin (α-

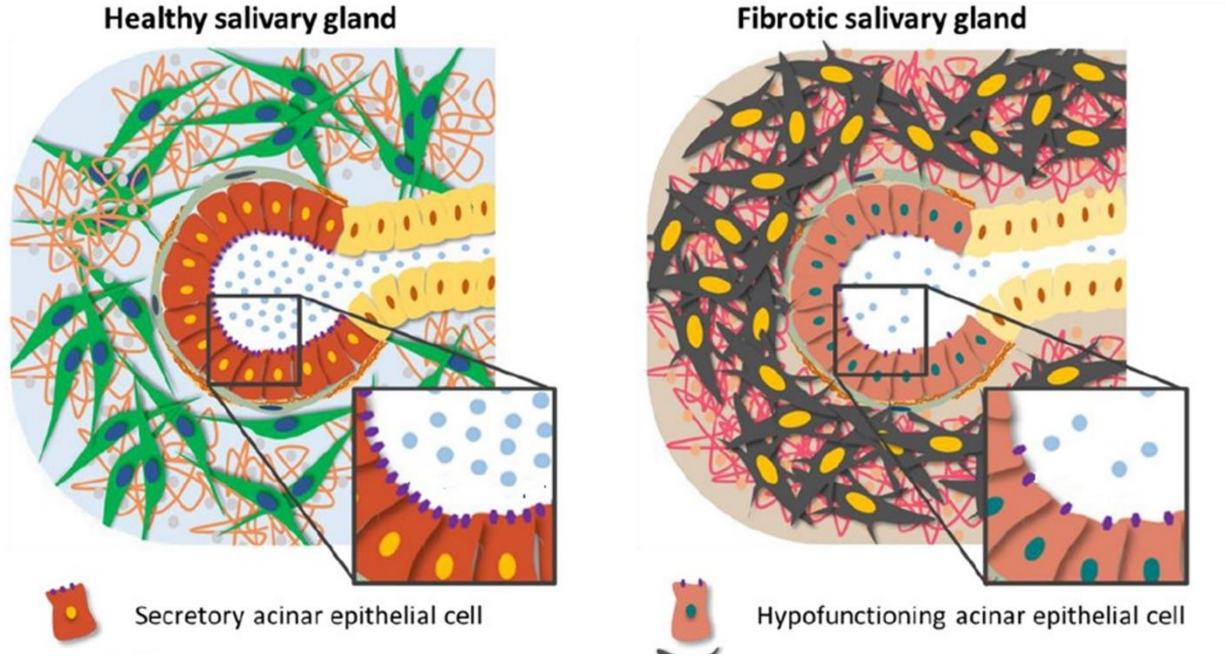

Figure. 1.1 Schematic comparison of healthy vs. fibrotic salivary gland: This illustration depicts the structural differences between a healthy salivary gland and one affected by fibrosis. On the left, the healthy gland shows normal acinar cells with intact, rounded structures for saliva production and a ductal system allowing saliva to flow freely. Surrounding connective tissue is minimal, ensuring efficient gland function. The fibrotic gland displays disrupted architecture on the right with significant collagen deposition, leading to thickened and scarred connective tissue. Acinar cells are hypofunctioning, compromising saliva production. These changes highlight the pathological impact of fibrosis on salivary gland function. Reprinted and modified with permission from Ramesh 2022. © 2022 by Ramesh[471]

SMA) and the acquisition of a contractile phenotype [14], myofibroblasts are the primary producers of the excessive deposition of ECM components that define fibrosis [15,16].

However, fibroblasts are not the sole culprits. Increasing evidence points to the involvement of epithelial cells through a process termed epithelial-mesenchymal transition (EMT) [17]. Here, epithelial cells lose their characteristic markers, such as E-cadherin, and gain mesenchymal traits, including vimentin expression, equipping them with migratory and ECM-producing capabilities [18]. Moreover, immune cells, particularly macrophages, play pivotal roles by releasing cytokines and growth factors that perpetuate fibroblast activation and ECM deposition [19].

It's crucial to understand that fibrosis, while a defense mechanism, is not without consequences. The excessive ECM disrupts the delicate architecture of the salivary gland, impinging on ductal structures and reducing the gland's secretory capabilities (See Figure 1.1). Clinically, this translates to xerostomia or dry mouth. This condition compromises oral health and significantly impacts the quality of life by interfering with speech, chewing, and swallowing [20,21].

Another dimension to the story is cellular senescence. Emerging research hints at a potential relationship between senescence and fibrosis. Senescent cells release myriad factors through their senescence-associated secretory phenotype (SASP), including pro-inflammatory cytokines, growth factors, and matrix-degrading enzymes, which can influence the fibrotic milieu [22,23]. Whether these cells are bystanders, perpetrators, or saviors in the context of salivary gland fibrosis remains a topic of active investigation and forms a core theme of this dissertation.

Salivary gland fibrosis is a complex interplay of cellular dynamics, signaling pathways, and molecular events. Understanding its intricacies unravels the mysteries of tissue remodeling and paves the way for potential therapeutic interventions, offering hope to those grappling with its consequences.

1.3 Senescence and its role in tissues

Historically introduced as a phenomenon where normal cells lose their ability to divide after a certain number of divisions, cellular senescence has evolved to be understood as a comprehensive biological response. Characterized by stable cell cycle arrest, senescent cells were first observed by Hayflick and Moorhead in the 1960s when they noted the limited proliferative capacity of human fibroblasts in culture [24]. Since then, the study of senescence has expanded from its initial focus on cellular aging to encompass broader roles in development, tissue repair, and pathology [25].

At the cellular level, senescent cells exhibit distinctive morphological changes such as enlarged and flattened appearance, increased lysosomal content (often detected by beta-galactosidase staining at pH 6), and altered gene expression patterns [25–27]. However, a defining hallmark of senescence is the irreversible cessation of cell division. The p53-p21 and p16INK4a primarily enforce this growth arrest-Rb pathways [28–30], though various other molecules and signaling cascades can modulate this process.

A myriad of factors can induce senescence:

1. Replicative senescence occurs due to telomere shortening after repeated cell divisions[24].
2. Stress-induced premature senescence (SIPS) is caused by various external stressors, such as oxidative stress, DNA-damaging agents, and even certain chemotherapeutic drugs [31].
3. Oncogene-induced senescence (OIS) results from activating specific oncogenes, serving as a protective mechanism to suppress tumor development [32].

Additionally, senescence plays a role during embryonic development, aiding tissue remodeling and organ formation [33].

While senescent cells are in a state of growth arrest, they are metabolically active and secrete many bioactive molecules, termed the senescence-associated secretory phenotype (SASP). The

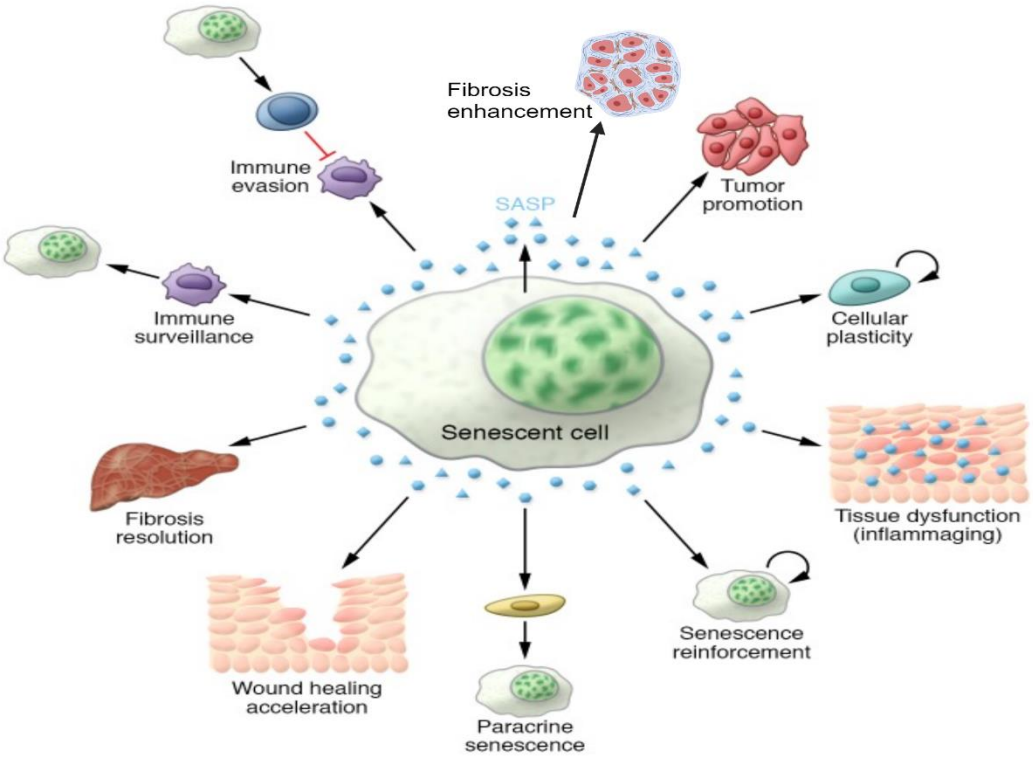

Figure 1.2. A schematic summary of some of the functions associated with the SASP as an essential mediator of the pathophysiological functions of senescent cells. Reprinted with permission from Herranz and Gill, 2018. © 2018 American Society for Clinical Investigation[431].

SASP includes pro-inflammatory cytokines, chemokines, growth factors, and ECM-degrading enzymes. SASP factors can affect neighboring cells differently, influencing inflammation, tissue repair, and even promoting tumorigenesis in specific contexts. Senescence, in physiological contexts, is beneficial. It plays roles in embryonic development and wound healing and safeguards against malignancy. However, with chronic inflammation or under persistent

damaging stimuli, the accumulation of senescent cells can become detrimental. In tissues, they can contribute to organ dysfunction, promote chronic inflammation, and further pathologies like fibrosis [25,34] (See Figure 1.2).

For instance, in salivary gland fibrosis, the accumulation of senescent cells could potentially influence the fibrotic process. Whether through the direct production of ECM components or the SASP-mediated modulation of the tissue microenvironment, senescent cells shape the tissue response to damage.

Given their involvement in many diseases, targeting senescent cells presents a promising therapeutic strategy. Senolytics selectively induce apoptosis in senescent cells, and interventions modulating SASP are under investigation [35,36]. However, given the beneficial roles of senescence in specific contexts, it's pivotal to approach it cautiously.

In sum, once viewed merely as a cell's response to aging, cellular senescence is now recognized as critical in various physiological and pathological processes. Its nuanced role, especially in tissue health and disease, warrants comprehensive exploration, as we'll delve into in the succeeding chapters of this dissertation.

1.4 3D microtissue models in biomedical research

For decades, the study of cellular behaviors and responses has predominantly relied on two-dimensional (2D) cell culture systems. While these models have significantly advanced our understanding of biological processes, they often fail to replicate living organisms' intricate spatial, mechanical, and biochemical cues. This gap has been bridged by the advent of three-dimensional (3D) microtissue models, which more closely mimic the in vivo environment and offer unparalleled insight into cell-cell and cell-matrix interactions [3].

Traditional 2D cultures involve cells growing flatly on rigid surfaces, an environment drastically different from the 3D context in which cells exist in vivo. These conditions can profoundly influence cell morphology, polarization, gene expression, and function. In contrast, 3D models offer a spatial arrangement, allowing cells to interact with their neighbors in all directions, much like in actual tissues [3].

On the other hand, 3D cell cultures offer diverse platforms that can simulate the in vivo environment more effectively than traditional 2D cultures. Various 3D models have emerged as research has progressed, each with unique advantages and applications. The following are some of the most widely recognized and employed 3D cell culture systems (See Figure 1.3).

- Spheroids: These spheroids are self-assembled spherical aggregates of cells. They can be single or multi-cellular types and have become particularly prominent in cancer research for modeling tumors[4].
- Organoids: Organoids are derived from stem cells, or progenitor or differentiated cells from healthy or diseased tissues. They are miniaturized and simplified versions of an organ. They recapitulate some specific organ functions and can reproduce several aspects of the organ's architecture [37].
- Hydrogels and Matrix-based Systems: Cells can be embedded or encapsulated within hydrogels or natural matrices such as collagen and Matrigel, allowing for a more genuine recreation of tissue biomechanics and biochemistry [38].
- Bioprinting and Chip Models: Advanced techniques such as 3D bioprinting enable the creation of more complex structures, while organ-on-a-chip models can replicate organ interfaces and dynamic physiological processes [39,40].

- Rotating Wall Vessel (RWV) Bioreactors: These bioreactors are specialized cell culture vessels that provide a low-shear environment that is conducive to the formation of 3D tissue-like aggregates [41].

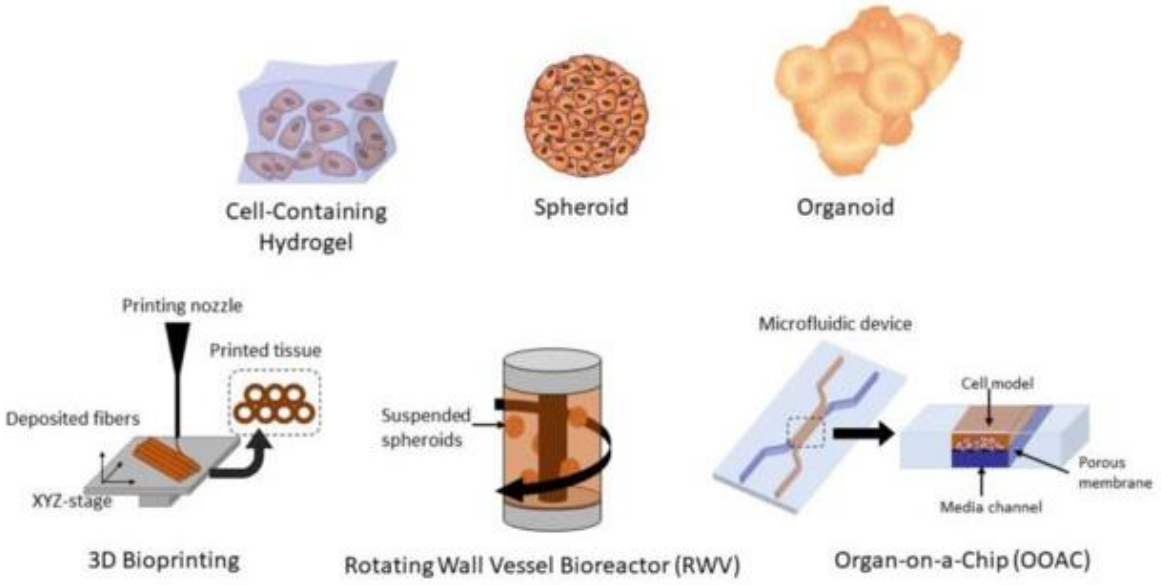

Figure 1.3 3D Cell Culture Methods. Different 3D cell culture methods include 3D hydrogels, spheroids, organoids, 3D bio-printed tissues, organ-on-a-chip (OOAC), and rotating wall vessel (RWV) bioreactors. Image by Nathan Lawko, licensed under CC BY 4.0."[472]

As shown in Figure 1.3 different 3D cell culture methods include 3D hydrogels, spheroids, organoids, 3D bio-printed tissues, organ-on-a-chip (OOAC), and rotating wall vessel (RWV) bioreactors. Three-dimensional cell cultures have revolutionized biomedical research, offering many advantages over traditional 2D models. These benefits are not limited to providing a more physiologically relevant environment but span various applications, from drug testing to understanding disease pathology. Here, we delve into the myriad advantages and the diverse applications of 3D cell culture systems in current research, which has revolutionized many areas in biomedical research:

- Disease Modeling: 3D systems have enabled a more accurate recapitulation of disease environments, from cancer metastasis to neurodegenerative conditions [42–44].
- Drug Screening: With structures more reminiscent of in vivo conditions, these models have improved the predictive validity for drug efficacy and toxicity, reducing the reliance on animal testing [45,46].
- Regenerative Medicine: Tissue engineering and regenerative medicine benefit from 3D cultures as they can produce tissue substitutes with architectures close to native tissues [47].

Given salivary glands' complex structural and functional attributes, 3D models are particularly advantageous. They facilitate understanding epithelial architecture, acinar and ductal cell interactions, extracellular matrix compositions, and secretory functions. In pathological states like fibrosis or radiation damage, 3D models can provide an unprecedented view of how cells respond within a more physiological context.

While 3D models have ushered in new research avenues, they come with challenges. Standardizing protocols, ensuring reproducibility, and optimizing culture conditions are ongoing concerns. Integrating emerging technologies, such as microfluidics and high-resolution imaging, promises to refine further and advance 3D modeling techniques [47].

In conclusion, 3D microtissue models have bridged the gap between traditional cell culture and in vivo studies, paving the way for breakthroughs in disease understanding and therapeutic developments. Their growing adoption underscores their potential to become mainstays in modern biomedical research.

1.5 Cell line selection and rationale

The selection of appropriate cell lines is pivotal to the integrity and relevance of any in vitro study. The cell lines chosen for this research, NIH-3T3, SCA-9, and senescent IMR-90 cells, are tailored to our study's objectives and questions.

NIH-3T3 fibroblasts serve as a representative mesenchymal cell model, which are stromal cells known for producing essential ECM components, including collagen and can be induced to fibrotic and senescence states. Originating from mouse embryo cultures, these cells are immortal, ensuring their consistent presence and performance in research settings. They have been widely acknowledged for their role in transfection experiments due to their capacity to incorporate foreign DNA [48] stably. The relevance of these cells in our study is further accentuated by their involvement in growth factors, oncogenes, and various cellular processes, notably cancer biology [48]. Moreover, being stromal cells, NIH-3T3 cells are significant producers of ECM components. An overproduction or disorganization of such ECM components, like collagen, can influence fibrotic processes [49].

SCA-9 cells are mouse SMG-derived epithelial cell lines originating from adult salivary gland ductal cells that provide insights into salivary gland biology. Their utility stems from their potential to form duct-like structures and express markers characteristic of salivary gland duct cells [50]. In the context of our study, NIH-3T3 cells, with their ECM-producing capabilities, can offer structural support to SCA-9 cells, which emulate the functional aspects of salivary gland cells. This relationship underscores the importance of stromal and functional cell interactions and their collective role in tissue maintenance and pathology.

The IMR-90 cell line, a human lung fibroblast derivative from a 16-week gestation male fetus, presents an intriguing and relevant model to our research focus. After a specified number of

population doublings or exposure to ionizing radiation, these cells undergo senescence, characterized by permanent cell-cycle arrest. Their distinctive features, such as an enlarged flat morphology and elevated SA-β-gal activity, have positioned them as a reliable tool in cellular biology [51]. More notably, the conditioned media from senescent IMR-90 cells, enriched with senescence-associated secretory phenotype (SASP) factors, is well-established and validated [52]. This SASP includes a plethora of factors that exert influence on surrounding cells and the local tissue microenvironment. Given our intention to employ senescent media in subsequent experiments, including IMR-90 cells offers a rational and methodologically sound choice. Their well-validated role in understanding the impact of senescence factors makes them invaluable in deciphering the intricate pathways involved in fibrotic conditions and other related biological processes.

In conclusion, the cell lines employed in this study have been carefully chosen to represent cellular interactions' complexity and multifaceted nature and their potential implications in fibrosis and tissue health. By studying these cells, we aim to unravel the cellular and molecular workings that drive pathologic conditions and offer potential therapeutic avenues.

1.6 Radiation and its' effects on salivary glands

Radiation, especially in cancer therapy, is a double-edged sword. While it effectively targets and destroys cancerous cells, the collateral damage to surrounding healthy tissues can be significant. The salivary glands stand out among the tissues vulnerable to radiation-induced damage due to their inherent sensitivity [53].

The mechanism behind radiation-induced damage is multifaceted. Primarily, ionizing radiation can damage DNA, including breaks in the DNA strands [54]. If these breaks are not

appropriately repaired, it can result in cell death or permanent cell cycle arrest. The latter

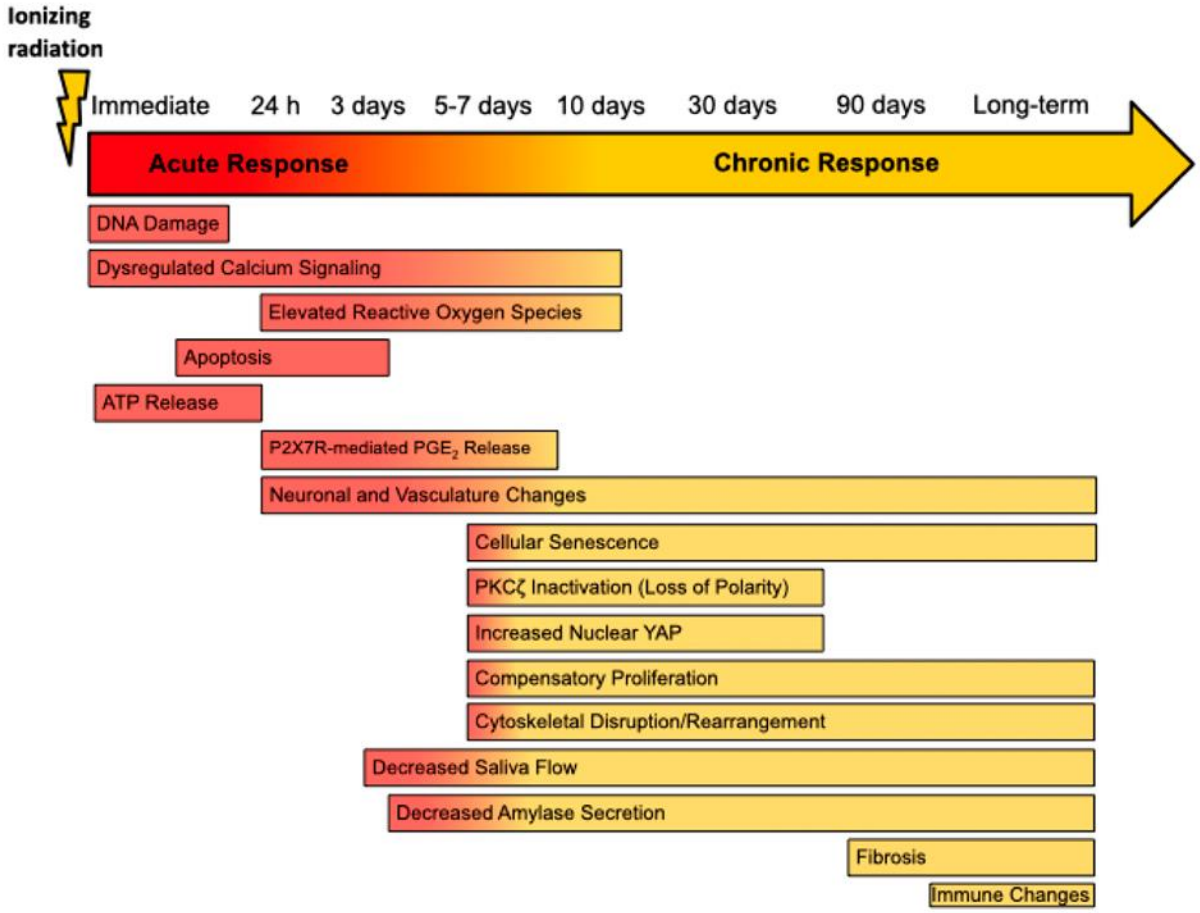

Figure 1.4 Timeline of Radiation-Induced Changes in the Rodent Salivary Gland. Following irradiation, rodent models show decreased saliva flow at approximately three days, and a loss of amylase secretion was reported as early as four days in rats post-IR. In the acute phase, immediate DNA damage, rapid apoptosis of acinar cells, and elevated levels of intracellular calcium and reactive oxygen species contribute to acute loss of glandular function following irradiation. This period is also marked by the release of ATP, which activates the P2X7 receptor (P2X7R), and the P2X7R-dependent release of prostaglandin E2 (PGE2) in murine parotid cells. During the transition phase, loss of apical/basolateral polarity because of PKCζ inactivation increases nuclear Yes-associated protein (Yap) levels, compensatory proliferation, cellular senescence, and cytoskeletal rearrangements, contributing to long-term dysfunction. Changes in innervation and vasculature have been reported as early as 24 h post-IR, as well as at chronic time points. Though inconsistently reported, fibrosis generally appears between 4- and 6-months following irradiation. There is little information regarding the effect of irradiation on the immune landscape of the salivary glands in rodent models. However, one study indicates changes at 300 days post-IR in mice**.** Image by Jasmer et al., licensed under CC BY 4.0."[55]

scenario, where cells enter a permanent cell cycle arrest state but remain metabolically active, is termed cellular senescence [52].

Radiation-induced senescence is particularly intriguing in the context of salivary glands. Post-radiation, the accumulation of senescent cells in the glandular tissue has been noted. These senescent cells can adopt various phenotypes, influencing tissue repair and regeneration differently. Specifically, specific senescent phenotypes secrete a range of inflammatory cytokines, growth factors, and proteases, collectively termed the senescence-associated secretory phenotype (SASP) [56]. An inflammatory SASP can exacerbate tissue damage and potentially promote fibrosis, leading to a loss of salivary gland function [57]. On the other hand, recent studies suggest that not all SASP components are detrimental. Some phenotypic shifts in senescent cells appear to mitigate damage and promote tissue repair [58]. The balance between these contrasting senescent cell behaviors might play a pivotal role in determining the outcome of radiation damage to the salivary glands (See Figure 1.4). However, the relationship between radiation, senescence, and salivary gland function remains complex and not entirely elucidated. While the role of senescent cells in tissue repair and fibrosis is becoming more apparent, questions remain on how their prevalence and phenotype post-radiation can be modulated to optimize tissue recovery.

1.7 Hypothesis and rationale

As senescent cells accumulate in salivary gland tissue with age, the SASP significantly influences the gland's response to radiation-induced damage. In specific contexts, senescent cells may reduce radiation damage by dampening tissue regeneration. Moreover, the SASP burden in the tissue might impact the success and efficacy of mesenchymal stem cell (MSC) transplantation for regenerative purposes. The central hypothesis is that the senescence-

associated secretory phenotype (SASP) significantly influences the response of salivary glands to radiation-induced damage.

The rationale lies in:

1. Cellular senescence is a complex process in which cells cease to divide but remain metabolically active, often in response to stressors [58]. As these cells accumulate in tissues, they can influence their surroundings through paracrine signaling, affecting various physiological and pathological processes, including tissue fibrosis [57,59].
2. Salivary glands are especially vulnerable to radiation's effects due to their specific cellular composition and functionality [60]. Radiation damages the tissue directly and can induce senescence in various cell types [61]. The resulting burden of these radiation-induced senescent cells within salivary glands has significant implications for tissue function, recovery, and attempts at regeneration.
3. The release of a wide array of factors known as the SASP is a hallmark of senescent cells. Depending on its composition, the SASP can either be detrimental—promoting inflammation and fibrosis—or beneficial, fostering tissue repair [58]. Initial findings suggest that under certain circumstances, senescent cells might offer protective effects against radiation damage, possibly because of a SASP profile that leans towards tissue repair and regeneration or perhaps because the SASP profile may inhibit cell growth and proliferation, which could make salivary gland cells more vulnerable to radiation damage [62].
4. Introducing mesenchymal stem cells (MSCs) into a tissue environment holds promise in regenerative medicine [63,64], but the tissue's existing state significantly dictates the MSCs' outcomes. A tissue environment with a high senescent cell burden might present a

challenging scenario for MSCs due to the altered cytokine milieu caused by the SASP [65]. This can impact the MSCs' survival, differentiation, and therapeutic efficacy [66].

5. Radiation, a cornerstone in cancer therapy, necessitates an in-depth understanding of the relationship between radiation, cellular senescence, tissue recovery, and regenerative interventions. Exploring the dynamic between radiation, senescence, and regenerative

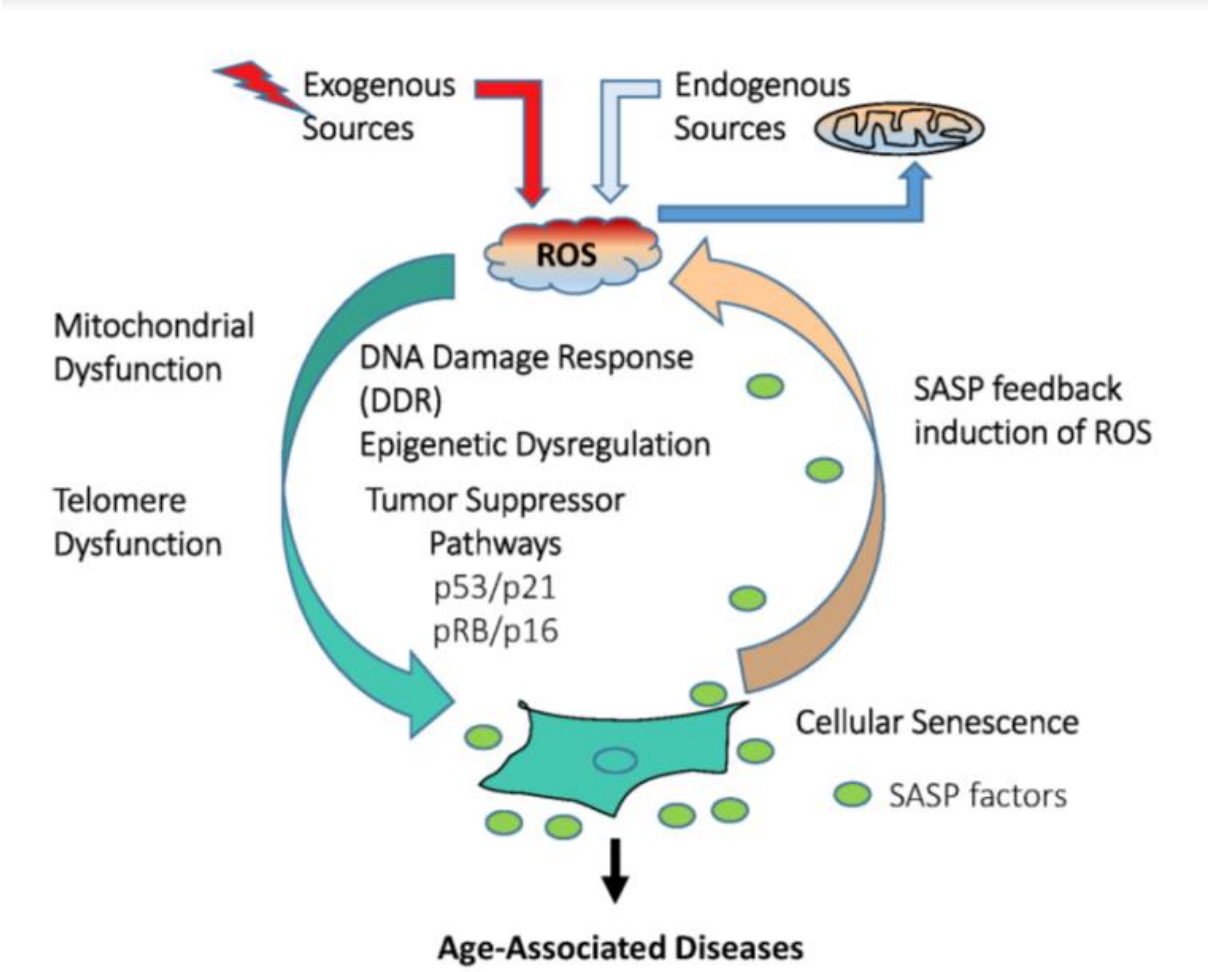

Figure 1.5 The Role of Reactive Oxygen Species in Cellular Senescence. ROS produced by exogenous sources such as radiation, smoke, and endogenous sources. ROS Produced by Endogenous and Exogenous Sources Image by Pole et al., CC 4.0 [64]

strategies like MSC transplantation holds vast clinical implications. Such insights could inform improved therapeutic strategies for patients undergoing radiation therapy and those seeking regenerative interventions.

6. By investigating these dynamics in 3D co-cultured salivary gland model, the research seeks to test the feasibility of using the 3D model to clarify the role of senescent cells in the salivary gland's radiation response and their potential influence on regenerative approaches, particularly future MSC transplantation. This knowledge could shape more effective therapeutic solutions for patients undergoing radiation and those needing regenerative treatments.

1.8 Organization of the dissertation

The organization of this dissertation is designed to provide a comprehensive exploration into the role of senescent cells in salivary gland tissue, particularly in the context of radiation damage and potential regenerative interventions. The structure logically guides the reader from fundamental concepts to specific experimental designs, results, and broader implications.

Chapter 1 Introduction and background

This chapter offers an overview of the existing knowledge in the field. It sets the stage by discussing the current understanding of salivary gland fibrosis, cellular senescence, 3D microtissue models, and the effects of radiation on salivary glands. The chapter concludes with the primary hypothesis and rationale, elucidating the motivation behind this research.

Chapter 2 Literature review: salivary gland bioengineering

This chapter examines the biology and pathology of salivary glands to inform their bioengineering. The chapter discusses the development and function of these glands, exploring

cellular aspects such as senescence and its implications on fibrosis and healing. It then explores cell selection for bioengineering, detailing the use of various cell types, including stem and progenitor cells. Additionally, it covers the design of biomaterials that facilitate cell survival, differentiation, and scaffold fabrication techniques like electrospinning and hydrogel synthesis. The chapter concludes by considering future strategies for enhancing vascularization and innervation of bioengineered tissues, suggesting innovative technologies like bioprinting and nanoparticles. The final section summarizes the potential future directions for research in salivary gland bioengineering.

Chapter 3 Development and characterization of 3D co-cultured salivary microtissue models

This chapter focuses on developing and characterizing a three-dimensional (3D) co-culture model that replicates the complex architecture and cell distribution of salivary gland tissue. The study establishes and optimizes a 3D co-cultured microtissue model using murine NIH 3T3 fibroblasts and SCA-9 submandibular gland salivary epithelial cells. It investigates multi-cellular interactions characteristic of salivary gland tissue, demonstrating the superior performance of non-adherent well plates over the conventional hanging drop method for consistent spheroid formation. The optimal cell seeding density was identified as 160 cells per well, consistently producing spheroids smaller than 200 μm, thereby preventing necrotic core development and maintaining spheroid roundness.

LIVE/DEAD staining confirmed high cell viability and the absence of central necrosis, while immunostaining with vimentin and TAS2R4 markers showed a mixed cell distribution within the spheroids. The chapter further explores the feasibility of using salivary gland spheroids for irradiation studies by exposing them to varying X-ray doses, revealing a dose-dependent increase in apoptosis. This self-assembled, Matrigel, and scaffold-free 3D co-culture model successfully

mimics critical features of the native salivary gland microenvironment, providing a valuable tool for future functional and pathological studies. The chapter concludes by discussing this model's potential applications and implications in salivary gland research.

Chapter 4 Senescence-conditioned medium exacerbates fibrotic response to radiation in a 3D salivary gland microtissue model

This chapter investigates the dynamics of radiation-induced fibrosis using a three-dimensional (3D) scaffold-free, necrotic core-free spheroid model of the salivary gland, comprised of NIH 3T3 fibroblasts and SCA-9 salivary epithelial cells. The study leverages this model to explore fibrotic responses to X-ray exposure, focusing on the modulatory role of senescent cell-conditioned medium. Initial analysis in two-dimensional (2D) cultures dissected individual reactions of NIH 3T3 and SCA-9 cells to radiation, identifying a 16-Gy radiation dose as optimal based on its cytotoxic effects, DNA damage, apoptosis, and senescence induction.

Transitioning to the 3D microtissue model, the study conducted a detailed investigation into how senescence-conditioned medium influences the fibrotic response of spheroids to 16-Gy radiation. Key aspects of this response, including cell viability, apoptosis, DNA damage, and senescence induction, were examined to understand the mechanisms driving radiation-induced fibrosis. A crucial element of this inquiry was the evaluation of fibrotic markers, specifically collagen I and alpha-smooth muscle actin (α-SMA), using quantitative assessments and Picrosirius Red staining. The results revealed significant exacerbation of fibrosis due to the senescence-conditioned medium.

The chapter concludes by discussing the implications of these findings for understanding the fibrotic responses in salivary gland tissues, highlighting the potential applications of this 3D model in further functional and pathological studies.

Chapter 5 Conclusions and future directions

The final chapter synthesizes the main findings, discusses broader implications, and suggests potential future research directions. It provides a holistic view of the research journey and its contributions to the field. Overall, this thesis is organized to offer a coherent and structured journey through a complex topic. Each chapter builds upon the previous, leading to a comprehensive understanding of the research's significance and potential applications.

Chapter 2 Literature review: salivary gland bioengineering

2.1.Introduction

In the United States, over twenty-four million people suffer from xerostomia, or dry mouth, with over a million people experiencing moderate to severe symptoms [67]. More than 400 medications cause xerostomia; elderly individuals suffer disproportionately from xerostomia as a result [68]. Other medical conditions such as Sjögren's disease and diabetes also cause xerostomia. Seventy-four to eighty-five percent of head and neck cancer patients receiving radiation therapy experience xerostomia [69]. According to World Cancer Report 2014, there were 550,000 head and neck cancer cases worldwide, suggesting the generation of at least 351,000 new cases of xerostomia from head and neck cancers alone [70]. The global xerostomia therapeutics market size was estimated at USD 625.3 million in 2018 and is expected to grow at a CAGR of 3.6% between 2019 and 2026 [71]. Xerostomia, the perception of dry mouth, typically results from a defect in saliva production or secretion, known as hyposalivation. Hyposalivation significantly decreases quality of life as it damages oral and general health, causing cracked lips, microbial proliferation, periodontitis, cavities, oral ulcerations, and difficulty in speaking, eating, tasting, swallowing, and digesting [72]. As a result of oral barrier compromise and subsequent systemic inflammation related to bacterial pathogens and endotoxin, poor oral health can contribute to cardiovascular and related diseases and is associated with rheumatoid arthritis, Alzheimer's disease, cardiovascular, diabetes, and cancer [73]. Currently, available treatments include medication changes, saliva stimulants (sialagogues), and moisturizers; however, these treatments offer only transient relief, and sialagogues can have side effects, including sweating, increased heartbeat, abdominal pain, diarrhea, nausea, changes in vision, among others. Temporary relief is a suboptimal solution, particularly for many head and

neck cancer survivors experiencing persistent xerostomia due to the limited salivary gland regenerative capacity [74]. Several approaches may improve the regenerative capacity of salivary gland tissues, including gene therapy, stem/progenitor cell-based therapy, and tissue engineering strategies, many of which are nearing clinical translation. Additionally, advances in organoid technology, organoid-enabled discovery of therapeutic targets, drug screening and testing, and tissue regeneration will provide new avenues to salivary gland tissue regeneration. This article

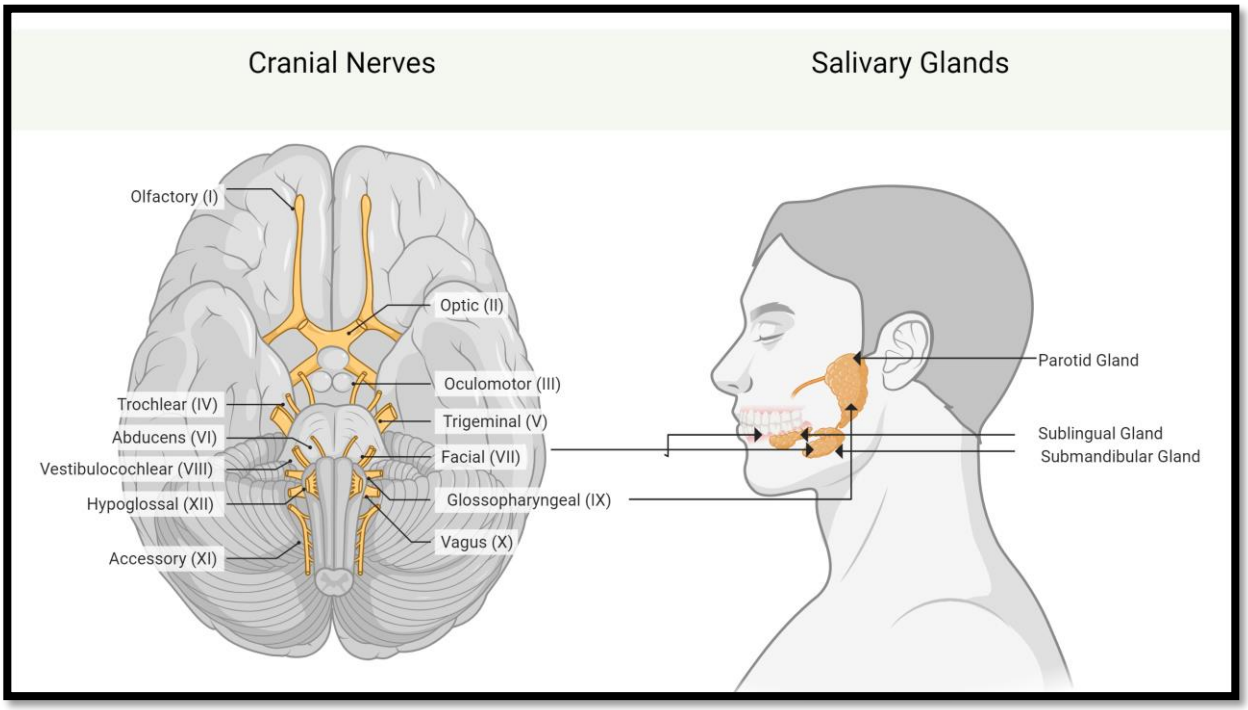

Figure 2.1 Primary salivary glands. There are three pairs of major salivary glands, parotid, submandibular, and sublingual, innervated by the facial and glossopharyngeal nerves. Created with BioRender.com (2023)[76].

will first review salivary gland biology and pathologies driving the development of regenerative medicine methods to restore salivary function and then review progress towards achieving regenerative medicine-based strategies for clinical application, followed by future perspectives on next-generation salivary gland tissue engineering and regenerative medicine.

2.2. Learning from salivary gland biology and pathology

2.2.1. Salivary gland development and function

Salivary glands and their functional units

Salivary glands function to produce a composite of water, electrolytes, enzymes, and mucus called saliva [75]. Ninety percent of saliva is made by three sets of major salivary glands: parotid, submandibular, and sublingual (Figure 2.1) [76]. Gland secretions vary between the

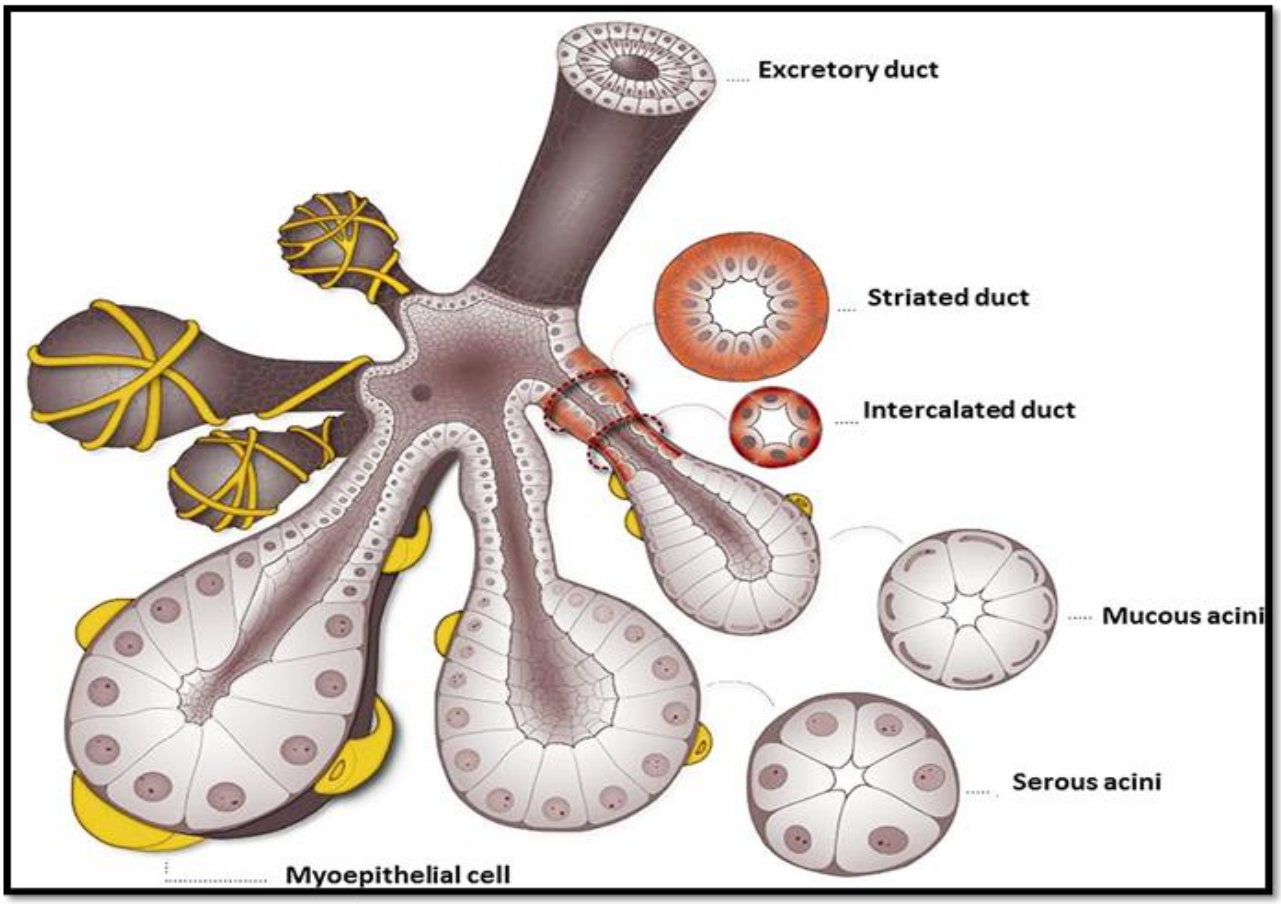

Figure 2.2. The adenomere functional unit of the human salivary gland. Reprinted with permission from de Paula et al, 2017. © 2017 Wiley Periodicals [1].

glands, with the parotid glands in front of and beneath the ear producing primarily the watery and proteinaceous components of saliva, the sublingual glands (SLGs) beneath the tongue primarily producing mucus, and submandibular glands (SMGs) on both sides, just under the jaw,

producing both components [77]. These salivary glands are innervated by the autonomic nervous system. Parasympathetic innervation via the cranial nerves tends to promote saliva secretion. The glossopharyngeal nerve innervates parotid glands, and the facial nerve innervates SMGs and SLGs[1]. Additionally, hundreds of minor salivary glands line the surface of the mouth and throat. Each gland is divided into lobules; these lobules, in turn, are made up of functional units called adenomeres. The adenomere contains several cell types: acinar (serous and mucous), myoepithelial, basal, and ductal (intercalated, striated, and excretory). The adenomere does not function independently but rather in an integrated fashion with neighboring parasympathetic ganglia and blood vessels [77,78].

Coordination of saliva secretion

The adenomere and the acinus have been referred to in the literature as the functional unit of the salivary gland. The distinction between the two is that the adenomere also includes the intercalated, striated, and excretory ducts, which provide the necessary conduits for saliva expulsion into the oral cavity and the acinus. In each adenomere, innervated myoepithelial cells surround clusters of acinar cells, each arranged in a bulb-shaped formation (Figure 2.2). Serous acinar cells secrete a watery fluid devoid of mucus; mucous acinar cells produce a secretion rich in mucins. Mucins are glycoproteins that combine with water to form a mucin hydrogel (mucus). The secretory products of each pair of glands are governed by the distribution of serous acinar versus mucous acinar cell types. Accordingly, the parotid gland, a serous gland, releases a watery secretion that contributes to around 25% of our daily saliva. Its secretions enter the oral cavity via ducts in the cheek lining, aligning roughly with the molar teeth. SMGs on the lower jaw produce both watery and mucous secretions, contributing to 70% of total salivary output. Their secretions flow into the mouth through ducts on both sides of the tongue's base, near the thin

frenulum. In contrast, the SLG produce primarily mucous secretions in smaller quantities, dispensed through several tiny ducts beneath the tongue [79]. It is worth noting that in humans, a given acini can be mixed (seromucous acini) and in mice, the SMG acini contain seromucous cells [80]Production of saliva requires the coordinated efforts of multiple cell types. Myoepithelial cells contain actin filaments, which contract to increase hydrostatic pressure in neighboring cells. This myoepithelial cell contraction results in the expulsion of acinar-cell secretory products into the ductwork of the adenomere [81]. Acinar secretions are deposited into the ductal system, initially entering through the intercalated duct. Acinar and ductal cells are linked together by multiple classes of complementary cell junctions such as occluding, anchoring, and communicating junctions, which maintain the structural and mechanical integrity of the adenomere structure [82]. Together with the basement membrane, the myoepithelial cells surround the acini and line the abluminal layer of the intercalated duct. The lumen of the intercalated duct is continuous with the striated duct. The characteristic appearance of the striated duct results from numerous folds in the apical plasma membrane that facilitate ion exchange to modify the acinar cell saliva. The apical domain of the striated duct cells secretes HCO_3^- and K^+ and reabsorbs Na^+ and Cl^- using the Na^+-K^+ pump and the Cl^--HCO_3^- pump to make the saliva hypotonic. This would not be the case were it not for the ductal cells being relatively impermeable to water. This causes the water in the saliva to remain in the duct and not be reabsorbed back into the bloodstream, and thus, the saliva becomes diluted or hypotonic compared to plasma by the time it exits the ducts into the oral cavity [77]. Further, the overall reabsorption of Na^+ and Cl^- is higher on a molar basis than the secretion of K^+ and HCO_3^-, which further contributes to the hypotonic nature of the saliva. The production of saliva requires the apicobasal polarity of the epithelial cells, which develops following epithelial cell-cell

interactions and interactions with basement membrane proteins [83] that are produced by both epithelial and stromal cells [84].

Salivary gland development

Branching morphogenesis creates the adult gland structure

Throughout nature, branching morphogenesis serves to form complex, well-ordered architectures. This meticulous formation arises from the cellular and molecular coordination that sets the stage for the unfolding of tissue development. Paramount in this orchestration are the molecular cues that navigate the dynamic cellular landscapes, ensuring their timely and spatial responses.Fibroblast growth factors (FGFs), especially FGF7 and FGF10, act as liaisons between the mesenchyme and epithelium. Their paracrine signaling is pivotal for driving epithelial proliferation and, in turn, shapes the eventual branching architecture of the gland [85,86]. Other morphogens, such as bone morphogenetic proteins (BMPs) and pivotal members of the transforming growth factor β (TGF-β) superfamily, orchestrate cellular proliferation and differentiation [87]. Their nuanced gradient distributions within developing tissues help establish unique cellular zones, dictating specific branching patterns within the salivary gland [88]. Not to be overshadowed, the Sonic Hedgehog (Shh) signaling pathway, central in many developmental processes, carves its niche particularly in the early stages of salivary gland morphogenesis [85,86,89][20,21]. Moving to the cellular adhesion process, cadherins emerge as central players. These calcium-dependent adhesion proteins ensure epithelial cell cohesion, with E-cadherin playing a lead role [90]. Its dynamic modulation during morphogenesis facilitates the flexible cellular rearrangements necessary for bud formation and clefting processes, as reviewed by Sisto et al. [90]. Integrins, the bridges between the cells and their extracellular matrix (ECM), transmit vital signals that inform cellular behavior. Their nuanced interactions with the ECM components, notably fibronectin and laminins, play a cardinal role in the epithelial invagination and migration

tales that underscore branching morphogenesis [91].As the story unfolds, these structures develop from a series of reciprocal interactions between tissue types, anchored in conserved molecular programs [18]. This process includes coordinated cellular actions, such as proliferation, ECM remodeling, differentiation, migration, and apoptosis. In the salivary gland, branching morphogenesis functions to maximize surface area, ensuring the flow of saliva from the salivary gland. Branching morphogenesis maximizes the surface area for the secretion of fluid across its underlying epithelium. Normal salivary gland function is dependent on branching morphogenesis of the epithelium to form the parenchymal tissue as well as the coordinated branching of the vasculature and nerves that support and innervate the gland, respectively [85,86].

Epithelium, endothelium, and neural crest derived cells regulate early salivary gland development

The orchestration of salivary gland development is a testament to the high-level interplay between diverse cell types. Each cell type not only carves its niche but also communicates actively with its neighbors to shape the mature gland. In coordinated unfolding of salivary gland development, the mesenchymal condensates and the thickening process of the oral epithelium precede formation of the primordial bud, or bud initiation, in morphogenesis. The mesenchymal condensates, clusters of mesenchymal cells, prominently express characteristic proteins such as FGF10 and FGFR2b. [85,92]. At the same time, as the oral epithelium thickens prior to bud formation, it exhibits a distinctive set of markers. E-cadherin marks the expanding adhesive interactions within this layer [93–95]. The epithelial cells initiate the very buds that subsequently undergo branching morphogenesis, setting the stage for the gland's elaborate architecture. This budding and subsequent branching rely on a myriad of signaling pathways, including those activated by growth factors such as FGFs and epidermal growth factors **(**EGFs) [32,33]. Proteins

such as SOX9, SOX10, and Pax-9 indicate evolving lineage commitments, steering the epithelial cells towards their predetermined roles in the salivary gland development [29,31]. Endothelia form the innermost lining of the blood vessels. Their intricate web ensures the delivery of essential nutrients and oxygen to the developing gland. Furthermore, the endothelial cell signaling can influence the behavior of nearby epithelial and mesenchymal cells, potentially impacting gland morphogenesis [96]. Neural crest-derived mesenchyme cells originate from the neural crest— a transient structure during embryonic development— and migrate to various parts of the embryo. In the context of the salivary gland, they provide crucial signals for epithelial morphogenesis. They secrete factors that guide the epithelial branching and possibly influence the differentiation of specific cell types within the gland [97]. Lineage tracing experiments have been instrumental in understanding the origins of various cell populations in the gland. The Sox17-2A-iCre/R26R experiments highlight the ectodermal origin of major salivary glands, emphasizing the shared developmental lineage between the skin, nervous system, and the glands [98]. This underscores the deeply evolutionarily conserved developmental pathways shared among various organs. Among the factors governing differentiation and lineage commitment in salivary gland development, the SOX transcription factors, particularly SOX2, SOX9, and SOX10, have emerged as pivotal regulators [95,99,100].SOX2 is a master regulator of the acinar cell lineage. It is expressed in progenitors that give rise to both acinar and ductal cells. However, in its absence, the formation of acinar cells is notably affected, while ductal formations remain largely unaffected. Peripheral nerves further play a role in acini formation through SOX2 regulation [99]. SOX9's significance in SMGs is underscored by its changing expression patterns from the embryonic to the adult stage. A lack of SOX9 during the early developmental phases leads to smaller initial SMG buds. Additionally, studies have shown that introducing SOX9 into

mouse embryonic stem cell-derived oral ectoderm can stimulate salivary gland rudiment development. ChIP-sequencing studies further reinforce the role of SOX9 in guiding genes involved in tube and branching formation [95].Lastly, SOX10 has proven crucial for both the maintenance and differentiation of specific epithelial progenitors in exocrine glands. Notably, these progenitors are marked by the KIT/FGFR2b/SOX10 axis, representing the earliest multi-potent and tissue-specific progenitors of exocrine glands. When SOX10 is genetically deleted in the epithelial context, there is a marked loss of secretory units, subsequently reducing organ size and function. However, intriguingly, the ductal tree persists. In the absence of SOX10, the remaining duct progenitors demonstrate a lack of adaptability and cannot properly form secretory units. Yet, when SOX10 is overexpressed in these ductal progenitors, there is an enhancement in their adaptability towards KIT^+ progenitors, driving the differentiation into secretory units. Thus, SOX10 emerges as a central regulator of plasticity and multi-potency in epithelial KIT^+ cells across several secretory organs, encompassing the mammary, lacrimal, and salivary glands [100]. Collectively, while the distinct roles of SOX2, SOX9, and SOX10 are becoming clearer in the context of salivary gland development, there remains much to be explored about their interplay, regulatory mechanisms, and potential therapeutic implications. The fact that parotid glands, SLGs, and SMGs arise from the oral epithelium sheds light on the potential shared molecular mechanisms between the salivary glands and other oral structures [101]. Meanwhile, the revelation from Wnt-1-cre lineage tracing, that mesenchymal and nerve cells in the gland originate from the neural crest, underscores the neural crest versatility and its profound influence on craniofacial development [102]. By mouse embryonic day 11 (E11) or human embryonic day 30 (H30), neural crest cells migrate to the oral epithelium, initializing a mesenchymal condensation (See Figure 2.3) [103]. This process prompts the oral epithelium to thicken into a

placode by mouse E11. The placode dives into the mesenchyme, forming an epithelial bud by E12, eventually becoming a primary bud. This action underpins salivary gland branching development. Simultaneously, nerve connections of the gland are established. Neural crest cells evolve into the parasympathetic fibers for the facial nerve, integrating with the SMG and SLG. By E12, these fibers structure the parasympathetic ganglion (PSG) [104–106]. For the gland's continued maturation at E12/H36, interactions between basal cells, marked by keratin 5 (K5), and the PSG are essential [107]. Wnt signals, emitted by $K5^+$ gland cells, regulate this nerve interaction [108].The parasympathetic ganglion cells also depend on neurotrophic factors such as neurturin (NRTN). Diminishing NRTN in adult mice experiments notably hampers gland regeneration and saliva production. At the molecular level, the glial-derived neurotrophic factor (GDNF) family, inclusive of NRTN, orchestrates nerve cell dynamics. Their receptors, glial cell-derived family receptors α, (GFRα 1-4), partner with ligands such as GDNF and NRTN. These ligand-receptor interactions, especially involving NRTN and GDNF, are pivotal for maintaining the health of the SMG's parasympathetic ganglion. Mechanistically, their association with GFRα and RET co-receptor triggers cellular pathways (e.g., MAPK and PI3K-Akt), overseeing cell growth and survival [109]. Reciprocal Wnt signaling from $K5^+$ salivary gland progenitors is necessary for innervation [108]. Wnt signaling, known for its role in cellular proliferation, differentiation, and stem cell maintenance, activates a cascade involving Dishevelled proteins, leading to the stabilization and nuclear translocation of β-catenin, where it can regulate gene expression [110]. In the context of the salivary gland, the specific genes targeted by this signaling might dictate progenitor cell behavior and further differentiation. The progenitors rely on the GDNF family members, such as NRTN. In adult mice, when NRTN and related GDNF family members were experimentally decreased, a 50% reduction in gland regeneration and a

40% reduction in saliva secretion were observed [111].In general, GDNF family members are involved in survival, proliferation, and differentiation of neuronal populations in the central and peripheral nervous systems. System receptors for these ligands include GFRα 1-4, which are the preferential co-receptors for GDNF, NRTN, Artemin (ARTN), and Persephone (PSPN), respectively. NRTN and GDNF are crucial neurotrophic factors with different temporal effects on prenatal and postnatal development and on survival of the SMG parasympathetic ganglion. These effects are mediated through binding to GFRα 1,2,3, and the "rearranged during transfection" co-receptor (RET co-receptor), which activates mitogen activated protein kinase (MAPK), phosphatidylinositol-3-kinase-protein kinase b (PI3K)-Akt, phospholipase c (PLC)-γ and sarcoma (Src) signaling pathways [109]. In conditions where NRTN and GDNF are experimentally decreased, the salivary gland exhibits marked dysfunction. A significant insight into the protective role of NRTN comes from studies involving irradiation-induced damage in salivary glands. Irradiation, commonly used in the treatment of head and neck cancers, frequently results in irreversible salivary gland hypofunction. Research has shown that NRTN plays a pivotal role in safeguarding the gland against such damage. NRTN assists in the epithelial regeneration of irradiated salivary glands by preventing the apoptosis of parasympathetic neurons, which are crucial for the gland's function. When delivered via gene therapy, NRTN effectively shields the gland against irradiation damage. Glands pre-treated with NRTN maintain their function post-irradiation, a stark contrast to untreated glands, which exhibit significant dysfunction. This protective mechanism of NRTN operates, at least in part, by bolstering parasympathetic innervation. Markers of parasympathetic function, negatively impacted by irradiation, remain stable when NRTN is present [112]. NRTN's essential function goes beyond its protective role against external damage like irradiation. In the developing and

adult salivary gland, NRTN pairs with GFRα2. While the gland parenchyma produces NRTN, GFRα2 is expressed in the parasympathetic ganglia. NRTN deficiency leads to a substantial loss of GFRα2-expressing parasympathetic neurons in the salivary gland, and the surviving ones appear smaller than in normal conditions. This finding suggests a pivotal role for NRTN as a trophic factor for specific parasympathetic neuron populations within the salivary gland [113]. The epithelium undergoes branching morphogenesis to elaborate its branched structure. At E13/H42, the endbud enlarges, and three to five clefts form in the epithelium as the salivary gland undergoes branching morphogenesis. These clefts later deepen to become the major lobules of the gland. In contrast to other organs in which branching morphogenesis is driven by proliferation, branching in the salivary gland is driven by the formation of clefts in the basement membrane on the surface of the buds [114]. Cleft formation is initiated by basement membrane fibronectin. Fibronectin drives BTB/POZ domain-containing protein 7 (Btdb7) expression, which induces snail family transcription factor 2 (Snail2) expression and E-cadherin suppression [115,116]. Cleft formation is further reinforced by the action of GSK 3-β, which phosphorylates β-catenin in cells at the base of the cleft, targeting it for degradation. A cytoplasmic shelf with a core of microfilaments occurs in cells at the base of the cleft [117], which may be a matrix attachment point to drive cleft elongation via cytoskeleton attachment. This notion is supported by studies showing that the inhibition of actin cytoskeletal polymerization inhibits cleft formation. Daley et al. proposed that a mechanochemical checkpoint involving rho-associated coiled-coil containing kinase (ROCK) regulates the transition of initiated clefts, which are proliferation independent, to a stabilized state that is competent to undergo cleft progression [118]. Basement membrane is required for cleft formation with laminin α5-null mice showing delayed SMG branching and delayed cleft formation. ROCK also controls organization of the

outer layer of cells adjacent to clefts by coordinating cell polarity via PAR-1b protein, which controls positioning of the basement membrane on the basal side of the outer layer of epithelial cells in the developing epithelial buds [119]. Epithelial cell proliferation drives the expansion of

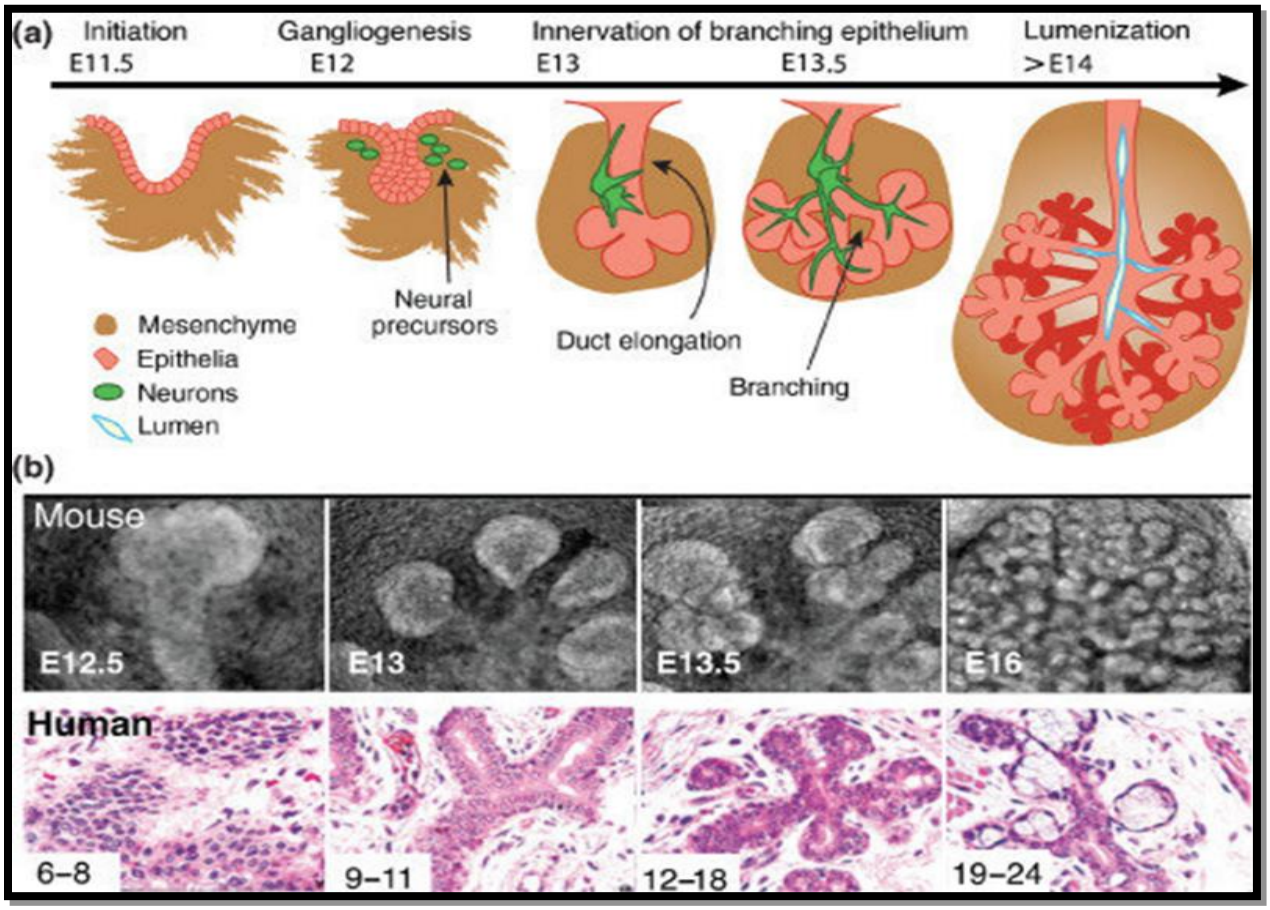

Figure 2.3. Stages of salivary gland development. Reprinted with permission from Mattingly et al., 2015. © 2015 Wiley Periodicals [87].

buds to drive the growth of the developing gland. EGFs and their receptors are important for SMG development. EGF-null mice show reduced epithelium proliferation, branching, and maturation [120]. Fibroblast growth factors such as FGF1, FGF3, FGF7, and FGF10 are produced from mesenchyme and modulated by platelet-derived growth factor (PDGF) [121]. FGFs are required for salivary gland development as the FGF10- and FGFR2b-null mice do not develop salivary glands [122]. Proliferation is driven by FGF10 and FGF7, both of which bind to

FGFR2b. When FGFR2b binds to FGF10, duct elongation is induced, while binding to FGF7 induces budding [123]. In vivo, FGF10 signaling is likely modulated by heparan sulfate as FGF10 binding to heparan sulfate increases its affinity for FGFR2b, and the ternary complex resulting from this binding increases proliferation [124]. Other growth factors are required for salivary gland development, including Wnt and ectodysplasin (Eda), as reviewed previously [125,126]. Defining the regulation of different cell populations is critical for the development of regenerative therapies. With recent studies to define distinct cell populations by single cell RNA sequencing (scRNASeq) [126,127], it will be possible to comprehensively define the specific cell populations responding to specific signals. The adult salivary glands appear to harbor various stem and progenitor cell populations essential for tissue maintenance, regeneration, and repair. Extensive studies have been conducted to pinpoint the exact locations of these cell pools within the salivary glands. The ductal regions, especially the intercalated and striated ducts, are seen as potential storehouses for progenitor cells. Notably, cells that express markers like c-Kit or Keratin 5 (K5) reside in these ductal regions, hinting at their stem-like properties [128].

Ascl3, a transcription factor that plays an essential role in determining cell fate, development, and differentiation, marks a progenitor cell population in the adult mouse salivary glands. Ascl3-expressing cells were shown to be intermediate lineage-restricted progenitor cells that exist in all major salivary glands that can differentiate into acinar and ductal cells in vitro in 3D spheres [129]. Basal cells, found at the basal side of the acinar units, are also proposed as potential stem or progenitor cells. They frequently express markers like Keratin 14 (K14) and are known to play a part in gland regeneration under certain conditions. [130].Although the primary role of acinar cells is saliva production, they have been observed to dedifferentiate and adopt progenitor-like abilities, suggestive of their ability to aid in glandular repair in specific contexts. Mesenchymal

stem cells (MSCs) present in salivary glands are typically found near blood vessels. These cells have the capacity to evolve into multiple cell types, potentially assisting in tissue repair post-injury [131]. In some conditions, salivary gland cells can develop spheroid formations when cultured. These spheroid-forming cells exhibit stem cell traits, positioning them as potential sources for regeneration. In specific mouse studies, Lgr5-positive cells, commonly recognized as stem cell markers in other tissues, have been identified within salivary glands and are suggested to contribute to tissue balance and recovery [132]. It should be noted that the exact roles, traits, and connections of these cell types within human salivary glands remain a subject of ongoing debate.

2.2.2. Fibrosis, cellular senescence, and salivary gland pathology

When salivary glands are damaged by immune dysfunction (e.g., Sjogren's syndrome), radiotherapy, or age-associated cellular senescence, an increase in senescent cells is typically accompanied by fibrosis. In each case, local inflammation is initially or subsequently driven by senescent cells and their secreted products, resulting in inflamed, fibrotic, and senescent cell-enriched salivary glands. In Sjögren's syndrome, autoimmune dysfunction leads to lymphocyte infiltration of the salivary gland, which is followed by an increase in senescent cells [133]. In salivary glands exposed to radiation, oxidative stress leads to DNA damage, which triggers the DNA-damage response pathways in cells that can lead to cellular senescence or apoptosis [134]. Finally, the number of senescent cells increases with advancing age due to replicative senescence and responses to environmental factors. As senescent cells produce secreted factors as part of their senescence associated secretory phenotype (SASP), senescent cells can affect otherwise healthy cells via bystander effects. This senescence-induced inflammation has many effects that include driving acinar cells to senescence, destroying their ability to produce saliva; dampening

or destroying existing stem cells that may exist in or migrate to salivary gland tissue, capping natural regenerative processes; and provoking phenotypic shifts in fibroblasts that drive the unremitting ECM production characteristic of fibrosis [135–137]. Numerous studies have shown that the SASP can exert deleterious effects on stem cell function. For example, geriatric stem cells could change reversible quiescence in satellite stem cells into senescence [138]. In the salivary gland, salivary gland stem cells (SGSCs) isolated from Sjögren's syndrome patients were regeneratively inferior; they were likely to be senescent or limited to intercalated duct cell differentiation only [139]. The impact of radiation on the salivary gland senescence is evidenced by a subtle interplay between different cell types and their physiological responses. A central response is the expression of p16, an inhibitor of cell division kinase 4, seen in the basal cells of the salivary duct, which are believed to act as progenitors. The correlation between p16 expression in these cells with saliva production and the infiltration of $CD45^+$ leukocyte cells in Sjögren's Syndrome (SS) patients suggests that basal cell senescence might be an early hallmark of SS, likely contributing to diminished salivary gland function [140]. After radiation exposure, there is a significant loss of acinar cells and shrinkage of the gland during the acute phase [141,142]. In the aftermath of radiation, the resilience and adaptability of different ductal progenitor populations within the gland including $KRT14^+$ progenitors is impressive. Fast-cycling cells display an increased proliferation in response to radiation-induced damage and asymmetrically divide to replenish the cells of the larger granulated ducts. On the other hand, KIT^+ intercalated duct cells are a stark contrast, being long-lived progenitors with minimal divisions both during homeostasis and post-radiation. These cells maintain ductal architecture with slow rates of cell turnover, emphasizing the heterogeneity in response mechanisms employed by salivary progenitor cells to sustain tissue structure [143].Another facet of radiation-

induced effects on salivary glands is their rapid functional impairment, which is evident as soon as 24 hours post-exposure. This response underscores the significant impairment of myoepithelial cells, offering a fresh perspective on the pathogenesis of radiogenic salivary gland dysfunction. Beyond the damage to acinar cells, this indicates that secretory retention, assessed scintigraphically, might be rooted in myoepithelial cell impairment [144,145].In general, salivary gland cellular senescence and its associated fibrosis create the need for tissue replacement, while simultaneously creating a host tissue environment that is not conducive to it [146].

SASP Signaling Drives Neighboring Proliferation-Competent Cells to Senescence (Bystander Effect)

Senescent cells induce the DNA-damage response in neighboring proliferation-competent cells through a variety of different mechanisms that often results in an increased senescent cell burden. This induction can occur via gap junction-mediated cell-cell contact and processes involving reactive oxygen species (ROS). Continuous exposure induced senescence in bystander fibroblasts [147]. Mikula-Pietrasik et al. showed that senescent human peritoneal mesothelial cells (HPMCs) elicited the bystander effect on neighboring HPMCs and human peritoneal fibroblasts (HPFCs). Further, they identified TGFβ1 as the essential soluble mediator eliciting this change. It was postulated that this effect occurred though the induction of ROS and p38 MAPK. HPMCs also released thrombospondin-1 (TSP-1), a major activator of TGFβ1 [148]. Nelson et al. asserted that ROS-activated NF-κB also elicits the DNA-damage response, leading to senescence in bystander cells [149]. Finally, Da Silva et al. demonstrated the bystander effect in vivo across multiple tissues using NOD SCID gamma mice, which support highly efficient engraftment of human hematopoietic stem cells (hu-$CD34^{+}$) and human peripheral blood mononuclear cells (hu-PBMC) [150]. These findings suggest a possible senescent cell-signaling

basis for fibrosis development in salivary glands and decreased saliva production. More importantly, they suggest a set of strategies for mitigating or reversing these effects, which will be explored in a later section.

Senescence and Its Impact of Normal Fibroblast Dynamics in Healing and Fibrosis

Fibroblasts have a set of functionally dynamic phenotypes that are temporally varied according to the healing stage of the tissue in which they reside. Oxidation and other factors associated with wounding prompt fibroblasts to shift their phenotype. While few studies have examined these transitions in the salivary gland, in response to a reversible injury where a metal clip is placed on the primary salivary gland duct, a transient fibrotic response occurs in which *Pdgfra*$^{+}$, *Pdgfrb*$^{+}$ fibroblasts overexpress ECM proteins [151]. Reversible phenotypic shifting among fibroblasts is thought to serve as a mechanism for tissue homeostasis [152,153]. In salivary gland organoid culture, *Pdgfra+* cells that support epithelial cell proacinar differentiation in response to FGF2 can transition to a fibrotic myofibroblast like phenotype in response to TGFβ1 [153]. In other contexts, these shifts can occur between fibroblast, senescent fibroblast, myofibroblast, and senescent myofibroblast phenotypes. However, it should be noted that fibroblasts may originate from different cell types, which may, in turn, dictate how they shift phenotypically [153,154].

The relationships between senescence and fibroblast dynamics have been explored in other organs and cultured cells. Damaris et al. found that wound-site damage prompted fibroblasts to become senescent and secrete PDGF-AA. PDGF-AA, in turn, prompts wound closure by inducing a phenotypic shift in fibroblasts to myofibroblasts. Contractile elements in the myofibroblasts are responsible for wound closure [155]. In tandem, the myofibroblasts emerge mainly, but not exclusively, as a phenotypic variant of the fibroblasts. Although not all myofibroblasts assume the same function, as a class they produce ECM, close wounds, and

release cytokines. IL-10 was shown to play a key role in fibrosis resolution by reversing a TGFβ1-induced, transiently activated, myofibroblast phenotype [156]. These two cytokines can cause neighboring macrophages to become oriented toward ECM degradation, which can lead to the resolution of fibrosis. ECM degradation reduces matrix stiffness, which shifts the apoptosis/senescence axis towards myofibroblast apoptosis. Apoptosis complements the macrophage degradation function to reestablish normal tissue homeostasis. Alternately, myofibroblasts may shift phenotype to become ECM-degrading fibroblasts (deactivation), or they may shift toward senescence as well, by the signaling action of cysteine-rich angiogenic inducer 61 (CYR61/CCN1) [157]. In general, pathological fibrosis is known to occur when myofibroblasts and senescent myofibroblasts escape apoptosis and engage in ongoing overproduction of ECM. Additionally, these cells produce several other compounds that further facilitate pathological remodeling. These pathological changes are readily observed in histological samples of salivary gland tissue that has been damaged due to autoimmune dysfunction, irradiation, or aging. Understanding the factors that control fibroblast dynamics is critical to successful salivary gland tissue engineering. Engineered and host tissue scaffold stiffness and local and systemic signaling aberrations are relevant to transplant success. The same is true of cell-signaling aberrations present in diseased salivary gland and the larger system in which the salivary glands operate. For example, individuals with systemic inflammation will likely have ongoing immune cell infiltration, while individuals with irradiated salivary glands may have different patterns of damage [69]. Aged individuals may have different kinds of cross-linking in their tissue, such as advanced glycation end products, which are less amenable to degradation [158]. Therefore, different patients may require different approaches to salivary gland engineering to optimize transplant and engraftment success. Scaffold stiffness and growth

factors such as TGFβ1 and connective tissue growth factor (CTGF) cue certain fibroblasts to phenotypically shift to the myofibroblast phenotype. This shift is evidenced by the expression of α-smooth muscle actin (α-SMA). ECM stiffness is driven via mechanotransduction pathways that involve lengthy cascades of signaling molecules to control α-SMA transcription. These pathways start at the surface of the cell via β1 integrins. β1 integrins are connected to F-actin stress fibers, which are bound, in sequence, to FAK, ROCK and myocardin-related transcription factor (MRTF). MRTF can translocate to the nucleus where it binds serum response factor (SRF), which leads directly to the production of α-SMA. MRTF also binds transcriptional co-activators yes-associated protein (YAP) and transcriptional co-activator with PDZ-binding motif (TAZ) to initiate α-SMA transcription. These proteins activate other transcription factors such as TEA domain family member (TEAD), T cell factor/lymphoid enhancer-binding factor (TCF/LEF), and β-catenin [159]. ECM stiffness and mechanical forces also regulate force-dependent activation of latent TGFβ1 by increasing resistance to traction forces generated by fibroblasts. In this mechanism, extracellular latent TGFβ1 (TGFβ1 with its latency-associated peptide) is released from latent TGFβ1-binding protein stores when αV integrins respond to mechanical pulling forces. Once activated, TGFβ1 binds to TGFβ receptors and promotes canonical mothers against decapentaplegic homolog 3 (SMAD3) activation [89][160]. Activated SMAD3 binds to SMAD4 and translocates to the nucleus, where it binds to SMAD-binding elements in the promoters of fibrogenic genes, such as ACTA2 (encoding α-SMA). Together, myofibroblast activation is controlled by both the TGFβ–SMAD pathway as well as biomechanical pathways such as integrin–FAK–ROCK–MRTF–YAP–TAZ signaling [161]. Moreover, ECM stiffness induces expression of the microRNAs miR-21 and miR-29a, which promote the survival of myofibroblasts by increasing the expression of pro-survival BCL-2

proteins [162]. Increased ECM stiffness, TGFβ1 and CTGF all cue fibroblasts to differentiate into collagen-producing, α-SMA^{+} myofibroblasts. These "activated" myofibroblasts also produce the anti-inflammatory cytokines, TGFβ1 and IL-10, which act on macrophages at the injury site, stimulating them to produce ECM degrading compounds. This shift in activity is a part of the resolution phase of normal wound healing (See Figure 2.4). Macrophages promote ECM softening in tandem with soluble pro-apoptotic factors, including IL-1B, FGF1, and PGE2, which, in turn, promote myofibroblast apoptosis. However, this is not the only potential fate of myofibroblasts. Myofibroblasts can revert to scar-resolving fibroblasts or temporarily be driven to senescence via CCN family member 1 (CCN1). Myofibroblast apoptosis, reversion to scar-resolving fibroblasts, and conversion to senescent myofibroblasts are all normal fates in the course of normal wound healing. However, myofibroblasts and senescent myofibroblasts can indefinitely escape apoptosis. This pathological turn of events leads to fibrosis and persistent tissue inflammation. Cells in the area are destroyed and replaced with scar tissue. Eventually this leads to tissue and organ failure. Several factors are postulated to account for apoptosis escape associated with the onset of pathological fibrosis. Pro-survival signaling through mechanotransduction pathways and integrin-mediated TGFβ activation have been shown to inhibit IL-1β, FGF1, and prostaglandin E2 (PGE_2) by shifting the senescence-apoptosis axis toward senescence. Additionally, factors that reinforce matrix stiffening also shift the orientation of myofibroblasts and senescent myofibroblasts toward persistence, survival, and senescence. Stiffening is reinforced by matrix-stabilizing, pro-fibrotic matrix metalloproteinases (MMPs) and crosslink-promoting lysyl oxidases (LOXs). Although MMPs are generally associated with matrix degradation, the reality is more nuanced. Weakening of the ECM by certain MMPs triggers fibroblasts to synthesize and deposit ECM. In addition, these same fibroblasts secrete

ECM-crosslinking enzymes such as LOXs [163]. Furthermore, tissue-stabilizing, fibroblast orientation of ECM fibers occurs during normal tissue repair [164], but the disruption of these orienting processes further defines pathological fibrosis. Lastly, advanced glycation products, which form crosslinks between collagen fibrils and also activate the receptor for advanced

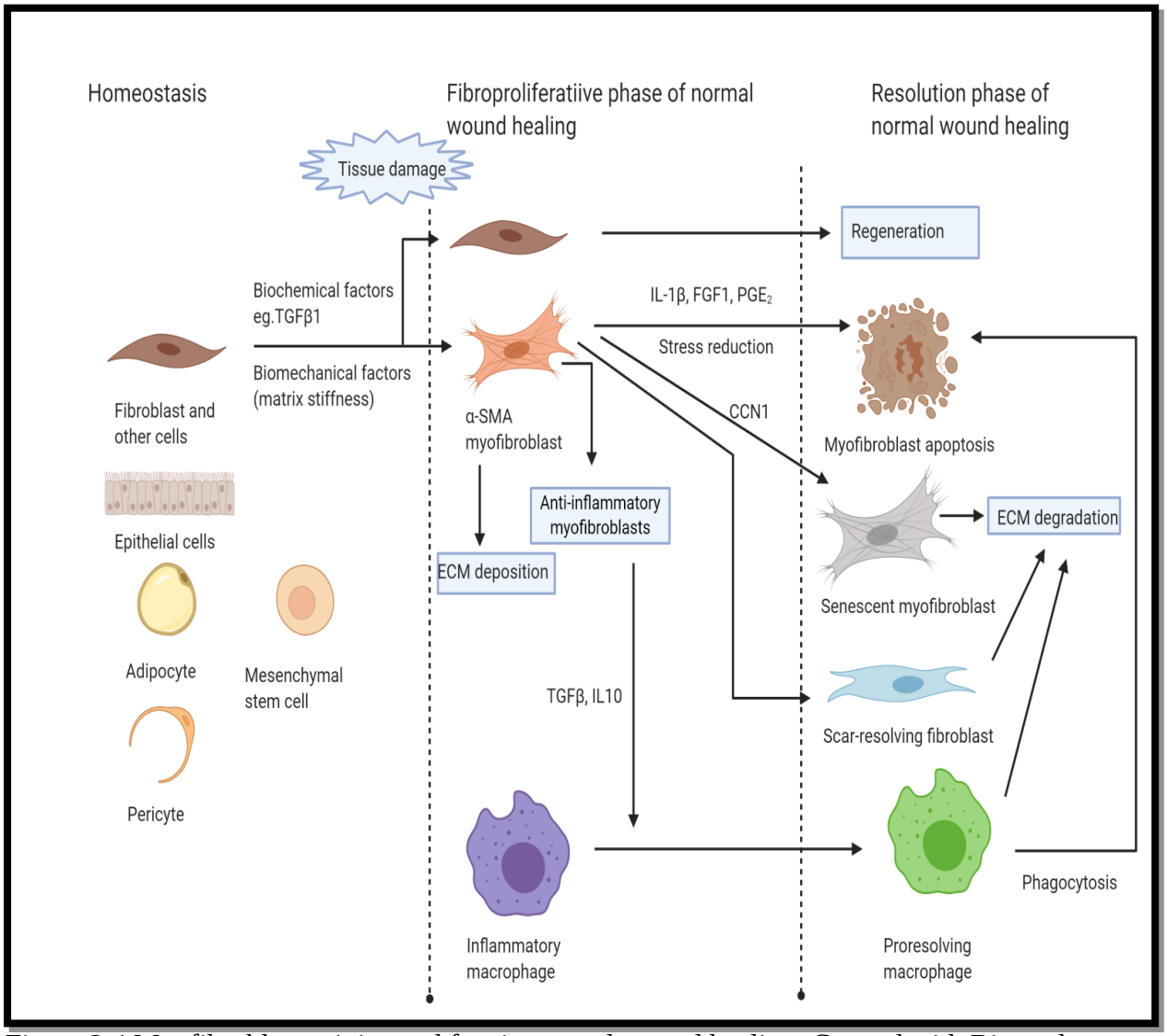

Figure 2.4 Myofibroblast origins and fate in normal wound healing. Created with Biorender.com [171].

glycation end products, may play a profound role in the emergence of fibrosis by irreversibly increasing matrix stiffness over time [165]. Myofibroblasts may originate from multiple cell

types; however, how they transition from one cell type to another is poorly understood and has not been characterized in the salivary gland. Myofibroblasts can be derived from pericytes, adipocytes, endothelial, epithelial cells, and mesenchymal stem cells (MSCs) [157]. Sun et al., transplanted bone marrow-derived MSCs into injured lung tissue hoping they would differentiate to lung epithelial cells [166]. Instead, these cells differentiated to myofibroblasts, which further exacerbated fibrosis. It was determined that this transition was mitigated by Wnt/β-catenin signaling, which could be attenuated using Dickkopf WNT Signaling Pathway Inhibitor 1 (DKK1) [167]. Sun's experimental outcomes speak to the complexities and potential problems investigators may encounter in their efforts to develop therapeutic approaches using MSCs. However, implantation of MSCs also showed potential to prevent fibrosis. Kim et al., determined adipose-derived MSCs could provoke salivary gland remodeling of fibrotic tissue and other beneficial effects in a mouse model of irradiated salivary gland tissue [168]. Saylam et al., showed adipose-derived MSCs could reduce differentiation of MSCs to myofibroblast after implantation, which may lie in a better understanding of factors that govern myofibroblast conversion in specific contexts. Engineered salivary gland tissues that incorporate strategies for shifting the senescence/apoptosis axis toward apoptosis can improve the likelihood of successful transplant engraftment and imaginably reverse or halt host tissue fibrosis. Conceptually, this approach to engineering salivary gland tissue is similar in nature to stent technology that not only provides scaffolding architecture to support arterial remodeling, but also integrates strategies for the timed release of chemistries that function to ensure proper engraftment and reduce the risk of complications [169]. Manipulatable factors that disrupt normal shifts of the senescence/apoptosis axis and pathological shifts in salivary gland tissue do exist. Apoptosis, a form of programmed cell death, is regulated by two intertwined pathways: the intrinsic (mitochondrial) and the

extrinsic (death receptor) pathways. The BCL-2 protein family plays a pivotal role, particularly in the intrinsic pathway, and can be classified into four categories: sensitizers, pro-survival (anti-apoptotic) proteins, activators, and effectors (pro-apoptotic proteins). Sensitizers inhibit pro-survival proteins that would otherwise inhibit the activators. The activators trigger effectors to initiate mitochondrial outer membrane permeabilization (MOMP) [170] and drive the myofibroblast phenotype toward apoptosis [171]. However, myofibroblasts will not undergo apoptosis in this state if pro-survival proteins are present and sequester pro-apoptotic proteins. BCL-2 homology domain 3 (BH3)-mimetic drugs have been used to circumvent this issue and trigger apoptosis by binding to pro-survival proteins, resulting in apoptosis [172,173].

Senolytics and SASP Depressants Support-Healing, Reduce Fibrosis, and Improve Transplant Engraftment

Senolytics and SASP depressants have been shown to support healing, reduce fibrosis, and improve transplant engraftment following salivary gland irradiation. Head and neck cancer patients acquire salivary gland damage caused by irradiation. Irradiation boosts mitochondrial ROS production, leading to a reduction in store-operated calcium entry (SOCE), which, in turn, decreases intracellular calcium necessary for the activation of calcium-dependent ion channels driving fluid secretion [174]. When cells are treated with H_2O_2, an increase in intracellular Ca^{2+} occurs, which leads to calpain-dependent processing of IL-1α [175], which ultimately leads to the production of inflammatory mediators IL-6 and IL-8 [176], suggesting that reducing oxidative stress would restrict inflammatory gene expression. Chelating Ca^{2+} during senescence inhibits calpain activation and subsequently, IL-1α processing, which attenuates the SASP phenotype. Another study by Ambudkar further validated this concept; H_2O_2 treatment resulted in a rapid calcium release from intracellular stores, mediated by the activation of PLC/IP3/IP3R pathway. Notably, further senescence development was accompanied by persistently elevated

$[Ca^{2+}]_i$ levels. In H_2O_2-treated human MSCs, $[Ca^{2+}]_i$ chelation by BAPTA-AM was sufficient to prevent the expansion of the senescence phenotype, decrease endogenous ROS levels, avoid G0/G1 cell-cycle arrest, and finally, retain proliferation [174]. Hai et al. generated a mouse model of irradiation-induced hyposalivation in which Sonic hedgehog (Shh) gene transfer repressed irradiation-induced cell-senescence. This effect was attributed to Shh upregulation of DNA repair pathways and decreased oxidative stress [177]. Lastly, numerous studies have demonstrated that pharmacologic (e.g., dasatinib, quercitin) or genetic elimination of senescent cells attenuates fibrosis and function in a variety of organ systems [178–185]. McCarthy et al., found senescence-associated oxidants and calcium drive the secretory phenotype, but antioxidant administration could limit SASP expression by restricting the expression of IL-1α [175]. Alternately, SASP repression strategies may offer a unique benefit, maintaining tumor suppression while eliminating other deleterious SASP-related effects [186–189] .

2.3.Cell Selection for Salivary Gland Bioengineering

2.3.1. Salivary Gland Cell Lines

Numerous cell lines have been developed for salivary gland basic research studies that inform engineering strategies [189]. These cell lines include human tumor-derived salivary gland cells and rodent immortalized or transformed salivary gland cells (Table 2.1). Representative human tumor-derived salivary gland cell lines include HSY, a neoplastic epithelial cell line derived from a thymic mouse tumor after transplantation with surgical specimens of a human parotid gland adenocarcinoma [190], and human salivary gland (HSG), a neoplastic intercalated ductal cell line derived from an irradiated human SMG [191]. Although these human cell lines are useful for biological studies, they are not useful for tissue engineering applications due to their tumor origins. Additionally, caution should be used with the HSG cell line as cross-contamination between this cell line and HeLa cells has been reported [192]. Rodent immortalized or

transformed salivary gland cell lines include mouse SIMS [193], rat submandibular cell lines (SMIE [194] and RSMT-A5 [195]), rat submandibular acinar cell lines (SMG-C6 and SMG-C10 [196]), murine mSG-PAC1 and mSG-DUC1 [197], and rat parotid cell lines (Par-C5 and Par-C10 [198]). Rodent cell lines have been useful for testing cell-cell and cell-material interactions and cell behaviors when seeded on engineered scaffolds for salivary gland regeneration.

A pertinent observation is that most of the aforementioned cell lines are epithelial in nature. While epithelial cells offer certain utilities, they may not fully capture the complex functionalities of acinar cells in salivary glands. While there is a potential for some of these epithelial cells to dedifferentiate, replicating the natural functions of acinar cells remains a challenge. This inherent limitation underscores the reliance on primary tissues in the field.

The gap in authentic acinar cell cultures impacts salivary gland bioengineering. Acinar cells, being paramount to saliva secretion, are indispensable for reconstituting a functional salivary gland. This gap not only impedes replicating gland function but reinforces dependence on primary tissues. These challenges provide an argument for exploring induced pluripotent stem cell (iPSC) technology. iPSCs, with their potential to differentiate into diverse cell types, could provide a way for generating acinar-like cells for salivary gland bioengineering, potentially addressing the challenges tied to primary acinar cells or epithelial-derived cell lines.

Table 2.1 Summary of representative salivary gland cell lines

Species	Cell lines	Tissue sources	Cell types	Characteristics
Human	HSY	Parotid gland adenocarcinoma	Ductal epithelial cells	Form desmosomes & tight junctions (TJs) and exhibit polarization [199]; Express amylase [200]; Respond to muscarinic and β-adrenergic autonomic agonists [201].
	HSG	Irradiated SMG	Intercalated duct epithelial cells	Form desmosomes with sporadic TJ and no AQP expression on plastics [202]Differentiate into acinar structures and express amylase on Matrigel; Respond to muscarinic & purinergic agonists; Express ductal differentiation markers (EGF, NGF & renin) [189]; Express TJs (claudin-1, -2, -3, -4, occludin, JAM-A & ZO-1) and AQP (AQP5) on Matrigel-coated permeable supports [203]. Reported to be derived from Hela cells [130]
Mouse	SIMS	A 22-day-old transgenic SMG	Immortalized ductal epithelial cells	Exhibit polarity and express E-cadherin & ZO-1 and duct-specific cytokeratins on Matrigel-coated surfaces; Form duct-like structures (cysts) on collagen Type I gels (Col I); Form a tight monolayer on filter supports, exhibiting microvilli, desmosomes & TJs, vectoral transport and exclusive basolateral localization Na^+/K^+-ATPase; Express EGF, NGF & renin [193].
	SIMP	A 12-day-old PyLT transgenic SMG	Immortalized striated ductal epithelial cells.	Exhibit polarity and express E-cadherin & ZO-1 and duct-specific cytokeratins on Matrigel-coated surfaces; Form duct-like structures on Col I; Express duct-specific cytokeratins and differentiation markers (EGF, NGF & renin) [204].
	mSG-DUC1	SMG	Genetically modified mice, homozygous for floxed alleles of the integrin α3 subunit	mSG-DUC1 cells express the ductal markers, keratin-7 and keratin-19, and form lumenized spheroids [197].
	mSG-PAC1	SMG	Genetically modified mice, homozygous for floxed alleles of the integrin α3 subunit	Express the ductal markers, keratin-7 and keratin-19, and form lumenized spheroids. express the pro-acinar markers SOX10 and aquaporin-5 [197].

Rat	SMIE	SMG	Immortalized salivary glandular epithelium-like cells	Form TJs on collagen-coated filters [194]; Resemble salivary glandular epithelium with an immature lumen; Express ZO-1 & E-cadherin, but low level claudin-3 [205]; Have a low level transepithelial resistance (TER) that can be regulated by IGF-1 [206]
	RSMT-A5	SMG	Transformed ductal cells	Exhibit a ductal epithelial phenotype and a high density of α1-adrenergic receptors [207].
	SMG-C6	SMG	Immortalized submandibular acinar epithelial cells	Form TJs and desmosomes, enabling polarization [196] ; Exhibit secretory features (i.e., domes, granules, and canaliculi) and more cytodifferentiation than SMG-C10 [208]; Respond to muscarinic and purinergic agonists (but not to α1 agonists) by increasing $[Ca^{2+}]_i$ and respond to β-adrenergic agonists by increasing [cAMP]; Lack ductal marker cytokeratin 19 expression and exhibit high TER on collagen-coated polycarbonate filters [209].
	SMG-C10	SMG	Immortalized submandibular acinar epithelial cells	Form TJs and desmosomes, enabling polarization [196] ; Respond to β-adrenergic agonists [208] ; Exhibit high TER on collagen-coated polycarbonate filters [209] ; Modulate Na^+ transport and regulate salivary cell volume [210].
	Par-C5	Rat parotid glands	Immortalized acinar epithelial cells	Form layers of plump cells containing intercellular lumen-like invaginations on their medial surfaces; Form secretory granules, TJs, intermediate junctions, desmosomes, and microvilli. Respond to α1-adrenergic agonists by increasing [cAMP] [211]; Respond to cholinergic, muscarinic & α1-adrenergic agonists by increasing $[Ca^{2+}]_i$ [212]; Express functional amylase [213].
	Par-C10		Immortalized acinar epithelial cells	Form monolayers of cuboidal cells with thick ECM at their bases [211]; Form secretory granules, TJs, intermediate junctions, desmosomes, and microvilli; Respond to α1-adrenergic agonists by increasing [cAMP] [212]; Respond to cholinergic, muscarinic & α1-adrenergic agonists by increasing $[Ca^{2+}]$ [213]; Do not express amylase [214]; Exhibit high TER [215];

				Express sodium bicarbonate cotransporters and anion exchange proteins on basolateral surfaces, which regulate transepithelial transport. Par-C10 cells achieve transepithelial transport that is sensitive to both intracellular Ca(2+)- and cAMP-dependent stimulation[215]; Form 3D differentiated acinar-like spheres on growth-factor-reduced Matrigel, expressing TJs, ion transporters, M3 muscarinic receptors & AQP3, increasing AQP5 expression under osmotic stress and showing changes in potential difference in response to muscarinic agonist stimulation [216].

2.3.2. Primary salivary gland cells

Primary cells have been used to explore cell interactions with scaffolds as well as for implantation in vivo. But critical problems exist with the ability of primary cells to achieve acinar formation in vitro, including a tendency to dedifferentiate when grown on plastic [217]. Salivary epithelial cells also become apoptotic when dissociated into single cell suspensions [218], demanding approaches that will maintain sufficient cell viability. However, single human parotid epithelial cells can differentiate into acinar and ductal structures when grown in a 3D environment [219]. When grown on hyaluronic acid hydrogels, these cells can assemble into acinar lobules, form tight junctions (TJs), develop central lumina, and express α-amylase [220]. A few studies show primary salivary gland cells can be transplanted into living organisms. Human parotid cells grown on polyglycolic acid polymers were implanted subcutaneously into athymic mice [221]. When the polymer scaffolds were retrieved, they had differentiated into acinar structures. Another study transplanted labeled rat SMG into atrophic salivary glands [222]. After several weeks, the labeled SMG cells were detectable over a broad area of the atrophic gland and localized around the acinar and ductal regions, suggesting that salivary gland cells can be transplanted and maintain differentiation. However, in these studies, it was not determined whether the transplanted salivary gland cells were able to function in response to

neurotransmitters. In a landmark study, embryonic salivary gland organ “germs” were transplanted in vivo and shown to integrate with existing ductal cells to restore some function [223].

2.3.3. Progenitor cells of the developing salivary gland

Salivary Gland Stem and Progenitor Cells During Development

The identity of salivary gland stem cells and their capacity to participate in gland development and regenerative responses has been a subject of intense study, since understanding how salivary gland stem and progenitor cells are regulated in development can inform regenerative medicine strategies. Lineage tracing studies, in which cells that are induced to express a fluorescent protein in a specific cell population that can then be traced along with its progeny as development proceeds, have been instrumental in defining the contribution of specific cell populations in developing salivary glands. Cells that express the transcription factors SOX2 and SOX9 and the intermediate filament protein, keratin 5 (K5), prior to emergence of the salivary gland can give rise to all cells in both the SMG and SLG [224–226]. During development, cell lineages become more restrictive and K5 is only expressed in ductal progenitor cells and SOX2 and SOX10 in acinar cells and progenitors (proacinar cells). SOX9 plays a pivotal role in determining the cellular differentiation and lineage commitment in the gland development [227].

Stromal-Epithelial Interactions During Development

Salivary gland branching morphogenesis requires interaction of epithelial cells with mesenchyme cells, and mesenchyme cells support the organization and differentiation of salivary gland epithelial clls in organoid cultures [228,229]. Different stromal-derived factors are required to stimulate different aspects of salivary gland development [126]. Although salivary gland progenitors, when combined with Matrigel and EGF to substitute for mesenchyme, could

recapitulate branching morphogenesis seen during embryonic development [230], FGF signaling is required for in vivo-like branching and FGF2 signaling in the salivary gland stroma is needed for those cells to support pro-acinar cell differentiation [231,232].

2.3.4. Stem cells for salivary gland tissue engineering

Studies targeted at increasing regenerative abilities of salivary glands are in progress. In addition, stem cell-based tissue engineering and cell therapy may improve function in damaged salivary glands [233]. Multiple types of stem cells and/or progenitor cells can be considered for regenerative therapies: the unipotent progenitor cells, elusive multipotent adult stem cell including salivary gland stem cells (SGSCs), MSCs, and induced pluripotent stem cells (iPSCs). There has been an ongoing search for a salivary gland stem cell for many years, based on the assumption that the hematopoietic stem cell-based paradigm is applicable to identify stem cells in all organs. However, recent studies suggest that such multipotent stem cells may not exist in adult salivary glands [234]. MSCs show great potential for tissue regeneration, including salivary gland tissue due to their anti-inflammatory, anti-fibrotic, and regenerative properties, while iPSCs possess the unique capabilities of unlimited self-renewal and the ability to undergo differentiation but with a risk of tumorigenesis. With stem cells, controlling their lineage commitment poses a new set of challenges, which can be better met with tailored biomaterial design strategies that influence transplanted cell fate as well as the host-tissue microenvironment.

Salivary Gland Stem Cells (SGSCs)

Lineage tracing studies in adult glands have enabled the isolation of SGSCs from the ducts of salivary gland tissues. SGSCs are characterized by the expression of a collection of stem cell markers including c-Kit, K5, K14, CD49f, CD90, and CD44 (See Table 2) [235]. However, Sui et al. asserted that there is no single, universal, definitive group of SGSC markers. For example, cells located in the striated ducts of the salivary gland expressed stem cell markers identified in

other organs, including CD24, CD49f, CD133, and c-Kit [236]. SGSCs can perhaps be best recognized by their behavior, which has been explored in 3D cultures. When human SMG stem/progenitor cell-derived human salispheres were cultured in a collagen I/Matrigel matrix for 2-3 weeks, they formed salivary organoids expressing markers such as cytokeratin, α-amylase, and AQP5 [139]. Human SMG stem/progenitor cells cultured in Matrigel formed aggregates on day 1; when FGF10 was added daily until day 14, they exhibited high expression of gland-specific markers such as AQP5 and Mist1 (acinar markers), α-amylase (functional marker), and α-SMA (salivary myoepithelial marker) and responsiveness to neurotransmitters responsible for salivary secretion [235]. However, the presence of mouse tumor-derived Matrigel makes this system unsuitable for future therapeutic applications. As another option, peptide-modified hyaluronic acid hydrogels supported long-term maintenance of human parotid gland stem/progenitor cells cultured for more than 100 days, showing increased gene expression of acinar markers (e.g., MIST1/BHLHA15, α-amylase/AMY1A) after treatment with β-adrenergic and cholinergic agonists, such as isoproterenol and carbachol for 20 hours [237]. However, mature differentiation into secretory acinar cells was not observed. The potential for implantation of cultured salivary gland organoids was shown by implantation in mice. In vivo transplantation of mouse salivary organoids with E12.5 mouse salivary gland mesenchyme showed natural morphology and saliva secretion, suggesting the role of salivary gland mesenchyme in promoting maturation and function of salivary organoids [238]. Further, Raman spectroscopy has been successfully used to identify the differentiation state of organoids, which may also be generalizable to cells on scaffolds to screen tissue constructs prior to implantation [239]. The therapeutic potential of stem cells is widely recognized. Yet, little is known about the engraftment and capacity of tissues derived from human adult epithelial stem cells. Pringle et al.

recently isolated human salivary gland stem/progenitor cells in vitro and observed self-renewal and multilineage differentiation of these cells into organoids. They further demonstrated in vivo functionality, long-term engraftment, and functional restoration of saliva production in irradiated salivary glands in a xenotransplantation model [240]. Additionally, the regenerative potential of stem cells transplanted into irradiated SGs was enhanced and further improved by selection for c-Kit expression. This groundbreaking work marks the first instance of salivary gland rescue using salispheres and the first clear demonstration of salivary gland stem/progenitor cell self-renewal and multilineage differentiation into functional organoids**.**

Table 2.2 Salivary gland stem cell markers

Stem Cell Marker	Salivary Gland Location	Method of Identification	Progenitor or Stem	Reference Number
c-KIT (CD117)	Ducts	Gene expression	Stem	[241]
SCA-1	Ducts	Gene expression	Stem	[241]
Keratin 5 (K5)	Ducts (developing)	Cytoskeletal protein expression, in vivo lineage tracing	Progenitor	[242,243]
Keratin 14 (K14)	Ducts (developing)	Cytoskeletal protein expression, in vivo lineage tracing	Progenitor	[242,243]
LGR5	Ducts (human parotid and submandibular)	Gene expression	Stem	[244]
CD44	Not specified	MSC surface antigen	Stem	[12,244–246]
CD49f (integrin)	Not specified	MSC surface antigen	Stem	[12,244–246]
CD90	Not specified	MSC surface antigen	Stem	[12,244–246]
CD105	Not specified	MSC surface antigen	Stem	[12,244–246]

Mesenchymal stem cells (MSCs)

MSCs are multipotent adult stem cells that can differentiate into several cell types, including adipocytes [247], osteoblasts [248], chondrocytes [249], myocytes [250], cardiomyocytes [251],

hepatocytes [252], neuronal cells [253], and salivary gland cells [254] among others. MSCs exhibit anti-inflammatory, anti-fibrotic, and regenerative potential [255,256]. Adult MSCs impact immune T- and B-cell responses through multiple pathways, including T-cell suppression, cytokine regulation, Th1/Th2 balance, Treg regulation, B-cell viability and proliferation, antibody secretion, co-stimulatory molecule production, dendritic cell maturation inhibition, and suppression of IL-2-induced NK cell activation [257]. MSCs that have been tried for salivary gland tissue regeneration include bone marrow-derived MSCs [258], adipose tissue-derived MSCs [259–262] and salivary gland-derived MSC-like cells [263,264]. Denewar et al. demonstrated bone marrow-derived MSCs prevented the development of diabetic-induced hyposalivation in rats [265]. MSCs have several advantages over alternate stem cell types. They are easily obtained from adipose tissues [266] and unlike ESCs and iPSCs, they are not potentially tumorigenic in vivo. However, newer research suggests the origin of MSCs may be an important consideration [267]. Additionally, MSCs can be used for allograft transplantation [268,269]. Moreover, by reducing lymphocyte infiltration, fibrotic processes may be mitigated under certain circumstances, as described more fully in the fibrosis section of this review [270]. Stromal cells derived from the mesenchyme compartment are not only important for development, they also have been used to restore function in hypofunctioning salivary gland. MSCs derived from bone marrow stroma have been shown to improve gland function in a mouse model of Sjögren's Syndrome [271], and adipose-derived MSCs restored salivary gland function in mice following a radioiodine-induced injury that mimics salivary hypofunction in patients treated for thyroid cancer [272]. In rabbit models, the application of MSCs and anti-inflammatory agents has been explored with improved function with dual treatment therapy as an experimental allogenic transplant [273]. Clinical trials are currently underway to evaluate the

ability of MSCs to restore salivary function for glands damaged by irradiation [274]. Thus, manipulating the stromal environment holds promise for clinical applications in salivary hypofunction.

Pluripotent Stem Cells (PSCs): ESCs and iPSCs

ESCs and iPSCs are pluripotent, i.e., they can self-renew and differentiate into somatic cells of all three germ layers—ectoderm, mesoderm, and endoderm [275–281]. As such, they offer more potency than adult stem cells. Due to ethical concerns and variable immunogenicity associated with ESCs, autologous iPSCs offer a feasible alternative to ESCs [282]. iPSCs were first generated by introducing four transcription factor genes (Oct 3/4, SOX2, Klf4, and c-Myc) into mouse and human fibroblasts [283]. More advanced methods that produce iPSCs with higher efficiency have since been developed and commercialized [281,284]. The use of both ESCs and iPSCs for more than 14 diseases in clinical trials has shown the promise of PSC-based cell therapies although there are still challenges to overcome, such as heterogeneity and a low, but non-negligible risk of teratoma or carcinoma formation in vivo [285]. Teratomas are thought to result from the presence of residual undifferentiated cells and differentiated but still proliferative progenitors, while carcinomas are thought to result from the use of the tumorigenic reprogramming factors (e.g., c-Myc) and viral vectors for generating iPSCs and genetic abnormalities of PSCs. Removing undifferentiated cells and genetically abnormal PSCs prior to implantation and using virus-free gene delivery methods can reduce the likelihood of teratoma development [286,287]. In vitro 3D culture models, including organoids and organ-on-chips, can be utilized to predict tumorigenicity and identify factors to reduce heterogeneity [285,288,289]. Kawakami et al. co-cultured mouse early ESCs (mEES-6) with mitomycin-treated human salivary gland-derived fibroblasts, attempting to differentiate mEES-6 cells to salivary gland cells (co-SG), and finally, to engraft these co-SG cells into the SMG of immune deficient mice.

These co-cultured cells expressed a variety of salivary gland-related markers and could generate new tissues by transplantation in vivo [290]. Additionally, these cells could reconstruct gland architecture in a 3D culture system. Similar results [290] were achieved by co-culturing mouse GFP-iPSCs with E13.5-day SMG cells for 4 days [291]. In a monoculture study, mouse ESCs were differentiated to early salivary gland organoids via stepwise viral induction, focusing on SOX9 and Foxc1, followed by microdissections of protruding buds [292]. The differentiation process was very tedious and inefficient, with loss of salivary organoids/cell aggregates during the frequent medium changes, highlighting the unmet need to differentiate not only mouse but also human iPSCs into mature salivary gland cells efficiently.

2.3.Biomaterials for salivary gland cells survival, differentiation, and engraftment

2.3.1. Cell support system overview

The design of an ideal cell support system for salivary gland tissue engineering necessitates a thorough understanding of the native ECM properties and composition. Native decellularized salivary gland tissue has unique properties, whose topography is characterized by honeycomb-like structures with pores in the range of 10-25 μm. Additionally, this tissue presents a notably low indentation modulus, approximately 120 Pa, indicative of its soft, gel-like nature. Such intrinsic properties play a pivotal role in facilitating cellular adhesion, proliferation, and differentiation, ultimately guiding the engineered tissue's functional outcomes[293,294]. Building on this foundational knowledge, early experiments examined the compatibility of salivary gland cell lines with different polymers and ECM proteins for salivary gland tissue engineering. Aframian et al. performed a 2D experiment wherein HSG cells were cultured on a poly(l-lactic acid) (PLLA), polyglycolide (PGA), or different poly (lactic-co-glycolic acid) (PLGA) co-polymer substrates. The purpose of this study was to examine the growth and

morphology of a salivary gland epithelial cell line (HSG) in vitro on several biodegradable substrates as part of an effort to develop an artificial salivary gland. Culture on copolymers alone was unsuccessful, but HSG cells grew particularly well on PLLA coated with ECM proteins, including fibronectin, collagen I, collagen IV, laminin, and gelatin, all of which promoted monolayer growth [295]. Since that time, many different fabrication techniques, such as bioprinting, electrospinning, thermal molding, freeze-drying, and in particular, hydrogel synthesis, have been used to produce scaffolds for salivary gland tissue engineering (Table 2.3 and Figure 2.5).

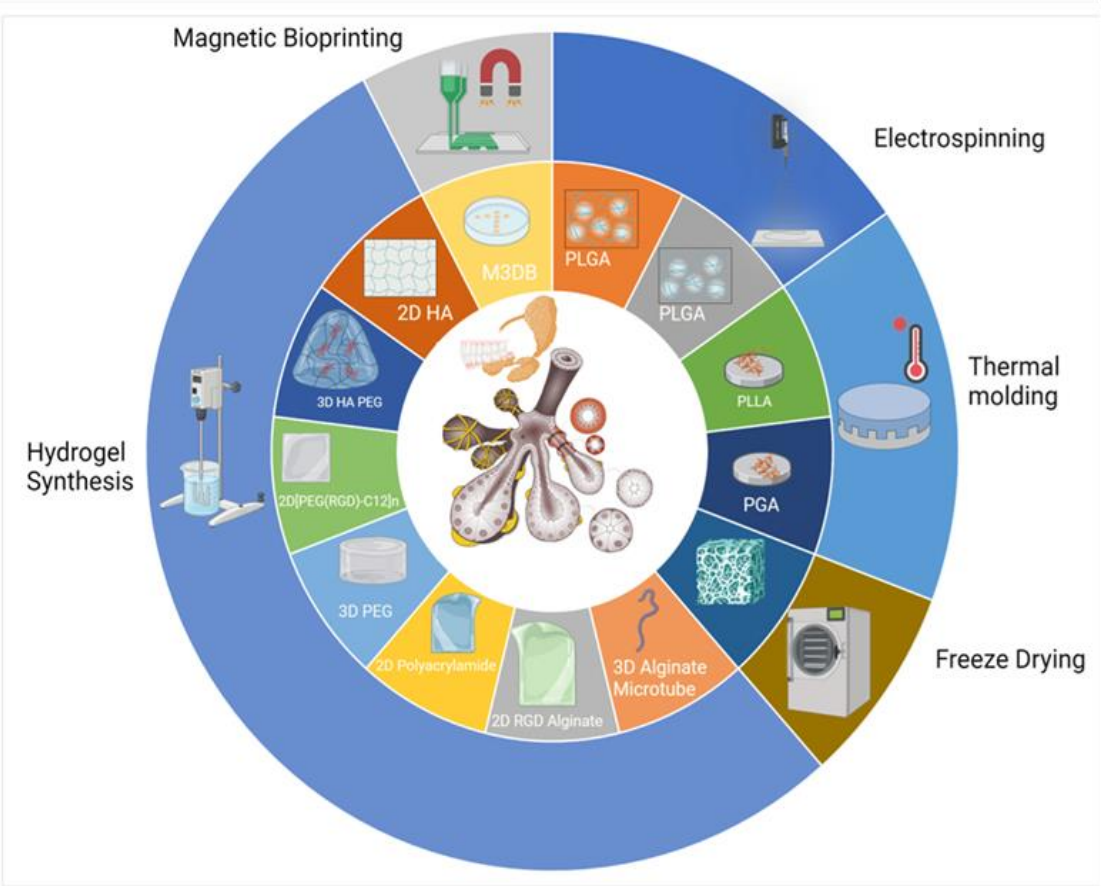

Figure 2.5. Major approaches to biofabrication of salivary gland tissues (Created using Biorender, Biorender.com)

Table 2.3 Major methods to biofabrication of scaffolds for salivary gland tissue engineering

Fabrication method	Biomaterial and dimensionality	Cell type	Advantages and disadvantages
Thermal molding	2D PLLA & PGA (flat disks)	HSG	Pros: Biodegradable; able to form into coverslip-like disks suitable for cell seeding; and versatile permitting melt-processing polymer pellets between sheets of aluminum foil using a Carver press at 350°F, 450°F, 175°F, and 200°F for PLLA, PGA, 50/50 PLGA, and 85/15 PLGA, respectively [295,296]. Cons: Require ECM coating to support cell attachment; lack 3D cues.
Electrospinning	PLGA (fibrous scaffolds) PLGA (fibrous scaffolds)	SIMS Par-C10	Pros: Provide topographic cues (e.g., nanofibers, curvature); exhibit more rounded and clustered cell shape vs. 2D flat disks; and enhance cell-polarization effects and expression of water channel proteins [297,298]. Cons: Require laminin coating for cell polarization and tight junctions; lack in vivo-like viscoelasticity.
Freeze-drying	Silk fibroin (porous scaffolds)	Primary salivary gland epithelial cells from rat SMG and parotid gland	Pros: Provide topographical cues; promote epithelial cell growth; facilitate the secretion of ECM proteins; and retain the differentiated function [299]. Cons: Require fibronectin coating; mimic the basement membrane for epithelial cells but might not be ideal for stromal cell culture; lack in vivo-like viscoelasticity.
Hydrogel synthesis	HA hydrogels (cell culture insert)	Primary human salivary gland acinar-like cells from the parotid gland	Pros: Mimic the hydrogel component of ECM; and exhibit acini-like structures with tight junctions, α-amylase expression and an apoptotic central lumen on HA gels with an elastic modulus of 2000 Pa and incorporating

		peptide derived from domain IV of perlecan [300]. Cons: Require coupling bioactive peptides; or form acinar-like structures that are less organized or slowly growing in 2D or 2.5D than those in 3D HA hydrogels [301].
3D HA/PEG hydrogels (cell culture insert)	Primary human salivary gland acinar-like cells from the parotid gland	Pros: Provide 3D microenvironment for encapsulated cells; facilitate cell self-assembly into acini-like spheroids of ~50 μm in size; demonstrate neurotransmitter-stimulated protein secretion and fluid production; and integration in an *in vivo* rat model with no obvious sign of inflammation [300,302,303]. Cons: Indicate reverse polarity; lack essential machinery for full salivary restoration [301].
$[PEG(RGD)\text{-}C12]_n$ microfibers	Human primary salivary gland myoepithelial cells	Pros:Fabricate meter-long multiblock copolymer microfibers via straightforward interfacial bioorthogonal polymerization; Provide guidance cues for the attachment and elongation of myoepithelial cells [304]. Cons: Cannot use for cell encapsulation; culture cells on the surface two dimensionally rather inside the microfiber three dimensionally.
3D PEG hydrogels	A mixture of primary acinar and ductal cells from mouse SMG	Pros: Improve cell viability and proliferation and facilitate cell-cell contacts by encapsulation of pre-assembled spheroids [305]. Cons: Remain as single cells without forming organized acini-like structures after cell encapsulation in 3D PEG hydrogels.
2D polyacrylamide	Mouse E13	Pros: Promote branching

gels	SMG	morphogenesis; partially rescue acini structure and differentiation by transferring glands from stiff to soft gels or by adding exogenous TGFβ1 [246,247][306] Cons: Require addition of exogenous TGFβ1 to polyacrylamide gels for partial acini structure rescue; lack 3D cues.
2D RGD-modified alginate hydrogel sheet	Mouse E13 mesenchymal cells and SMG	Pros: Promote mesenchymal (not epithelial) cell adhesion by RGD surface modification; enhance the bud expansion and cleft formation in SMG by softer gels, whereas stiffer gels attenuate them and decrease gene expression of FGF7 and FGF10; partially rescue acini structure and differentiation by adding exogenous FGF7 or FGF10, or by transferring SMGs from stiff to soft gels [307]. Cons: Stiffer RGD-modified alginate hydrogel sheets attenuate bud expansion and decrease gene expression of FGF7 and FGF10.
3D Alginate hydrogel microtubes	Co-culture of SIMS with mouse NIH 3T3 fibroblasts or E16 mesenchyme cells	Pros: Provide 3D microenvironment in hydrogel that is easy to handle; allow for high density cell growth; facilitate 3D mesenchymal-epithelial interaction; allow salivary gland epithelial cell organization into 3D cavitated structures with lumen formation; exhibit potential for formation of uniform organoids and functional units [308]. Cons: Require 3D arrangement of microtubes with organoids and additional elements to construct the full machinery of the salivary gland.
2D Fibrin-based hydrogels	Par-C10	Pros: Support differentiation of salivary gland cell clusters with mature lumens[309] Cons: 2D culture on the hydrogel

			surface; require laminin-111 peptide-modification.
	Fibrin-based hydrogels	Acellular, laminin I peptide functionalized	Pros: Mitigate the risk of tumor development; results in restoration of functional salivary tissue [247]. Cons: Require decoration with laminin-1 peptides; require injection of liquid followed by internal gelation to avoid hydrogel clogging the needle.
	Gelatin-based hydrogel sheet	Acellular, controlled release of growth factors (EGF, FGF, NGF)	Pros: Demonstrate atrophy and regeneration of the SMG; and enable observation of effects of sustained release of physiologically active substances contained within an implanted hydrogel sheet. Cons: Collapse of the hydrogel mesh began by day 7, in conjunction with invasion of surrounding fibrotic connective tissue, without regeneration of the salivary gland tissue [310].
Cryoelectrospinning	3D Alginate-elastin cryoelectrospinning scaffolds	NIH 3T3 fibroblasts	Pros: Produce porous nanofiber-sponge scaffolds that recapitulate the topography and viscoelasticity of salivary gland ECM; allow cell penetration deeply and 3D culture; support stromal cell viability and homeostatic marker expression[293] ons: Require dynamic seeding to achieve high seeding efficiency; require dynamic culture to achieve high density cell growth.
Bioprinting	Magnetic 3D bioprinting (M3DB)	Neural crest derived MSCs and human dental pulp stem cells	Pros: Develop innervated secretory epithelial organoids in the presence of FGF using cells tagged with magnetic nanoparticles that are ordered using magnetic dots. Cons: Require magnetic nanoparticles; challenge to determine an apicobasal polarization due to tightly packed

	epithelial cells; and exhibit limited vascularization in the organoids [311].

3D scaffolds that mimic salivary gland tissues can be produced using a variety of top-down or bottom-up approaches. Scaffold fabrication approaches to salivary gland tissue engineering include electrospinning, phase-separation, freeze-drying, hydrogel synthesis, self-assembly, and bioprinting. Top-down approaches typically entail scaffold development, which may integrate essential constituents of native ECM. Cells seeded on such scaffolds are expected to attach, migrate, grow, and proliferate in a systematic way in accord with cues provided by the engineered bioscaffold. On the other hand, bottom-up methods involve the fabrication of tissue building blocks, which can be developed in several ways, cell-encapsulated hydrogels, self-assembled cell aggregates, 2D cell sheets, and bioprinted cells. The specific cell types best suited for transplantation on or within scaffolds are unclear. But immature stem or progenitor cells survive longer than other cell types during the dissociation and transplantation stages than all other tested cell types [312,313]. Based on clinically translatable successes with hematopoietic stem cell transplants [314,315], cell transplantation to reverse incurable disease and regenerate tissue holds promise. However, transplanted cells must survive longer, aggregate less, and integrate into host tissue better than cells have in any study to date [316–318], underscoring the unmet need for scaffolds for efficient salivary gland tissue regeneration.

2.3.2. Scaffold fabrication approaches to salivary gland tissue engineering

Electrospinning is used to fabricate microfibers and nanofibers less than 1000 nm in diameter for tissue engineering. It uses a syringe pump, high-voltage source, and collector plate, which

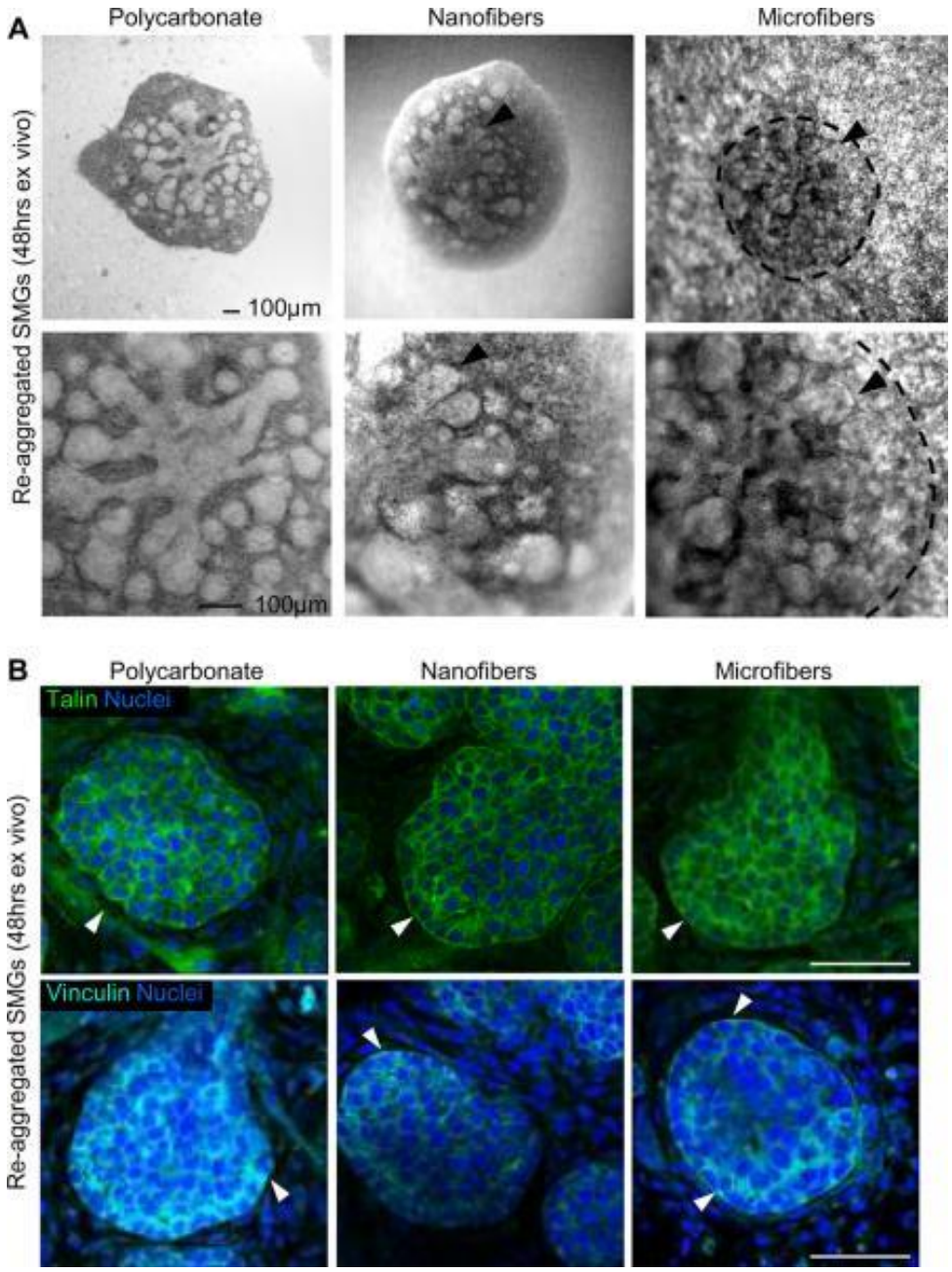

Figure 2.6 Nanofiber scaffolds promote self-organization and branching morphogenesis of dissociated embryonic salivary gland cells. (A) Bright field images of spontaneously re-aggregated cell pellets from dissociated embryonic day 13 (E13) SG cells cultured on polycarbonate filter membrane, PLGA nanofibers and microfibers for 48 h. (B) Confocal images through the equatorial section of re-aggregated buds immunostaining for talin (green, top panels) or vinculin (cyan, bottom panels), co-stained for nuclei (DAPI, blue), showed diffuse cortical expression with stronger staining along the basal cell membranes at the bud periphery (arrowheads), similar to that observed in intact glands, scale bars = 50 μm. Reprinted with permission from Sequeira et al., 2012. © 2012 Elsevier [298].

comprise the basic setup. Generally, a capillary spinning tip is filled with polymer solution with a certain conductivity and viscosity. The solution will stay at the opening of the tip due to surface tension. An electric field is used to oppose the surface tension. Once the force of the electric field exceeds the surface tension forces, a Taylor cone is formed at the opening of the spinning tip, causing a jet of particles to emanate from the tip. Due to molecular cohesion, a continuous stream of liquid results, leading to an unstable and whipping motion of the jet, which is generally

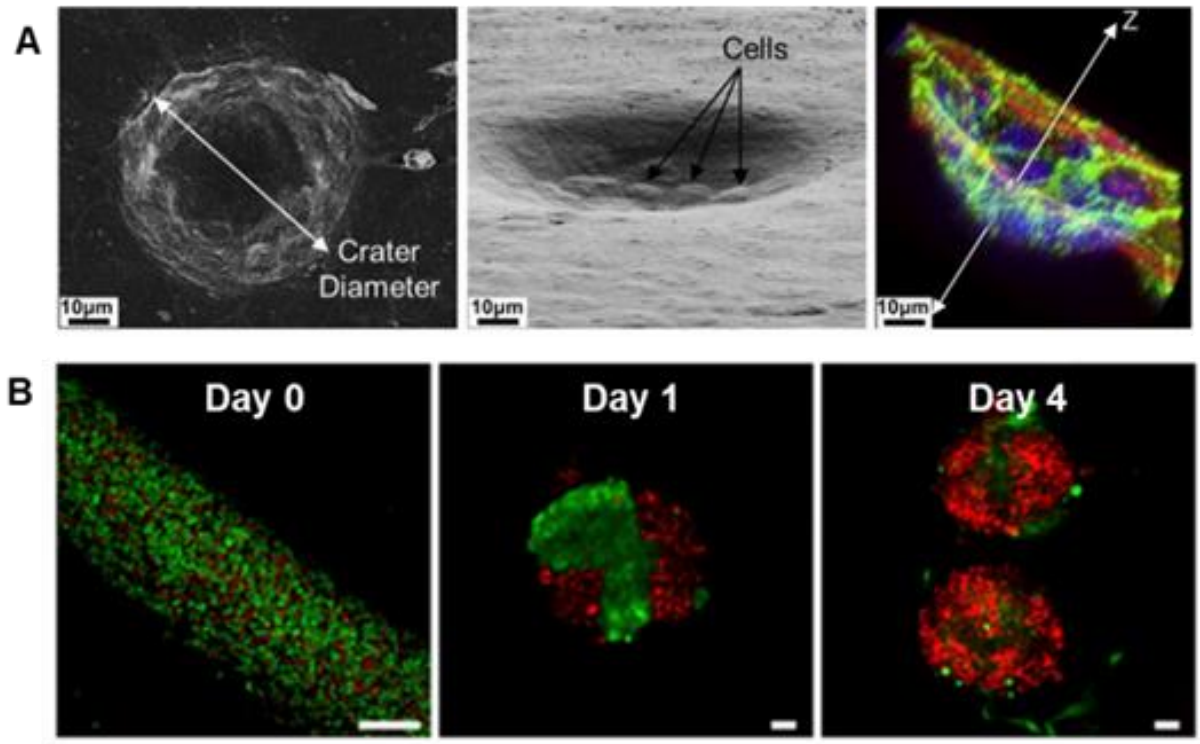

Figure 2.7 Biomaterials Can Control The Shape of Organized Tissue Constructs. (A) Confocal image (right) of SIMS cells stained for F-actin (green, phalloidin) and nuclei (blue, DAPI) grown in 30-μm nanofibrous craters (SEM of top view, left and angled view, middle) for 96 h, scale bar = 10 μm. The arrow denotes the Z-plane. Reprinted with permission from Soscia et al., 2013. © 2022 Elsevier [234]. (B) Confocal images of CellTracker™ Red CMTPX-labeled SIMS cells and CellTracker™ Green CMFDA-labeled NIH 3T3 fibroblasts showed cellular organization after co-cultured in microtubes for 4 days, scale bar = 250 μm. Reprinted and modified with permission from Jorgensen et al., 2022. © 2022 by the authors [308].

termed bending instability. The bending instability and solvent evaporation result in the elongation and thinning of fibers as the jet travels to the collector plate. Fiber dimensions can be controlled by regulating solution constituents, humidity, temperature, viscosity, surface tension, and other factors. Numerous synthetic and natural polymers have been used to produce electrospun micro- and nanofibers, e.g., PLLA, PLGA, Poly (glycerol-sebacate) (PGS)/PLGA, polycaprolactone (PCL), alginate, collagen, chitosan, chitin, and silk fibroin [319–324]. PLGA

nanofiber scaffolds were used to investigate physical characteristics of the scaffolds and their influence on cell behavior for application in salivary gland tissue engineering. Sequeira et al. compared PLGA nanofibers from 250-1200 nm in diameter [325] and observed a decreased number of focal adhesion complexes in epithelial cells cultured on the nanofibers relative to microfibers or flat

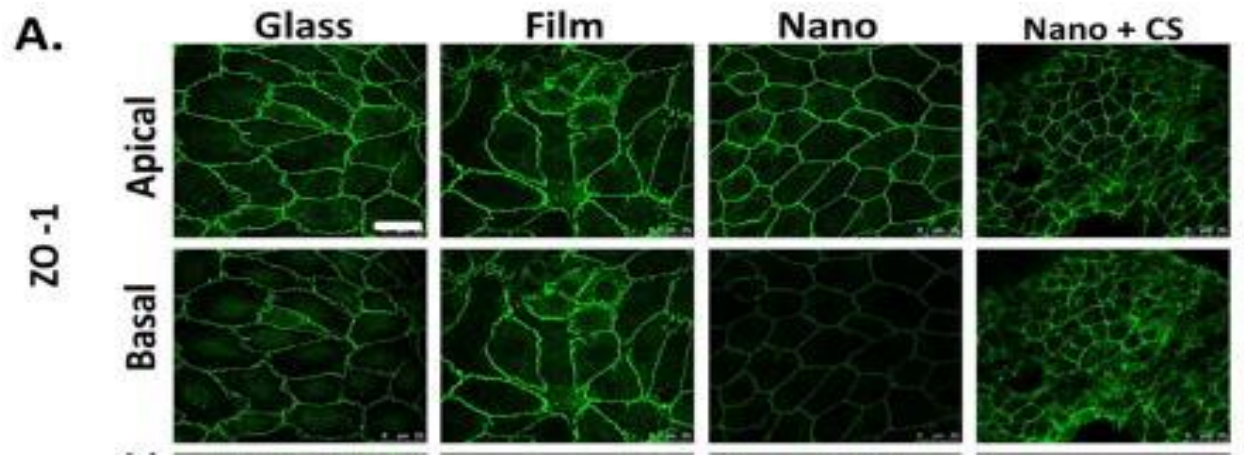

Figure 2.8 Cell behavior in organoids can be achieved through cell surface modifications of nanofibrous scaffolds. Confocal images of immunostained SIMS cells seeded on PLGA nanofibers (Nano) showed apical restriction of ZO-1 (green), which was disrupted by chitosan-modified nanofibers (Nano + CS) compared to 2D culture on glass or PLGA film. Scale bar = 25 µm. Reprinted with permission from Cantara et al., 2012. © 2012 Elsevier [328].

surfaces. As the material stiffness was the same for micro- and nanofibers, the topography was assumed to be a significant factor in determining the structure of cell attachments. Additionally, they observed spontaneous self-organization and branching of dissociated embryonic salivary gland cells grown on these nanofibers (Figure 2.6) [325]. The intent was to increase surface area and better recapitulate the 3D architecture of the basement membrane surrounding spherical acini of salivary gland epithelial cells. They subsequently cultured SIMS ductal and Par-C10 acinar cells in these nanofiber-lined craters, concluding that increasing curvature yielded more polarized cells expressing the tight junction protein, occludin, localized at the apical surface of

the cells and increased expression of the water channel protein AQP5 in Par-C10 cells (Figure 2.7) [326]. Cantara et al. examined effects of PLGA nanofiber scaffolds on cell proliferation and apicobasal polarity. Using murine SIMS ductal and rat SMGC10 parotid acinar salivary gland epithelial cell lines, they observed that cell proliferation was greater on chitosan-coated nanofiber scaffolds than uncoated scaffolds, but that chitosan interfered with apicobasal cell polarity, as indicated by decreased apical localization of the tight junction protein, ZO-1 [298]. Neither salivary gland acinar nor ductal cells are fully polarized on these nanofiber scaffolds, as indicated by the homogenous membrane distribution of occluding. Functionalizing nanofibers with laminin-111 promoted more mature TJs and demonstrated more apicobasal polarization. To recapitulate the varied functional capabilities of the basement membrane, bifunctional PLGA nanofibers were generated by coating the nanofibers with both chitosan and laminin-111. The signals provided by bifunctional scaffolds prompted a response from both acinar and ductal cell lines, demonstrating the applicability of such scaffolds for epithelial cell types (Figure 2.8) [327].

Phase separation to produce composite scaffolds

As scaffolds comprised of one material are rarely sufficient to support and direct cell behavior, the combination of multiple materials is typically needed. Although they have not been widely applied in the development of salivary gland bioscaffolds, phase separation methods can be used to create scaffolds from multiple materials. With these methods, the polymer of choice is dissolved, and then thermal or non-solvent-addition phase separation is induced. In either case, thermodynamic instability results in a two-phase separation. The solvent is generally extracted using water. Next, the temperature is lowered, which causes the polymer-rich phase to solidify into a 3D porous scaffold [328].

Freeze-drying to fabricate porous scaffolds

Freeze-drying, also known as lyophilization, is a method of producing porous scaffolds that does not degrade bioactive molecules [329]. Polymeric and/or proteinaceous materials in solution are frozen, followed by sublimation of the solvent under vacuum, creating materials with a sponge-like structure full of pores. The pore characteristics, including their size, volume fraction, and shape, hinge on several factors. These include the temperature at which the freezing occurs, the concentration of the initial solution, the types of solvent and solute involved, and the way the freezing is managed directionally. Researchers have experimented with a variety of solutions—ranging from water-based to organic, including mixtures with fine particles and solutions where CO_2 is used in a supercritical fluid state—to produce diverse porous and particulate formations. Innovative techniques, such as spray freezing and controlled, directional freezing are pushing the boundaries even further, paving the way for not just porous particles but also materials with pores arranged in a specific alignment, expanding the potential applications of this fascinating process [330].

Hydrogel synthesis to form injectable cell delivery vehicles

Hydrogels are networks of cross-linked hydrophilic polymers that form gels upon hydration. Crosslinked polymers may be chemically synthesized or made from naturally occurring polysaccharides (e.g., alginate, chitosan, hyaluronic acid) and proteins (e.g., collagen, gelatin, fibrin). There are many synthetic crosslinking materials including polyvinyl alcohols, polyethylene glycol (PEG), and polyacrylate as well. These materials can be modified in ways that enable transplantation by injection, a cleaner, less invasive means than surgical implantation. To use this method, two critical factors must be considered: first, the mechanical properties of the hydrogel should be optimized for injection, and second, ECM components may be included

to prevent apoptosis. Salivary gland engineers have used $CaCl_2$-crosslinked alginate [307], polyacrylamide [331], and PEG hydrogels [305] among others in their research efforts. Miyajima et al. used arginine-glycine-aspartic acid (RGD)-modified alginate hydrogel sheets of different stiffness to demonstrate enhanced bud expansion and cleft formation of submandibular salivary glands. Softer alginate gels facilitated bud expansion and cleft formation, whereas increasing stiffness attenuated these results [307]. RGD-modified alginate hydrogel beads (20, 50, or 100 μm in diameter) also enhanced the ratio of cleft formation and tissue morphogenesis of SMGs [332]. Chitosan-coated alginate hydrogel sheets demonstrated enhanced cell growth, bud expansion, and neural innervation of isolated SMGs [333]. Chitosan also facilitated essential ECM deposition and enhance SMG branch formation [334,335]. Supplemental chitosan added to medium enhanced the morphogenic effects of mesenchyme and mesenchyme-derived growth factors (e.g., FGF7, FGF10 and HGF) on salivary gland epithelial morphogenesis [336] through spatial and temporal regulation of basement membrane [337]. Additionally, egg white-alginate hydrogel discs were synthesized and supported survival and spheroid formation of salivary gland cell lines [338]. Srinivasan et. al., study showed that parotid cells seeded in hyaluronic acid-based environments self-assembled into acini-like structures expressing functional neurotransmitter receptors. These structures, particularly in 3D hydrogel setups, grew into organized spheroids, exhibiting a range of markers such as CD168/RHAMM, CD44, Keratin-5 (K5), Keratin-14 (K14), integrin-β1, and α-amylase. Methodologies like staining, immunocytochemistry, and suspension culture techniques were crucial in identifying and verifying the markers and spheroid characteristics. Hyaluronic acid hydrogels may potentially be used as implantable cell delivery vehicles for salivary gland tissue restoration as well. Prodhan et al. used photo-crosslinked hyaluronic acid hydrogel inserts coupled with perlecan domain IV

peptides to culture human parotid gland acinar cells, exhibiting lobular acini-like structures and lumen formation [220]. Shubin et al., employed PEG hydrogels synthesized by step-growth thiol-ene polymerization to encapsulate primary SMG cells in thiol-ene PEG microspheres, which promoted duct and acinar cell proliferation, improved cell viability relative to controls, and maintained the differentiation of salivary gland epithelial cell phenotypes [305]. Fibrin hydrogels have gained traction in the realm of salivary gland bioengineering due to their biomimetic properties and ability to support cellular functions. Fibrin's inherent ability to guide tissue repair and promote regeneration has been further augmented by chemically conjugating it with Laminin-111 peptides [309]. Furthermore, an additional aspect of this research is the potential therapeutic application of these modified fibrin hydrogels in addressing radiation-induced salivary gland damage. Nam et al., assessed the regenerative potential of transdermally injected fibrin solution chemically conjugated with Laminin-1 peptides A99 and YIGSR on irradiated salivary glands, forming hydrogels through internal polymerization using endogenous thrombin. The results were promising; the treated irradiated glands showed substantial regeneration, culminating in the restoration of functional salivary tissue. In stark contrast, untreated irradiated glands continued to manifest significant structural and functional degradation [339].Gelatin-based hydrogels have demonstrated profound potential in the domain of salivary gland regeneration. In a study by Miyaki, et. Al., aimed at creating a model to elucidate the impacts of physiologically active substances on the atrophy and regeneration of salivary gland acinar cells in vivo, acellular gelatin-based hydrogel sheets were employed. These sheets were implanted into resection wounds made in the SMG of Wistar rats. Notably, by Day 10 post-implantation, the hydrogel sheets had almost entirely dissipated. The subsequent histochemical examinations revealed that in atrophic regions, a remarkable transition was

observed from the initial state of acinar cell atrophy to the emergence of newly formed, mature acinar cells by Day 10. These results were further accentuated by the observed transformation of striated and granular ducts into duct-like structures between Days 5 and 7. In contrast, necrotic regions showcased a slightly different progression, with a conspicuous destruction of acinar and ductal cells post-resection, followed by the appearance of new acinar cells by Day 10 [310]. The significance of this model lies in its capacity to mimic and elucidate the processes of atrophy and subsequent regeneration in the SMG. Moreover, it offers a valuable framework for evaluating the sustained release impacts of physiologically active substances embedded within an implanted hydrogel sheet.

Self-Assembly to generate cellular clusters and organoids

Scaffold-free methods of developing tissues and organs have emerged, yielding self-assembled and self-organized sets of cells. To implement this approach, cells are selected and exposed over time to a variety of growth regulators. Two distinct forms of scaffold-free technology have evolved, self-assembling processes (SAP), and self-organizing techniques (SOT) [340]. In the self-assembling process, non-adherent culture substrates like agarose support high-density seeding, prevent cell-attachment, and encourage cell-cell interaction. Differential adhesion and differential interfacial tension are important concepts in self-assembly, pointing to the idea that cells minimize free energy via cell-cell binding. Consequently, cells with similar surface tension aggregate with one another. Cells with the highest surface tension will sort to the center of a nascent tissue. N-cadherin often plays a role in this process via its expression and localization on cell surfaces. ECM secretions can anchor or free cells from their location. Chemotactic secretions can create concentration gradients that guide cells from one place to another as well [340]. Salivary gland cells have inherent self-assembly properties. This was first revealed when

Wei et al. used E13 mouse SMG cells to study tissue assembly. They found that dissociated SMG epithelial cells self-organized into structures that underwent significant branching. Significant insights were garnered by this study. One such insight was that β1-integrin inhibition blocked cell aggregation, but E-cadherin inhibition hampered aggregate compaction. SMG mesenchymal cells added to the epithelial cell cultures facilitated branching and proacinar differentiation [341].

2.4. Potential engineering strategies to improve salivary gland tissue vascularization, innervation, and engraftment

Significant hurdles must be overcome before organ-level tissue engineering becomes clinically translatable. Recapitulating the vascular and neural architecture of engineered salivary glands are big challenges, but new technologies and methods may soon mitigate these two issues. 3D bioprinting, tissue-nanoparticle integration, and mesh electronics are relatively new technologies, which have not been applied to SG engineering in significant measure, but the proof of principle to support their application to SG engineering is abundant. This section will explore these relatively new technologies and prospective approaches for their application to salivary gland engineering.

2.4.1. Prospects for engineering vascularized salivary gland tissue

Salivary glands need blood vessels to remain viable as oxygen cannot diffuse more than 200 μm due to mass transfer limitations. Salivary gland thickness surpasses that length along every axis. The human SMGs, for instance, have an anterior-posterior length of 35 ± 5.7 mm, a paramandibular extension to gland depth of 14.3 ± 5.7 mm, and an extension in frontal scanning of 33.7 ± 5.4 mm [342]. Emerging 3D bioprinting technologies can precisely deposit a variety of cell-laden biomaterials with spatiotemporal controls. [343]. In another strategy is to produce

perfusable vascular tubes, Koroleva developed a 3D co-culture of vasculogenic cells (e.g., human umbilical vascular endothelial cells, HUVECs) and human adipose-derived stem cells (hASCs) within a synthetically modified fibrin hydrogel [344].

2.4.2. Prospects for engineering innervated salivary gland tissue

Innervation of engineered tissue has been a long-standing, but an elusive goal of tissue engineers. As both salivary gland development and saliva secretion depend upon sympathetic and parasympathetic innervation, engineered salivary glands must have the capacity to interface with

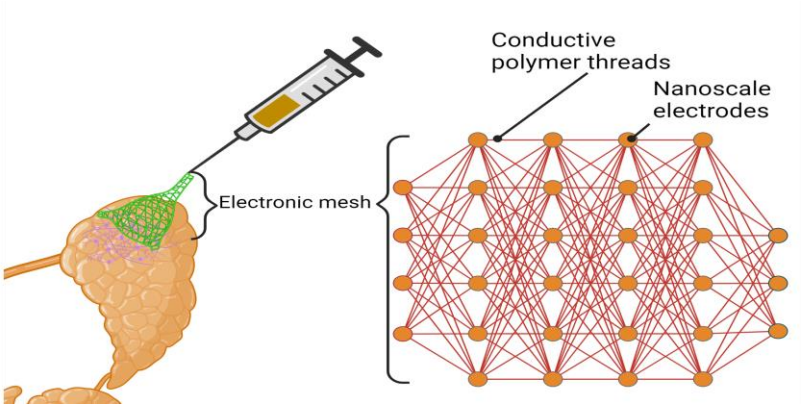

Figure 2.9. Electronic mesh schematic (created using Biorender, Biorender.com)[473]

the nervous system. Evidence indicates that normal salivary gland development will not occur in the absence of the PSG [224,345]

Mesh electronics and bio-hybrid systems

Normal development and maintenance of salivary gland tissue is severely undermined when the parasympathetic ganglion is damaged [346]. Mesh electronics may offer a way to circumvent salivary gland innervation problems that emerge after damage. Mesh electronics are a class of ultra-flexible and scalable neural probes originally designed to seamlessly integrate with the neural tissues (Figure 9). These semiconductor electronics resemble a 3D mesh or network,

allowing them to be implanted in the brain (or other tissues) with minimal inflammation or damage over long durations. Their design aims to achieve a biologically compatible interface, where the implanted electronic mesh can move with the tissue, reducing the relative motion between the device and the surrounding neurons. This ensures long-term stability and a reduced immune response. Bridging is enabled by the structural and mechanical properties of mesh electronics, which mimic native neurons. Mesh electronics are small enough to be injected directly into tissue or integrated into engineered tissues and transplanted. These probes are neuro-attractive and non-immunogenic. Further, they are capable of long-term mapping and modulation of neural activity [347,348]. Mesh electronics show promise for restoration of function in damaged glands and for creating functional engineered glands (Figure 2.9).

Biocompatible, endocytosed nanotubes in salivary gland tissue

Nanotubes can be comprised of a single sheet of atoms or multiple layers formed into a tube having a diameter in the nanometer range. Goldman et al. discovered that multiwall inorganic tungsten disulfide ([WS2], INT-WS2) nanotubes, which are 40-150 nm in diameter/ 75-100 nm in length and fullerene-like nanoparticles (IF-WS2), which are 120-150 nm in diameter were biocompatible with rat submandibular cells. Transmission electron microscopy (TEM) images indicated nanoparticle (NP) endocytosis and accumulation in cytoplasmic vesicles, suggesting promising future uses as these NPs have many potential medical applications [349]. NPs of different compounds form nanotubes and fullerene-like particles and can be functionalized with proteins and other biomolecules, enabling targeted drug delivery and bioimaging capabilities [350]. These nanomaterials have superior mechanical and tribological (interacting surface in relative motion) properties. Additionally, carbon nanotubes have demonstrated the potential to induce axonal regeneration and peripheral nerve repair because of their unique properties, such as biocompatibility, electrical conductivity, and flexibility [351].

Bioprinting of neurons and innervation of tissues

Bioprinting offers the possibility of printing stem cells, nerve cells, and nerve conduits for integration with engineered salivary gland tissue. Owens et al. developed a synthetic nerve graft using murine bone-marrow stem cells (BMSCs) and Schwann cells. The cells were cast into 500 μm diameter tubes then loaded into an extrusion bioprinter, which formed Schwann cell tubes surrounded by BMSCs [352] . Lorber et al. printed rat ganglion cells and glia using an inkjet printing system [353]. Pateman et al. used micro-stereolithography to print PEG-based nerve guidance conduits for nerve repair studies, which performed similarly to autograft controls [354]. As bioprinting technology continues to improve, we can anticipate more papers and technological advances in this important area to facilitate the innervation of engineered tissues.

Nanoparticles offer essential spatiotemporal control over scaffold development and engraftment

NPs range in size from 1-100 nm, creating extremely high surface area-to-volume ratios. The surface area and size of NPs make them highly mobile and interactive, with the potential for highly tunable interactions. The NP surface and its interior can be functionalized for many tissue engineering-relevant purposes including cell-specific targeting and penetration, heat production, vibration, antimicrobial activity, contrast, magnetic control, and conductance. These particles can be designed with biocompatibility and non-immunogenicity in mind and can be engineered to mimic the size of ECM components. Researchers have developed NP applications specific to tissue engineering fields across several basic areas, including biological, electrical, and mechanical property enhancement, mechanotransduction stimulators, gene delivery, magnetic cell patterning, 3D tissue construction, and biomolecular detection. NPs can be directed and delivered to salivary gland tissue or integrated into engineered salivary gland tissue and are demonstrably biocompatible and easily endocytosed [355]. NPs can improve the engraftment

environment by reducing apoptosis and can also be used to promote PSG innervation through the controlled release of growth factors to drive branching morphogenesis of neurites. Further, Arany et al. targeted the pro-apoptotic PKCδ gene using a novel, pH-responsive nanoparticle complexed with siRNA. The knockdown of PKCδ not only reduced the number of apoptotic cells during the acute phase of radiation damage, but also markedly improved saliva secretion at 3 months in irradiated animals. Treatment was administered prior to ionizing radiation. Varghese et al. developed a protocol for nanoparticle delivery to salivary gland tissue using retroductal injection of the SMG via Wharton's duct and parotid gland via Stetson's duct. As nanoparticles can be delivered in combinations and with spatiotemporal controls, future advancements will further increase their applicability for salivary gland tissue engineering and other medical applications [355].

Injectable engineered salivary gland transplants

Injectable scaffolds allow for minimally invasive cell delivery in vivo and can be used to increase survival rates upon cell implantation. However, this process can be hampered by mechanical stress during cell injection [356,357]. Shear-thinning biomaterials are materials that decrease in viscosity or become less viscous when subjected to increasing shear stress. This is a non-Newtonian flow property wherein the material becomes more fluid-like under mechanical stress or agitation and returns to its more viscous or semi-solid state once the stress is removed. Shear-thinning biomaterials, such as alginate[356] and hyaluronic acid [358], have been shown to form a lubricating layer on the syringe wall, which reduces resistance to flow, which, in turn, leads to increased cell viability after injection [356,357]. Once these cells are transferred, they are still subject to apoptosis as many cells undergo integrin-mediated apoptosis, or anoikis, in the absence of ECM binding [359,360]. Injectant inclusion of ECM components, such as collagen, laminin, fibronectin, and HA, can prevent this anoikis. Other compounds can also improve post-

transplant survival, and biomaterials can be modified to mimic ECM-mediated signaling through inclusion of integrin-binding domains. RGD is a well-known integrin-binding domain that binds to at least eight different integrin complexes [361,362]. These integrin-binding domains offer many benefits. First, RGD is the main integrin-binding domain present within ECM proteins such as fibronectin and vitronectin; hence, it is widely recognized by many cell types. Second, short peptides like RGD are more stable than their corresponding proteins. Third, as functionalization components, they easily fit biomaterial spatial and conformational parameters [363]. Studies have shown a marked increase in in vitro MSC survival following the use of RGD-modified alginate [364]. Like RGD, laminin-derived peptides, isoleucine-lysine-valine-alanine-valine (IKVAV) and tyrosine-isoleucine-glycine-serine-arginine (YIGSR) and the collagen-derived peptide glycine-phenylalanine-hydroxyproline-glycine-glutamic acid-arginine (GFOGER) [365,366] can improve cell survival for specific cell types. Two examples are laminin- and collagen-mimetic peptides, which can be used for neural cell transplantation and musculoskeletal system transplantation, respectively [367,368]. Injectable scaffolds hold promise for salivary gland engineering and also for repair of damaged glands. An exploration of the various strategies aimed at enhancing glandular vascularization, innervation, and engraftment would not be complete without consideration of how these methods would be applied in different pathological environments, particularly radiation-damaged versus diseased or senescent ones. Radiation damage often results in acute and chronic inflammation, vascular damage, and fibrosis [369]. Strategies employed for this environment need to not only promote tissue regeneration but also combat the detrimental effects of radiation. For instance, antioxidants, anti-inflammatory agents, and growth factors might be incorporated into the tissue engineering approach to mitigate the radiation-induced damage. Furthermore, given the compromised vasculature post-radiation,

strategies that promote early rapid vascularization will be vital to ensure the viability of the engineered tissue in the radiation-damaged environment or a diseased or senescent glandular environment that is characterized by cell aging, reduced proliferative capacity, and often, chronic inflammation [61]. In such a context, strategies should focus on rejuvenating the tissue, possibly through the introduction of younger, more proliferative cells or stem cells. Additionally, given the chronic inflammation often seen in these settings, anti-inflammatory approaches will also be of value. Tissue engineering solutions here might prioritize restoring normal cellular function, potentially utilizing signaling molecules that combat senescence or promote cellular rejuvenation. Lastly, an emerging class of compounds knowns as senolytics offer promise in reducing the effects of senescent cell burden in diseased or senescent tissue [370]. In summary, while the goal remains the restoration of gland function, the specific challenges posed by radiation damage versus inherent glandular disease or senescence necessitate tailored strategies. The effectiveness of any tissue engineering approach will hinge on its adaptability to the unique challenges of the environment under consideration.

2.5. Conclusions and future perspectives

As current treatments for salivary hypofunction are inadequate and only offer transient relief, regenerative medicine-based treatments are being developed. Efforts to date have included gene therapy, stem/progenitor cell-based therapy, and tissue engineering strategies. Understanding salivary gland development and its relevance to normal and dysregulated wound healing provides a foundation for the development of engineered salivary gland tissues. The salivary gland, stromal cells, nerves, and vasculature engage in reciprocal signaling that leads to branching morphogenesis of the epithelium, integration with the vascular and nervous systems, and the eventual elaboration of mature secretory salivary glands. Depending on the cause,

hyperfunctioning salivary gland tissue can be characterized histologically by degenerated acinar epithelial cells, an increase in the ductal/acinar epithelial ratio, exaggerated numbers of senescent cells, fibrotic stromal tissue, and increased immune infiltration. Efforts to develop salivary gland [1]tissue models must carefully consider what biomaterials and fabrication methods will be used to provide a substrate for culturing cells, and many natural, synthetic, and semi-synthetic materials have been used to create scaffolds for elucidation of cell interactions with scaffolds and for implantation in vivo. Fabrication strategies have included electrospinning, phase separation, freeze-drying, self-assembly, enhanced hydrogels, photolithography, and bioprinting. For eventual clinical application, bioengineering a tissue greater than 200 µm thick that is perfusable and innervated remains a major challenge in developing engineered salivary gland tissue that fully recapitulates the features inherent in natural tissue. Significant progress has been made in overcoming these hurdles using innovative

Table 2.4. Future perspectives of salivary gland bioengineering

Category	Details and Strategies
Origins and Development	• Ectodermal origin of major salivary glands • Role of epithelial, stromal, endothelial, and nerve cells
Histological Features of Hypofunctioning Tissue	• Degenerated acinar epithelial cells; Increased ductal/acinar ratio • Fibrotic stromal tissue • Increased immune infiltration
Fabrication Strategies for Scaffolds	• Electrospinning, phase separation, freeze-drying • Self-assembly, enhanced hydrogels, photolithography • Bioprinting
Major Challenges	• Creating tissue >200 µm thick that is perfusable & innervated • Integration with the in vivo environment • Integration with vasculature and nervous systems
Emerging Technologies	• Bioprinting, microfluidics, cryoelectrospinning • Nanotubes, mesh electronics
Outlook	• Redefining current techniques • Precise integration of cellular components • Exploring new approaches on the horizon in regenerative medicine for salivary hypofunction

[1] Part of this chapter has previously appeared as : Rose, S.C.; Larsen, M.; Xie, Y.; Sharfstein, S.T. *Bioengineering* **2024**, *11*, 28. https://doi.org/10.3390/bioengineering11010028Salivary Gland Bioengineering

technologies, including bioprinting, microfluidics, nanotubes and NPs, mesh electronics, and other nascent technologies (See Table 2.4).

Chapter 3: Development and characterization of a non-necrotic core 3D microtissue model of salivary gland tissue for radiation studies

3.1 Introduction

Traditional in vitro co-culture models have predominantly utilized two-dimensional (2D) surfaces to investigate cell-cell interactions, which fall short of accurately reflecting living tissues' complex three-dimensional (3D) architecture. These simplified 2D systems cannot replicate the intricate cellular arrangements and the full spectrum of biochemical interactions found in vivo. 2D culture significantly alters cell morphology, metabolism, and gene expression patterns from the in vivo state, particularly in higher organisms. Furthermore, the constraints of 2D cultures limit essential biological processes, such as cellular communication, nutrient and oxygen diffusion, waste removal, and overall cellular metabolism [371,372].

In response to these limitations, there has been a concerted effort within the scientific community to develop 3D in vitro models that better emulate the tissue microenvironment. These models aim to offer a more accurate representation of the spatial and chemical cues encountered by cells within actual tissues, thus facilitating a deeper understanding of cell behaviors, including direct and indirect interactions like autocrine and paracrine signaling [373,374]Understanding the properties and composition of the native extracellular matrix (ECM) is central to integrating these 3D models, which are crucial for cellular adhesion, proliferation, and differentiation.

Recent advances have utilized biomaterials and bioengineering strategies to create various 3D models, employing natural ECM proteins such as collagen gels and laminin to synthesize matrices. The unique properties of native decellularized salivary gland tissues, such as their honeycomb-like topography and soft, gel-like nature, have inspired these developments (Ramesh, 2022). Song et al. used engineered extracellular matrices combined with microbubble

array technology to evaluate radiosensitivity and the mitigation of radiation damage using a radioprotective compound [375]. The exploration of various polymers and ECM proteins for salivary gland tissue engineering has underscored the importance of substrate compatibility, highlighting the critical role of material science in tissue engineering [376–378]. Advanced biofabrication techniques, including bioprinting, conventional electrospinning and cryoelectrospinning, and hydrogel synthesis, have expanded possibilities for creating scaffolds that support and direct the development of salivary gland tissues, as reviewed in Rose et al., 2023.

The widespread presence of xerostomia, the subjective feeling of dry mouth, which can be related to salivary gland hypofunction, is the primary driver for interest in salivary gland models. Xerostomia affects over 24 million people in the United States alone (Sasportas et al., 2013), with more than one million experiencing moderate to severe symptoms. Xerostomia primarily results from hyposalivation—a defect in saliva production or secretion, which significantly diminishes the quality of life through its detrimental effects on oral and general health, including cracked lips, microbial proliferation, periodontitis, cavities, oral ulcerations, and challenges in speaking, eating, tasting, swallowing, and digesting. Salivary hypofunction is disproportionately suffered by the elderly, partly due to the side effects of over 154 medications [381]. Additionally, diseases such as Sjögren's disease and diabetes contribute to its prevalence [21,382]. Notably, 74-85% of head and neck cancer patients undergoing radiation therapy develop salivary hypofunction, with the World Cancer Report 2014 indicating that head and neck cancers alone could lead to at least 351,000 new cases of xerostomia worldwide [380,383–385]. The prevalence of radiation-associated salivary hypofunction underscores the urgency to develop models for irradiated salivary gland tissue.

An additional application of in vitro-developed 3D salivary gland models garnering interest is their potential role in cell-based therapies, such as the transplantation of non-differentiated, patient-derived organoids into the glands of irradiated patients to alleviate conditions like xerostomia. This innovative approach aims to restore glandular function by leveraging the regenerative capacity of organoids, thus providing a promising avenue for improving patient outcomes in cases of severe hyposalivation[386].

The global xerostomia therapeutics market, valued at USD 625.3 million in 2018, is expected to grow at a CAGR of 3.6% between 2019 and 2026, reflecting the escalating demand for effective treatments. [387] Despite the availability of treatments, such as medication adjustments, saliva stimulants (sialagogues), and moisturizers, these interventions often provide only transient relief. Side effects, such as sweating, increased heartbeat, and nausea, can accompany them. This situation is particularly challenging for head and neck cancer survivors, whose persistent xerostomia underscores the limited regenerative capacity of salivary glands (Konkel et al., 2019; Polaris Market Research, 2023b; Weng et al., 2018; Yoo et al., 2014).

The current state-of-the-art salivary gland tissue models, including 3D bioprinting and organoid cultures, have played a pivotal role in understanding the pathophysiology of salivary gland diseases and testing new therapeutic approaches. These advances set the stage for our approach to accurately simulate glandular biology and pathology, directly addressing the unmet need for effective salivary gland regeneration strategies. The development of models that accurately mimic the salivary gland environment is crucial for facilitating the exploration and eventual application of regenerative therapies, offering hope for substantial improvements in the quality of life for individuals suffering from xerostomia and related conditions.

In our study, we harness cells' intrinsic ability to self-assemble and produce their own ECM, preceding using exogenous scaffolds. By co-culturing murine NIH 3T3 fibroblasts with SCA-9 submandibular gland salivary epithelial cells in a 5:1 mesenchymal to epithelial ratio (based on prior research, [391] within non-adherent well plates, we have facilitated the formation of spheroids with desired size and high viability from a small initial cell number, through natural migratory and adhesive behaviors of mesenchymal and epithelial cells. We have further demonstrated the utility of the spheroid model for investigating the effects of X-ray irradiation on salivary tissues. This scaffold-free, 3D co-culture system successfully simulates the cell-cell and cell-matrix interactions crucial to the physiology of the salivary gland, presenting a more physiologically relevant platform for the study of tissue dynamics.

3.2 Materials and methods

3.2.1 Cell culture

NIH 3T3 mouse embryonic fibroblasts (passage 12-17) [392] and SCA-9 mouse submandibular gland (SMG)-derived epithelial cell line (ATCC® CRL-1734™), which was developed from an undifferentiated, chemically induced carcinoma of adult mouse SMG [393–395], were routinely maintained (separately) in cell culture medium, consisting of Dulbecco's Modified Eagles Medium (DMEM, high glucose, Thermo Fisher Scientific, Waltham, MA) supplemented with 10% fetal bovine serum (Thermo Fisher Scientific) and 1% penicillin-streptomycin (Thermo Fisher Scientific). Cell culture media were changed one day before subculturing and cells were passaged every 3 or 4 days at 70-80% confluence. Cultures were maintained in a humidified 37°C incubator with 5% CO_2.

3.2.2 Spheroid formation and culture

The hanging drop method used 160-2560 NIH-3T3 fibroblasts and SCA-9 epithelial cells at a 5:1 ratio. Cells mixed with cell culture medium were seeded in 15 µL drops on the inverted lids of 50 mm Petri dishes with 200 µL of distilled water in the base to maintain humidity. An additional 15 µL of medium was added on days 3 and 7, respectively.

Non-adherent 96-well Biofloat® plates (faCellitate, Mannheim, Germany) were also evaluated for spheroid generation. Cell densities ranging from 40 to 620 cells/well for NIH-3T3 and SCA-9 cells (at a 5:1 ratio) were tested for optimal spheroid formation. Briefly, 800-12,400 cells/mL were seeded in each well in 50 µL of cell culture medium, centrifuged at 250 x g for 5 minutes, and then incubated in a 37°C incubator with 5% CO_2. On days 3, 6, and 9, 30 µL of medium was removed, and 30 µL of fresh medium was added. All cultures were incubated and imaged daily for ten days to monitor spheroid formation using an EVOS M7000 microscope imaging system (Thermo Fisher Scientific Invitrogen, Carlsbad, CA).

3.2.3 Viability assay and determination of spheroid core structure

Cell viability within spheroids was assessed by fluorescence using the Thermo Fisher LIVE/DEAD^{TM} Viability/Cytotoxicity Kit. Live cells are detected by the presence of intracellular esterases that convert the nonfluorescent cell-permeant calcein AM to fluorescent calcein; simultaneously, dead cells are detected by the permeation of red fluorescent ethidium homodimer-1 due to loss of plasma membrane integrity. Briefly, on day 10 after seeding, spheroids were washed with PBS three times, and then calcein AM and ethidium homodimer-1 were added to final concentrations of 2 µM and 4 µM, respectively. After addition of calcein AM and ethidium homodimer-1, spheroids were incubated at room temperature for 40 minutes per

the manufacturer's instructions (Thermo Fisher Scientific, Invitrogen). Images were captured using the EVOS M7000 microscope imaging system with GFP (482/524 nm) and RFP (542/593 nm) filters (Thermo Fisher Scientific) and processed using ImageJ.

As an additional measure to determine whether the core structure was hollow or solid, spheroids were cultured over ten days, after which they underwent a systematic preparation process for cryosectioning and staining. This process involved fixation (Thermo Fisher Scientific, Liverpool, N.Y.), a graded series of dehydration steps in solutions of sucrose (Thermo Fisher Chemical, Waltham, MA.), and embedding in tissue freezing media (Electron Microscopy Sciences, Hatfield, PA) for solidification (Supplementary Methods). The core integrity of the spheroids was confirmed using picrosirius red staining, which highlights collagen fibers, thereby providing a clear indication of the solid-core structure within the spheroids (Supplementary Figure S1).

3.2.4 Immunocytochemistry and fluorescence microscopy

To determine cell distribution within spheroids, immunofluorescence staining of NIH 3T3 fibroblasts, SCA-9 epithelial cells, and co-cultured NIH 3T3 and SCA-9 cells was performed using an anti-vimentin antibody to recognize NIH 3T3 fibroblasts and anti-TAS2R4 to recognize epithelial cells [396]. Cells were fixed in 4% paraformaldehyde (Thermo Fisher Scientific) for 30 min, washed four times with PBS-Tween (0.5% v/v Tween 20 (Thermo Fisher Scientific) in 1X PBS, PBS-T), permeabilized using 0.4% v/v Triton-X 100 (Sigma-Aldrich, St. Louis, MO) in 1X PBS for 30 min, and blocked in 20% donkey serum (Jackson ImmunoResearch Laboratories, West Grove, PA) in PBS-T. Spheroids were then incubated with primary antibodies, anti-TAS2R4 (polyclonal rabbit anti-mouse, Osenses, Keswick, Australia [Catalog # Rb2950-010217-WS]) at a 1:400 dilution in PBS and/or anti-vimentin (mouse-μ chain specific, Sigma-Aldrich [Catalog # V2258]) at a 1:400 dilution in PBS at 4 °C overnight, followed by incubation

with 4′,6-diamidino-2-phenylindole (DAPI, Sigma-Aldrich) at 1 µg/mL. five washes with PBS-T, and incubation with secondary antibodies at room temperature for 4 hours. Secondary antibodies used were Alexa Fluor 488 AffiniPure F(ab')$_2$ fragment, donkey-anti-mouse IgM, µ chain specific (Jackson ImmunoResearch [Catalog # 715-546-020]) at a 1:400 dilution in PBS-T with 5% donkey serum and 3 wt.% BSA to reveal vimentin and Alexa Fluor 647 donkey-anti rabbit IgG (H+L) (Thermo Fisher [Catalog# A-31573]) at a 1:400 dilution in PBS-T with 5% donkey serum and 3 wt.% BSA to reveal TAS2R4. Images were captured using the EVOS M7000 microscope imaging system with DAPI (357/447 nm), GFP (482/524 nm), and RFP (542/593 nm) filters and processed using ImageJ.

3.2.5 Irradiation of salivary spheroids and apoptosis assay

Spheroids in covered, round-bottomed 96-well plates containing 30 µL of medium were placed in the Faxitron RX 650 Cabinet X-Radiator™ System (Faxitron X-Ray LLC, Lincolnshire, IL). The energy of the X-ray beam was 120 kV, and the rate of exposure was 150 cGy per minute. Spheroids were exposed for various times to deliver a single dose of 0 Gy, 4 Gy, 8 Gy, 12 Gy, or 16 Gy. After X-ray exposure, spheroids were incubated for four hours in a humidified 37°C incubator with 5% CO_2 before being washed with PBS and transferred to Annexin V binding buffer (10 mM HEPES, 140 mM NaCl, and 2.5 mM CaCl2, pH 7.4). At four hours post irradiation, apoptosis was quantified by staining with a solution of 25 µL Annexin V – Alexa Fluor 488 conjugate (Invitrogen) in 100 µL Annexin V binding buffer per 96 round-bottom well to detect apoptotic cells and 7.48 µM propidium iodide (Invitrogen) to detect dead cells. The spheroids were imaged using fluorescence microscopy. Images were captured using the EVOS M7000 microscope imaging system with DAPI (357/447 nm), GFP (482/524 nm), and RFP

(542/593 nm) filters and processed using ImageJ, and the percentage of early and late apoptotic cells were calculated.

3.2.6 Quantification using ImageJ

3.2.6.1 Quantification of spheroid size and roundness

Cell cultures and spheroids were imaged daily for ten days using an EVOS M7000 microscope imaging system to monitor spheroid formation. Size and roundness were determined using ImageJ analysis. The spheroid size was determined using ImageJ by observing and measuring the total 2D area from a section at the center of the microtissue of each DAPI-stained spheroid. The roundness of a spheroid was defined as the ratio of its 2D surface area to the area of a circle whose diameter matches the spheroid maximum diameter. Therefore, the roundness can be mathematically expressed as the surface area of the spheroid divided by the product of pi and the square of half the maximum diameter (Eq. 1).

$$Roundness = 4 * \frac{Area}{\pi * (Maximum\ Diameter)^2} \quad (1)$$

3.2.6.2 Quantification of cell viability

Cell viability in spheroids was determined via ImageJ analysis of the fluorescent images of calcein AM and ethidium homodimer-1-stained spheroids, calculated by the ratio of green fluorescence area relative to the combined green and red fluorescence areas.

3.2.6.3 Quantification of cell apoptosis

Cell apoptosis in spheroids was quantified using ImageJ to measure the ratio of the area of Annexin V green fluorescence to the area of propidium iodide red-stained fluorescence. To quantify the Annexin V and propidium iodide-related fluorescence areas, images were split into

separate color channels (green and red) and then converted to 8-bit grayscale. Next, the threshold function was used to measure the respective areas.

3.2.7 Statistical analysis

Statistical analysis was performed using GraphPad Prism version 10.0.0 for Windows. Results were expressed as mean ± the standard error of the mean**.** The statistical significance of differences in apoptosis among treated groups was analyzed using one-way analysis of variance (ANOVA), with further assessments of variance homogeneity conducted using Brown-Forsythe and Bartlett's tests. A P-value of less than 0.05 was considered statistically significant.

3.3 Results

3.3.1 Optimization of cell seeding density for spheroid formation

To establish a consistent and uniform 3D co-culture model of salivary gland tissue, we initially assessed the formation of spheroids using the hanging drop method and subsequently using 96-well non-adherent Biofloat™ plates, seeding NIH 3T3 fibroblasts and SCA-9 submandibular gland salivary epithelial cells in a 5:1 mesenchymal to epithelial ratio at varying densities.

We maintained spheroids for ten days using the hanging drop method with seeding densities of 160, 320, 1280, or 2560 cells per 15 µL drop (Figure 3.1). We found that uniform spheroids only consistently formed at higher densities (≥ 2560 cells per drop). However, these conditions also resulted in spheroids larger than 400 µm in diameter, which would be predicted to develop necrotic cores based on mass transfer principles in addition to prior research [397]—this was deemed inconsistent with our objective to maintain cell viability throughout the spheroid. We subsequently evaluated the formation of spheroids in 96-well non-adherent Biofloat™ plates with seeding densities of 40, 80, 160, 320, or 640 cells per well in an NIH 3T3 to SCA-9 ratio of

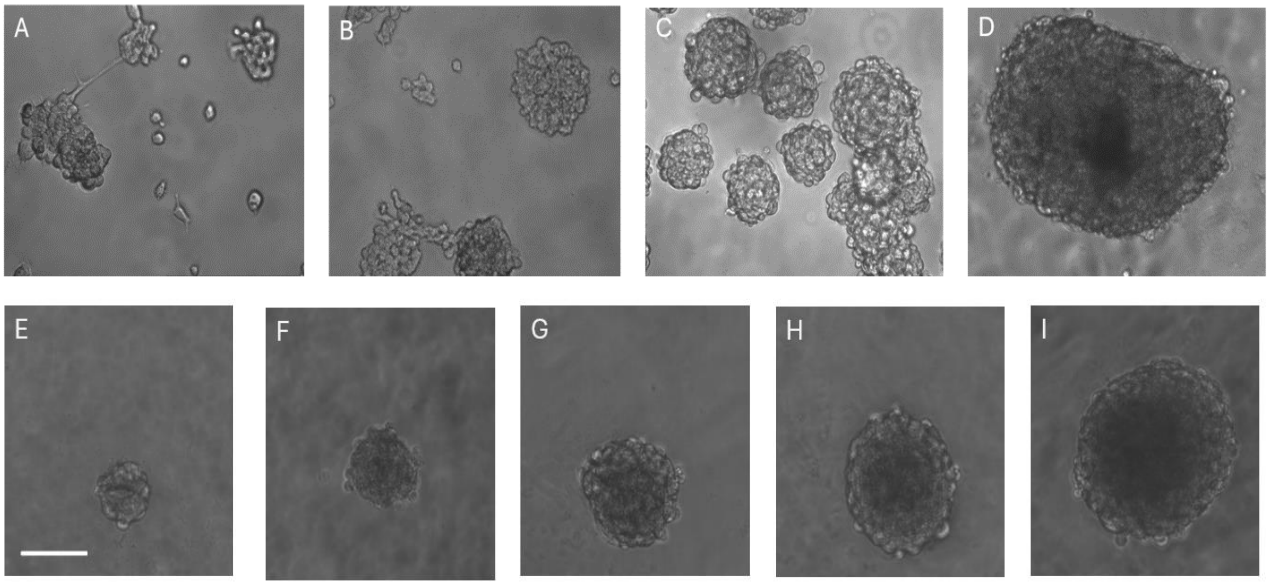

Figure 3.1. Spheroid development using hanging drop method and non-adherent 96 well plates. Top: Spheroid development using the hanging drop method. NIH 3T3 fibroblasts and SCA-9 epithelial cells were co-cultured in a mesenchymal to epithelial ratio of 5:1 and seeded at varying densities using the hanging drop method for 10 days. (A) 160 cells/drop. (B) 320 cells/drop. (C) 1280 cells/drop. (D) 2560 cells/drop. Scale bar = 100 µm. Bottom: Spheroid development in non-adherent 96-well plates. NIH 3T3 fibroblasts and SCA-9 epithelial cells were co-cultured in a mesenchymal to epithelial ratio of 5:1 and seeded at varying densities in a 96-well non-adherent Biofloat™ plate for 10 days. (E) 40 cells/well. (F) 80 cells/well. (G) 160 cells/well. (H) 320 cells/well. (I) 640 cells/well. Scale bar =100 µm.

5:1, with cells cultured for ten days (Figure 3.1). One hundred and sixty cells per well yielded optimal results as follows. The spheroid diameter ranged from a minimum of 145.0 µm to a maximum of 185.0 µm, with a mean diameter of 166.4 µm ± 9.7 µm and a median diameter of 167.5 µm. The range of differences in diameters observed was 40.0 µm, highlighting the controlled size distribution of the spheroids formed. The lower and upper 95% confidence intervals for the mean diameter were 162.7 µm and 170.2 µm, respectively (Figure 3.2).

We measured each spheroid's roundness as a measure of morphological consistency. A perfect sphere would have a roundness ratio of 1. The minimum measured value was 0.60, and the maximum was 0.91, with a mean roundness of 0.76 ± 0.08, indicating a relatively consistent

spheroidal shape across samples. The lower and upper 95% confidence intervals for the mean roundness were 0.74 and 0.79, respectively. The coefficient of variation was calculated at 9.8%, underscoring the uniformity in spheroid roundness (Figure 2).

These data suggest that a cell seeding density of 160 cells per well in non-adherent Biofloat™ plates is optimal for generating uniform spheroids with minimal variation in diameter and roundness. This density ensures the formation of spheroids within the desired size range (< 200 µm diameter), which is crucial for avoiding necrotic core development and maintaining overall cell viability. Therefore, this seeding density was adopted to investigate cell-cell interactions

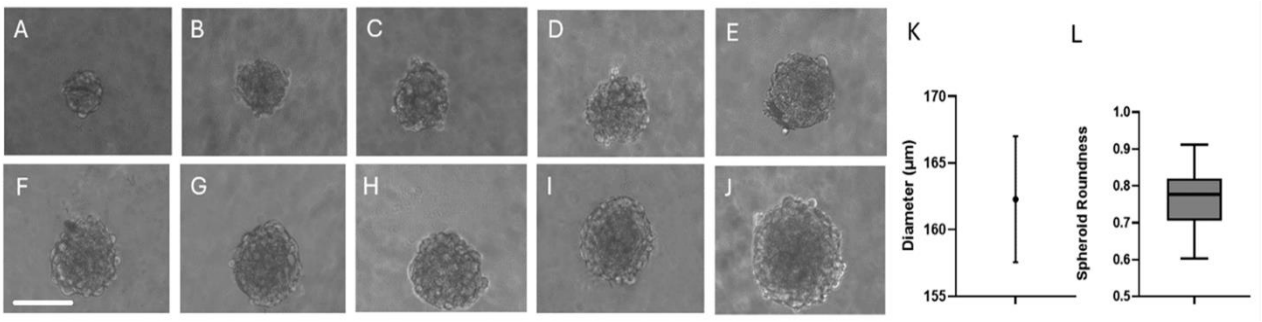

Figure 3.2. Typical growth pattern over 10-day period of NIH 3T3: SCA-9 spheroids seeded at 160 cells/well. (A-J) Days 1-10, respectively. The cell seeding density of 160 cells per well formed spheroids within 24 hours, with a mean diameter increase of 13.8% over a 10-day period. Under these conditions, 99.7% of spheroids remained below the 200 µm threshold, minimizing the risk of necrotic core formation. (K) Mean and standard deviation for average spheroid diameter measured on day 10. (L) Box and whiskers plot highlighting the spheroid roundness, interquartile values, and outliers measured on day 10. Scale bar = 100 µm.

within the spheroids further.

3.3.2 Assessment of spheroid viability

LIVE/DEAD staining was used to evaluate the viability of NIH 3T3: SCA-9 spheroids within our 3D co-culture model produced from 160 cells per well (Figure 3.3). Spheroids were assayed on day 10, revealing high levels of cell viability across all examined spheroids. The percentage of viable cells within the spheroids ranged from a minimum of 97.4% to a maximum of 100%.

The mean viability was determined to be 99.5 ± 1.0%, capped at 100%, indicating a consistently high viability across the spheroids. The standard error of the mean was calculated at 0.4%,

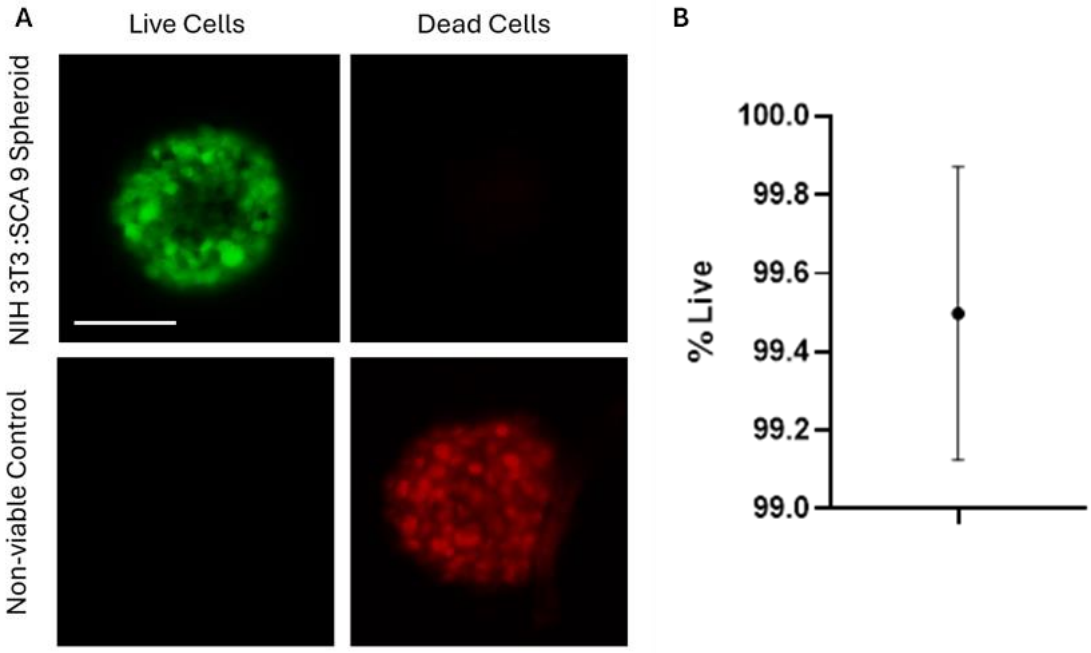

Figure 3.3. Cell viability of NIH 3T3: SCA-9 spheroids determined by LIVE/DEAD assay. (A) Confocal images of LIVE/DEAD stained NIH 3T3: SCA-9 spheroids grown under normal culture conditions for 10 days, in which the absence of red fluorescence in the center of the normal spheroid indicates a non-necrotic core (top panels), in contrast to the non-viable spheroid control (treated with 70% methanol) (bottom panels). Green, live cells. Red, dead cells. Scale bar = 100 µm. (B) Percentage of live cells in the NIH 3T3: SCA-9 spheroids after 10 days in culture. N=7.

further underscoring the consistency of high cell viability in NIH 3T3: SCA-9 spheroids (Figure 3.3B).

The absence of red fluorescence in the NIH 3T3: SCA-9 spheroid centers indicates a non-necrotic core, contrasting sharply with the non-viable control spheroids treated with 70% methanol, which showed extensive red fluorescence. These observations, supported by the quantitative data, confirm the high level of viability sustained by the NIH 3T3: SCA-9 spheroids under the specified culture conditions. Additionally, to determine whether or not the spheroids contained cells all the way through or were hollow, spheroids were subjected to cryosectioning

followed by picrosirius red staining. As shown in Figure S1, the spheroids harbored a solid core. These outcomes highlight the effectiveness of using the NIH 3T3: SCA-9 spheroids as a co-cultured microtissue model in maintaining spheroid integrity and cell viability, a crucial aspect of its application in studying cell-cell interactions within a simulated tissue environment.

3.3.3 Expression of mesenchymal and salivary epithelial markers in co-cultured spheroids

The distribution of cell types and their ability to maintain characteristic mesenchymal and salivary epithelial marker expression within our NIH 3T3: SCA-9 spheroids over ten days were examined using immunofluorescence to identify and localize the NIH 3T3 fibroblasts and SCA-9 salivary epithelial cells within the co-culture spheroids. Cell-specific markers vimentin, an intermediate filament protein characteristic of fibroblasts, and TAS2R4, a taste receptor protein expressed in SCA-9 cells [398,399], were utilized to distinguish between these two cell populations.

Vimentin and TAS2R4 immunostaining identified NIH 3T3 and SCA-9 cells in the co-cultured spheroids. The immunofluorescence image delineates the presence of both markers, confirming the coexistence of both cell types within a single spheroid structure (Figure 4A). To verify that NIH 3T3 and SCA-9 cells exclusively expressed their respective markers, we created and immunostained NIH 3T3 spheroids as well as SCA-9 spheroids, demonstrating exclusivity (Figure 4B-G).

These findings highlight the association of the two cell types when cultured in spheroids, emphasizing the ability of our co-culture system to preserve cell-type specificity within a heterogeneous population. The absence of cross-staining in the single-population spheroids

validates the specificity of the immunofluorescent markers used, confirming the reliability of our

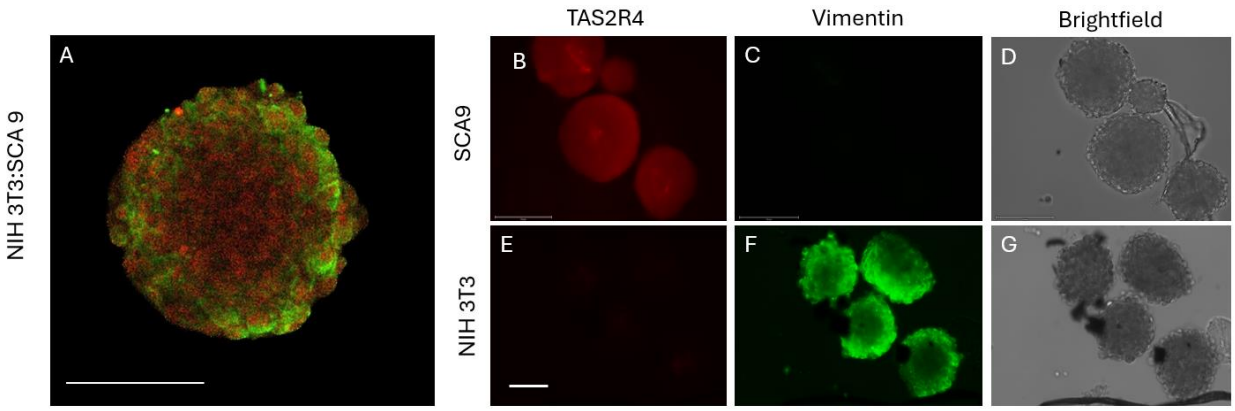

Figure 3.4 Cell distribution within NIH 3T3: SCA-9 spheroids. (A) Fluorescence image of NIH 3T3: SCA-9 spheroid, demonstrating expression of both vimentin (mesenchymal marker to reveal NIH 3T3 fibroblasts in green) and TAS2R4 (SCA-9-specific marker in red). (B-D) Fluorescence images of SCA-9 spheroids showing only expression of TAS2R4 (B), not vimentin (C), along with the brightfield image (D) showing the total spheroid cell population. (E-G) Fluorescence images of NIH 3T3 spheroids showing the absence of TAS2R4 (E) and presence of vimentin expression (F), along with the brightfield image (G). Red, TAS2R4. Green, vimentin. Scale bar = 100 μm.

method for assessing cell distribution within the spheroids. This result ensures that our 3D co-culture accurately reflects the cellular heterogeneity characteristic of native salivary gland tissue, which is crucial for studying cell-cell interactions and tissue function in vitro. However, it is essential to clarify that while our system adeptly replicates cellular heterogeneity, it does not fully emulate the complex cellular structures found in native tissue. This distinction underscores the limitations of our model in replicating the full spectrum of tissue architecture and should be considered when interpreting our findings.

3.3.4 Exposure of the 3D co-cultured salivary gland to X-rays

To evaluate the utility of the spheroid model for investigating the effect of X-rays on salivary tissues, spheroids were exposed to varying radiation doses: 0 Gy (control), 4 Gy, 8 Gy, 12 Gy, and 16 Gy, followed by apoptosis assay to assess the response of our 3D microtissue spheroid

model. Spheroids were stained with Annexin V and propidium iodide to identify early and late apoptotic (cell membrane rupture and death) events, respectively (Figure 5). The ratio of apoptotic to necrotic cells increased with increasing radiation dosage (Figure 5F).

Our experiment successfully delineated early versus late apoptosis proportions across the different radiation doses (Figure 5A-E). The fluorescent staining within the NIH 3T3: SCA-9

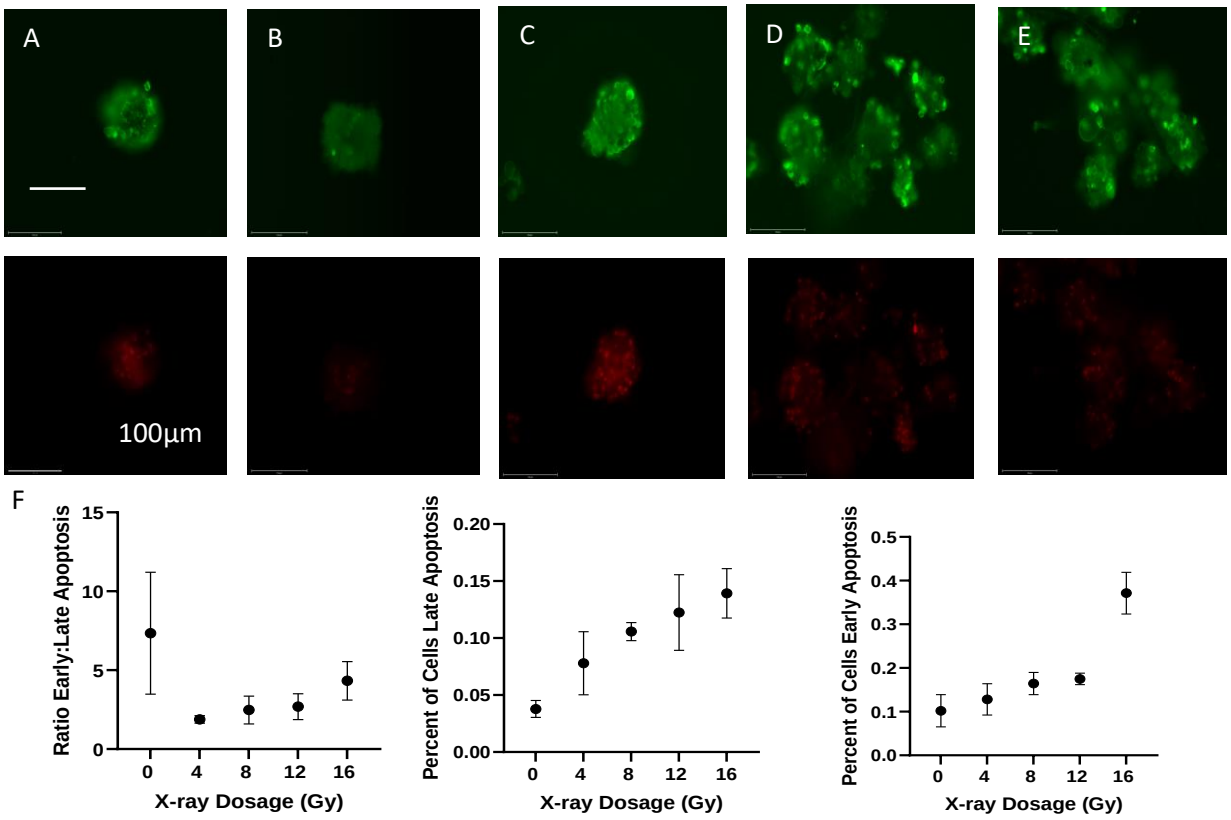

Figure 3.5. Radiation-associated apoptosis in NIH 3T3: SCA-9 spheroids. NIH 3T3: SCA 9 spheroids stained for Annexin V to detect early apoptotic cells in green (top panel) and propidium iodide to detect late apoptotic cells in red (bottom panel). Spheroids were cultured in non-adherent 96-well plates and irradiated. (A) 0 Gy (negative control), (B) 4 Gy, (C) 8 Gy, (D) 12 Gy, or (E) 16 Gy. Scale bars = 100 µm. (F) Quantification of cell apoptosis: ratio of early to late apoptosis (left panel), percentage of cells in late apoptosis (middle panel), and percentage of cells in early apoptosis (right panel).

spheroids demonstrated increased green fluorescence (Annexin V) across the spheroids exposed to increasing X-ray dosage, indicating a dose-dependent increase in early apoptotic events.

Simultaneously, red fluorescence (propidium iodide) indicated late apoptotic events, particularly at higher doses of radiation.

One-way ANOVA was performed to determine the significance of the differences in the ratio of apoptotic to dead cells with increasing radiation doses. The analysis revealed an F-value of 3.292 with a P-value of 0.0486, indicating a statistically significant difference among the means of the treatment groups ($P < 0.05$) (Figure 5F)

These results demonstrate that our 3D co-culture spheroid model is sensitive to X-ray exposure. An X-ray dosage of 16 Gy generated a significantly different response from the negative control, thus validating the utility of this 3D co-culture spheroid model for studying cellular responses to radiation and evaluating the efficacy of radioprotective or radiosensitizing agents.

3.4 Discussion

This study aimed to advance tissue engineering and regenerative medicine by developing efficiently produced, necrotic core-free, self-assembled, 3D co-cultured spheroids for salivary gland research that simulate the in vivo environment, which traditional 2D cell cultures and typical 3D spheroid cultures do not. A distinctive feature of our model is its necrosis-free core, addressing the limitations of oxygen and nutrient transfer in spheroid models over 200 micrometers in diameter [397]. Additionally, our model incorporated both stromal and epithelial cells at a low starting cell number (160 cells in 50 µL of medium) or low initial cell seeding density (3,200 cells/mL), enhancing its suitability for high-throughput screening and simplifying experimental setups.

The model's Matrigel-free and scaffold-free design ensures more natural cell interactions and growth dynamics, offering a physiologically relevant platform for studying cellular behaviors

and treatment responses. We successfully established a model that overcomes many limitations associated with traditional 2D cultures and scaffold-based 3D models, introducing a methodological innovation in cultivating and characterizing 3D spheroids. Our findings demonstrate that optimizing cell seeding density and leveraging the natural propensity for self-assembly in a scaffold-free environment can produce spheroids that maintain high viability and structural integrity without necrosis for at least 16 days. This necrosis-free microtissue model represents a significant step in creating physiologically relevant in vitro models for studying tissue-level responses to various stimuli, including radiation, and exploring potential radioprotective treatments.

A noteworthy application of our model is its potential in radiation therapy research and protecting healthy salivary glands. The spheroids were exposed to single X-ray doses slightly above the range used in the total course of head and neck cancer radiation treatment. The dose-dependent increase in cell apoptosis highlights the model's sensitivity to radiation-induced cellular changes, offering a promising avenue for exploring radioprotective treatments, which may mitigate irreversible collateral damage to the salivary glands when total exposure exceeds 30 Gy [400,401]. Furthermore, our model's adaptability to incorporate patient-specific cells in the future positions it as a valuable tool for personalized medicine. By testing therapeutic interventions on patient-derived spheroids, we can develop patient-tailored treatments.

Over the past few decades, the technology for producing spheroids in 3D cell culture has evolved significantly. Innovations include agarose molds, microfluidic devices, magnetic levitation, bioreactors, and non-adherent well plates [402]. Despite these advancements, the quest for a model that genuinely encapsulates the complexity of in vivo tissue environments continues. Our

study introduces a scaffold-free, self-assembled 3D co-culture model that addresses several limitations inherent to existing methodologies.

Historically, salivary gland tissue engineering has evolved significantly, with foundational work by Arnold et al. exploring stromal-epithelial interactions in co-culture models, demonstrating the stroma's regulatory role on epithelial cell growth [403]. Progress continued with Ozdemir et al. and Sfakis advancing tissue-engineered constructs aimed at restoring salivary gland function, primarily through hydrogel-based or compliant scaffolds [378,404]. The field leapt forward with the development of transplantable 3D salivary gland organoids by Tanaka and Mishima (2020) using Yamanaka factors and further innovations by Lindberg et al. (2021) with secondary structures from co-cultured spheroids, alongside Ramesh and coworkers engineered cryoelectrospun elastin-alginate scaffolds for transplantable bioengineered tissues [405–407]. These recent studies highlight the efficacy of 3D co-culture models and the potential for mimicking tissue architecture and functionality, underscoring the dynamic progression towards developing therapeutic applications and enhancing our understanding of tissue engineering [408].

In contrast to prevailing methods, our research adopted a scaffold-free approach that simplifies the construction of our model and enhances its physiological relevance, thanks to a matrix composed entirely of naturally produced ECM. We have developed spheroids that maintain structural integrity and high viability without external scaffolds by optimizing the cell seeding density in non-adherent well plates. This methodological advancement provides a more accurate platform for examining tissue-level responses, addressing a critical gap left by previous studies. Unlike research in oncology, which often tolerates the presence of necrotic cores within larger

spheroids, our focus on mimicking healthy tissue structures demands models that maintain cellular viability throughout, ensuring relevance to tissue engineering and regenerative medicine.

Our study contributes to understanding salivary gland tissue engineering and sets a new benchmark for producing spheroids in research. The ability to generate smaller, viable spheroids without necrosis presents an important advance, highlighting the importance of controlling spheroid size for maintaining a viable microenvironment. Due to oxygen and nutrient diffusion limitations, traditional spheroid models over 200 μm in diameter promote necrotic cores. While this may be acceptable in oncological research, given that tumors frequently have necrotic cores, it is not the norm in other in vivo environments, including salivary gland tissues. Thus, eliminating necrosis from our 3D model creates a better mimic of normal salivary gland tissue [409].

Necrotic cells release damage-associated molecular patterns (DAMPs) or alarmins, which include high mobility group box 1 (HMGB1), heat shock proteins (HSPs), ATP, and extracellular DNA and RNA. These signals activate the immune system, releasing pro-inflammatory cytokines such as TNF-α, IL-1, and IL-6, and attract phagocytic cells [410]. Additionally, reactive oxygen species (ROS) and fragments of extracellular matrix proteins like hyaluronan can be released, further perpetuating inflammation and tissue damage [409]. The release of intracellular proteins from necrotic cells can also alter pH and ionic balance, potentially influencing cell viability and function. Lastly, enzymatic degradation caused by the release of matrix metalloproteinases can degrade ECM [411–414]. Overall, the presence of a necrotic core introduces significant variability and potentially masks or alters the phenomena intended for study. Therefore, our model offers substantial improvements over existing 2D and 3D models in this fundamental respect.

This finding is particularly relevant given the sparse literature on sub-200-µm spheroids and the limited efforts to produce smaller spheroids in non-oncological contexts. Pinto et al. defined spheroids as being at least 200 µm. They cite 23 studies, which include scaffold-free and scaffold-based approaches; curiously, no study cited by Pinto uses an initial cell seeding density of fewer than 625 cells for microtissue formation [415]. Lee and colleagues generated size-controllable spheroids using 100,000-200,000 gingiva-derived mesenchymal stem cells, utilizing concave microwells for spheroid formation with controlled sizes and high viability [416]. Our approach allowed us to form uniform co-cultured spheroids with diameters less than 200 µm using 160 cells in 50 µL of medium, highlighting a technological advancement in the field.

Our study introduces a scaffold-free, self-assembled 3D co-culture model that significantly advances salivary gland bioengineering. Leveraging the natural propensity for self-assembly, our model allows the constituent cells to produce their own ECM, mimicking the normal in vivo environment rather than relying on artificial scaffolds or mouse tumor-derived Matrigel, which are not specific to salivary gland tissue.

These advancements offer a simplified and physiologically relevant platform for studying tissue morphogenesis, tissue-level responses, and the effects of therapeutic interventions. Our model's versatility and potential scalability make it applicable to various research and clinical scenarios, providing valuable insights and methodologies for salivary gland bioengineering. Through our methodological refinements, we can observe cellular responses in a 3D microenvironment where our controls are not contaminated by necrotic cell signaling from the core of the spheroid.This innovative approach allows for the study of tissue-level responses, drug screening, disease modeling, and the development of personalized treatments for salivary gland disorders. Our

findings pave the way for further advancements in tissue engineering, regenerative medicine, and personalized medicine in the context of salivary gland bioengineering.

Chapter 4 Senescence-conditioned medium exacerbates fibrotic response to radiation in a 3D salivary gland microtissue model

4.1 Introduction

While small and often overlooked, salivary glands play an essential role in our daily lives. From aiding digestion to maintaining oral health and facilitating speech, their importance cannot be overstated [1]. Yet, like all tissues, they are susceptible to various insults and damage, one of the most potent being radiation (Deasy et al., 2010). The increasing application of radiation in the medical field, particularly in oncology treatments, underscores the need to understand its repercussions on these delicate tissues.

Salivary gland fibrosis is characterized by the excessive accumulation of extracellular matrix (ECM) components, mainly collagen, resulting in glandular scarring and functional decline. This condition results from various causes, including chronic inflammation, autoimmune diseases such as Sjögren's disease, radiation therapy, and aging [417–419], which trigger complex molecular and cellular responses [10,12,271] Central to the fibrosis process are fibroblasts, which transform into myofibroblasts under stimuli such as TGF-β, producing large amounts of ECM [14–16,420–422] . Epithelial cells also contribute through epithelial-mesenchymal transition, gaining mesenchymal traits and contributing to ECM production[17,18] or through epithelial defects, contributing to abnormal ECM remodeling and fibroblast activation [422,423]. Additionally, macrophages play a significant role by activating fibroblasts through cytokines and growth factors [19]. The resultant disruption in the gland architecture causes a loss of functional cells, often leading to xerostomia (the perception of dry mouth) and can severely impact oral health and quality of life .[20,21,424].

Radiation has been shown to profoundly affect cultured cells, impacting cellular structure, function, and viability. The primary mechanism through which radiation exerts its effects is by

causing DNA damage. This damage can be in the form of single-strand breaks, double-strand breaks, and the formation of reactive oxygen species (ROS), which can further damage cellular components. Such DNA damage can lead to mutations, apoptosis (programmed cell death), and senescence (permanent cell cycle arrest), depending on the dose and type of radiation. High doses of radiation are particularly lethal to cells, leading to significant cell death and reduced proliferation rates. Even at lower doses, radiation can cause sublethal damage that affects the cell cycle, often resulting in delayed cell division and altered cellular functions [425].

The type of radiation also plays a crucial role in determining the extent and type of cellular damage. For example, ionizing radiation, which includes X-rays and gamma rays, is highly penetrative and can cause extensive DNA damage. In contrast, non-ionizing radiation, such as ultraviolet (UV) light, primarily affects the surface layers of cells, causing damage to DNA and other cellular components through the production of ROS and direct absorption by DNA molecules. The cellular response to radiation-induced damage includes activating repair mechanisms, such as the DNA damage response (DDR) pathways, which work to repair the damaged DNA. However, the efficiency of these repair mechanisms varies, and failure to correctly repair the damage can result in genomic instability and potentially lead to carcinogenesis, fibrosis, and other pathological conditions. Studies have demonstrated that prolonged radiation exposure, even at low levels, can lead to significant long-term effects, including increased mutation rates and reduced cellular functionality. X-rays were chosen in our work as they are commonly used in the treatment of head and neck cancers, which cause collateral damage to the salivary glands. In the series of experiments that followed, we attempted to determine a radiation dose that would be adequate to induce effects including; DNA damage, cell apoptosis, senescence and fibrosis, comparable to those experienced by individuals

subject to head and neck cancer irradiation, which commonly results in collateral damage to salivary glands, including loss of functional cells, fibrosis, and senescence [426]. A dosage too low would have negligible effects on these characteristics; a dosage too high would result in necrosis.

Radiation therapy is a double-edged sword in the field of oncology, offering life-saving treatment for various cancers, particularly those of the head and neck. However, this treatment does not come without its costs, particularly to the salivary glands, which are highly sensitive to radiation damage [427,428]. Even with protective measures and advances in radiation delivery such as intensity-modulated radiation therapy (IMRT), patients often experience a significant reduction in salivary function [429]. This reduction in salivary function is primarily due to the susceptibility of salivary gland acinar cells, which are responsible for saliva production, to radiation-induced apoptosis and necrosis. As these cells deteriorate, saliva production diminishes, leading to xerostomia, or the sensation of dry mouth, which severely compromises digestion, oral hygiene, and overall quality of life [427].

Further, radiation prompts the activation of fibroblasts into myofibroblasts, increasing the deposition of extracellular matrix proteins and leading to the stiffening and scarring of glandular tissues [430]. This fibrotic change not only further reduces gland function but also complicates potential recovery, as the fibrotic tissue is less responsive to regenerative therapies. Additionally, radiation-induced senescence contributes to an inflammatory milieu, characterized by the secretion of pro-inflammatory cytokines and chemokines, which can perpetuate the cycle of damage and fibrosis [427]. These processes underline the critical need for targeted therapeutic strategies to protect and regenerate salivary gland tissue during and following radiation therapy, ensuring better outcomes for patients undergoing treatment for head and neck cancers.

Cellular senescence is another layer of complexity in understanding tissue responses, especially post-radiation. Senescence, a state of irreversible cell cycle arrest, has garnered attention for its implications in aging and various pathological contexts, including fibrosis and cancer [6,7]. As cells transition into senescence, they undergo significant morphological, physiological, and secretory changes that can profoundly impact the surrounding microenvironment and, by extension, tissue functionality [8,9].

Once seen as a simple cessation of cell division due to aging, cellular senescence is now understood as a complex response impacting development, tissue repair, and disease progression [24] .Senescent cells exhibit distinct changes and secrete various bioactive molecules through the senescence-associated secretory phenotype (SASP), influencing neighboring cells and potentially contributing to conditions like fibrosis [26,27,431] Factors inducing senescence include replicative limits, external stressors, and oncogene activation, each playing roles in physiological and pathological contexts Brandl et al., 2011; Courtois-Cox et al., 2008; Hayflick & Moorehead,1964) The accumulation of senescent cells in tissues can promote dysfunction and chronic diseases, making them targets for therapeutic strategies such as senolytics[35,36,432].

Traditional two-dimensional (2D) cell culture systems have driven our cellular and molecular biology understanding. However, they often fail to capture the complex three-dimensional (3D) interactions and microenvironments in vivo (Ravi et al ., 2015). This discrepancy between 2D cultures and the in vivo microenvironment can lead to misrepresentations and limit the applicability of findings. Hence, recent years have witnessed a rising interest in 3D microtissue models, which promise to bridge this gap. 3D microtissue models, particularly spheroids, have emerged as powerful tools in biomedical research. They offer a more physiologically relevant representation of in vivo tissues, recapitulating essential cellular interactions, ECM

compositions, and gradient-driven behaviors [4]. This has rendered them particularly invaluable in studying tissue-specific responses.

Recent advances in 3D culture systems for salivary gland cells and organoids have made significant strides, offering more physiologically relevant models for research and potential therapeutic applications. These systems can be broadly categorized into scaffold-based, hydrogel-based, and bioprinting/magnetic bioassembly techniques[433–437]. Scaffold-based techniques include micropatterned PLGA nanofiber craters, which provide a structured environment that promotes cell attachment and organization, supporting glandular differentiation[438]. Similarly, PEG hydrogel-micropatterned PCL nanofibrous microwells combine PEG hydrogels with micropatterned PCL nanofibers to create a conducive niche for salivary gland cells, enhancing cell viability and function[439,440]. Cryoelectrospun elastin-alginate scaffolds mimic the native extracellular matrix, steering cell adhesion and proliferation[441].

Hydrogel-based techniques are also pivotal. Matrigel, widely used for its ECM-like properties, supports the formation of complex organoid structures, facilitating functional studies of salivary glands[442–446]. A blend of collagen and Matrigel has been shown to enhance the structural and functional mimicry of native tissues [447,448]. Laminin-peptide conjugated fibrin hydrogel offers improved cell-matrix interactions, promoting better cell differentiation and organoid formation than fibrin hydrogels alone [449]. Growth factor-encapsulated HA/alginate hydrogel provides a sustained release of growth factors to support cell growth and differentiation[450]. Alginate hydrogel microtubes support 3D cell culture, enhancing cell viability and function[451,452]. Versatile and tunable, PEG hydrogels offer a customizable environment for salivary gland cell culture[453,454].

Magnetic bioassembly and 3D bioprinting are innovative techniques in this field. Magnetic bioassembly uses magnetic forces to assemble cells into desired structures, offering precision and scalability [455,456]. 3D bioprinting leverages bioinks and printing technologies to create complex, functional salivary gland constructs[457]. These studies highlight the ongoing progress and diverse methodologies employed to develop effective 3D salivary gland models, contributing to advancements in regenerative medicine and disease model . In particular, see Chapter 3, we successfully developed a scaffold-free, spheroid model with a non-necrotic core for non-oncologic studies by co-culturing stromal cells (e.g., NIH 3T3 fibroblasts) and salivary epithelial cells (e.g., SCA-9 cells), establishing a more consistent and controlled environment for observing cellular dynamics than prior models, which are greater than 200 µm in diameter [458–460]. Building upon this advancement, the current study aims to employ this innovative model to explore the effects of radiation in the milieu of cellular senescence. We hypothesized that the burden of the senescence-associated secretory phenotype would elicit a significant increase in fibrotic markers post-radiation in a 3D salivary gland model.

To test the hypothesis, we simulated the senescence microenvironment using a senescence-conditioned medium generated from senescent IMR-90 fibroblasts, which is a widely used cell line for senescence studies. Furthermore, we confirmed the effects of X-ray radiation at the optimal dose in a scaffold-free, 3D co-cultured salivary spheroid model and, in particular, evaluated fibrotic responses to radiation in the presence of the senescence-conditioned medium. This study would establish and validate a 3D radiated salivary gland model that can be used to reveal mechanisms that drive fibrotic processes and potentially influence future therapeutic approaches for conditions characterized by enhanced fibrotic activity.

4.2 Materials and methods

4.2.1 Cell culture

NIH 3T3 mouse embryonic fibroblasts (at passages 12-17)[461] Click or tap here to enter text.and SCA-9 mouse salivary epithelial cell line [393], derived from an undifferentiated chemically induced carcinoma of the murine submandibular gland, were utilized to model salivary gland stromal and epithelial components. Cell lines were maintained in DMEM (high glucose) medium supplemented with 10% fetal bovine serum (FBS) and 1% penicillin-streptomycin, all sourced from Thermo Fisher Scientific (Waltham, MA). Cultures were incubated in a humidified environment at 37°C with 5% CO_2 and passaged every three or four days upon reaching 70-80% confluence.

4.2.2 Preparation of senescence-conditioned medium

4.2.2.1. culture of senescent IMR-90 fibroblasts

IMR-90 cells (ATCC CCL-186, fibroblasts isolated from normal human lung tissue derived from a 16-week-old female fetus)[462] were used to generate senescence-conditioned medium(Dulbecco's Modified Eagle Medium (DMEM)(ThermoFisher Scientific, Waltham, MA. with 1% PenStrep (ThermoFisher Scientific, Waltham, MA.) , which is a well-established model for inducing cellular s enescence [462,463]. A total of 7 x 10^5 cells were seeded into T75 flasks (Thermo Fisher, Fairport, NY), maintained in xxx medium, supplemented with xxx, and incubated at 37°C at 5% CO_2 until reaching 70-80% confluence, typically within 3-4 days, indicative of a thriving, low population doubling (PD) culture. Cells were then detached using 0.05% trypsin/EDTA?? (Thermo Fisher Scientific). Trypsin activity was halted by adding fresh medium and centrifugation to segregate viable cells from debris. Next, the cell pellet was resuspended, and cell counts, viability, and cumulative PD were checked using a Bio-Rad TC20 Automated Cell Counter (Bio-Rad, Hercules, CA) to calculate the cumulative PD, a critical

metric in the assessment of cell aging. This calculation integrated the initial and final cell counts, adjusted for the PD levels at both the seeding and counting phases. Through repeated cycles of seeding, growing, and splitting the fibroblasts, we observed an extension in the time required for cultures to achieve confluence, eventually resulting in the discontinuation of cell division. This phase marked the onset of senescence, at which point the cells were evaluated for senescence markers or prepared for downstream analysis. Notably, due to the enlarged size of senescent cells, we observed that the apparent confluence of the culture did not correlate with actual cell count, underscoring the importance of PD stability and the presence of senescence markers as more reliable indicators of the senescent state. Throughout this procedure, we utilized proliferating primary fibroblasts as the control group, providing a benchmark against evaluating the progression toward senescence.

4.2.2.2. Collection and storage of senescence-conditioned medium

After reaching senescence, 7 x 10^5 senescent IMR-90 fibroblasts were seeded in a T75 flask and cultured in xxx mL xxx medium. After culturing for xxx days, senescence-conditioned medium was collected. The "strength" of the senescence-conditioned medium was normalized based on cell number to maintain specific metabolic conditions and ensure consistent nutrient availability across different experimental setups. Hence, cells were counted after removing the senescence-conditioned medium to ascertain the cell number before replating or other analyses. The collected senescence-conditioned medium was centrifuged at 500 x g for 5-10 minutes to remove cell debris. The supernatant was then transferred to 50-milliliter conical tube for storage at -80°C adapted from previous report (Neri et al., 2021).

4.2.3 2D and 3D irradiated cell culture models

4.2.3.1. Radiation of 2D culture of fibroblasts or salivary epithelial cells

For 2D experiments, NIH 3T3 fibroblasts or SCA-9 salivary epithelial cells were cultured in 24-well plates until they reached 70-80% confluence. Subsequent X-ray exposure was performed using the Faxitron RX 650 Cabinet X-Radiator™ System (Faxitron X-Ray LLC, Tucson, AZ), applying doses of 0 Gy (as a negative control), 4 Gy, 8 Gy, 12 Gy, and 16 Gy to investigate dose-dependent effects on cell viability, DNA damage, apoptosis, and senescence.

4.2.3.2. 3D spheroids of co-cultured NIH 3T3 fibroblasts and SCA-9 salivary epithelial cells

For 3D experiments, including DNA damage, apoptosis, senescence, and fibrosis in NIH 3T3: SCA-9 spheroids, we generated spheroids by culturing NIH 3T3 fibroblasts and SCA-9 cells in a 5:1 ratio. We seeded 160 cells per well in 50 µL of cell culture medium in non-adherent Biofloat® 96-well plates (faCellitate, Mannheim, Germany). The 96-well plates with added cells were then centrifuged at 250 x g for 5 minutes and incubated at 37°C with 5% CO_2 to form spheroids. The medium was exchanged every three days by removing 30 µL of medium and then adding 30 µL of fresh medium.

Four different conditions were established through this experiment: negative control (C) with regular medium; senescence-conditioned medium (CM); X-ray exposure to 16 Gy (X), which is the optimal dose determined by radiation of 2D culture; and senescence-conditioned medium for three days prior to a 16 Gy radiation dose (CMX). All spheroids were cultured in regular medium for three days to allow them to reach size maturity (160 µm). On day three, the medium in half of the wells (conditions (C) and (X)) was replaced with fresh regular medium, and the medium in the other half of the wells (conditions (CM) and (CMX)) was replaced with the senescence-conditioned medium. The cells were incubated for an additional 72 hours. After the 72-hour incubation, the X and CMX spheroids were subject to 16 Gy of radiation. The (C) and (X) conditions were placed in the X-ray chamber for the same period, but with no radiation.

Additionally, spheroids were consolidated by systematically transferring spheroids from individual wells to two or three wells corresponding to their condition (e.g., CM). Spheroids were then fixed in 4% paraformaldehyde (Thermo Fisher Scientific) for 30 min on ice, washed four times with PBS-Tween (0.5% v/v Tween 20 (Thermo Fisher Scientific) in 1X PBS, PBS-T before treatment with reagents such as H2AX.

4.2.3.3 Radiation studies of 3D co-cultured spheroids

Spheroids in covered, round-bottomed 96-well plates containing 30 µL of medium were placed in the Faxitron RX 650 Cabinet X-Radiator™ System (Faxitron X-Ray LLC, Lincolnshire, IL). The energy of the X-ray beam was 120 kV and the exposure rate was 150 Gy per minute. Spheroids were exposed to deliver a single dose of 16 Gy. Control spheroids were placed in the X-Radiator for the same period without irradiation.

4.2.4 Cell viability assay in 2D culture

Cell viability for 2D cultures was assessed at 72 hours post-irradiation using the LIVE/DEAD^{TM} Viability/Cytotoxicity Kit (Thermo Fisher Scientific). Live cells were detected by the presence of intracellular esterases that convert the nonfluorescent cell-permeant calcein AM to fluorescent calcein; simultaneously, dead cells were detected by the permeation of red fluorescent ethidium homodimer-1 due to loss of plasma membrane integrity. Briefly, cells were washed with phosphate-buffered saline (PBS) three times, and then calcein AM and ethidium homodimer-1 were added to final concentrations of 2 µM and 4 µM, respectively. After adding calcein AM and ethidium homodimer-1, cells were incubated at room temperature for 40 minutes per the manufacturer's instructions (Thermo Fisher Scientific, Invitrogen). Images were captured using the EVOS M7000 microscope imaging system with GFP (482/524 nm) and RFP (542/593 nm) filters (Thermo Fisher Scientific) and processed using ImageJ. The viability metric (% dead

cells) was calculated using ImageJ by determining the percentage of red fluorescence (dead cells) to the total fluorescence, which is the sum of both green and red fluorescence (dead cells). Treatment with 70% methanol for ten minutes was used as a positive control of cell death.

4.2.5 Immunocytochemistry analysis of phosphorylated H2AX to detect DNA damage

4.2.5.1. DNA damage detection in irradiated 2D culture

To detect DNA double-strand breaks in NIH 3T3 and SCA-9 cells cultured in 2D cultures, we utilized Anti-phospho-Histone H2A.X (Ser139) Antibody (clone JBW301, FITC conjugate) (Millipore, Darmstadt, Germany). This FITC-conjugated mouse monoclonal antibody is specifically designed to bind to the phosphorylated form of histone H2AX, a marker indicative of DNA damage. Following radiation exposure, cells were incubated at 37 °C for 30 minutes before proceeding with the staining protocol. Cells were fixed in 4% paraformaldehyde in 5% (w/v) sucrose and 0.6X PBS for 15 minutes at room temperature, permeabilized with 0.1% Triton X-100 in PBS for 10 minutes and blocked with 5% bovine serum albumin (BSA) in PBS for 1 hour to minimize non-specific antibody binding. The fixed cells were then incubated overnight at 4°C with the anti-phospho-histone H2A.X antibody at a dilution of 3 µg/mL

Following incubation, cells were washed three times with PBS. Etoposide-treated cells were employed as a positive control to ensure the assay's sensitivity to DNA damage, while the 0 Gy dose served as a negative control. Each radiation dose, including controls, was replicated across 12 wells. After washing DAPI was added at a concentration of 1 µg/mL for nuclear visualization of the total cell population. Images were captured using an EVOS M7000 imaging system with DAPI (357/447 nm) and GFP (482/524 nm) filters and processed using ImageJ to determine % fluorescent H2AX by dividing the total area of phosphorylated H2AX by total area of DAPI

staining, providing a quantitative measure of H2AX phosphorylation, thereby reflecting the extent of DNA damage induced by X-ray exposure.

4.2.5.2. DNA damage detection in 3D Spheroids

3D spheroids were produced and cultured as described in Section 4.4.2.3.2, including treatment with normal medium and senescence-conditioned medium. On day six, thirty minutes after irradiation at 16 Gy (or no irradiation), the spheroids initially in individual wells were combined into two wells per condition within the 96-well Biofloat plates. This consolidation process made handling and processing the spheroids easier, allowing for more efficient media changes and treatment applications. These spheroids were then fixed in 4% paraformaldehyde in 5% (w/v) sucrose and 0.6X PBS for 30 minutes, followed by permeabilization with 0.4% Triton X-100 for 30 minutes. After permeabilization, the spheroids were washed again using PBS and then blocked for 2 hours in 5% BSA in PBS at room temperature to prevent nonspecific binding. Spheroids were then incubated overnight at 4 °C with Anti-phospho-Histone H2A.X (Ser139) Antibody (clone JBW301, FITC conjugate). After staining, spheroids were washed in PBS and counterstained with DAPI for nuclear visualization. The stained spheroids were carefully transferred to an 8-chamber glass-bottomed cell culture slide, (CELLTREAT®, Port Washington, NY) for imaging. Fluorescence microscopy was employed to capture the FITC signal from the anti-phospho-histone H2A.X antibody and the DAPI signal for nuclei. Images were captured using an EVOS M7000 imaging system with DAPI (357/447 nm) and GFP (482/524 nm) filters and processed using ImageJ to determine % fluorescent H2AX as described above, with comparisons made across the four treatment groups to assess the impact of senescence-conditioned medium and X-ray irradiation on DNA damage within the 3D spheroids.

4.2.6 Apoptosis assay in irradiated 2D cultures

After radiation exposure, cells were incubated for four hours in a humidified 37°C incubator with 5% CO_2. After incubation, cells were washed with PBS. The PBS was then removed and replaced with a solution of 25 µL Annexin V– Alexa Fluor 488 Conjugate (Thermo Fisher Scientific) in 100 µL Annexin V binding buffer (10 mM HEPES, 140 mM NaCl, and 2.5 mM $CaCl_2$, pH 7.4) per well to detect apoptotic cells and 7.48 µM propidium iodide (Thermo Fisher Scientific) to detect necrotic/late apoptotic cells. The cells were incubated in the stain for 15 minutes. After staining, cells were washed with Annexin V binding buffer and then imaged using fluorescence microscopy. Images were captured using the EVOS M-7000 with GFP (482/524 nm), and RFP (542/593 nm) filters (Thermo Fisher Scientific, Carlsbad, CA) and processed using ImageJ. The percentage of apoptotic cells was calculated by dividing the area of apoptotic cells by the total area occupied by cells. Staurosporine treatment was used as a positive control for Annexin V assays.

4.2.7 Determination of Senescence Using a Fluorescent Beta-galactosidase Substrate

4.2.7.1 Cellular senescence detection in 2D cultures

Following radiation exposure, cells were washed with PBS, the medium was replaced, and the cells were returned to the incubator. The medium was changed again on days six and nine. On day ten, cells were washed with PBS, and then 100 µL of fixation solution containing 4% paraformaldehyde in 5% (w/v) sucrose and 0.6X PBS was added to each well for 15 minutes. The cells were kept on ice in the dark during fixation. Following fixation, cells were washed with 1% BSA in PBS. Next, 100 µL of prewarmed working solution was added to each well. The prewarmed working solution was prepared by diluting CellEvent™ Senescence Green Probe (Thermo Fisher Scientific) 1:1000 into the pre-warmed CellEvent™ Senescence Buffer (Thermo Fisher). Next, the plates were then covered with plastic film to minimize evaporation. Cells

were incubated at 37°C for 2 hours in a non-CO_2 environment to maintain the optimal pH for the enzymatic reaction. After incubation, the working solution was discarded, and the cells were washed 3 times with PBS to remove unreacted stain. Images were captured using the EVOS M7000 with GFP (482/524 nm) and processed using ImageJ. The percentage of senescence-associated beta-galactosidase activity was measured by quantitation of green fluorescence relative to the total area covered by DAPI-stained?? cells.

4.2.7.2 Cellular senescence detection in 3D spheroids

Ten days post-irradiation, spheroids were stained to detect senescence-associated beta-galactosidase activity. Spheroids were consolidated in round-bottomed 96-well plates and then washed with PBS. Next, 100 µL of fixation solution containing 4% paraformaldehyde in 5% (w/v) sucrose in PBS was added to each well; these spheroids were kept on ice for 30 minutes. Following fixation, spheroids were washed with 1% BSA in PBS to eliminate any leftover fixation solution and to block nonspecific sites. Next, 100 µL of prewarmed working solution was added to each well. The prewarmed working solution was prepared by diluting the CellEvent™ Senescence Green Probe (1,000X concentration) into the pre-warmed CellEvent™ Senescence Buffer. Next, the plates were covered with plastic film to minimize evaporation. Cells were incubated at 37°C for 2 hours in a non-CO_2 environment to maintain the optimal pH for the enzymatic reaction. After incubation, the working solution was discarded, and the cells were washed 3 times with PBS to remove unreacted stains. Next, 100 µL of pre-prepared DAPI solution (1µg/mL in PBS) was added to each well and the spheroids were incubated for 15 minutes at room temperature in the dark. Following incubation, the cells were washed three times with PBS to remove excess DAPI. Finally, 100 µL of PBS was added to each well before imaging. Imaging was carried out using an EVOS M7000 imaging system with GFP (470/525

nm) and DAPI (357/447 nm) filters and processed using ImageJ. The percentage of green fluorescence was measured as a percentage of the total 2D area of the spheroid, which was determined by measuring the area of blue stain from DAPI.

4.2.8 Evaluation of Fibrotic Response in Irradiated 3D Spheroids

4.2.8.1 Immunocytochemistry analysis of expression of fibrosis markers in 3D spheroids

Immunocytochemistry was performed to assess the expression of fibrosis marker, collagen I and myofibroblast marker, α-SMA in NIH 3T3: SCA-9 spheroids subjected to various treatments as described above. For immunocytochemistry, spheroids 10 days post-irradiation were fixed using a solution containing 4% paraformaldehyde in 5% (w/v) sucrose and 0.6X PBS for 30 minutes at room temperature, permeabilized with 0.4% Triton X-100 in PBS for 30 minutes and blocked with 5% BSA in PBS for 2 hours at room temperature to minimize non-specific antibody binding. Following the blocking step, spheroids were incubated overnight at 4°C with primary antibodies targeting α-SMA (mouse Anti-Actin, α-Smooth Muscle antibody, 1:300 dilution) (Sigma Aldrich, Catalog # A5228) and collagen I (rabbit Anti-Collagen I, 1:300 dilution) (Millipore Sigma, Catalog # AB745) Following the incubation period, the spheroids were washed five more times followed by incubation with DAPI and secondary antibodies for 4 hours. Alexa Fluor 488 Donkey Anti-Rabbit IgG was the secondary antibody to identify collagen I. (catalog# ab150073, 1:400 dilution) and to identify α-SMA was Alexa Fluor 647 Donkey Anti-Mouse IgG (catalog# 715-606-150, 1:400 dilution) (Jackson ImmunoResearch Laboratories). Images were captured using the EVOS M-7000 with DAPI (357/447 nm), GFP (482/524 nm), and RFP (542/593 nm) filters (Thermo Fisher Scientific) and processed using ImageJ. The expression of each marker was quantified by % fluorescence that was calculated by dividing the

total area of α-SMA by the total area of DAPI and the total area of Collagen I fluorescence by the total area of DAPI.

4.2.8.2 Picrosirius red staining of collagen fibers in 3D spheroids

After culturing, spheroids were consolidated, fixed, and washed as described in section 2.3. After washing, the spheroids were subjected to a series of dehydration steps using sucrose solutions. Spheroids were first exposed to a 10% sucrose solution, followed by increasing concentrations up to 30% sucrose. Each step involved an hour of refrigeration at 4 °C, except for the final sucrose solution, which was refrigerated overnight.

Subsequently, spheroids, were placed into a silicone mold with about 32 spheroids per mold. A very thin layer (~0.8 mm) of tissue freezing medium (Leica, Deer Park, IL) was added to cover the spheroids, and they were refrigerated at 4 °C and frozen the following day using liquid nitrogen, which was poured around the silicone molds (molds were not submerged). Next, more tissue freezing medium was added to create a thicker block, which was also frozen with liquid nitrogen. This method positioned the spheroids near the surface of the block, making it easier to section them for analysis. The samples were then stored horizontally at -80°C until they were sectioned into 5-μm sections using a cryostat (CM 1950, Leica Biosystems, Nussloch, Germany). After cryopreservation and sectioning, picrosirius red (PSR) staining was employed to quantify and assess the distribution of collagen in spheroid sections. Samples were dipped in Bouin's fluid (Newcomer Supply, Middleton, WI., Catalog # 1020B) five times, then removed and allowed to dry overnight at room temperature to fix the sample. The following day, the Bouin's fluid temperature was increased to 60°C, and the samples were placed in the Bouin's fluid for one hour to enhance fixation. After fixation, the samples underwent ten dips in tap water to remove excess fixative. The samples were then stained with PSR (Scytek, Logan, UT, Catalog #

SRS999) by immersion for 15 minutes, followed by rinsing under running tap water for one minute to wash off unbound dye. The samples were subsequently immersed in picric acid (Newcomer Supply, Middleton, WI. Catalog # 1336B) for 40 minutes to enhance staining contrast. Following this, the samples were dehydrated in 100% isopropanol for five minutes. Dehydration continued with five dips in 100% ethanol, which was repeated once with unused 100% ethanol, to ensure thorough water removal. This was followed by 10 dips in a xylene/ethanol mixture (1:1 ratio) and three consecutive xylene washes—lasting one minute, one minute, and two minutes, respectively—to clear the tissue of any remaining ethanol. Finally, the slides were mounted using a non-aqueous mounting medium, Fisher Chemical™ Permount™ Mounting Medium (Thermo Fisher Scientific), to preserve the stained tissue for microscopic examination.

Brightfield images of the samples, stained with PSR, were captured using the EVOS M7000 imaging system. The captured images were subsequently analyzed using ImageJ software. To quantify the proportion of collagen in each section, images were first converted to 8-bit grayscale. The total area of each section was quantified via thresholding as follows: First, the images were split into three color channels: red, green, and blue. Next, the green channel lower and upper thresholds for pixel intensity were set to (0,146) respectively to measure the total area. Subsequently, the red area lower and upper thresholds for pixel intensity were set to (0,75). This red area was subtracted from the total section area to calculate the percentage of the area occupied by collagen.Heat maps were generated to examine differences in signal intensity visually and depict areas of increasing signal intensity within the collagen-defined area. This was achieved using the Heatmap Histogram plugin for ImageJ. The plugin counts pixels for each

gray value in an 8-bit or 16-bit image within a defined interval, transforming the image into a heatmap complete with a calibration bar.

4.2.9 Statistical analysis

Quantitative data were expressed as mean ± SEM (standard error of mean). Descriptive statistics were compiled to summarize cell viability, DNA damage, apoptosis, and collagen deposition across the four treatment groups. One-way ANOVA was performed to determine the significance of treatment effects on collagen accumulation, followed by Tukey's multiple comparisons test to discern differences between specific treatment groups. The Brown-Forsythe and Bartlett's tests were utilized to evaluate the homogeneity of variances among the groups. These analyses were performed using GraphPad Prism version 10.0.0 for Windows, GraphPad Software, Boston, Massachusetts USA, www.graphpad.com"

4.3 Results

4.3.1 Effects of radiation dosages on 2D cultured SCA-9 salivary epithelial cells and NIH 3T3 fibroblasts

4.3.1.1 SCA-9 and NIH 3T3 viability post-irradiation

We examined the effects of X-ray exposure on SCA-9 cell viability across a range of doses (0, 4, 8, 12, and 16 Gy). Our study revealed a significant increase in percentage of dead cells (i.e., reduction in viability) as radiation dose increased from 0 to 16 Gy (Fig. 1, A-F, M). One-way ANOVA indicated a profound effect of radiation on cell viability ($p < 0.0001$), with the dose variation accounting for 99% of the response variability (R-squared = 0.99). Tukey's multiple comparisons further confirmed that viability at all irradiated doses was significantly lower compared to the control group. Particularly, the transition from non-irradiated cells to 4 Gy exposure showed an average viability decrease of over 11%, and the reduction continued to be

significant at higher doses. However, the difference between 8 Gy and 12 Gy was insignificant, suggesting a threshold effect within this range. The most significant decrease in cell viability occurred at 16 Gy, indicating severe cytotoxic effects.

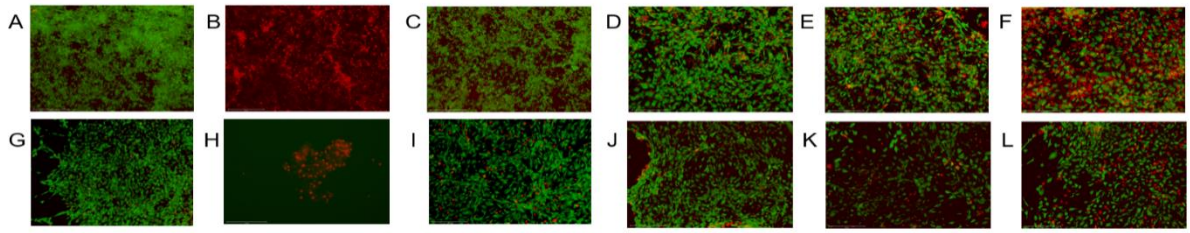

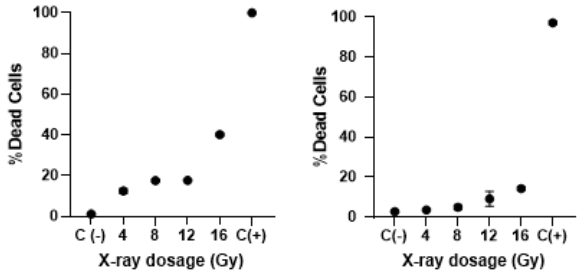

Figure. 4.1. Effect of the radiation dosage on cell viability. (A-L) Fluorescence images of LIVE/DEAD staining of 2D cultures of SCA-9 (A-F) and NIH 3T3 (G-H) cells exposed to increasing doses of radiation. (A,G) negative control (C(-), 0 Gy); (B,H) positive control (C(+), treated with 70% methanol); (C,I) 4 Gy; (D,J) 8 Gy; (E,K) 12 Gy; (F,L) 16 Gy. Scale bar = 275 μm. (M,N) Quantification of LIVE/DEAD stained SCA-9 (M) and NIH 3T3 (N) show the percentage of dead cells (mean ± SEM) under different X-ray exposures. SCA-9, N=4. NIH 3T3, N=2,3,4,3,4,4 for C (-), 4,8,12,16 Gy and C (+), respectively.

Similarly, the effects of radiation on NIH 3T3 cell viability showed that higher doses significantly increased cell mortality, especially at 16 Gy (Figure 4.1, G-L, N). One-way ANOVA results showed a significant impact of radiation dose on cell death ($p = 0.0108$), with about 70% of variability in cell death explained by dose differences. However, lower doses did not exhibit significant increases in mortality compared to the control, suggesting a higher threshold for observable effects on NIH 3T3 fibroblasts. The homogeneity of variances,

confirmed by the Brown-Forsythe test (p = 0.5578), supported the validity of the ANOVA findings.

4.3.1.2 Analysis of DNA damage in 2D cultures of SCA-9 and NIH 3T3 post-irradiation

NIH 3T3 fibroblasts showed a significant increase in phosphorylated H2AX expression at 16 Gy compared to the control group (Fig. 4.2), indicating DNA damage; the ANOVA results approached statistical significance, F(4, 33) = 2.366, P = 0.0729, indicating potential differences in DNA damage between the groups.

In SCA-9 cells, Following the ANOVA results, Tukey's posthoc analysis revealed a significant difference in phosphorylated H2AX expression at 16 Gy compared to all other doses (0, 4, 8, and 12 Gy) (Fig. 4.3).

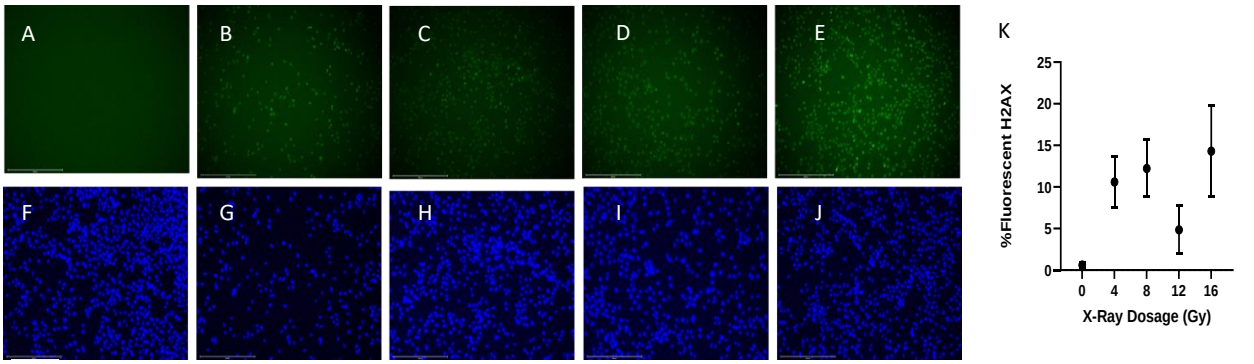

Figure 4.2 2D DNA damage assay of NIH 3T3 cells subject to 0 Gy, 4 Gy, 8 Gy, 12 Gy, or 16 Gy of X-ray exposure as indicated by H2AX phosphorylation. (A-E) Fluorescence images of phosphorylated H2AX expression in green. (F-J) Fluorescence images of DAPI-stained nuclei to show total cell population. (A,F) negative control (0 Gy); (B,G) 4 Gy; (C,H) 8 Gy; (D,I) 12 Gy; (E,J) 16 Gy. Scale bar = 275 μm. (K) Quantification of H2AX fluorescence percentage (total area of phosphorylated H2AX / total area of DAPI staining).

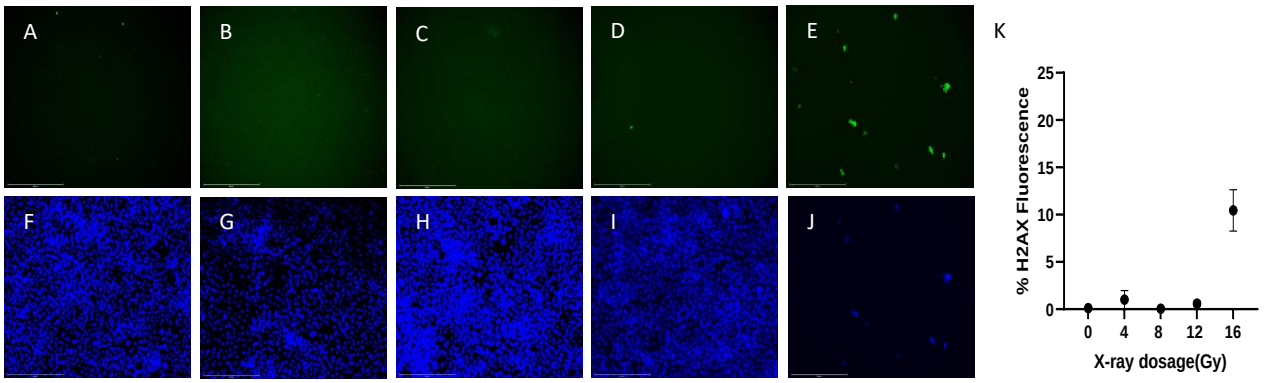

Figure 4.3. 2D DNA damage in SCA-9 cells subjected to X-ray exposure as indicated by H2AX phosphorylation. (A-E) Fluorescence images of H2AX expression in green. (F-J) Fluorescence images of DAPI-stained nuclei to show total cell population. (A,F) 0 Gy; (B,G) 4 Gy; (C,H) 8 Gy; (D,I) 12 Gy; (E,J) 16 Gy. Scale bar = 275 μm. (K) Quantification of H2AX fluorescence percentage (total area of phosphorylated H2AX / total area of DAPI staining).

4.3.1.3 SCA-9 and NIH 3T3 cell apoptosis post-irradation

Apoptosis in SCA-9 and NIH 3T3 fibroblasts was evaluated after exposure to varying radiation doses and quantified using Annexin V fluorescence, a marker for early apoptotic events (Fig. 4.4). In SCA-9 cells, apoptosis was significantly induced only at the highest radiation dose of 16 Gy, with no significant changes observed at lower doses (0, 4, 8, and 12 Gy, Fig. 4A-E, K). One-way ANOVA confirmed the effect of radiation dose on apoptosis ($F(4, 64) = 2.894$, $p = 0.0289$), although the variance explained by the treatment was relatively low (R-squared = 0.1531). Tukey's post hoc test further isolated the 16 Gy dose as significantly different, indicating a threshold effect where apoptosis markedly increased only at this high dose. The variance across treatment groups was not homogenous, suggesting differing responses to radiation doses.

In contrast, the NIH 3T3 cells displayed a more pronounced dose-dependent increase in apoptosis. The ANOVA results showed a significant effect of radiation dose on apoptosis levels for by the radiation dose. The highest dose of 16 Gy notably increased apoptosis compared to both the control and the lower radiation doses. Tukey’s multiple comparisons indicated

significant differences between the highest dose and the control and across increasing dose levels from 4 to 16 Gy. No significant increases were observed among the lower doses or between these doses and the control, highlighting a threshold effect at 16 Gy. However, NIH 3T3 cells showed generally lower level of annexin V staining.

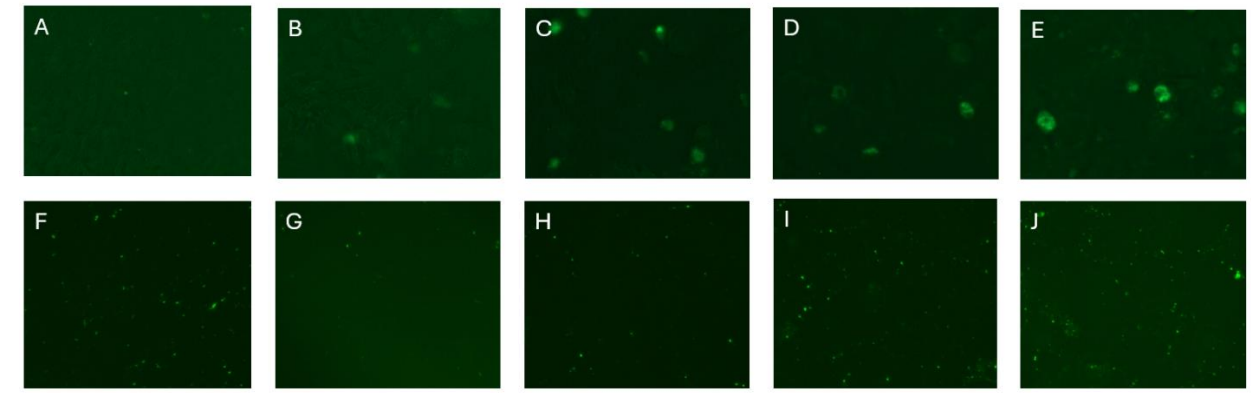

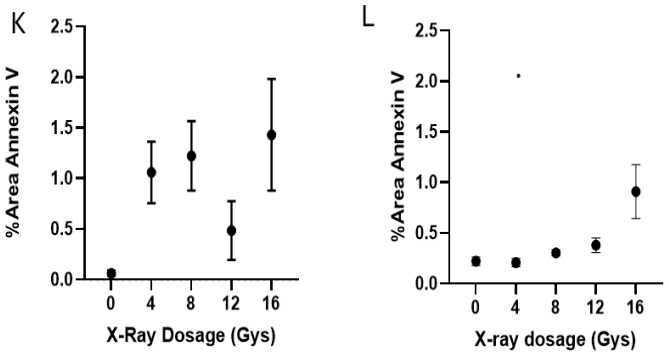

Figure 4.4. Apoptosis in 2D cultures of SCA-9 and NIH 3T3 cells as a function of radiation dose ranging from 0 to 16 Gy. Four hours post-irradiation, cultures were stained for Annexin V (in green) to assess apoptosis. (A-E) Fluorescence images of SCA-9 cells. Scale bar = 125 µm. (F-J) Fluorescence images of NIH 3T3 fibroblasts. Scale bar = 275 µm. (A,F) Negative control (0 Gy). (B,G) 4 Gy. (C,H)8 Gy. (D,I) 12 Gy. (E,J) 16 Gy. (K,L) Quantification of cell apoptosis of SCA-9 (K) and NIH 3T3 (L). SCA-9, N = 14. NIH 3T3, N=18, 19, 22, 19, and 18 for 0 Gy, 4 Gy, 8 Gy, 12 Gy, and 16 Gy, respectively.

4.3.1.4 SCA-9 and NIH 3T3 cell senescence post irradiation

Examination of senescence in SCA-9 and NIH 3T3 cells exposed to radiation revealed differing responses across varying doses (Fig. 4.5). SCA-9 cells showed no significant increase in senescence-associated beta-galactosidase activity with increasing radiation doses up to 16 Gy (Fig. 5, A-E, K). One-way ANOVA confirmed no significant differences in senescence levels

(F(4, 75) = 2.141, P = 0.0840), and the R-squared value was relatively low (0.1025), suggesting minimal influence of radiation dose on senescence in these cells. Tests for homogeneity of variance confirmed consistent variability across groups.

In contrast, NIH 3T3 cells showed an observable, though not statistically significant, increase in senescence at higher radiation doses, particularly at 16 Gy (Figure 4.3, F-J, L). Despite the visible increase in senescence-associated activity, statistical analyses (One-way ANOVA: F(4, 135) = 1.893, p = 0.1152) did not show significant differences, with a low R-squared value

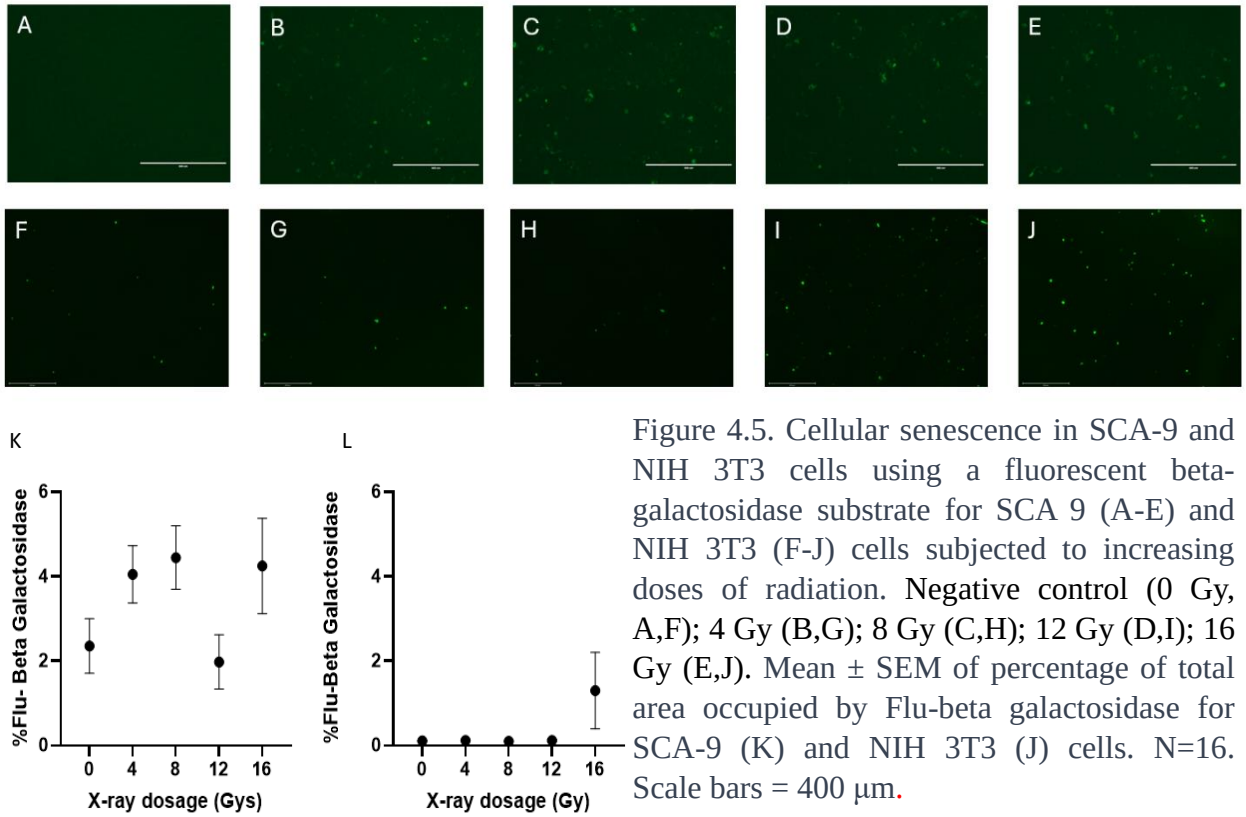

Figure 4.5. Cellular senescence in SCA-9 and NIH 3T3 cells using a fluorescent beta-galactosidase substrate for SCA 9 (A-E) and NIH 3T3 (F-J) cells subjected to increasing doses of radiation. Negative control (0 Gy, A,F); 4 Gy (B,G); 8 Gy (C,H); 12 Gy (D,I); 16 Gy (E,J). Mean ± SEM of percentage of total area occupied by Flu-beta galactosidase for SCA-9 (K) and NIH 3T3 (J) cells. N=16. Scale bars = 400 μm.

(0.05311) indicating that radiation dose poorly explained the variance in senescence. The variance homogeneity tests yielded conflicting results, suggesting potential disparities in data distribution, especially at higher doses.

We chose 16 Gy as the best dosage to use for the reabased on several key findings from prior experiments. Initially, we conducted dose-response studies on NIH 3T3 fibroblasts and SCA-9 salivary epithelial cells cultured in two-dimensional (2D) systems. These studies examined a range of doses: 0 Gy, 4 Gy, 8 Gy, 12 Gy, and 16 Gy. Our results indicated that 16 Gy was the most effective in inducing significant levels of cytotoxic effects, DNA damage, apoptosis, and senescence in these cells.

Specifically, the 16 Gy dose resulted in a notable increase in apoptosis compared to both the control and lower radiation doses, as demonstrated by Annexin V staining. The ANOVA results confirmed a significant effect of radiation dose on apoptosis levels, with the highest dose showing significant differences from the control and lower doses, highlighting a threshold effect at 16 Gy. Additionally, 16 Gy was found to increase phosphorylated H2AX expression significantly, indicating substantial DNA damage.

Given these findings, we concluded that 16 Gy was the optimal dose for further experiments, particularly in our 3D co-culture spheroid model, as it provided a clear and pronounced response across multiple cellular and molecular endpoints

4.3.2 DNA Damage Response in NIH 3T3: SCA-9 Spheroids Cultured in Senescence-conditioned Medium and Subject to X-ray Irradiation at 16 Gy

Next, NIH 3T3 fibroblasts and SCA-9 salivary epithelial cells were co-cultured in a 5:1 ratio, seeded at 160 cells per well in non-adherent 96-well plates, and centrifuged to form spheroids,

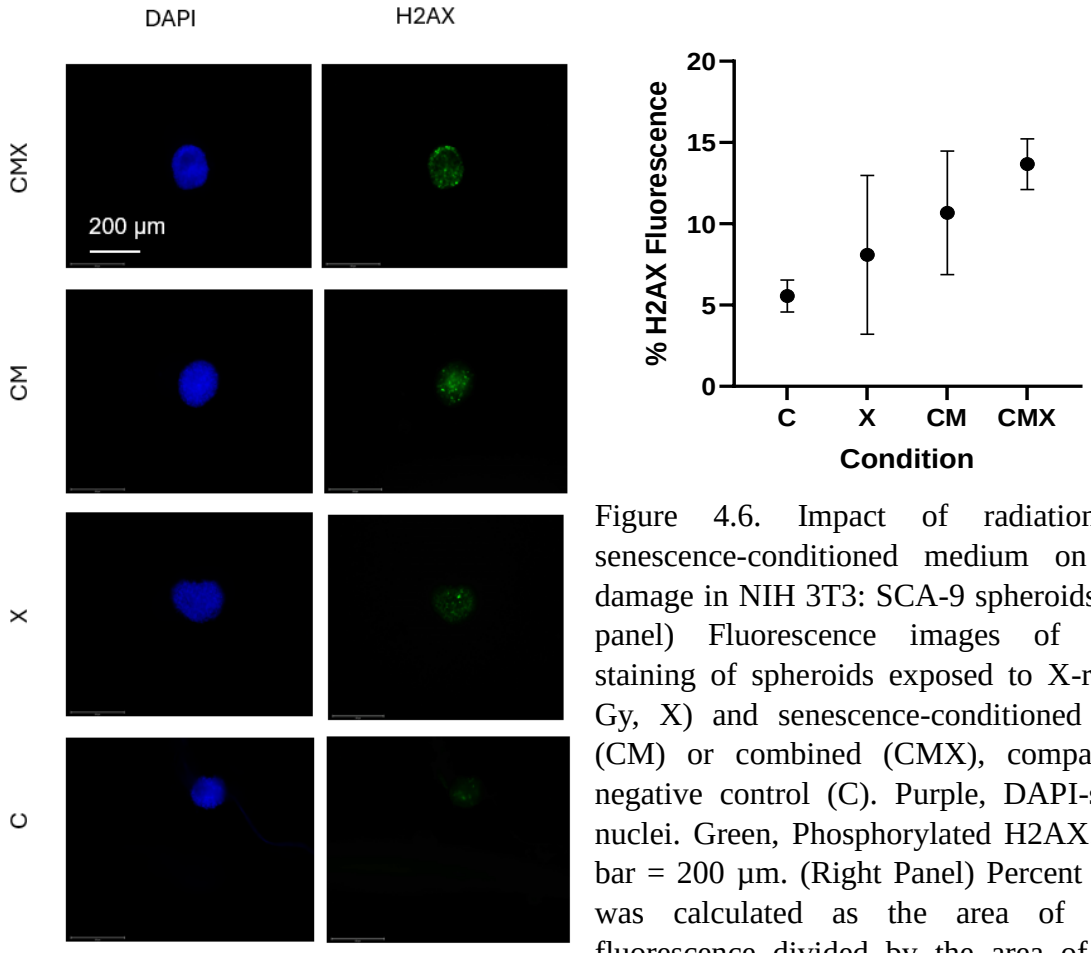

Figure 4.6. Impact of radiation and senescence-conditioned medium on DNA damage in NIH 3T3: SCA-9 spheroids. (Left panel) Fluorescence images of H2AX staining of spheroids exposed to X-ray (16 Gy, X) and senescence-conditioned media (CM) or combined (CMX), compared to negative control (C). Purple, DAPI-stained nuclei. Green, Phosphorylated H2AX. Scale bar = 200 µm. (Right Panel) Percent H2AX was calculated as the area of H2AX fluorescence divided by the area of DAPI fluorescence using ImageJ. C, N=12; X, N=2; CM, N=3; CMX, N= 43.

which were then incubated at 37°C with 5% CO2 with regular medium changes every three days. We evaluated spheroid responses to four different experimental conditions: control (C), spheroids cultured in regular medium; X-ray exposure only (X) at 16 Gy; senescence-conditioned medium only (CM); and combined senescence-conditioned medium with X-ray

exposure (CMX), starting with assessment of DNA damage by expression of phosphorylated H2AX (Figure. 4.6). While both the X-ray-treated and senescence-conditioned medium-treated spheroids showed apparent increases in DNA damage, statistical comparisons between the control and either the X or CM groups alone an tween the X and CM groups compared to the CMX group did not reach statistical significance, suggesting that the observed effect is specifically associated with the combined treatment. Notably, the CMX group exhibited the highest mean value, suggesting a potential additive effect of the senescence-conditioned medium and X-ray exposure on DNA damage. Group standard deviation varied minimally, indicating consistent responses within each treatment condition. One-way ANOVA revealed a statistically significant difference among the four treatment groups ($F(3, 17) = 15.38$, $p < 0.0001$), explaining approximately 73.08% of the variance in H2AX phosphorylation levels. The absence of significant variance in standard deviations among the groups, as indicated by the Brown-Forsythe test ($p = 0.4241$), suggests that the observed differences in means are not due to the heterogeneity of variance. Post hoc analyses using Tukey's HSD test identified a significant increase in DNA damage in the CMX group compared to the control (mean difference = -0.2779, $p < 0.0001$), indicating that the combination of senescence-conditioned medium and X-ray exposure significantly exacerbates DNA damage. These results support the hypothesis that senescence-conditioned medium exacerbates DNA damage in NIH 3T3: SCA-9 spheroids exposed to radiation, as evidenced by a significant increase in H2AX phosphorylation levels in the CMX group compared to controls. The absence of significant differences between the control and either the X or CM groups alone, and between these groups and the CMX group, underscores the specificity of the senescence-conditioned medium effect when combined with X-ray exposure.

4.3.3 The Impact of senescence-conditioned medium on senescence induction in NIH 3T3: SCA-9 spheroids post X-ray irradiation

The effects of senescence-conditioned medium on the induction of senescence in NIH 3T3: SCA-9 spheroids exposed to radiation were explored using a fluorescent substrate to assay beta-galactosidase activity (Figure. 4.7). This study aimed to determine if pre-treatment with senescence-conditioned medium would amplify the senescence response to radiation. Overall, the study demonstrated that pre-treatment with senescence-conditioned medium significantly amplified the senescence response to radiation in NIH 3T3 SCA-9 spheroids, whereas X-ray exposure alone or CM alone did not significantly increase senescence levels compared to the control. The ANOVA results showed a significant influence of the treatment conditions on senescence induction ($F(3, 17) = 15.38$, $P < 0.0001$), with an R-squared value of 0.7308. This

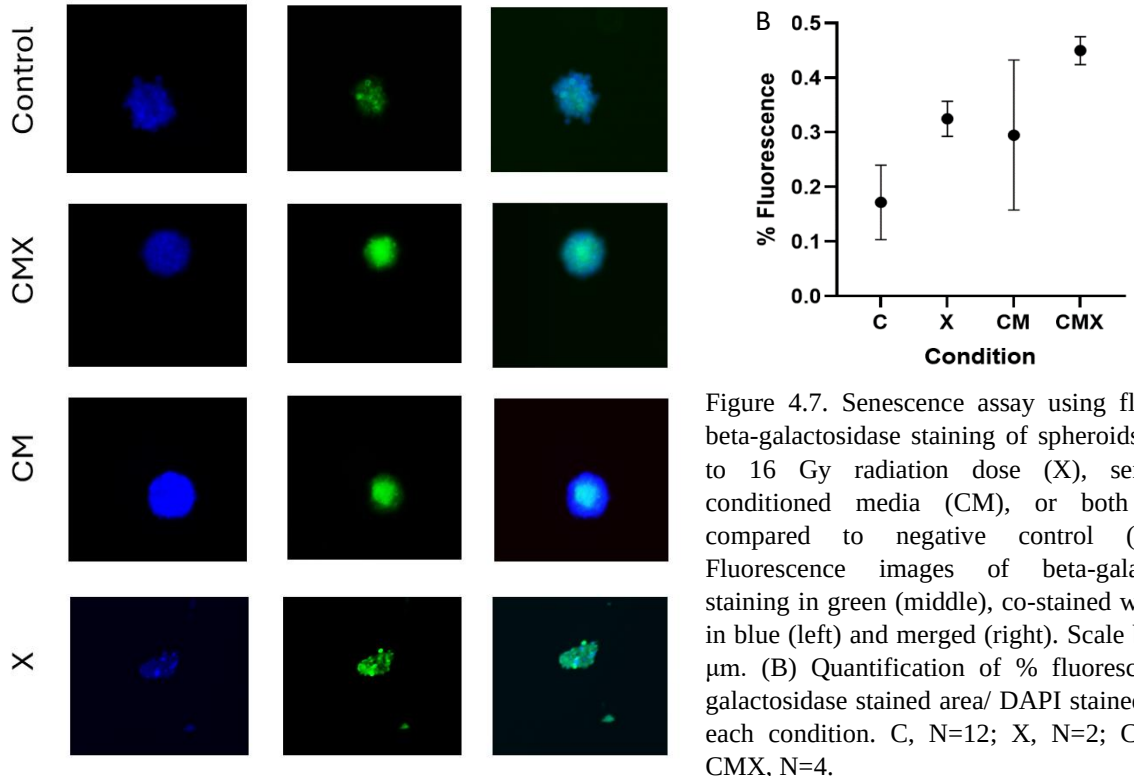

Figure 4.7. Senescence assay using fluorescent beta-galactosidase staining of spheroids exposed to 16 Gy radiation dose (X), senescence-conditioned media (CM), or both (CMX), compared to negative control (C). (A) Fluorescence images of beta-galactosidase staining in green (middle), co-stained with DAPI in blue (left) and merged (right). Scale bar = 200 µm. (B) Quantification of % fluorescent beta-galactosidase stained area/ DAPI stained area for each condition. C, N=12; X, N=2; CM, N=3; CMX, N=4.

indicates that the treatment conditions explained approximately 73% of the variance in senescence levels. Subsequent post hoc analysis using Tukey's multiple comparisons tests revealed detailed differences between the groups. The most notable finding was a significant increase in senescence levels in spheroids pre-treated with senescence-conditioned medium. Then, it was exposed to radiation (CMX), with a mean difference of -0.2779 compared to the control group, indicating a heightened senescence response ($P < 0.0001$). No significant differences were observed between the control and the other two treatment conditions (X and CM), suggesting that neither X-ray exposure alone nor senescence-conditioned medium alone was sufficient to increase senescence levels significantly compared to the control. Future studies with larger sample sizes would be warranted given the trend observed.

The comparisons between X-ray-only (X) and senescence-conditioned medium-only (CM) conditions did not show significant differences, nor did the comparison between X-ray exposure alone and the combination of senescence-conditioned medium with X-ray exposure (X vs. CMX). However, a trend was noted towards increased senescence in the CMX group compared to other treatments, albeit not reaching statistical significance in all cases.

4.3.4 Effect of senescence-conditioned medium on fibrosis NIH 3T3: SCA-9 spheroids post X-ray irradiation

4.3.4.1 Expression of collagen I and α-SMA in response to 16 Gy X-ray exposure

We investigated the fibrotic response of NIH 3T3: SCA-9 spheroids to radiation and senescence-conditioned medium, starting with the expression of myofibroblast marker, α-SMA and fibrosis marker, collagen I. As before, four experimental conditions were analyzed: control (C), X-ray

only (X), senescence-conditioned medium only (CM), and senescence-conditioned medium followed by irradiation (CMX).

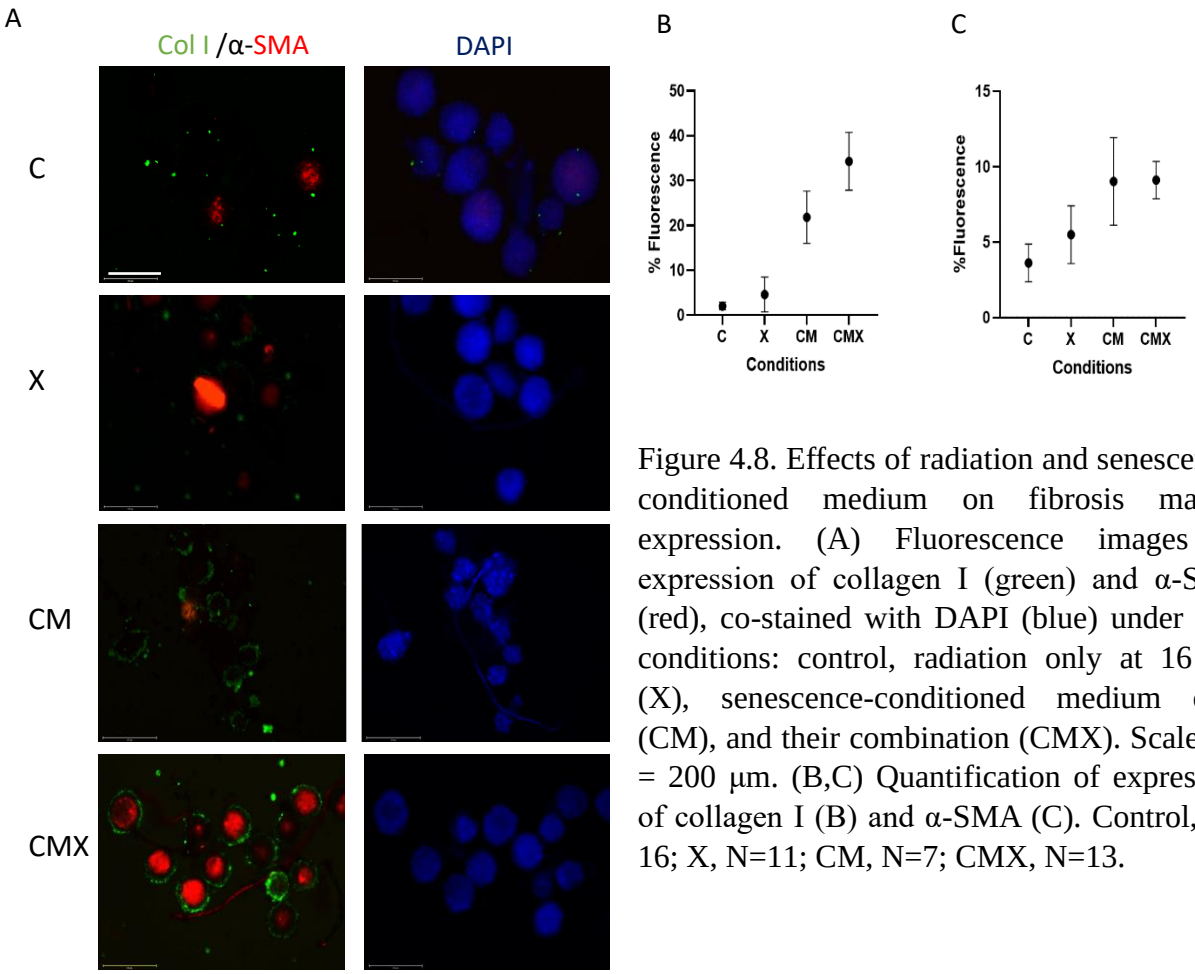

Figure 4.8. Effects of radiation and senescence-conditioned medium on fibrosis marker expression. (A) Fluorescence images of expression of collagen I (green) and α-SMA (red), co-stained with DAPI (blue) under four conditions: control, radiation only at 16 Gy (X), senescence-conditioned medium only (CM), and their combination (CMX). Scale bar = 200 μm. (B,C) Quantification of expression of collagen I (B) and α-SMA (C). Control, N= 16; X, N=11; CM, N=7; CMX, N=13.

No significant differences were observed in the mean expression levels of α-SMA across the four groups. One-way ANOVA was performed to assess the statistical significance of differences among the mean expression levels of α-SMA across the four groups. The analysis yielded a P-value of 0.6204, indicating no significant difference among the groups. Further analysis using Tukey's multiple comparisons test confirmed the lack of statistically significant differences. This outcome challenges our initial hypothesis and highlights the complexity of fibrotic signaling pathways in the context of senescence and radiation exposure.

The study further investigated the effects of senescence-conditioned medium and X-ray exposure on the expression of collagen I in NIH 3T3: SCA-9 spheroids, exploring another facet of the fibrotic response (Figure 4.8). A one-way ANOVA revealed significant differences in collagen I expression among the four groups. Subsequent Brown-Forsythe and Bartlett tests confirmed the significance.

4.3.4.2. Picrosirius red staining of cryosectioned spheroids

Further investigation into fibrotic responses across different culture conditions in a 3D microtissue model of the salivary gland using PSR staining of cryosectioned spheroids revealed significant variations in collagen deposition. The senescence-conditioned medium and irradiation (CMX) combination significantly enhanced collagen deposition within the microtissue model. Furthermore, these findings highlight the differential impact of culture conditions on the fibrotic phenotype of 3D salivary gland microtissues, with the combined effect of senescence conditioning and radiation exposure markedly accelerating collagen accumulation, a hallmark of fibrosis (Figure 4.9).

Statistical evaluation via one-way ANOVA demonstrated a profound effect of treatment on collagen deposition ($F(3, 37) = 69.47$, $p < 0.0001$, R-squared = 0.8492), confirming significant differences among the groups. These findings highlight the differential impact of culture conditions on the fibrotic phenotype of 3D salivary gland microtissues, with the combined effect of senescence-conditioning and radiation exposure markedly accelerating collagen accumulation, a hallmark of fibrosis.

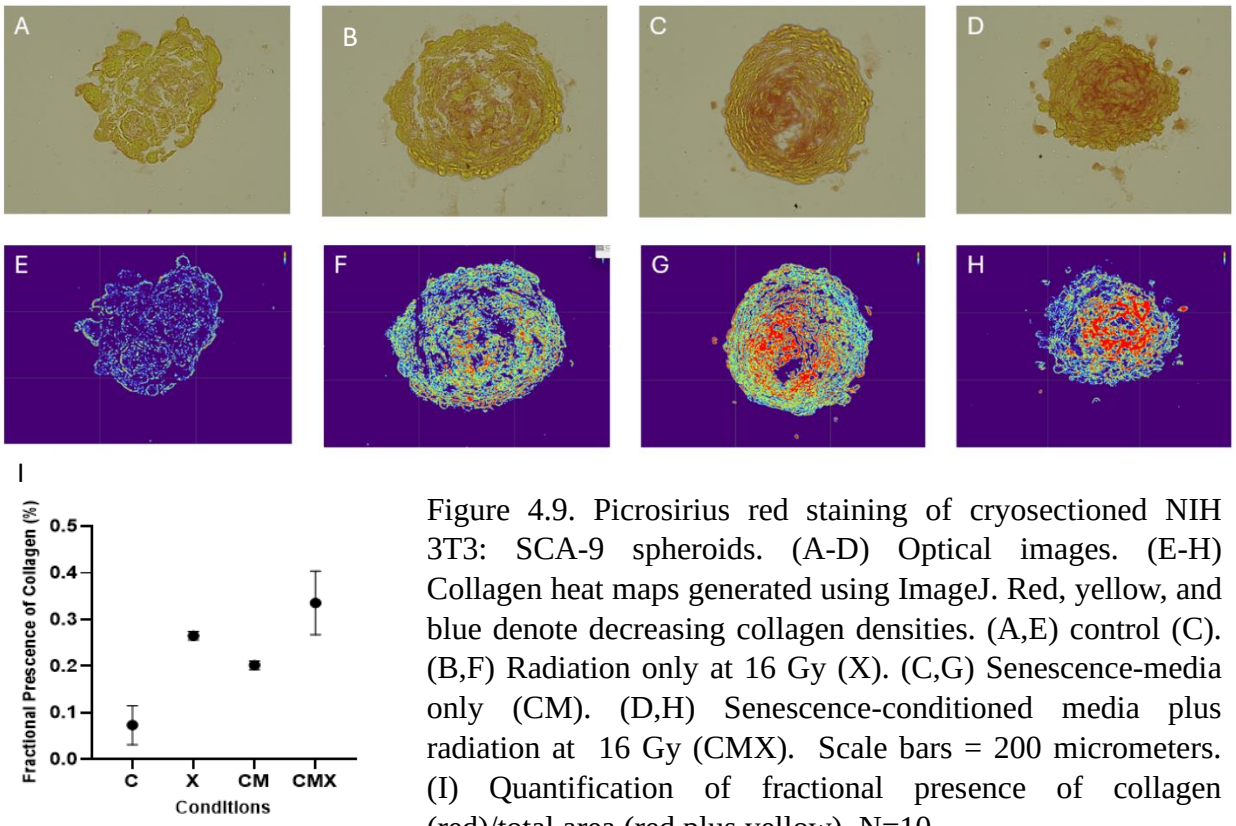

Figure 4.9. Picrosirius red staining of cryosectioned NIH 3T3: SCA-9 spheroids. (A-D) Optical images. (E-H) Collagen heat maps generated using ImageJ. Red, yellow, and blue denote decreasing collagen densities. (A,E) control (C). (B,F) Radiation only at 16 Gy (X). (C,G) Senescence-media only (CM). (D,H) Senescence-conditioned media plus radiation at 16 Gy (CMX). Scale bars = 200 micrometers. (I) Quantification of fractional presence of collagen (red)/total area (red plus yellow). N=10.

4.4 Discussion

Our study highlights the complex interplay between cellular senescence, the SASP, and the fibrogenic processes following radiation exposure. The significant increase in collagen deposition, particularly in the presence of a senescence-conditioned medium, underscores the role of senescent cells in promoting fibrotic environments. The SASP, characterized by the secretion of pro-inflammatory cytokines, chemokines, and growth factors, influences the behavior of neighboring cells and tissue microenvironment. In our study, the use of the senescence-conditioned medium, which contains these SASP factors, provides a relevant context to explore their impact on fibrotic responses. Conversely, the nuanced response of α-SMA expression points to the multifaceted nature of fibrosis, suggesting that fibrogenesis can be

modulated through various cellular actors and signaling pathways beyond the traditional myofibroblast-centric view.

This study's contributions to the field extend beyond the empirical findings; they stimulate further inquiry into the mechanisms driving fibrosis and offer a foundation for developing strategies to mitigate such effects in radiation therapy. The detailed examination of SASP components and their impacts on fibrotic outcomes would provide a roadmap for identifying new therapeutic targets within the complex senescence-associated secretome.

Translating these findings into therapeutic strategies offers a promising horizon for managing radiation-induced fibrosis. Identifying key SASP factors in promoting fibrosis allows targeted interventions to neutralize these components or inhibit their production. Furthermore, exploring senolytic agents that can selectively clear senescent cells presents an opportunity to alleviate the profibrotic pressures within irradiated tissues. These approaches, grounded in a deep understanding of the cellular responses to radiation and the senescence phenotype, promise to enhance the therapeutic efficacy of radiation therapy while minimizing its adverse sequelae.

As we advance our understanding of the cellular dynamics in radiation-induced fibrosis, the insights from this study beckon a more nuanced approach to cancer treatment that harmonizes the oncological imperative of eradicating tumor cells while preserving tissue integrity and function. The journey from bench to bedside is fraught with challenges. However, the potential to improve patient outcomes by integrating these molecular insights into therapeutic strategies offers an inspiring direction for future research and clinical practice.

Our experiments with SCA-9 cells with a tumorigenic origin revealed no significant increase in senescence when treated with a senescence-conditioned medium and subjected to X-ray irradiation. This resilience against senescence-inducing stressors, likely due to inherent defense

mechanisms in tumor-derived cells, underscores the complexity of cellular aging and the adaptive strategies of tumor cells to bypass growth arrest [432].

Contrastingly, the same conditions led to pronounced DNA damage in co-cultured spheroids, as indicated by increased H2AX phosphorylation. This result suggests that factors in the senescence-conditioned medium, part of the SASP, sensitize cells to radiation, potentially exacerbating DNA damage through interference with repair mechanisms or increased oxidative stress [465]. To confirm these findings, further investigation with possibly larger sample sizes or different statistical methods might be warranted.

Moreover, our findings highlight a significant role of senescence-conditioned medium in enhancing fibrotic responses, notably through increased collagen deposition in spheroids. This suggests that SASP factors facilitate the transformation of fibroblasts into myofibroblasts, enhancing extracellular matrix production and fibrosis and compromising tissue function [466].

The synergy between senescence signals and radiation in promoting fibrogenesis underscores the therapeutic potential of targeting the senescent microenvironment. Approaches like senolytics or senomorphics, which modulate detrimental senescence pathways, could theoretically enhance treatments like mesenchymal stem cell therapy for fibrosis, providing a dual strategy to counteract radiation-induced fibrosis.

The differential expression of fibrotic markers such as collagen I and α-SMA in response to radiation and senescence-conditioned medium further delineates the complex regulatory mechanisms of fibrosis influenced by the cellular microenvironment.

Our study highlights the significant role of the senescence-conditioned medium and X-ray irradiation in enhancing collagen I deposition across treatment groups, particularly in those receiving both treatments (CMX group). This enhanced collagen deposition, a hallmark of

fibrotic diseases, suggests that factors in the senescence-conditioned medium, particularly SASP components, might stimulate profibrotic cytokines and growth factors, thereby promoting increased collagen production by fibroblasts and myofibroblasts [466–469].

Interestingly, despite the increase in collagen deposition, α-SMA expression remained unchanged, suggesting a dissociation between collagen production and myofibroblast activation. This finding indicates that collagen deposition may be regulated through alternative pathways independent of myofibroblast transdifferentiation, highlighting the complexity of fibrotic processes and suggesting the need for further research into specific pathways and cell types involved in fibrosis under senescent and genotoxic stress conditions [470].

These observations contribute to a nuanced understanding of fibrosis, emphasizing that fibrogenic responses can vary significantly depending on the cellular environment and external stimuli. The absence of increased α-SMA expression alongside elevated collagen levels underscores the diversity of fibrotic pathways. This could lead to new therapeutic strategies targeting specific aspects of fibrosis, such as collagen deposition, without impacting myofibroblast activity.

Furthermore, our findings underline the complexities of radiation therapy, particularly the challenge of inducing fibrosis in adjacent healthy tissues, highlighting the importance of precision in radiation dosing. Modulating the tissue microenvironment to inhibit SASP could mitigate fibrosis, improving the therapeutic ratio of radiation therapy by minimizing its adverse effects on healthy tissue.

The role of senescence-conditioned medium in enhancing fibrotic responses highlights a novel therapeutic opportunity. By targeting the senescence-associated secretory phenotype (SASP), characterized by pro-inflammatory cytokines, chemokines, and growth factors, we can

potentially limit the fibrogenic consequences of radiation therapy. Therapeutic strategies include senolytics to eliminate senescent cells, thereby reducing the SASP or modulators to adjust the secretion profiles of these cells, minimizing their impact on tissue fibrosis. Identifying specific SASP factors exacerbating fibrosis could lead to targeted therapies to neutralize these factors or block their effects on responsive cells.

4.5 Conclusion and future research directions

Our findings suggest new avenues for optimizing radiation therapy by targeting the mechanisms of radiation-induced fibrosis and the modulatory effects of the senescent microenvironment. Future research should focus on translating these benchtop insights into clinical strategies to improve treatment efficacy and patient quality of life. Bridging the gap between in vitro results and clinical applications is essential, recognizing the complexity of in vivo biological systems. To confirm these findings, further investigation with possibly larger sample sizes or different statistical methods might be warranted.

Limitations and prospects for further study

Our findings underscore the importance of exploring the temporal dynamics of senescence and fibrosis to understand the initiation and progression of fibrosis post-radiation. Investigating these patterns through longitudinal studies could reveal critical intervention points to alter the course of fibrosis. Furthermore, there is substantial potential for developing targeted interventions against the SASP. Strategies include designing small molecule inhibitors, monoclonal antibodies, and other biologics to neutralize specific SASP factors or block their receptor interactions. Employing senolytics to enhance the clearance of senescent cells could also reduce the profibrotic effects of the SASP.

Chapter 5: Conclusions and Future Directions

5. Summary of key findings

Throughout this investigative journey, we explored the intricate dynamics between cellular senescence and radiation-induced damage, primarily focusing on 3D salivary gland spheroid models. As we progressed through each chapter, a sequence of significant findings emerged, laying the foundation for future research in this domain.

One of the most striking discoveries was the pivotal role that senescent cells play in modulating radiation responses. These cells, which have undergone a permanent growth arrest, displayed unique properties in the face of radiation. Their distinct secretory profile, the Senescence-Associated Secretory Phenotype (SASP), was revealed to influence neighboring cells significantly.

Our experiments suggested that conditioned media, enriched with factors from senescent cells, provided a protective shield against radiation-induced DNA damage. This observation was counterintuitive and highlighted the potential therapeutic avenues that might be derived from understanding the SASP.

We observed a clear link between the presence of senescent cells and the onset of fibrosis in the spheroid models. This connection is especially critical given the detrimental impact of fibrosis on tissue functionality.

It was also intriguing to note that not all senescent cells responded uniformly. Depending on their induction method—whether replicative senescence or stress-induced premature senescence—their behavior and impact on surrounding cells varied, indicating a layered complexity within the realm of senescence.

By drawing these key conclusions, we have expanded the existing knowledge base on the subject and set the stage for further studies that can dive deeper into each of these findings. This journey through the world of senescence and radiation has shed light on areas previously shrouded in mystery and opened up new, promising avenues for therapeutic interventions.

6.1 Implications of research conclusions

The findings from this research have opened a window into the complex interplay between senescence, radiation, and tissue response, and revelations bear far-reaching implications across various scientific domains.

The understanding that senescent cells, particularly the SASP, can modulate tissue response to radiation is groundbreaking for regenerative medicine. Recognizing the protective or detrimental roles of senescent cells can guide strategies for tissue regeneration, especially in scenarios where radiation therapy is a prerequisite. Harnessing the protective properties of conditioned media or modulating the senescent cell population might offer avenues for enhanced tissue recovery post-radiation.

The protective effect of conditioned media against radiation-induced DNA damage reshapes our understanding of radiation biology. Traditional views have often considered radiation to exert uniform effects across tissues. However, this research underscores that specific cellular factors can significantly influence radiation outcomes. Such insights can guide the development of treatments that reduce the side effects of radiation or enhance its therapeutic efficacy.

Our exploration of senescence has illuminated the heterogeneity of senescent responses based on the nature of their induction. It underscores that senescent cells are passive, aged entities and active in shaping tissue microenvironments. This expanded understanding can have implications in aging research, where the accumulation of senescent cells is a hallmark, and in diseases where senescence plays a role, such as fibrotic disorders or certain cancers.

The discovery that senescent cell behavior can vary based on its induction mode suggests that therapies targeting senescent cells must be fine-tuned based on the specific context. Broad-spectrum anti-senescence or senolytic treatments might not be universally beneficial, and a more tailored approach could be the key to maximizing therapeutic gains.

The successful use of 3D salivary gland spheroids in this research underscores the potential advantages of employing physiologically relevant model systems. Such systems can bridge the gap between in vitro and in vivo studies, providing more accurate representations of in vivo scenarios.

The insights gleaned from this research have paved the way for reevaluating established norms in multiple scientific areas. They remind us that biological systems are dynamic and interconnected, and a shift in one component can ripple through the entire system, influencing outcomes in ways previously unimagined.

6.2 Future directions

The journey undertaken in this dissertation has traversed the intricate pathways of cellular senescence, radiation response, and tissue repair, offering a fresh perspective on how these entities interact, influence, and are influenced by one another. Some key conclusions drawn from this body of work include:

One of the pivotal findings has been the protective role of senescence-conditioned media against radiation-induced DNA damage. This observation underscores the multifaceted nature of senescent cells, highlighting their potential as end-of-the-line cells marked by growth arrest and as dynamic entities that can actively influence their surroundings.

The research has revealed that while senescence can be protective against immediate radiation damage, its prolonged presence or the continuous influence of senescence-associated secretory phenotype (SASP) can promote fibrotic changes, emphasizing the dual role senescence plays in tissue health.

The evident transformation of tissue towards a fibrotic state in the presence of conditioned media from senescent cells post-radiation underscores the profound influence that senescent cells exert on tissue microenvironments. This relationship between senescence and fibrosis can have profound implications for several pathologies where fibrosis is a detrimental outcome.

The research also emphasized the robustness and relevance of 3D salivary gland spheroids as a model system. Their physiological relevance enabled a closer mimicry of in vivo conditions, yielding insights that might have been overlooked in traditional 2D models.

The variations observed in cellular response based on the media condition, whether regular, senescence-conditioned, or DMEM, emphasize the intricate nature of cellular metabolism, growth, and response mechanisms. Such findings highlight the need for meticulous experimental designs in future studies, ensuring that variables like media composition are appropriately considered.

In summing up, this dissertation has expanded the understanding of senescence beyond its traditionally perceived roles. By delving deep into the intersections of senescence, radiation, and

tissue health, we have unraveled layers of complexity that, while challenging established norms, offer exciting possibilities for the future of regenerative medicine, radiation therapy, and aging research.

The discoveries and insights from this dissertation contribute to the existing body of knowledge and illuminate paths for further exploration. As the boundaries of our understanding expand, so too do the horizons of what can be achieved. Here are some critical areas of exploration that emerge as future directions based on the work presented.

6.2.1 Senolytic and anti-senescent treatments

Targeting Senescent Cells with Senolytics: Senolytic agents, which selectively target and eliminate senescent cells, have gained significant attention in recent years for their potential in rejuvenation therapies and combating age-related diseases. Given the findings of this dissertation, exploring how these agents impact radiation-damaged tissues that harbor senescent cells could be transformative. Can they effectively reduce the senescent cell burden in such tissues? And if so, does this alleviation improve tissue health and function post-radiation?

Another avenue is modulating the SASP. Given that SASP factors have been seen to influence radiation response and tissue fibrosis, understanding how to manipulate these secretions could hold the key to mitigating detrimental effects. This endeavor involves studying molecules or interventions that can suppress the pro-fibrotic elements of SASP or enhance its beneficial components.

Understanding the therapeutic window for these interventions is needed. When is the optimal time post-radiation to introduce senolytic or anti-senescent treatments to achieve the best outcomes? Is there a "golden hour" post-exposure when intervention is most beneficial?

A promising strategy would be the combination of radiation with senolytics or anti-senescent agents. Such a synergistic approach might enhance the therapeutic effects of radiation while minimizing its side effects, especially in cancer treatment, where radiation is a mainstay.

While immediate effects can be gauged, the long-term implications of using senolytic or anti-senescent treatments in the context of radiation exposure remain an open question. Would these treatments confer long-term benefits to tissue health and function? Or might there be unforeseen complications that emerge over time?

Incorporating these future directions into subsequent research endeavors would be instrumental in achieving a holistic understanding of senescence modulation in radiation biology. Moreover, these investigations could pave the way for innovative therapeutic strategies that address the immediate aftermath of radiation exposure and sculpt long-term outcomes for improved health and longevity.

6.2.2 Enhanced 3D models for studying radiation response

Significance of 3D Models: Traditional 2D cell culture systems, while foundational to our understanding of cellular processes, often lack the complex intercellular interactions and microenvironments found in vivo. 3D culture systems, conversely, can more closely mimic the physiological conditions of tissues and organs. Given the intricate dynamics of radiation response involving multiple cell types and intricate cell-cell and cell-matrix interactions, employing advanced 3D tissue models is crucial for generating physiologically relevant and translatable data.

Incorporation of Multiple Cell Types: One key feature that advanced 3D models can incorporate is the co-culture of multiple cell types. Given that radiation affects not just a single cell type but

the entire tissue ecosystem, models that include numerous resident cell types of a particular tissue (e.g., fibroblasts, epithelial cells, immune cells) can offer a more comprehensive understanding of radiation response.

Leveraging microfluidic technologies allows for creating "organ-on-a-chip" models where dynamic cellular interactions can be studied in real time. Such models could be instrumental in understanding radiation's immediate and delayed effects at a microphysiological level.

Different types of radiation (e.g., X-rays, gamma rays, alpha particles) may have varying effects on tissues. Advanced 3D models can be employed to understand these differential effects, providing insights into the mechanistic underpinnings of tissue response to diverse radiation types.

With the advancement of imaging technologies, it's now possible to monitor cellular and subcellular processes in 3D models in real time. Such dynamic monitoring post-radiation exposure could provide invaluable insights into the immediate cellular responses, onset of senescence, and emergence of other radiation-induced phenotypes.

3D models can be complemented by computational modeling to predict radiation responses based on various parameters. Such integrative approaches can be powerful in anticipating outcomes and guiding experimental designs.

In summary, the enhancement and employment of advanced 3D tissue models stand as a frontier in radiation biology. By their ability to emulate physiological conditions, these models promise to unveil deeper and more relevant insights into how tissues and organs respond to radiation. The knowledge gleaned from such studies can be instrumental in devising strategies to protect, mitigate, or repair radiation-induced damage.

6.2.3 Exploring molecular mechanisms further

Understanding the Interplay: While this dissertation has touched upon some critical molecular pathways, especially concerning the transition between senescence and fibrosis, there is still a vast landscape of molecular interactions yet to be explored. The cellular response to radiation and the interplay between senescence and fibrosis is multifaceted, with multiple molecular pathways likely contributing to the observed phenotypes.

Role of Non-Coding RNAs: Recent research has highlighted the significance of non-coding RNAs, including microRNAs and long non-coding RNAs, in modulating cellular responses to various stimuli, including radiation. Their potential role in governing the transition between senescence and fibrosis or modulating the SASP could be fertile ground for exploration.

Post-Translational Modifications: Beyond gene expression changes, post-translational modifications (such as phosphorylation, acetylation, and ubiquitination) can dramatically influence protein activity and stability. Exploring these modifications, especially in critical proteins involved in senescence or fibrosis, can provide a deeper understanding of radiation-induced changes at the molecular level.

Interplay with Metabolism: Cellular metabolism is tightly linked to many cellular processes, including senescence. Exploring shifts in metabolic pathways, such as glycolysis or oxidative phosphorylation, in response to radiation can shed light on the metabolic requirements of senescent cells and how they may differ from non-senescent counterparts.

Systems Biology Approach: Instead of focusing on individual pathways or molecules, a systems biology approach considers the network of interactions and how they collectively contribute to

cellular outcomes. Employing this approach can help understand the complex interplay of molecular pathways following radiation exposure.

Feedback Mechanisms: Cellular responses are often regulated by feedback mechanisms, where the output of a pathway can influence its input. Identifying and understanding these feedback loops, especially in radiation response, senescence, and fibrosis, could be pivotal in predicting long-term outcomes and potential therapeutic interventions.

Integration with Clinical Data: While molecular studies in laboratory models provide invaluable insights, integrating these findings with clinical data can validate their relevance in real-world scenarios. Such an integrative approach can ensure that the explored mechanisms directly affect patient care and treatment outcomes.

In summary, while significant strides have been made in understanding the molecular underpinnings of radiation response, senescence, and fibrosis, much terrain remains to be charted. Delving deeper into these mechanisms, with advanced technologies and integrative approaches, will pave the way for a more comprehensive understanding and potentially novel therapeutic interventions.

6.2.4 Recommendations for further studies

Expanding the Cell Types: While the current dissertation has centered on salivary gland spheroids and their response to radiation in the presence of senescent cues, it is crucial to expand the study to other cell types. Different cells might have unique radiation responses, and understanding these nuances could offer a broader perspective on radiation biology.

In Vivo Models: While 3D spheroid models provide a more physiological context than 2D cultures, in vivo animal models are a step closer to understanding responses in a living organism.

For instance, mouse or rat models could provide insights into systemic responses, tissue-tissue interactions, and more comprehensive physiological outcomes post-radiation.

A detailed time-course study of post-radiation exposure could provide insights into the immediate and long-term molecular and cellular changes. Such a study could delineate the chronological sequence of events, from the immediate DNA damage response to the eventual tissue remodeling or fibrosis.

In the clinical setting, radiation is often given with other treatments, such as chemotherapy. Understanding how these combined treatments impact senescence and subsequent tissue outcomes could be of significant relevance.

With the advent of single-cell RNA sequencing technologies, dissecting cellular responses at an individual cell level is now possible. Given the heterogeneity of cellular responses to stimuli like radiation, single-cell studies could unearth previously unappreciated nuances in how different cells within a tissue or spheroid respond.

Beyond transcriptomics, incorporating proteomics, metabolomics, and even epigenomics could offer a multi-dimensional view of the cellular response to radiation in the context of senescence. Such an integrative approach can provide a holistic understanding of the changes occurring within the cells.

Given the rising interest in senolytic agents that selectively target senescent cells, understanding which senescent cells (induced by radiation or otherwise) are sensitive to which senolytic agents could be pivotal. It could also pave the way for combining treatments that utilize radiation and senolytics for therapeutic benefits.

Beyond molecular markers, functional assays that assess cellular capabilities (e.g., migration assays, wound healing assays for fibrosis studies) could provide a more tangible measure of the impact of radiation and senescence on cellular behavior.

Numerous avenues remain to be explored in the vast and ever-evolving field of radiation biology intersecting with cellular senescence. While not exhaustive, the above recommendations provide a direction for subsequent research endeavors to deepen our understanding and uncover novel therapeutic possibilities.

REFERENCES

1. de Paula, F.; Teshima, T.H.N.; Hsieh, R.; Souza, M.M.; Nico, M.M.S.; Lourenco, S.V. Overview of Human Salivary Glands: Highlights of Morphology and Developing Processes. *Anat Rec* **2017**, *300*, 1180–1188, doi:10.1002/AR.23569.

2. Deasy, J.O.; Moiseenko, V.; Marks, L.; Chao, K.S.C.; Nam, J.; Eisbruch, A. Radiotherapy Dose–Volume Effects on Salivary Gland Function. *International Journal of Radiation Oncology*Biology*Physics* **2010**, *76*, S58–S63, doi:10.1016/J.IJROBP.2009.06.090.

3. Ravi, M.; Paramesh, V.; Kaviya, S.R.; Anuradha, E.; Paul Solomon, F.D. 3D Cell Culture Systems: Advantages and Applications. *J Cell Physiol* **2015**, doi:10.1002/jcp.24683.

4. Schmidt, M.; Scholz, C.J.; Polednik, C.; Roller, J. Spheroid-Based 3-Dimensional Culture Models: Gene Expression and Functionality in Head and Neck Cancer. *Oncol Rep* **2016**, *35*, 2431–2440, doi:10.3892/or.2016.4581.

5. Aging and Cellular Senescence.Pdf.

6. Stojanovic, S.D.; Fiedler, J.; Bauersachs, J.; Thum, T.; Sedding, D.G. Senescence-Induced Inflammation: An Important Player and Key Therapeutic Target in Atherosclerosis. *Eur Heart J* **2020**, *41*, 2983–2996, doi:10.1093/eurheartj/ehz919.

7. Campisi, J. Aging, Cellular Senescence, and Cancer. *Annu Rev Physiol* **2013**, *75*, 685–705, doi:10.1146/ANNUREV-PHYSIOL-030212-183653.

8. Coppé, J.P.; Desprez, P.Y.; Krtolica, A.; Campisi, J. The Senescence-Associated Secretory Phenotype: The Dark Side of Tumor Suppression. *Annu Rev Pathol* **2010**, *5*, 99–118, doi:10.1146/ANNUREV-PATHOL-121808-102144.

9. Basisty, N.; Kale, A.; Jeon, O.H.; Kuehnemann, C.; Payne, T.; Rao, C.; Holtz, A.; Shah, S.; Sharma, V.; Ferrucci, L.; et al. A Proteomic Atlas of Senescence-Associated Secretomes for Aging Biomarker Development. *bioRxiv* **2019**, doi:10.1101/604306.

10. Ficarra, B.J. Submandibular Salivary Gland Fibrosis. *J Med* **1996**, *27*, 103–113.

11. Khalili, S.; Liu, Y.; Kornete, M.; Roescher, N.; Kodama, S.; Peterson, A.; Piccirillo, C.A.; Tran, S.D. Mesenchymal Stromal Cells Improve Salivary Function and Reduce Lymphocytic Infiltrates in Mice with Sjögren's-like Disease. *PLoS One* **2012**, *7*, 1–11, doi:10.1371/journal.pone.0038615.

12. Jeong, J.; Baek, H.; Kim, Y.; Choi, Y.; medicine, H.L.-… & molecular; 2013, undefined Human Salivary Gland Stem Cells Ameliorate Hyposalivation of Radiation-Damaged Rat Salivary Glands. *nature.comJ Jeong, H Baek, YJ Kim, Y Choi, H Lee, E Lee, ES Kim, JH Hah, TK Kwon, IJ Choi, H KwonExperimental & molecular medicine, 2013•nature.com*.

13. Zhang, X.; Yun, J.S.; Han, D.; Yook, J.I.; Kim, H.S.; Cho, E.S. Tgf-β Pathway in Salivary Gland Fibrosis. *Int J Mol Sci* **2020**, *21*, 1–20, doi:10.3390/ijms21239138.

14. Hu, B.; Wu, Z.; Phan, S.H. Smad3 Mediates Transforming Growth Factor-β–Induced α-Smooth Muscle Actin Expression. *https://doi.org/10.1165/rcmb.2003-0063OC* **2012**, *29*, 397–404, doi:10.1165/RCMB.2003-0063OC.

15. Desmoulière, A.; Chaponnier, C.; Gabbiani, G. Tissue Repair, Contraction, and the Myofibroblast. *Wound Repair and Regeneration* **2005**, *13*, 7–12, doi:10.1111/J.1067-1927.2005.130102.X.

16. Gabbiani, G. The Myofibroblast in Wound Healing and Fibrocontractive Diseases. *J Pathol* **2003**, *200*, 500–503, doi:10.1002/PATH.1427.

17. Stone, R.C.; Pastar, I.; Ojeh, N.; Chen, V.; Liu, S.; Garzon, K.I.; Tomic-Canic, M. Epithelial-Mesenchymal Transition in Tissue Repair and Fibrosis. *Cell and Tissue Research 2016 365:3* **2016**, *365*, 495–506, doi:10.1007/S00441-016-2464-0.

18. Mendez, M.G.; Kojima, S.; Goldman, R.D. Vimentin Induces Changes in Cell Shape, Motility, and Adhesion during the Epithelial to Mesenchymal Transition. *FASEB J* **2010**, *24*, 1838–1851, doi:10.1096/FJ.09-151639.

19. Van Linthout, S.; Miteva, K.; Tschöpe, C. Crosstalk between Fibroblasts and Inflammatory Cells. *Cardiovasc Res* **2014**, *102*, 258–269, doi:10.1093/CVR/CVU062.

20. Villa, A.; Connell, C.L.; Abati, S. Diagnosis and Management of Xerostomia and Hyposalivation. **2015**, 45–51.

21. Jensen, S.B.; Vissink, A. Salivary Gland Dysfunction and Xerostomia in Sjögren's Syndrome. *Oral Maxillofac Surg Clin North Am* **2014**, *26*, 35–53, doi:10.1016/j.coms.2013.09.003.

22. Tchkonia, T.; Zhu, Y.; Van Deursen, J.; Campisi, J.; Kirkland, J.L. Cellular Senescence and the Senescent Secretory Phenotype: Therapeutic Opportunities. *J Clin Invest* **2013**, *123*, 966–972, doi:10.1172/JCI64098.

23. Schafer, M.J.; Haak, A.J.; Tschumperlin, D.J.; LeBrasseur, N.K. Targeting Senescent Cells in Fibrosis: Pathology, Paradox, and Practical Considerations. *Curr Rheumatol Rep* **2018**, *20*, 1–11, doi:10.1007/S11926-018-0712-X/METRICS.

24. HAYFLICK, L.; MOORHEAD, P.S. THE LIMITED IN VITRO LIFETIME OF HUMAN DIPLOID CELL STRAINS. *Cytogenetics of Cells in Culture* **1964**, 155–173, doi:10.1016/B978-1-4832-3076-4.50017-8.

25. Herranz, N.; Gil, J. Mechanisms and Functions of Cellular Senescence. *J Clin Invest* **2018**, *128*, 1238–1246, doi:10.1172/JCI95148.

26. Carnero, A. Markers of Cellular Senescence. *Methods in Molecular Biology* **2013**, *965*, 63–81, doi:10.1007/978-1-62703-239-1_4/COVER.

27. González-Gualda, E.; Baker, A.G.; Fruk, L.; Muñoz-Espín, D. A Guide to Assessing Cellular Senescence in Vitro and in Vivo. *FEBS J* **2021**, *288*, 56–80, doi:10.1111/FEBS.15570.

28. Mijit, M.; Caracciolo, V.; Melillo, A.; Amicarelli, F.; Giordano, A. Role of P53 in the Regulation of Cellular Senescence. *Biomolecules* **2020**, *10*, 1–16, doi:10.3390/biom10030420.

29. Shtutman, M.; Chang, B.D.; Schools, G.P.; Broude, E. V. Cellular Model of P21-Induced Senescence. *Methods in Molecular Biology* **2017**, *1534*, 31–39, doi:10.1007/978-1-4939-6670-7_3/COVER.

30. Baker, D.J.; Wijshake, T.; Tchkonia, T.; Lebrasseur, N.K.; Childs, B.G.; Van De Sluis, B.; Kirkland, J.L.; Van Deursen, J.M. Clearance of P16 Ink4a-Positive Senescent Cells Delays Ageing-Associated Disorders. *Nature* **2011**, *479*, 232–236, doi:10.1038/nature10600.

31. Brandl, A.; Meyer, M.; Bechmann, V.; Nerlich, M.; Angele, P. Oxidative Stress Induces Senescence in Human Mesenchymal Stem Cells. *Exp Cell Res* **2011**, *317*, 1541–1547, doi:10.1016/J.YEXCR.2011.02.015.

32. Courtois-Cox, S.; Jones, S.L.; Cichowski, K. Many Roads Lead to Oncogene-Induced Senescence. *Oncogene 2008 27:20* **2008**, *27*, 2801–2809, doi:10.1038/sj.onc.1210950.

33. Van Deursen, J.M. The Role of Senescent Cells in Ageing. *Nature 2014 509:7501* **2014**, *509*, 439–446, doi:10.1038/nature13193.

34. Coppé, J.P.; Desprez, P.Y.; Krtolica, A.; Campisi, J. The Senescence-Associated Secretory Phenotype: The Dark Side of Tumor Suppression. *https://doi.org/10.1146/annurev-pathol-121808-102144* **2010**, *5*, 99–118, doi:10.1146/ANNUREV-PATHOL-121808-102144.

35. Tchkonia, T.; Palmer, A.K.; Kirkland, J.L. New Horizons: Novel Approaches to Enhance Healthspan through Targeting Cellular Senescence and Related Aging Mechanisms. *J. Clin. Endocrinol. Metab.* **2021**, *106*, e1481–e1487, doi:10.1210/clinem/dgaa728.

36. Chaib, S.; Tchkonia, T.; Kirkland, J.L. Cellular Senescence and Senolytics: The Path to the Clinic. *Nature Medicine 2022 28:8* **2022**, *28*, 1556–1568, doi:10.1038/s41591-022-01923-y.

37. Lombaert, I.; Movahednia, M.M.; Adine, C.; Ferreira, J.N. Concise Review: Salivary Gland Regeneration: Therapeutic Approaches from Stem Cells to Tissue Organoids. **2018**, *35*, 97–105, doi:10.1002/stem.2455.Concise.

38. Huang, G.Y.; Zhou, L.H.; Zhang, Q.C.; Chen, Y.M.; Sun, W.; Xu, F.; Lu, T.J. Microfluidic Hydrogels for Tissue Engineering. *Biofabrication* 2011.

39. Orlo, N.D.; Truong, C.; Cira, N.; Koo, S.; Hamilton, A.; Choi, S.; Wu, V.; Riedel-kruse, I.H. RSC Advances Networkable Desktop Experimentation † Bioprinter Assembly. **2014**, 34721–34728, doi:10.1039/C4RA05932H.

40. Mandrycky, C.; Wang, Z.; Kim, K.; Kim, D. 3D Bioprinting for Engineering Complex Tissues. **2017**, *34*, 422–434, doi:10.1016/j.biotechadv.2015.12.011.3D.

41. Licata, J.P.; Schwab, K.H.; Har-el, Y. El; Gerstenhaber, J.A.; Lelkes, P.I. Bioreactor Technologies for Enhanced Organoid Culture. *International Journal of Molecular Sciences 2023, Vol. 24, Page 11427* **2023**, *24*, 11427, doi:10.3390/IJMS241411427.

42. Sant, S.; Johnston, P.A. The Production of 3D Tumor Spheroids for Cancer Drug Discovery. *Drug Discov Today Technol* **2017**, *23*, 27–36.

43. Rodrigues, T.; Kundu, B.; Silva-Correia, J.; Kundu, S.C.; Oliveira, J.M.; Reis, R.L.; Correlo, V.M. Emerging Tumor Spheroids Technologies for 3D in Vitro Cancer Modeling. *Pharmacol Ther* **2018**, *184*, 201–211, doi:10.1016/J.PHARMTHERA.2017.10.018.

44. Centeno, E.G.Z.; Cimarosti, H.; Bithell, A. 2D versus 3D Human Induced Pluripotent Stem Cell-Derived Cultures for Neurodegenerative Disease Modelling. *Molecular Neurodegeneration 2018 13:1* **2018**, *13*, 1–15, doi:10.1186/S13024-018-0258-4.

45. Kunz-Schughart, L.A.; Freyer, J.P.; Hofstaedter, F.; Ebner, R. The Use of 3-D Cultures for High-Throughput Screening: The Multicellular Spheroid Model. *J. Biomol. Screen* **2004**, *9*, 273–285, doi:10.1177/1087057104265040.

46. Friedrich, J.; Seidel, C.; Ebner, R.; Kunz-Schughart, L.A. Spheroid-Based Drug Screen: Considerations and Practical Approach. *Nature Protocols 2009 4:3* **2009**, *4*, 309–324, doi:10.1038/nprot.2008.226.

47. Kim, S. jeong; Kim, E.M.; Yamamoto, M.; Park, H.; Shin, H. Engineering Multi-Cellular Spheroids for Tissue Engineering and Regenerative Medicine. *Adv Healthc Mater* **2020**, *9*, 2000608, doi:10.1002/ADHM.202000608.

48. Expression of Multidrug Resistance-Associated Protein in NIH/3T3 Cells Confers Multidrug Resistance Associated with Increased Drug Efflux and Altered Intracellular Drug Distribution1 | Cancer Research | American Association for Cancer Research Available online: https://aacrjournals.org/cancerres/article/55/22/5342/501720/Expression-of-Multidrug-Resistance-associated (accessed on 5 October 2023).

49. Ryu, J.K.; Song, S.U.; Man, J.Y.; Chu, Y.C.; Lee, M.; Kim, J.S.; Kim, S.J.; Suh, J.K. Establishment of Penile Fibrosis Model in a Rat Using Mouse NIH 3T3 Fibroblasts Expressing Transforming Growth Factor B1. *Biol Reprod* **2005**, *72*, 916–921, doi:10.1095/BIOLREPROD.104.035089.

50. Barka, T.; Gresik, E.S.; Miyazaki, Y. Differentiation of a Mouse Submandibular Gland-Derived Cell Line (SCA) Grown on Matrigel. *Exp Cell Res* **2005**, *308*, 394–406, doi:10.1016/J.YEXCR.2005.04.025.

51. Nichols, W.W.; Murphy, D.G.; Cristofalo, V.J.; Toji, L.H.; Greene, A.E.; Dwight, S.A. Characterization of a New Human Diploid Cell Strain, IMR-90. *Science (1979)* **1977**, *196*, 60–63, doi:10.1126/SCIENCE.841339.

52. Neri, F.; Basisty, N.; Desprez, P.Y.; Campisi, J.; Schilling, B. Quantitative Proteomic Analysis of the Senescence-Associated Secretory Phenotype by Data-Independent Acquisition. *Curr Protoc* **2021**, *1*, e32, doi:10.1002/CPZ1.32.

53. Jasmer, K.J.; Gilman, K.E.; Forti, K.M.; Weisman, G.A.; Limesand, K.H. Radiation-Induced Salivary Gland Dysfunction: Mechanisms, Therapeutics and Future Directions. *J Clin Med* **2020**, *9*, 1–37, doi:10.3390/JCM9124095.

54. Meyer, S.; Chibly, A.M.; Burd, R.; Limesand, K.H. Insulin-Like Growth Factor-1-Mediated DNA Repair in Irradiated Salivary Glands Is Sirtuin-1 Dependent. *J Dent Res* **2017**, *96*, 225–232, doi:10.1177/0022034516677529.

55. Jasmer, K.J.; Gilman, K.E.; Forti, K.M.; Weisman, G.A.; Limesand, K.H. Radiation-Induced Salivary Gland Dysfunction: Mechanisms, Therapeutics and Future Directions. *J Clin Med* **2020**, *9*, 1–37, doi:10.3390/JCM9124095.

56. Özcan, S.; Alessio, N.; Acar, M.B.; Mert, E.; Omerli, F.; Galderisi, U. Unbiased Analysis of Senescence Associated Secretory Phenotype (SASP) to Identify Common Components Following Different Genotoxic Stresses. **2016**, *8*, 16–27.

57. Schafer, M.J.; White, T.A.; Iijima, K.; Haak, A.J.; Ligresti, G.; Atkinson, E.J.; Oberg, A.L.; Birch, J.; Salmonowicz, H.; Zhu, Y.; et al. Cellular Senescence Mediates Fibrotic Pulmonary Disease. *Nature Communications 2017 8:1* **2017**, *8*, 1–11, doi:10.1038/ncomms14532.

58. Antelo-Iglesias, L.; Picallos-Rabina, P.; Estévez-Souto, V.; Da Silva-Álvarez, S.; Collado, M. The Role of Cellular Senescence in Tissue Repair and Regeneration. *Mech Ageing Dev* **2021**, *198*, 111528, doi:10.1016/J.MAD.2021.111528.

59. Nelson, G.; Wordsworth, J.; Wang, C.; Jurk, D.; Lawless, C.; Martin-Ruiz, C.; von Zglinicki, T. A Senescent Cell Bystander Effect: Senescence-Induced Senescence. *Aging Cell* **2012**, *11*, 345–349, doi:10.1111/j.1474-9726.2012.00795.x.

60. Grundmann, O.; Mitchell, G.C.; Limesand, K.H. Sensitivity of Salivary Glands to Radiation: From Animal Models to Therapies. *J Dent Res* **2009**, *88*, 894, doi:10.1177/0022034509343143.

61. Marmary, Y.; Adar, R.; Gaska, S.; Wygoda, A.; Maly, A.; Cohen, J.; Eliashar, R.; Mizrachi, L.; Orfaig-Geva, C.; Baum, B.J.; et al. Radiation-Induced Loss of Salivary Gland Function Is Driven by Cellular Senescence and Prevented by IL6 Modulation. *Cancer Res* **2016**, *76*, 1170–1180, doi:10.1158/0008-5472.CAN-15-1671.

62. Reactor Concepts Manual Biological Effects of Radiation.

63. Newman, R.E.; Yoo, D.; LeRoux, M.A.; Danilkovitch-Miagkova, A. Treatment of Inflammatory Diseases with Mesenchymal Stem Cells. *Inflamm Allergy Drug Targets* **2009**, *8*, 110–123, doi:10.2174/187152809788462635.

64. El Agha, E.; Kramann, R.; Schneider, R.K.; Li, X.; Seeger, W.; Humphreys, B.D.; Bellusci, S. Mesenchymal Stem Cells in Fibrotic Disease. *Cell Stem Cell* **2017**, *21*, 166–177, doi:10.1016/j.stem.2017.07.011.

65. Dimri, M.; Dimri, G.P.; Pole, A. Oxidative Stress, Cellular Senescence and Ageing Akshaj Pole APA Citation Oxidative Stress, Cellular Senescence and Ageing. **2016**, doi:10.3934/molsci.2016.3.300.

66. Denu, R.A.; Hematti, P. Effects of Oxidative Stress on Mesenchymal Stem Cell Biology. *Oxid Med Cell Longev* **2016**, *2016*, doi:10.1155/2016/2989076.

67. Sasportas, M.; Hosford, A.; Sodini, M.; Waters, J.; Zambricki, A.; Barral, J.; Graves, E.; Brinton, T.; Yock, P.; Quyhh-Thu, L.; et al. Cost-Effectiveness Landscape Analysis of Treatments Addressing Xerostomia in Patients Receiving Head and Neck Radiation Therapy. *Oral Surg Oral Med Oral Pathol Oral Raiol* **2014**, *23*, 1–7, doi:10.1038/jid.2014.371.

68. Turner, M.; Ship, J. Dry Mouth and Its Effects on the Oral Health of Elderly People. *The Journal of the American Dental Association* **2007**, *138*, S15–S20, doi:10.14219/jada.archive.2007.0358.

69. Jensen, S.B.; Pedersen, A.M.L.; Vissink, A.; Andersen, E.; Brown, C.G.; Davies, A.N.; Dutilh, J.; Fulton, J.S.; Jankovic, L.; Lopes, N.N.F.; et al. A Systematic Review of Salivary Gland Hypofunction and Xerostomia Induced by Cancer Therapies: Prevalence, Severity and Impact on Quality of Life. *Supportive Care in Cancer* 2010.

70. Stewart, B.W.; Wild, C.P. World Cancer Report 2014. *World Health Organization* **2014**, doi:9283204298.

71. Polaris No Title Available online: https://www.polarismarketresearch.com/industry-analysis/xerostomia-therapeutics-market.

72. Yoo, C.; Vines, J.B.; Alexander, G.; Murdock, K.; Hwang, P.; Jun, H.W. Adult Stem Cells and Tissue Engineering Strategies for Salivary Gland Regeneration: A Review. *Biomater Res* **2014**, *18*, 1–12, doi:10.1186/2055-7124-18-9.

73. Konkel, J.E.; O'Boyle, C.; Krishnan, S. Distal Consequences of Oral Inflammation. *Front Immunol* **2019**, *10*, 1–16, doi:10.3389/fimmu.2019.01403.

74. Weng, P.; Aure, M.; Maruyama, T.; Ovitt, C. Limited Regeneration of Adult Salivary Glands after Severe Injury Involves Cellular Plasticity. *Cell Rep* **2018**, *24*, 1464–1470, doi:10.1016/j.celrep.2018.07.016. Limited.

75. Nash, A.; Saßmannshausen, J.; Bozec, L.; Birch, H.L.; De Leeuw, N.H.; Sarma, R.H. Computational Study of Glucosepane–Water and Hydrogen Bond Formation: An Electron Topology and Orbital Analysis. *J Biomol Struct Dyn* **2016**, *1102*, 1–11, doi:10.1080/07391102.2016.1172026.

76. Rose, S. Primary Salivary Glands Available online: https://app.biorender.com/illustrations/60149f828a786b606b577576 (accessed on 23 August 2023).

77. Treuting, P.M.; Dintzis, S.M. Comparative Anatomy and Histology: A Mouse and Human Atlas. In *Comparative Anatomy and Histology: A Mouse and Human Atlas*; 2012 ISBN 9780123813619.

78. de Paula, F.; Teshima, T.H.N.; Hsieh, R.; Souza, M.M.; Nico, M.M.S.; Lourenco, S.V. Overview of Human Salivary Glands: Highlights of Morphology and Developing Processes. *Anat Rec* **2017**, *300*, 1180–1188, doi:10.1002/AR.23569.

79. Carlson, B.M. The Human Body: Linking Structure and Function. *The Human Body: Linking Structure and Function* **2018**, 1–417, doi:10.1016/C2015-0-00205-2.

80. Munger, B.L. Histochemical Studies on Seromucous- and Mucoussecreting Cells of Human Salivary Glands. *American Journal of Anatomy* **1964**, *115*, 411–429, doi:10.1002/AJA.1001150303.

81. Shah, A.; Mulla, A.; Mayank, M. Pathophysiology of Myoepithelial Cells in Salivary Glands. *J Oral Maxillofac Pathol* **2016**, *20*, 480, doi:10.4103/0973-029X.190952.

82. Ozdemir, T.; Fowler, E.W.; Hao, Y.; Ravikrishnan, A.; Harrington, D.A.; Witt, R.L.; Farach-Carson, M.C.; Pradhan-Bhatt, S.; Jia, X. Biomaterials-Based Strategies for Salivary Gland Tissue Regeneration. *Biomater Sci* **2016**, *4*, 592–604, doi:10.1039/c5bm00358j.

83. Chou, Y.S.; Lin, Y.C.; Young, T.H.; Lou, P.J. Effects of Fibroblasts on the Function of Acinar Cells from the Same Human Parotid Gland. *Head Neck* **2016**, doi:10.1002/hed.23986.

84. Larsen, M.; Wei, C.; Yamada, K.M. Cell and Fibronectin Dynamics during Branching Morphogenesis. *J Cell Sci* **2006**, doi:10.1242/jcs.03079.

85. Patel, V.N.; Likar, K.M.; Zisman-rozen, S.; Cowherd, S.N.; Lassiter, K.S.; Sher, I.; Yates, E.A.; Turnbull, J.E.; Ron, D.; Hoffman, M.P. Specific Heparan Sulfate Structures Modulate FGF10-Mediated Submandibular Gland Epithelial Morphogenesis. **2008**, *283*, 9308–9317, doi:10.1074/jbc.M709995200.

86. Jaskoll, T.; Abichaker, G.; Witcher, D.; Sala, F.G.; Bellusci, S.; Hajihosseini, M.K.; Melnick, M. FGF10/FGFR2b Signaling Plays Essential Roles during in Vivo Embryonic Submandibular Salivary Gland Morphogenesis. *BMC Dev Biol* **2005**, *5*, 1–12, doi:10.1186/1471-213x-5-11.

87. Mattingly, A.; Finley, J.K.; Knox, S.M. Salivary Gland Development and Disease. *Wires Dev Biol* **2015**, *194*, doi:10.1002/wdev.194.

88. Retting, K.N.; Lyons, K.M. BMPs in Development. *Handbook of Cell Signaling, Second Edition* **2010**, *2*, 1905–1912, doi:10.1016/B978-0-12-374145-5.00233-3.

89. Jaskoll, T.; Leo, T.; Witcher, D.; Ormestad, M.; Astorga, J.; Bringas, P.; Carlsson, P.; Melnick, M. Sonic Hedgehog Signaling Plays an Essential Role during Embryonic Salivary Gland Epithelial Branching Morphogenesis. *Developmental Dynamics* **2004**, *229*, 722–732, doi:10.1002/DVDY.10472.

90. Sisto, M.; Ribatti, D.; Lisi, S. E-Cadherin Signaling in Salivary Gland Development and Autoimmunity. *Journal of Clinical Medicine 2022, Vol. 11, Page 2241* **2022**, *11*, 2241, doi:10.3390/JCM11082241.

91. Lourenço, S.V.; Kapas, S. Integrin Expression in Developing Human Salivary Glands. *Histochem Cell Biol* **2005**, *124*, 391–399, doi:10.1007/S00418-005-0784-3.

92. Chatzeli, L.; Gaete, M.; Tucker, A.S. Fgf10 and Sox9 Are Essential for the Establishment of Distal Progenitor Cells during Mouse Salivary Gland Development. *Development* **2017**, *144*, 2294–2305, doi:10.1242/DEV.146019.

93. Schöck, F.; Perrimon, N. Molecular Mechanisms of Epithelial Morphogenesis. *https://doi.org/10.1146/annurev.cellbio.18.022602.131838* **2003**, *18*, 463–493, doi:10.1146/ANNUREV.CELLBIO.18.022602.131838.

94. Kriangkrai, R.; Iseki, S.; Eto, K.; Chareonvit, S. Dual Odontogenic Origins Develop at the Early Stage of Rat Maxillary Incisor Development. *Anat Embryol (Berl)* **2006**, *211*, 101–108, doi:10.1007/S00429-005-0068-7/METRICS.

95. Tanaka, J.; Takamatsu, K.; Yukimori, A.; Kujiraoka, S.; Ishida, S.; Takakura, I.; Yasuhara, R.; Mishima, K. Sox9 Function in Salivary Gland Development. *J Oral Biosci* **2021**, *63*, 8–13, doi:10.1016/J.JOB.2021.01.005.

96. Kwon, H.R.; Nelson, D.A.; Desantis, K.A.; Morrissey, J.M.; Larsen, M. Endothelial Cell Regulation of Salivary Gland Epithelial Patterning. *Development (Cambridge)* **2017**, *144*, 211–220, doi:10.1242/DEV.142497.

97. Takahashi, M.; Suzawa, T.; Yamada, A.; Yamaguchi, T.; Mishima, K.; Osumi, N.; Maki, K.; Kamijo, R. Identification of Gene Expression Profile of Neural Crest-Derived Cells Isolated from Submandibular Glands of Adult Mice. *Biochem Biophys Res Commun* **2014**, *446*, 481–486, doi:10.1016/J.BBRC.2014.02.130.

98. Rothova, M.; Thompson, H.; Lickert, H.; Tucker, A.S. Lineage Tracing of the Endoderm during Oral Development. *Developmental Dynamics* **2012**, *241*, 1183–1191, doi:10.1002/DVDY.23804.

99. Emmerson, E.; May, A.J.; Nathan, S.; Cruz-Pacheco, N.; Lizama, C.O.; Maliskova, L.; Zovein, A.C.; Shen, Y.; Muench, M.O.; Knox, S.M. SOX2 Regulates Acinar Cell Development in the Salivary Gland. *Elife* **2017**, *6*, doi:10.7554/ELIFE.26620.

100. Athwal, H.K.; Iii, G.M.; Tibbs, E.; Cornett, A.; Hill, E.; Yeoh, K.; Berenstein, E.; Hoffman, M.P.; Lombaert, I.M.A. Stem Cell Reports Article Sox10 Regulates Plasticity of Epithelial Progenitors toward Secretory Units of Exocrine Glands. **2019**, doi:10.1016/j.stemcr.2019.01.002.

101. Cutler, L.S. The Role of Extracellular Matrix in the Morphogenesis and Differentiation of Salivary Glands. *Adv Dent Res* **1990**, *4*, 27–33, doi:10.1177/08959374900040010401.

102. Aure, M.H.; Symonds, J.M.; Mays, J.W.; Hoffman, M.P. Epithelial Cell Lineage and Signaling in Murine Salivary Glands. *https://doi.org/10.1177/0022034519864592* **2019**, *98*, 1186–1194, doi:10.1177/0022034519864592.

103. Patel, V.N.; Hoffman, M.P. Salivary Gland Development: A Template for Regeneration. *Semin Cell Dev Biol* **2014**, *0*, 52, doi:10.1016/J.SEMCDB.2013.12.001.

104. Clark, W.D. Embryology and Anomalies of the Facial Nerve and Their Surgical Implications. *JAMA: The Journal of the American Medical Association* **1991**, doi:10.1001/jama.1991.03470020111050.

105. Johnson, C.M.; Hoffer, M.E. Facial Nerve, Embryology. *Encyclopedia of Otolaryngology, Head and Neck Surgery* **2013**, 879–882, doi:10.1007/978-3-642-23499-6_855.

106. Knox, S.M.; Lombaert, I.M.A.; Reed, X.; Vitale-Cross, L.; Gutkind, J.S.; Hoffman, M.P. Parasympathetic Innervation Maintains Epithelial Progenitor Cells during Salivary Organogenesis. *Science (1979)* **2010**, doi:10.1126/science.1192046.

107. Knox, S.M.; Lombaert, I.M.A.; Reed, X.; Vitale-Cross, L.; Gutkind, J.S.; Hoffman, M.P. Parasympathetic Innervation Maintains Epithelial Progenitor Cells during Salivary Organogenesis. *Science* **2010**, *329*, 1645–1647, doi:10.1126/SCIENCE.1192046.

108. Knosp, W.M.; Knox, S.M.; Lombaert, I.M.A.; Haddox, C.L.; Patel, V.N.; Hoffman, M.P. Submandibular Parasympathetic Gangliogenesis Requires Sprouty-Dependent Wnt Signals from Epithelial Progenitors. *Dev Cell* **2015**, doi:10.1016/j.devcel.2015.01.023.

109. Paratcha, G.; Ledda, F. GDNF and GFRα: A Versatile Molecular Complex for Developing Neurons. *Trends Neurosci* **2008**, doi:10.1016/j.tins.2008.05.003.

110. Sharma, M.; Castro-Piedras, I.; Simmons, G.E.; Pruitt, K. Dishevelled: A Masterful Conductor of Complex Wnt Signals. *Cell Signal* **2018**, *47*, 52, doi:10.1016/J.CELLSIG.2018.03.004.

111. Ferreira, J.N.; Hoffman, M.P. Interactions between Developing Nerves and Salivary Glands. *Organogenesis* **2013**, *9*, 152–158, doi:10.4161/ORG.25224.

112. Ferreira, J.N.A.; Zheng, C.; Lombaert, I.M.A.; Goldsmith, C.M.; Cotrim, A.P.; Symonds, J.M.; Patel, V.N.; Hoffman, M.P. Neurturin Gene Therapy Protects Parasympathetic Function to Prevent Irradiation-Induced Murine Salivary Gland Hypofunction. *Mol Ther Methods Clin Dev* **2018**, *9*, 172–180, doi:10.1016/j.omtm.2018.02.008.

113. Heuckeroth, R.O.; Enomoto, H.; Grider, J.R.; Golden, J.P.; Hanke, J.A.; Jackman, A.; Molliver, D.C.; Bardgett, M.E.; Snider, W.D.; Johnson, E.M.; et al. Gene Targeting Reveals a Critical Role for Neurturin in the Development and Maintenance of Enteric, Sensory, and Parasympathetic Neurons. *Neuron* **1999**, *22*, 253–263, doi:10.1016/S0896-6273(00)81087-9.

114. Wang, S.; Sekiguchi, R.; Daley, W.P.; Yamada, K.M. Patterned Cell and Matrix Dynamics in Branching Morphogenesis. *Journal of Cell Biology* **2017**, *216*, 559–570, doi:10.1083/JCB.201610048.

115. Onodera, T.; Sakai, T.; Hsu, J.C.F.; Matsumoto, K.; Chiorini, J.A.; Yamada, K.M. Btbd7 Regulates Epithelial Cell Dynamics and Branching Morphogenesis. *Science (1979)* **2010**, doi:10.1126/science.1191880.

116. Sakai, T.; Larsen, M.; Yamada, K.M. Fibronectin Requirement in Branching Morphogenesis. *Nature* **2003**, doi:10.1038/nature01712.

117. Kadoya, Y.; Yamashina, S. Cellular Dynamics of Epithelial Clefting during Branching Morphogenesis of the Mouse Submandibular Gland. *Developmental Dynamics* **2010**, doi:10.1002/dvdy.22312.

118. Daley, W.P.; Gulfo, K.M.; Sequeira, S.J.; Larsen, M. Identification of a Mechanochemical Checkpoint and Negative Feedback Loop Regulating Branching Morphogenesis. *Dev Biol* **2009**, doi:10.1016/j.ydbio.2009.09.037.

119. Daley, W.P.; Gervais, E.M.; Centanni, S.W.; Gulfo, K.M.; Nelson, D.A.; Larsen, M. ROCK1-Directed Basement Membrane Positioning Coordinates Epithelial Tissue Polarity. *Development* **2012**, doi:10.1242/dev.075366.

120. Häärä, O.; Koivisto, T.; Miettinen, P.J. EGF-Receptor Regulates Salivary Gland Branching Morphogenesis by Supporting Proliferation and Maturation of Epithelial Cells and Survival of Mesenchymal Cells. *Differentiation* **2009**, doi:10.1016/j.diff.2008.10.006.

121. Yamamoto, S.; Fukumoto, E.; Yoshizaki, K.; Iwamoto, T.; Yamada, A.; Tanaka, K.; Suzuki, H.; Aizawa, S.; Arakaki, M.; Yuasa, K.; et al. Platelet-Derived Growth Factor Receptor Regulates Salivary Gland Morphogenesis via Fibroblast Growth Factor Expression. *Journal of Biological Chemistry* **2008**, *283*, 23139–23149, doi:10.1074/jbc.M710308200.

122. Jaskoll, T.; Abichaker, G.; Witcher, D.; Sala, F.G.; Bellusci, S.; Hajihosseini, M.K.; Melnick, M. FGF10/FGFR2b Signaling Plays Essential Roles during in Vivo Embryonic Submandibular Salivary Gland Morphogenesis. *BMC Dev Biol* **2005**, *5*, doi:10.1186/1471-213X-5-11.

123. Steinberg, Z.; Myers, C.; Heim, V.M.; Lathrop, C.A.; Rebustini, I.T.; Stewart, J.S.; Larsen, M.; Hoffman, M.P. FGFR2b Signaling Regulates Ex Vivo Submandibular Gland Epithelial Cell Proliferation and Branching Morphogenesis. *Development* **2005**, *132*, 1223–1234, doi:10.1242/dev.01690.

124. Patel, V.N.; Likar, K.M.; Zisman-Rozen, S.; Cowherd, S.N.; Lassiter, K.S.; Sher, I.; Yates, E.A.; Turnbull, J.E.; Ron, D.; Hoffman, M.P. Specific Heparan Sulfate Structures Modulate FGF10-Mediated Submandibular Gland Epithelial Morphogenesis and Differentiation. *Journal of Biological Chemistry* **2008**, doi:10.1074/jbc.M709995200.

125. Patel, V.N.; Hoffman, M.P. Salivary Gland Development: A Template for Regeneration. *Semin Cell Dev Biol* **2014**, *0*, 52, doi:10.1016/J.SEMCDB.2013.12.001.

126. Ligtenberg, A.J.M.; Veerman, E.C.I. Saliva: Secretion and Functions. *Saliva: Secretion and Functions* **2014**, *24*, 1–154, doi:10.1159/ISBN.978-3-318-02596-5.

127. Hauser, B.R.; Aure, M.H.; Kelly, M.C.; Hoffman, M.P.; Chibly, A.M. Generation of a Single-Cell RNAseq Atlas of Murine Salivary Gland Development. *iScience* **2020**, *23*, doi:10.1016/J.ISCI.2020.101838.

128. Nanduri, L.S.Y.; Lombaert, I.M.A.; Van Der Zwaag, M.; Faber, H.; Brunsting, J.F.; Van Os, R.P.; Coppes, R.P. Salisphere Derived C-Kit+ Cell Transplantation Restores Tissue Homeostasis in Irradiated Salivary Gland. *Radiotherapy and Oncology* **2013**, *108*, 458–463, doi:10.1016/J.RADONC.2013.05.020.

129. Rugel-Stahl, A.; Elliott, M.E.; Ovitt, C.E. Ascl3 Marks Adult Progenitor Cells of the Mouse Salivary Gland. *Stem Cell Res* **2012**, *8*, 379–387, doi:10.1016/J.SCR.2012.01.002.

130. Lombaert, I.M.A.; Brunsting, J.F.; Wierenga, P.K.; Kampinga, H.H.; de Haan, G.; Coppes, R.P. Keratinocyte Growth Factor Prevents Radiation Damage to Salivary Glands by Expansion of the Stem/Progenitor Pool. *Stem Cells* **2008**, *26*, 2595–2601, doi:10.1634/STEMCELLS.2007-1034.

131. Pringle, S.; Maimets, M.; Van Der Zwaag, M.; Stokman, M.A.; Van Gosliga, D.; Zwart, E.; Witjes, M.J.H.; De Haan, G.; Van Os, R.; Coppes, R.P. Human Salivary Gland Stem Cells Functionally Restore Radiation Damaged Salivary Glands. *Stem Cells* **2016**, *34*, 640–652, doi:10.1002/STEM.2278.

132. Yi, T.G.; Lee, S.; Choi, N.; Shin, H.S.; Kim, J.; Lim, J.Y. Single Cell Clones Purified from Human Parotid Glands Display Features of Multipotent Epitheliomesenchymal Stem Cells. *Sci Rep* **2016**, *6*, doi:10.1038/SREP36303.

133. Katsiougiannis, S.; Wong, D.T.W. The Proteomics of Saliva in Sjögren's Syndrome. *Rheum Dis Clin North Am* **2016**, *42*, 449–456, doi:10.1016/J.RDC.2016.03.004.

134. Marmary, Y.; Adar, R.; Gaska, S.; Wygoda, A.; Maly, A.; Cohen, J.; Eliashar, R.; Mizrachi, L.; Orfaig-geva, C.; Baum, B.J.; et al. Radiation-Induced Loss of Salivary Gland Function Is Driven by Cellular Senescence and Prevented by IL-6 Modulation. *Cancer Res* **2016**, *15*, doi:10.1158/0008-5472.CAN-15-1671.

135. Avouac, J.; Sordet, C.; Depinay, C.; Ardizonne, M.; Vacher-Lavenu, M.C.; Sibilia, J.; Kahan, A.; Allanore, Y. Systemic Sclerosis-Associated Sjögren's Syndrome and Relationship to the Limited Cutaneous Subtype: Results of a Prospective Study of Sicca Syndrome in 133 Consecutive Patients. *Arthritis Rheum* **2006**, *54*, 2243–2249, doi:10.1002/art.21922.

136. Davis, M.A.; Reynolds, A.B. Blocked Acinar Development, E-Cadherin Reduction, and Intraepithelial Neoplasia upon Ablation of P120-Catenin in the Mouse Salivary Gland. *Dev Cell* **2006**, doi:10.1016/j.devcel.2005.12.004.

137. Ellis, G.L.; Auclair, P.L. *Salivary Glands*; Second Edi.; Elsevier Inc., 2009;

138. Sousa-Victor, P.; Gutarra, S.; García-Prat, L.; Rodriguez-Ubreva, J.; Ortet, L.; Ruiz-Bonilla, V.; Jardí, M.; Ballestar, E.; González, S.; Serrano, A.L.; et al. Geriatric Muscle Stem Cells Switch Reversible Quiescence into Senescence. *Nature* **2014**, *506*, 316–321, doi:10.1038/nature13013.

139. Pringle, S.; Wang, X.; Verstappen, G.M.P.J.; Terpstra, J.H.; Zhang, C.K.; He, A.; Patel, V.; Jones, R.E.; Baird, D.M.; Spijkervet, F.K.L.; et al. Salivary Gland Stem Cells Age Prematurely in Primary Sjögren's Syndrome. *Arthritis and Rheumatology* **2019**, *71*, 133–142, doi:10.1002/art.40659.

140. Wang, X.; Bootsma, H.; Terpstra, J.; Vissink, A.; Van Der Vegt, B.; Spijkervet, F.K.L.; Kroese, F.G.M.; Pringle, S. Progenitor Cell Niche Senescence Reflects Pathology of the Parotid Salivary Gland in Primary Sjögren's Syndrome. *Rheumatology (Oxford)* **2020**, *59*, 3003–3013, doi:10.1093/RHEUMATOLOGY/KEAA012.

141. Hoebers, F.J.P.; Kartachova, M.; De Bois, J.; Van Den Brekel, M.W.M.; Van Tinteren, H.; Van Herk, M.; Rasch, C.R.N.; Valdés Olmos, R.A.; Verheij, M. 99mTc Hynic-Rh-Annexin V Scintigraphy for in Vivo Imaging of Apoptosis in Patients with Head and Neck Cancer Treated with Chemoradiotherapy. *Eur J Nucl Med Mol Imaging* **2008**, *35*, 509–518, doi:10.1007/S00259-007-0624-X.

142. Robar, J.L.; Day, A.; Clancey, J.; Kelly, R.; Yewondwossen, M.; Hollenhorst, H.; Rajaraman, M.; Wilke, D. Spatial and Dosimetric Variability of Organs at Risk in Head-and-Neck Intensity-Modulated Radiotherapy. *Int J Radiat Oncol Biol Phys* **2007**, *68*, 1121–1130, doi:10.1016/J.IJROBP.2007.01.030.

143. May, A.J.; Cruz-Pacheco, N.; Emmerson, E.; Gaylord, E.A.; Seidel, K.; Nathan, S.; Muench, M.O.; Klein, O.D.; Knox, S.M. Diverse Progenitor Cells Preserve Salivary Gland Ductal Architecture after Radiation-Induced Damage. *Development* **2018**, *145*, doi:10.1242/DEV.166363.

144. Hakim, S.G.; Kosmehl, H.; Lauer, I.; Nadrowitz, R.; Wedel, T.; Sieg, P. The Role of Myoepithelial Cells in the Short-Term Radiogenic Impairment of Salivary Glands. An Immunohistochemical, Ultrastructural and Scintigraphic Study. *Anticancer Res* **2002**, *22*, 4121–4128.

145. Chibly, A.M.; Patel, V.N.; Aure, M.H.; Pasquale, M.C.; Morell, R.J.; Izquierdo, D.M.; Boger, E.; Martin, G.E.; Ghannam, M.; Andrade, J.; et al. Neurotrophin Signaling Is a Central Mechanism of Salivary Dysfunction after Irradiation That Disrupts Myoepithelial Cells. *npj Regenerative Medicine 2023 8:1* **2023**, *8*, 1–16, doi:10.1038/s41536-023-00290-7.

146. Borodkina, A. V.; Deryabin, P.I.; Giukova, A.A.; Nikolsky, N.N. "Social Life" of Senescent Cells: What Is SASP and Why Study It? *Acta Naturae* **2018**, *10*, 4–14.

147. Nelson, G.; Wordsworth, J.; Wang, C.; Jurk, D.; Lawless, C.; Martin-Ruiz, C.; von Zglinicki, T. A Senescent Cell Bystander Effect: Senescence-Induced Senescence. *Aging Cell* **2012**, *11*, 345–349, doi:10.1111/j.1474-9726.2012.00795.x.

148. Mikuła-Pietrasik, J.; Sosinska, P.; Janus, J.; Rubis, B.; Brewinska-Olchowik, M.; Piwocka, K.; Ksiãzek, K. Bystander Senescence in Human Peritoneal Mesothelium and Fibroblasts Is Related to Thrombospondin-1-Dependent Activation of Transforming Growth Factor-B1. *International Journal of Biochemistry and Cell Biology* **2013**, *45*, 2087–2096, doi:10.1016/j.biocel.2013.07.004.

149. Nelson, G.; Kucheryavenko, O.; Wordsworth, J.; von Zglinicki, T. The Senescent Bystander Effect Is Caused by ROS-Activated NF-KB Signalling. *Mech Ageing Dev* **2018**, *170*, 30–36, doi:10.1016/j.mad.2017.08.005.

150. da Silva, P.F.L.; Ogrodnik, M.; Kucheryavenko, O.; Glibert, J.; Miwa, S.; Cameron, K.; Ishaq, A.; Saretzki, G.; Nagaraja-Grellscheid, S.; Nelson, G.; et al. The Bystander Effect Contributes to the Accumulation of Senescent Cells in Vivo. *Aging Cell* **2019**, *18*, doi:10.1111/acel.12848.

151. Altrieth, A.L.; O'Keefe, K.J.; Gellatly, V.A.; Tavarez, J.R.; Feminella, S.M.; Moskwa, N.L.; Cordi, C. V.; Turrieta, J.C.; Nelson, D.A.; Larsen, M. Identifying Fibrogenic Cells Following Salivary Gland Obstructive Injury. *Front Cell Dev Biol* **2023**, *11*, doi:10.3389/FCELL.2023.1190386.

152. Fulda, S. Evasion of Apoptosis as a Cellular Stress Response in Cancer. *Int J Cell Biol* **2010**, *2010*, doi:10.1155/2010/370835.

153. Moskwa, N.; Mahmood, A.; Nelson, D.A.; Altrieth, A.L.; Forni, P.E.; Larsen, M. Single-Cell RNA Sequencing Reveals PDFGRα+ Stromal Cell Subpopulations That Promote Proacinar Cell Differentiation in Embryonic Salivary Gland Organoids. *Development (Cambridge)* **2022**, *149*, doi:10.1242/DEV.200167/274560/AM/SINGLE-CELL-SEQUENCING-REVEALS-PDFGR-STROMAL-CELL.

154. Mack, M.; Yanagita, M. Origin of Myofibroblasts and Cellular Events Triggering Fibrosis. *Kidney Int* **2015**, *87*, 297–307, doi:10.1038/ki.2014.287.

155. Demaria, M.; Ohtani, N.; Youssef, S.A.; Rodier, F.; Toussaint, W.; Mitchell, J.R.; Laberge, R.M.; Vijg, J.; VanSteeg, H.; Dollé, M.E.T.; et al. An Essential Role for Senescent Cells in Optimal Wound Healing through Secretion of PDGF-AA. *Dev Cell* **2014**, *31*, 722–733, doi:10.1016/j.devcel.2014.11.012.

156. Sapudom, J.; Wu, X.; Chkolnikov, M.; Ansorge, M.; Anderegg, U.; Pompe, T. Fibroblast Fate Regulation by Time Dependent TGF-B1 and IL-10 Stimulation in Biomimetic 3D Matrices. *Biomater Sci* **2017**, *5*, 1858–1867, doi:10.1039/c7bm00286f.

157. Hinz, B.; Lagares, D. Evasion of Apoptosis by Myofibroblasts: A Hallmark of Fibrotic Diseases. *Nat Rev Rheumatol* **2020**, *16*, 11–31, doi:10.1038/s41584-019-0324-5.

158. Panwar, P.; Lamour, G.; Mackenzie, N.C.W.; Yang, H.; Ko, F.; Li, H.; Brömme, D. Changes in Structural-Mechanical Properties and Degradability of Collagen during Aging-Associated Modifications. *Journal of Biological Chemistry* **2015**, doi:10.1074/jbc.M115.644310.

159. Fedintsev, A.; Moskalev, A. Stochastic Non-Enzymatic Modification of Long-Lived Macromolecules - A Missing Hallmark of Aging. *Ageing Res Rev* **2020**, *62*, doi:10.1016/j.arr.2020.101097.

160. Tzavlaki, K.; Moustakas, A. TGF-β Signaling. *Biomolecules* **2020**, *10*, doi:10.3390/BIOM10030487.

161. Dupont, S.; Morsut, L.; Aragona, M.; Enzo, E.; Giulitti, S.; Cordenonsi, M.; Zanconato, F.; Le Digabel, J.; Forcato, M.; Bicciato, S.; et al. Role of YAP/TAZ in Mechanotransduction. *Nature* **2011**, doi:10.1038/nature10137.

162. Olivieri, F.; Rippo, M.R.; Monsurrò, V.; Salvioli, S.; Capri, M.; Procopio, A.D.; Franceschi, C. MicroRNAs Linking Inflamm-Aging, Cellular Senescence and Cancer. *Ageing Res Rev* **2013**, *12*, 1056–1068, doi:10.1016/j.arr.2013.05.001.

163. Lampi, M.C.; Reinhart-King, C.A. Targeting Extracellular Matrix Stiffness to Attenuate Disease: From Molecular Mechanisms to Clinical Trials. *Sci Transl Med* **2018**, *10*, 1–15, doi:10.1126/scitranslmed.aao0475.

164. Hildebrand, A.; Romaris, M.; Rasmussen, M.; Heinegard, D.; Twardzik, D.R.; Border, W.A.; Ruoslahti, E. Interaction of the Small Interstitial Proteoglycans Biglycan, Decorin and Fibromodulin with Transforming Growth Factor β. *Biochemical Journal* **1994**, doi:10.1042/bj3020527.

165. Rojas, A.; Añazco, C.; González, I.; Araya, P. Extracellular Matrix Glycation and Receptor for Advanced Glycation End-Products Activation: A Missing Piece in the Puzzle of the Association between Diabetes and Cancer. *Carcinogenesis* **2018**, *39*, 515–521, doi:10.1093/carcin/bgy012.

166. Wondrak, G.T.; Roberts, M.J.; Jacobson, M.K.; Jacobson, E.L. Photosensitized Growth Inhibition of Cultured Human Skin Cells: Mechanism and Suppression of Oxidative Stress from Solar Irradiation of Glycated Proteins. *Journal of Investigative Dermatology* **2002**, *119*, 489–498, doi:10.1046/j.1523-1747.2002.01788.x.

167. Sun, Z.; Wang, C.; Shi, C.; Sun, F. Activated Wnt Signaling Induces Myofibroblast Differentiation of Mesenchymal Stem Cells , Contributing to Pulmonary Fibrosis. *Int J Mol Med* **2014**, *33*, 1097–1109, doi:10.3892/ijmm.2014.1672.

168. Kim, J.W.; Kim, J.M.; Choi, M.E.; Kim, S.K.; Kim, Y.M.; Choi, J.S. Adipose-Derived Mesenchymal Stem Cells Regenerate Radioiodine-Induced Salivary Gland Damage in a Murine Model. *Sci Rep* **2019**, *9*, 1–9, doi:10.1038/s41598-019-51775-9.

169. Stone, G.W.; Ellis, S.G.; Cox, D.A.; Hermiller, J.; O'Shaughnessy, C.; Mann, J.T.; Turco, M.; Caputo, R.; Bergin, P.; Greenberg, J.; et al. A Polymer-Based, Paclitaxel-Eluting Stent in Patients with Coronary Artery Disease. *https://doi.org/10.1056/NEJMoa032441* **2004**, *350*, 221–231, doi:10.1056/NEJMOA032441.

170. Onat, D.; Brillon, D.; AM, S.; PC, C. Human Vascular Endothelial Cells: A Model System for Studying Vascular Inflammation in Diabetes and Atherosclerosis. *Curr Diab Rep* **2012**, *11*, 193–202, doi:10.1007/s11892-011-0182-2.Human.

171. Rose, S. Myofibroblast Origins and Fate in Normal Wound Healing Available online: https://app.biorender.com/illustrations/64e6225156a3787ce7161c9e (accessed on 20 July 2023).

172. Deng, J.; Carlson, N.; Takeyama, K.; Dal Cin, P.; Shipp, M.; Letai, A. BH3 Profiling Identifies Three Distinct Classes of Apoptotic Blocks to Predict Response to ABT-737 and Conventional Chemotherapeutic Agents. *Cancer Cell* **2007**, *12*, 171–185, doi:10.1016/j.ccr.2007.07.001.

173. Green, D.R.; Llambi, F. Cell Death Signaling. *Cold Spring Harb Perspect Biol* **2015**, doi:10.1101/cshperspect.a006080.

174. Ambudkar, I. Calcium Signaling Defects Underlying Salivary Gland Dysfunction. *Biochim Biophys Acta Mol Cell Res* **2018**, *1865*, 1771–1777, doi:10.1016/j.bbamcr.2018.07.002.

175. Mccarthy, D.A.; Clark, R.R.; Toni, R.; Trebak, M.; Andres, J.; Mccarthy, D.A.; Clark, R.R.; Bartling, T.R.; Trebak, M.; Melendez, J.A. Redox Control of the Senescence Regulator Interleukin-1 Alpha and the Secretory Phenotype *. *J Biol Chem* **2013**, doi:10.1074/jbc.M113.493841.

176. Orjalo, A. V.; Bhaumik, D.; Gengler, B.K.; Scott, G.K.; Campisi, J. Cell Surface-Bound IL-1α Is an Upstream Regulator of the Senescence-Associated IL-6/IL-8 Cytokine Network. *Proc Natl Acad Sci U S A* **2009**, doi:10.1073/pnas.0905299106.

177. Hai, B.; Zhao, Q.; Deveau, M.A.; Liu, F. Delivery of Sonic Hedgehog Gene Repressed Irradiation-Induced Cellular Senescence in Salivary Glands by Promoting DNA Repair and Reducing Oxidative Stress. *Theranostics* **2018**, *8*, 1159–1167, doi:10.7150/thno.23373.

178. Lehmann, M.; Korfei, M.; Mutze, K.; Klee, S.; Skronska-Wasek, W.; Alsafadi, H.N.; Ota, C.; Costa, R.; Schiller, H.B.; Lindner, M.; et al. Senolytic Drugs Target Alveolar Epithelial Cell Function and Attenuate Experimental Lung Fibrosis Ex Vivo. *European Respiratory Journal* **2017**, *50*, doi:10.1183/13993003.02367-2016.

179. Pan, J.; Deguan, L.; Zhang, J.; Wang, Y.; Chen, M.; Lin, S.; Huang, L.; Chung, J.E.; Citrin, D.; Wang, Y.; et al. Inhibition of Bcl-2/Xl With ABT-263 Selectively Kills Senescent Type II Pneumocytes and Reverses Persistent Pumonary Fibrosis Induced by Ionizing Radiation in Mice. *Int J Radiat Oncol Biol Phys* **2017**, *99*, 352–361, doi:10.1016/j.physbeh.2017.03.040.

180. Schafer, M.J.; White, T.A.; Iijima, K.; Haak, A.J.; Ligresti, G.; Atkinson, E.J.; Oberg, A.L.; Birch, J.; Salmonowicz, H.; Zhu, Y.; et al. Cellular Senescence Mediates Fibrotic Pulmonary Disease. *Nat Commun* **2017**, *8*, doi:10.1038/ncomms14532.

181. Baker, D.J.; Wijshake, T.; Tchkonia, T.; Lebrasseur, N.K.; Childs, B.G.; Van De Sluis, B.; Kirkland, J.L.; Van Deursen, J.M. Clearance of P16 Ink4a-Positive Senescent Cells Delays Ageing-Associated Disorders. *Nature* **2011**, *479*, 232–236, doi:10.1038/nature10600.

182. Humphreys, B.D. Mechanisms of Renal Fibrosis. *Annu Rev Physiol* **2018**, *80*, 309–326, doi:10.1146/annurev-physiol-022516-034227.

183. Jin, H.; Zhang, Y.; Ding, Q.; Wang, S.S.; Rastogi, P.; Dai, D.-F.; Lu, D.; Purvis, M.; Cao, C.; Wang, A.; et al. Epithelial Innate Immunity Mediates Tubular Cell Senescence after Kidney Injury. *JCI Insight* **2019**, *4*, doi:10.1172/jci.insight.125490.

184. Luo, C.; Zhou, S.; Zhou, Z.; Liu, Y.; Yang, L.; Liu, J.; Zhang, Y.; Li, H.; Liu, Y.; Hou, F.F.; et al. Wnt9a Promotes Renal Fibrosis by Accelerating Cellular Senescence in Tubular Epithelial Cells. *Journal of the American Society of Nephrology* **2018**, doi:10.1681/ASN.2017050574.

185. Justice, J.N.; Nambiar, A.M.; Tchkonia, T.; LeBrasseur, N.K.; Pascual, R.; Hashmi, S.K.; Prata, L.; Masternak, M.M.; Kritchevsky, S.B.; Musi, N.; et al. Senolytics in Idiopathic Pulmonary Fibrosis: Results from a First-in-Human, Open-Label, Pilot Study. *EBioMedicine* 2019, *40*, 554–563.

186. Jin, H.; Zhang, Y.; Ding, Q.; Wang, S.S.; Rastogi, P.; Dai, D.-F.; Lu, D.; Purvis, M.; Cao, C.; Wang, A.; et al. Epithelial Innate Immunity Mediates Tubular Cell Senescence after Kidney Injury. *JCI Insight* **2019**, *4*, doi:10.1172/jci.insight.125490.

187. Luo, C.; Zhou, S.; Zhou, Z.; Liu, Y.; Yang, L.; Liu, J.; Zhang, Y.; Li, H.; Liu, Y.; Hou, F.F.; et al. Wnt9a Promotes Renal Fibrosis by Accelerating Cellular Senescence in Tubular Epithelial Cells. *Journal of the American Society of Nephrology* **2018**, doi:10.1681/ASN.2017050574.

188. Justice, J.N.; Nambiar, A.M.; Tchkonia, T.; LeBrasseur, N.K.; Pascual, R.; Hashmi, S.K.; Prata, L.; Masternak, M.M.; Kritchevsky, S.B.; Musi, N.; et al. Senolytics in Idiopathic Pulmonary Fibrosis: Results from a First-in-Human, Open-Label, Pilot Study. *EBioMedicine* **2019**, *40*, 554–563, doi:10.1016/j.ebiom.2018.12.052.

189. Nelson, J.; Manzella, K.; Baker, O.J. Current Cell Models for Bioengineering a Salivary Gland: A Mini-Review of Emerging Technologies. *Oral Dis* **2013**, *19*, 236–244, doi:10.1111/J.1601-0825.2012.01958.X.

190. Yanagawa, T.; Hayashi, Y.; Nagamine, S.; Yoshida, H.; Yura, Y.; Sato, M. Generation of Cells with Phenotypes of Both Intercalated Duct-Type and Myoepithelial Cells in Human Parotid Gland Adenocarcinoma Clonal Cells Grown in Athymic Nude Mice. *Virchows Arch B Cell Pathol Incl Mol Pathol* **1986**, doi:10.1007/BF02899028.

191. Search for Specific Markers of Neoplastic Epithelial Duct and Myoepithelial Cell Lines Established from Human Salivary Gland and Characterization of Their Growth in Vitro - PubMed Available online: https://pubmed.ncbi.nlm.nih.gov/6093988/ (accessed on 4 April 2023).

192. Lin, L.C.; Elkashty, O.; Ramamoorthi, M.; Trinh, N.; Liu, Y.; Sunavala-Dossabhoy, G.; Pranzatelli, T.; Michael, D.G.; Chivasso, C.; Perret, J.; et al. Cross-Contamination of the Human Salivary Gland HSG Cell Line with HeLa Cells: A STR Analysis Study. *Oral Dis* **2018**, *24*, 1477–1483, doi:10.1111/ODI.12920.

193. Laoide, B.M.; Courty, Y.; Gastinne, I.; Thibaut, C.; Kellermann, O. Immortalised Mouse Submandibular Epithelial Cell Lines Retain Polarised Structural and Functional Properties. **1996**, *2800*, 2789–2800.

194. Xinjun, H.; Frank, D.; Tabak, L. ESTABLISHMENT IMMORTALIZED AND CHARACTERIZATION OF 12s ADENOVIRAL ElA RAT SUBMANDIBULAR GLAND EPITHELIAL CELLS. *Biochem Biophys Res Commun* **1990**, *170*, 336–343.

195. Brown, A.M. In Vitro Transformation of Submandibular Gland Epithelial Cells and Fibroblasts of Adult Rats by Methylcholanthrene. *Cancer Res* **1973**.

196. Quissell, D.O.; Barzen, K.A.; Redman, R.S.; Camden, J.M.; Turner, J.T. Development and Characterization of SV40 Immortalized Rat Submandibular Acinar Cell Lines Department Of. *In Vitro Cellular & Developmental Biology* **1997**, 164–173.

197. Thiemann, R.F.; Nelson, D.A.; Michael DiPersio, C.; Larsen, M.; LaFlamme, S.E. Establishment of a Murine Pro-Acinar Cell Line to Characterize Roles for FGF2 and A3β1 Integrins in Regulating Pro-Acinar Characteristics. *Sci Rep* **2019**, *9*, doi:10.1038/S41598-019-47387-Y.

198. Zhu, Y.; Aletta, J.M.; Wen, J.; Zhang, X.; Higgins, D.; Rubin, R.P. Rat Serum Induces a Differentiated Phenotype in a Rat Parotid Acinar Cell Line. *Am J Physiol Gastrointest Liver Physiol* **1998**, doi:10.1152/ajpgi.1998.275.2.g259.

199. An Adenoid Squamous Carcinoma-Forming Cell Line Established from an Oral Keratinizing Squamous Cell Carcinoma Expressing Carcinoembryonic Antigen - PubMed Available online: https://pubmed.ncbi.nlm.nih.gov/2429552/ (accessed on 4 April 2023).

200. Imai, A.; Nashida, T.; Shimomura, H. Roles of Munc18-3 in Amylase Release from Rat Parotid Acinar Cells. *Arch Biochem Biophys* **2004**, *422*, 175–182, doi:10.1016/j.abb.2003.12.021.

201. Patton, L.L.; Pollack, S.; Wellner, R.B. Responsiveness of a Human Parotid Epithelial Cell Line (HSY) to Autonomic Stimulation: Muscarinic Control of K+ Transport. *In Vitro Cell Dev Biol Anim* **1991**, *27 A*, 779–785, doi:10.1007/BF02631243.

202. Sato, M.; Yoshida, H.; Yanagawa, T.; Yura, Y.; Urata, M. Sensitivity of a Neoplastic Epithelial Duct Cell Line from a Human Submandibular Salivary Gland to Human Leukocyte Interferon as Assessed by an in Vitro Semi-Solid Agar Technique. *Int J Oral Surg* **1982**, *11*, 183–189, doi:10.1016/s0300-9785(82)80006-9.

203. Maria, O.M.; Maria, O.; Liu, Y.; Komarova, S. V.; Tran, S.D. Matrigel Improves Functional Properties of Human Submandibular Salivary Gland Cell Line. *Int J Biochem Cell Biol* **2011**, *43*, 622–631, doi:10.1016/J.BIOCEL.2011.01.001.

204. Laoide, B.M.; Courty, Y.; Gastinne, I.; Thibaut, C.; Kellermann, O.; Rougeon, F. Immortalised Mouse Submandibular Epithelial Cell Lines Retain Polarised Structural and Functional Properties. *J Cell Sci* **1996**, *109*, 2789–2800.

205. He, X.; Kuijpers, G.A.J.; Goping, G.; Kulakusky, J.A.; Zheng, C.; Delporte, C.; Tse, C.M.; Redman, R.S.; Donowitz, M.; Pollard, H.B.; et al. A Polarized Salivary Cell Monolayer Useful for Studying

Transepithelial Fluid Movement in Vitro. *Pflugers Arch* **1998**, *435*, 375–381, doi:10.1007/s004240050526.

206. Mitsui, R.; Fujita-Yoshigaki, J.; Narita, T.; Matsuki-Fukushima, M.; Satoh, K.; Qi, B.; Guo, M.Y.; Katsumata-Kato, O.; Sugiya, H. Maintenance of Paracellular Barrier Function by Insulin-like Growth Factor-I in Submandibular Gland Cells. *Arch Oral Biol* **2010**, *55*, 963–969, doi:10.1016/j.archoralbio.2010.07.023.

207. Brown, A.M. In Vitro Transformation of Submandibular Gland Epithelial Cells and Fibroblasts of Adult Rats by Methylcholanthrene. *Cancer Res* **1973**, *33*, 2779–2789.

208. Liu, X. bing; Mörk, A.C.; Sun, X.; Castro, R.; Martinez, J.R.; Zhang, G.H. Regulation of CA2+ Signals in a Parotid Cell Line Par-C5. *Arch Oral Biol* **2001**, *46*, 1141–1149, doi:10.1016/S0003-9969(01)00074-7.

209. Castro, R.; Barlow-Walden, L.; Woodson, T.; Kerecman, J.D.; Zhang, G.H.; Martinez, J.R. Ion Transport in an Immortalized Rat Submandibular Cell Line SMG-C6 (44550). *Exp Biol Med* **2000**, doi:10.1046/j.1525-1373.2000.22505.x.

210. Aure, M.H.; Røed, A.; Galtung, H.K. Intracellular Ca2+ Responses and Cell Volume Regulation upon Cholinergic and Purinergic Stimulation in an Immortalized Salivary Cell Line. *Eur J Oral Sci* **2010**, *118*, 237–244, doi:10.1111/J.1600-0722.2010.00738.X.

211. Quissell, D.O.; Barzen, K.A.; Redman, R.S.; Camden, J.M.; Turner, J.T. Development and Characterization of SV40 Immortalized Rat Parotid Acinar Cell Lines. *In Vitro Cell Dev Biol Anim* **1998**, doi:10.1007/s11626-998-0054-5.

212. Liu, X. bing; Mörk, A.C.; Sun, X.; Castro, R.; Martinez, J.R.; Zhang, G.H. Regulation of CA2+ Signals in a Parotid Cell Line Par-C5. *Arch Oral Biol* **2001**, doi:10.1016/S0003-9969(01)00074-7.

213. Zhu, Y.; Aletta, J.M.; Wen, J.; Zhang, X.; Higgins, D.; Rubin, R.P. Rat Serum Induces a Differentiated Phenotype in a Rat Parotid Acinar Cell Line. *Am J Physiol Gastrointest Liver Physiol* **1998**, doi:10.1152/ajpgi.1998.275.2.g259.

214. Turner, J.T.; Redman, R.S.; Camden, J.M.; Landon, L.A.; Quissell, D.O. A Rat Parotid Gland Cell Line, Par-C10, Exhibits Neurotransmitter-Regulated Transepithelial Anion Secretion. *Am J Physiol* **1998**, *275*, doi:10.1152/AJPCELL.1998.275.2.C367.

215. Demeter, I.; Szucs, A.; Hegyesi, O.; Foldes, A.; Racz, G.Z.; Burghardt, B.; Steward, M.C.; Varga, G. Vectorial Bicarbonate Transport by Par-C10 Salivary Cells. *J Physiol Pharmacol* **2009**.

216. Baker, O.J. Tight Junctions in Salivary Epithelium. *J Biomed Biotechnol* **2010**, *2010*, doi:10.1155/2010/278948.

217. Szlávik, V.; Szabó, B.; Vicsek, T.; Barabás, J.; Bogdán, S.; Gresz, V.; Varga, G.; O'Connell, B.; Vág, J. Differentiation of Primary Human Submandibular Gland Cells Cultured on Basement Membrane Extract. *Tissue Eng Part A* **2008**, *14*, 1915–1926, doi:10.1089/ten.tea.2007.0208.

218. Walsh, G.M.; Dewson, G.; Wardlaw, A.J.; Levi-Schaffer, F.; Moqbel, R. A Comparative Study of Different Methods for the Assessment of Apoptosis and Necrosis in Human Eosinophils. *J Immunol Methods* **1998**, doi:10.1016/S0022-1759(98)00103-3.

219. Joraku, A.; Sullivan, C.A.; Yoo, J.; Atala, A. In-Vitro Reconstitution of Three-Dimensional Human Salivary Gland Tissue Structures. *Differentiation* **2007**, doi:10.1111/j.1432-0436.2006.00138.x.

220. Pradhan, S.; Liu, C.; Zhang, C.; Jia, X.; Farach-Carson, M.C.; Witt, R.L. Lumen Formation in Three-Dimensional Cultures of Salivary Acinar Cells. *Otolaryngology - Head and Neck Surgery* **2010**, *142*, 191–195, doi:10.1016/J.OTOHNS.2009.10.039.

221. Joraku, A.; Sullivan, C.A.; Yoo, J.J.; Atala, A. Tissue Engineering of Functional Salivary Gland Tissue. *Laryngoscope* **2005**, doi:10.1097/01.mlg.0000154726.77915.cc.

222. Sugito, T.; Kagami, H.; Hata, K.; Nishiguchi, H.; Ueda, M. Transplantation of Cultured Salivary Gland Cells into an Atrophic Salivary Gland. *Cell Transplant* 2004, *13*, 691–699.

223. Yoo, C.; Vines, J.B.; Alexander, G.; Murdock, K.; Hwang, P.; Jun, H.W. Adult Stem Cells and Tissue Engineering Strategies for Salivary Gland Regeneration: A Review. *Biomater Res* **2014**, *18*, doi:10.1186/2055-7124-18-9.

224. Knox, S.M.; Lombaert, I.M.A.; Reed, X.; Vitale-Cross, L.; Gutkind, J.S.; Hoffman, M.P. Parasympathetic Innervation Maintains Epithelial Progenitor Cells during Salivary Organogenesis. *Science* **2010**, *329*, 1645–1647, doi:10.1126/SCIENCE.1192046.

225. Athwal, H.K.; Murphy, G.; Tibbs, E.; Cornett, A.; Hill, E.; Yeoh, K.; Berenstein, E.; Hoffman, M.P.; Lombaert, I.M.A. Sox10 Regulates Plasticity of Epithelial Progenitors toward Secretory Units of Exocrine Glands. *Stem Cell Reports* **2019**, *12*, 366, doi:10.1016/J.STEMCR.2019.01.002.

226. Emmerson, E.; May, A.J.; Nathan, S.; Cruz-Pacheco, N.; Lizama, C.O.; Maliskova, L.; Zovein, A.C.; Shen, Y.; Muench, M.O.; Knox, S.M. SOX2 Regulates Acinar Cell Development in the Salivary Gland. *Elife* **2017**, *6*, doi:10.7554/ELIFE.26620.

227. Lombaert, I.M.A.; Hoffman, M.P. Epithelial Stem/Progenitor Cells in the Embryonic Mouse Submandibular Gland. **2010**, 90–106, doi:10.1159/000313709.

228. Koslow, M.; O'Keefe, K.J.; Hosseini, Z.F.; Nelson, D.A.; Larsen, M. ROCK Inhibitor Increases Proacinar Cells in Adult Salivary Gland Organoids. *Stem Cell Res* **2019**, *41*, doi:10.1016/J.SCR.2019.101608.

229. Takahashi, Y.; Nogawa, H. Branching Morphogenesis of Mouse Salivary Epithelium in Basement Membrane-like Substratum Separated from Mesenchyme by the Membrane Filter. *Development* **1991**, *111*, 327–335, doi:10.1242/dev.111.2.327.

230. Okumura, K.; Shinohara, M.; Endo, F. Capability of Tissue Stem Cells to Organize into Salivary Rudiments. *Stem Cells Int* **2012**, *2012*, doi:10.1155/2012/502136.

231. Hosseini, Z.F.; Nelson, D.A.; Moskwa, N.; Sfakis, L.M.; Castracane, J.; Larsen, M. FGF2-Dependent Mesenchyme and Laminin-111 Are Niche Factors in Salivary Gland Organoids. *J Cell Sci* **2018**, *131*, doi:10.1242/JCS.208728.

232. Steinberg, Z.; Myers, C.; Heim, V.M.; Lathrop, C.A.; Rebustini, I.T.; Stewart, J.S.; Larsen, M.; Hoffman, M.P. FGFR2b Signaling Regulates Ex Vivo Submandibular Gland Epithelial Cell Proliferation and Branching Morphogenesis. *Development* **2005**, *132*, 1223–1234, doi:10.1242/DEV.01690.

233. Feng, J.; van der Zwaag, M.; Stokman, M.A.; van Os, R.; Coppes, R.P. Isolation and Characterization of Human Salivary Gland Cells for Stem Cell Transplantation to Reduce Radiation-Induced Hyposalivation. *Radiotherapy and Oncology* **2009**, doi:10.1016/j.radonc.2009.06.023.

234. Rocchi, C.; Barazzuol, L.; Coppes, R.P. The Evolving Definition of Salivary Gland Stem Cells. *npj Regenerative Medicine 2021 6:1* **2021**, *6*, 1–8, doi:10.1038/s41536-020-00115-x.

235. Sui, Y.; Zhang, S.; Li, Y.; Zhang, X.; Hu, W.; Feng, Y.; Xiong, J.; Zhang, Y.; Wei, S. Generation of Functional Salivary Gland Tissue from Human Submandibular Gland Stem/Progenitor Cells. *Stem Cell Res Ther* **2020**, *11*, 127, doi:10.1186/s13287-020-01628-4.

236. Nanduri, L.S.Y.; Maimets, M.; Pringle, S.A.; Van Der Zwaag, M.; Van Os, R.P.; Coppes, R.P. Regeneration of Irradiated Salivary Glands with Stem Cell Marker Expressing Cells. *Radiotherapy and Oncology* **2011**, doi:10.1016/j.radonc.2011.05.085.

237. Srinivasan, P.P.; Patel, V.N.; Liu, S.; Harrington, D.A.; Hoffman, M.P.; Jia, X.; Witt, R.L.; Farach-Carson, M.C.; Pradhan-Bhatt, S. Primary Salivary Human Stem/Progenitor Cells Undergo Microenvironment-Driven Acinar-Like Differentiation in Hyaluronate Hydrogel Culture. *Stem Cells Transl Med* **2017**, doi:10.5966/sctm.2016-0083.

238. Sui, Y.; Zhang, S.; Li, Y.; Zhang, X.; Hu, W.; Feng, Y.; Xiong, J.; Zhang, Y.; Wei, S. Generation of Functional Salivary Gland Tissue from Human Submandibular Gland Stem/Progenitor Cells. *Stem Cell Res Ther* **2020**, *11*, 1–13, doi:10.1186/S13287-020-01628-4/FIGURES/4.

239. Tubbesing, K.; Moskwa, N.; Khoo, T.C.; Nelson, D.A.; Sharikova, A.; Feng, Y.; Larsen, M.; Khmaladze, A. Raman Microspectroscopy Fingerprinting of Organoid Differentiation State. *Cell Mol Biol Lett* **2022**, *27*, 1–20, doi:10.1186/S11658-022-00347-3/FIGURES/7.

240. Pringle, S.; Van Os, R.; Coppes, R.P. Concise Review: Adult Salivary Gland Stem Cells and a Potential Therapy for Xerostomia. *Stem Cells* 2013.

241. Hisatomi, Y.; Okumura, K.; Nakamura, K.; Matsumoto, S.; Satoh, A.; Nagano, K.; Yamamoto, T.; Endo, F. Flow Cytometric Isolation of Endodermal Progenitors from Mouse Salivary Gland Differentiate into Hepatic and Pancreatic Lineages. *Hepatology* **2004**, *39*, 667–675, doi:10.1002/HEP.20063.

242. Knox, S.M.; Lombaert, I.M.A.; Reed, X.; Vitale-Cross, L.; Gutkind, J.S.; Hoffman, M.P. Parasympathetic Innervation Maintains Epithelial Progenitor Cells during Salivary Organogenesis. *Science* **2010**, *329*, 1645–1647, doi:10.1126/SCIENCE.1192046.

243. Lombaert, I.; Abrams, S.; Li, L.; reports, V.E.-S. cell; 2013, undefined Combined KIT and FGFR2b Signaling Regulates Epithelial Progenitor Expansion during Organogenesis. *cell.comIMA*

Lombaert, SR Abrams, L Li, VP Eswarakumar, AJ Sethi, RL Witt, MP HoffmanStem cell reports, 2013•cell.com.

244. Yi, T.G.; Lee, S.; Choi, N.; Shin, H.S.; Kim, J.; Lim, J.Y. Single Cell Clones Purified from Human Parotid Glands Display Features of Multipotent Epitheliomesenchymal Stem Cells. *Sci Rep* **2016**, *6*, doi:10.1038/SREP36303.

245. Sato, A.; Okumura, K.; Matsumoto, S.; Hattori, K.; Hattori, S.; Shinohara, M.; Endo, F. Isolation, Tissue Localization, and Cellular Characterization of Progenitors Derived from Adult Human Salivary Glands. *Cloning Stem Cells* **2007**, *9*, 191–205, doi:10.1089/CLO.2006.0054.

246. Rotter, N.; Oder, J.; Schlenke, P.; Lindner, U.; Böhrnsen, F.; Kramer, J.; Rohwedel, J.; Huss, R.; Brandau, S.; Wollenberg, B.; et al. Isolation and Characterization of Adult Stem Cells from Human Salivary Glands. *Stem Cells Dev* **2008**, *17*, 509–518, doi:10.1089/SCD.2007.0180.

247. Zuk, P.A.; Zhu, M.; Ashjian, P.; De Ugarte, D.A.; Huang, J.I.; Mizuno, H.; Alfonso, Z.C.; Fraser, J.K.; Benhaim, P.; Hedrick, M.H. Human Adipose Tissue Is a Source of Multipotent Stem Cells. *Mol Biol Cell* **2002**, *13*, 4279–4295, doi:10.1091/MBC.E02-02-0105/ASSET/IMAGES/LARGE/MK1222051007.JPEG.

248. Pittenger, M.F.; Mackay, A.M.; Beck, S.C.; Jaiswal, R.K.; Douglas, R.; Mosca, J.D.; Moorman, M.A.; Simonetti, D.W.; Craig, S.; Marshak, D.R. Multilineage Potential of Adult Human Mesenchymal Stem Cells. *Science (1979)* **1999**, *284*, 143–147, doi:10.1126/SCIENCE.284.5411.143/SUPPL_FILE/983855S5_THUMB.GIF.

249. Mackay, A.M.; Beck, S.C.; Murphy, J.M.; Barry, F.P.; Chichester, C.O.; Pittenger, M.F. Chondrogenic Differentiation of Cultured Human Mesenchymal Stem Cells from Marrow. *Tissue Eng* **1998**, *4*, 415–428, doi:10.1089/TEN.1998.4.415.

250. Dezawa, M.; Ishikawa, H.; Itokazu, Y.; Yoshihara, T.; Hoshino, M.; Takeda, S.I.; Ide, C.; Nabeshima, Y.I. Developmental Biology: Bone Marrow Stromal Cells Generate Muscle Cells and Repair Muscle Degeneration. *Science (1979)* **2005**, *309*, 314–317, doi:10.1126/SCIENCE.1110364/SUPPL_FILE/DEZAWA.SOM.PDF.

251. Makino, S.; Fukuda, K.; Miyoshi, S.; Konishi, F.; Kodama, H.; Pan, J.; Sano, M.; Takahashi, T.; Hori, S.; Abe, H.; et al. Cardiomyocytes Can Be Generated from Marrow Stromal Cells in Vitro. *Journal of Clinical Investigation* **1999**, *103*, 697, doi:10.1172/JCI5298.

252. Snykers, S.; Vanhaecke, T.; Papeleu, P.; Luttun, A.; Jiang, Y.; Vander Heyden, Y.; Verfaillie, C.; Rogiers, V. Sequential Exposure to Cytokines Reflecting Embryogenesis: The Key for in Vitro Differentiation of Adult Bone Marrow Stem Cells into Functional Hepatocyte-like Cells. *Toxicological Sciences* **2006**, *94*, 330–341, doi:10.1093/TOXSCI/KFL058.

253. Scintu, F.; Reali, C.; Pillai, R.; Badiali, M.; Sanna, M.A.; Argiolu, F.; Ristaldi, M.S.; Sogos, V. Differentiation of Human Bone Marrow Stem Cells into Cells with a Neural Phenotype: Diverse Effects of Two Specific Treatments. *BMC Neurosci* **2006**, *7*, 1–12, doi:10.1186/1471-2202-7-14/TABLES/1.

254. Marinkovic, M.; Tran, O.N.; Wang, H.; Abdul-Azees, P.; Dean, D.D.; Chen, X.D.; Yeh, C.K. Autologous Mesenchymal Stem Cells Offer a New Paradigm for Salivary Gland Regeneration. *International Journal of Oral Science 2023 15:1* **2023**, *15*, 1–19, doi:10.1038/s41368-023-00224-5.

255. Caplan, A.I. Adult Mesenchymal Stem Cells for Tissue Engineering versus Regenerative Medicine. *J Cell Physiol* **2007**, *213*, 341–347, doi:10.1002/JCP.21200.

256. Dominici, M.; Le Blanc, K.; Mueller, I.; Slaper-Cortenbach, I.; Marini, F.C.; Krause, D.S.; Deans, R.J.; Keating, A.; Prockop, D.J.; Horwitz, E.M. Minimal Criteria for Defining Multipotent Mesenchymal Stromal Cells. The International Society for Cellular Therapy Position Statement. *Cytotherapy* **2006**, *8*, 315–317, doi:10.1080/14653240600855905.

257. Gao, F.; Chiu, S.M.; Motan, D.A.L.; Zhang, Z.; Chen, L.; Ji, H.L.; Tse, H.F.; Fu, Q.L.; Lian, Q. Mesenchymal Stem Cells and Immunomodulation: Current Status and Future Prospects. *Cell Death Dis* **2016**, *7*, e2062, doi:10.1038/CDDIS.2015.327.

258. Lim, J.Y.; Yi, T.; Choi, J.S.; Jang, Y.H.; Lee, S.; Kim, H.J.; Song, S.U.; Kim, Y.M. Intraglandular Transplantation of Bone Marrow-Derived Clonal Mesenchymal Stem Cells for Amelioration of Post-Irradiation Salivary Gland Damage. *Oral Oncol* **2013**, *49*, 136–143, doi:10.1016/j.oraloncology.2012.08.010.

259. Kojima, T.; Kanemaru, S.I.; Hirano, S.; Tateya, I.; Ohno, S.; Nakamura, T.; Ito, J. Regeneration of Radiation Damaged Salivary Glands with Adipose-Derived Stromal Cells. *Laryngoscope* **2011**, *121*, 1864–1869, doi:10.1002/lary.22080.

260. Lee, J.; Park, S.; Roh, S. Transdifferentiation of Mouse Adipose-Derived Stromal Cells into Acinar Cells of the Submandibular Gland Using a Co-Culture System. *Exp Cell Res* **2015**, doi:10.1016/j.yexcr.2015.03.006.

261. Lim, J.Y.; Ra, J.C.; Shin, I.S.; Jang, Y.H.; An, H.Y.; Choi, J.S.; Kim, W.C.; Kim, Y.M. Systemic Transplantation of Human Adipose Tissue-Derived Mesenchymal Stem Cells for the Regeneration of Irradiation-Induced Salivary Gland Damage. *PLoS One* **2013**, *8*, doi:10.1371/journal.pone.0071167.

262. Xiong, X.; Shi, X.; Chen, F. Human Adipose Tissue-Derived Stem Cells Alleviate Radiation-Induced Xerostomia. *Int J Mol Med* **2014**, doi:10.3892/ijmm.2014.1837.

263. Lim, J.Y.; Yi, T.; Lee, S.; Kim, J.; Kim, S.N.; Song, S.U.; Kim, Y.M. Establishment and Characterization of Mesenchymal Stem Cell-like Clonal Stem Cells from Mouse Salivary Glands. *Tissue Eng Part C Methods* **2015**, doi:10.1089/ten.tec.2014.0204.

264. Jeong, J.; Baek, H.; Kim, Y.J.; Choi, Y.; Lee, H.; Lee, E.; Kim, E.S.; Hah, J.H.; Kwon, T.K.; Choi, I.J.; et al. Human Salivary Gland Stem Cells Ameliorate Hyposalivation of Radiation-Damaged Rat Salivary Glands. *Exp Mol Med* **2013**, *45*, e58-7, doi:10.1038/emm.2013.121.

265. Denewar, M.; Amin, L.E. Role of Bone Marrow-Derived Mesenchymal Stem Cells on the Parotid Glands of Streptozotocin Induced Diabetes Rats. *J Oral Biol Craniofac Res* **2020**, *10*, 33–37, doi:10.1016/j.jobcr.2020.02.003.

266. Lindroos, B.; Suuronen, R.; Miettinen, S. The Potential of Adipose Stem Cells in Regenerative Medicine. *Stem Cell Rev Rep* 2011.

267. Gaebel, R.; Furlani, D.; Sorg, H.; Polchow, B.; Frank, J.; Bieback, K.; Wang, W.; Klopsch, C.; Ong, L.L.; Li, W.; et al. Cell Origin of Human Mesenchymal Stem Cells Determines a Different Healing Performance in Cardiac Regeneration. *PLoS One* **2011**, *6*, doi:10.1371/journal.pone.0015652.

268. Skardal, A.; Mack, D.; Kapetanovic, E.; Atala, A.; Jackson, J.D.; Yoo, J.; Soker, S. Bioprinted Amniotic Fluid-Derived Stem Cells Accelerate Healing of Large Skin Wounds. *Stem Cells Transl Med* **2012**, doi:10.5966/sctm.2012-0088.

269. De Coppi, P.; Bartsch, G.; Siddiqui, M.M.; Xu, T.; Santos, C.C.; Perin, L.; Mostoslavsky, G.; Serre, A.C.; Snyder, E.Y.; Yoo, J.J.; et al. Isolation of Amniotic Stem Cell Lines with Potential for Therapy. *Nat Biotechnol* **2007**, doi:10.1038/nbt1274.

270. Gao, F.; Chiu, S.M.; Motan, D.A.L.; Zhang, Z.; Chen, L.; Ji, H.L.; Tse, H.F.; Fu, Q.L.; Lian, Q. Mesenchymal Stem Cells and Immunomodulation: Current Status and Future Prospects. *Cell Death Dis* 2016.

271. Khalili, S.; Liu, Y.; Kornete, M.; Roescher, N.; Kodama, S.; Peterson, A.; Piccirillo, C.A.; Tran, S.D. Mesenchymal Stromal Cells Improve Salivary Function and Reduce Lymphocytic Infiltrates in Mice with Sjögren's-like Disease. *PLoS One* **2012**, *7*, doi:10.1371/JOURNAL.PONE.0038615.

272. Kim, J.W.; Kim, J.M.; Choi, M.E.; Kim, S.K.; Kim, Y.M.; Choi, J.S. Adipose-Derived Mesenchymal Stem Cells Regenerate Radioiodine-Induced Salivary Gland Damage in a Murine Model. *Scientific Reports 2019 9:1* **2019**, *9*, 1–9, doi:10.1038/s41598-019-51775-9.

273. Almansoori, A.A.; Khentii, N.; Kim, B.; Kim, S.M.; Lee, J.H. Mesenchymal Stem Cell Therapy in Submandibular Salivary Gland Allotransplantation: Experimental Study. *Transplantation* **2019**, *103*, 1111–1120, doi:10.1097/TP.0000000000002612.

274. Grønhøj, C.; Jensen, D.H.; Glovinski, P. V.; Jensen, S.B.; Bardow, A.; Oliveri, R.S.; Specht, L.; Thomsen, C.; Darkner, S.; Kiss, K.; et al. First-in-Man Mesenchymal Stem Cells for Radiation-Induced Xerostomia (MESRIX): Study Protocol for a Randomized Controlled Trial. *Trials* **2017**, *18*, 1–10, doi:10.1186/S13063-017-1856-0/FIGURES/2.

275. Martin, G.R. Isolation of a Pluripotent Cell Line from Early Mouse Embryos Cultured in Medium Conditioned by Teratocarcinoma Stem Cells. *Proc Natl Acad Sci U S A* **1981**, *78*, 7634–7638, doi:10.1073/PNAS.78.12.7634.

276. Evans, M.J.; Kaufman, M.H. Establishment in Culture of Pluripotential Cells from Mouse Embryos. *Nature* **1981**, *292*, 154–156, doi:10.1038/292154A0.

277. JA, T.; J, I.-E.; SS, S.; MA, W.; JJ, S.; VS, M.; JM, J. Embryonic Stem Cell Lines Derived from Human Blastocysts. *Science* **1998**, *282*, 1145–1147, doi:10.1126/SCIENCE.282.5391.1145.

278. Thomson, J.A.; Kalishman, J.; Golos, T.G.; Durning, M.; Harris, C.P.; Becker, R.A.; Hearn, J.P. Isolation of a Primate Embryonic Stem Cell Line. *Proc Natl Acad Sci U S A* **1995**, *92*, 7844–7848, doi:10.1073/PNAS.92.17.7844.

279. Takahashi, K.; Yamanaka, S. Induction of Pluripotent Stem Cells from Mouse Embryonic and Adult Fibroblast Cultures by Defined Factors. *Cell* **2006**, *126*, 663–676, doi:10.1016/J.CELL.2006.07.024.

280. Takahashi, K.; Tanabe, K.; Ohnuki, M.; Narita, M.; Ichisaka, T.; Tomoda, K.; Yamanaka, S. Induction of Pluripotent Stem Cells from Adult Human Fibroblasts by Defined Factors. *Cell* **2007**, *131*, 861–872, doi:10.1016/J.CELL.2007.11.019.

281. Yu, J.; Vodyanik, M.A.; Smuga-Otto, K.; Antosiewicz-Bourget, J.; Frane, J.L.; Tian, S.; Nie, J.; Jonsdottir, G.A.; Ruotti, V.; Stewart, R.; et al. Induced Pluripotent Stem Cell Lines Derived from Human Somatic Cells. *Science* **2007**, *318*, 1917–1920, doi:10.1126/SCIENCE.1151526.

282. Yamanaka, S. Induced Pluripotent Stem Cells: Past, Present, and Future. *Cell Stem Cell* 2012.

283. Takahashi, K.; Tanabe, K.; Ohnuki, M.; Narita, M.; Ichisaka, T.; Tomoda, K.; Yamanaka, S. Induction of Pluripotent Stem Cells from Adult Human Fibroblasts by Defined Factors. *Cell* **2007**, doi:10.1016/j.cell.2007.11.019.

284. Park, A.; Hong, P.; Won, S.T.; Thibault, P.A.; Vigant, F.; Oguntuyo, K.Y.; Taft, J.D.; Lee, B. Sendai Virus, an RNA Virus with No Risk of Genomic Integration, Delivers CRISPR/Cas9 for Efficient Gene Editing. *Mol Ther Methods Clin Dev* **2016**, *3*, 16057, doi:10.1038/MTM.2016.57.

285. Yamanaka, S. Pluripotent Stem Cell-Based Cell Therapy-Promise and Challenges. *Cell Stem Cell* **2020**, *27*, 523–531, doi:10.1016/J.STEM.2020.09.014.

286. Singh, V.K.; Kalsan, M.; Kumar, N.; Saini, A.; Chandra, R. Induced Pluripotent Stem Cells: Applications in Regenerative Medicine, Disease Modeling, and Drug Discovery. *Front Cell Dev Biol* 2015.

287. Miura, K.; Okada, Y.; Aoi, T.; Okada, A.; Takahashi, K.; Okita, K.; Nakagawa, M.; Koyanagi, M.; Tanabe, K.; Ohnuki, M.; et al. Variation in the Safety of Induced Pluripotent Stem Cell Lines. *Nat Biotechnol* **2009**, doi:10.1038/nbt.1554.

288. Sato, Y.; Bando, H.; Di Piazza, M.; Gowing, G.; Herberts, C.; Jackman, S.; Leoni, G.; Libertini, S.; MacLachlan, T.; McBlane, J.W.; et al. Tumorigenicity Assessment of Cell Therapy Products: The Need for Global Consensus and Points to Consider. *Cytotherapy* **2019**, *21*, 1095–1111, doi:10.1016/J.JCYT.2019.10.001.

289. Kunitomi, A.; Yuasa, S.; Sugiyama, F.; Saito, Y.; Seki, T.; Kusumoto, D.; Kashimura, S.; Takei, M.; Tohyama, S.; Hashimoto, H.; et al. H1foo Has a Pivotal Role in Qualifying Induced Pluripotent Stem Cells. *Stem Cell Reports* **2016**, *6*, 825–833, doi:10.1016/J.STEMCR.2016.04.015.

290. Kawakami, M.; Ishikawa, H.; Tachibana, T.; Tanaka, A.; Mataga, I. Functional Transplantation of Salivary Gland Cells Differentiated from Mouse Early ES Cells in Vitro. *Hum Cell* **2013**, *26*, 80–90, doi:10.1007/s13577-013-0061-z.

291. Ono, H.; Obana, A.; Usami, Y.; Sakai, M.; Nohara, K.; Egusa, H.; Sakai, T. Regenerating Salivary Glands in the Microenvironment of Induced Pluripotent Stem Cells. *Biomed Res Int* **2015**, *2015*, doi:10.1155/2015/293570.

292. Tanaka, J.; Ogawa, M.; Hojo, H.; Kawashima, Y.; Mabuchi, Y.; Hata, K.; Nakamura, S.; Yasuhara, R.; Takamatsu, K.; Irié, T.; et al. Generation of Orthotopically Functional Salivary Gland from Embryonic Stem Cells. *Nat Commun* **2018**, *9*, 1–13, doi:10.1038/s41467-018-06469-7.

293. Ramesh, P.; Moskwa, N.; Hanchon, Z.; Koplas, A.; Nelson, D.A.; Mills, K.L.; Castracane, J.; Larsen, M.; Sharfstein, S.T.; Xie, Y. Engineering Cryoelectrospun Elastin-Alginate Scaffolds to Serve as Stromal Extracellular Matrices. *Biofabrication* **2022**, *14*, 035010, doi:10.1088/1758-5090/AC6B34.

294. Mosier, A.P.; Peters, S.B.; Larsen, M.; Cady, N.C. Microfluidic Platform for the Elastic Characterization of Mouse Submandibular Glands by Atomic Force Microscopy. *Biosensors 2014, Vol. 4, Pages 18-27* **2014**, *4*, 18–27, doi:10.3390/BIOS4010018.

295. Aframian, D.J.; Cukierman, E.; Nikolovski, J.; Mooney, D.J.; Yamada, K.M.; Baum, B.J. The Growth and Morphological Behavior of Salivary Epithelial Cells on Matrix Protein-Coated Biodegradable Substrata. *Tissue Eng* **2000**, *6*, 209–216, doi:10.1089/10763270050044380.

296. Wang, S.; Cukierman, E.; Swaim, W.D.; Yamada, K.M.; Baum, B.J. Extracellular Matrix Protein-Induced Changes in Human Salivary Epithelial Cell Organization and Proliferation on a Model Biological Substratum. *Biomaterials* **1999**, doi:10.1016/S0142-9612(98)00255-5.

297. Soscia, D.; Sequeira, S.; Schramm, R.; Jayarathanam, K.; Cantara, S.; Larsen, M.; Castracane, J. Salivary Gland Cell Differentiation and Organization on Micropatterned PLGA Nanofiber Craters. *Biomaterials* **2013**, *34*, 6773–6784, doi:10.1038/jid.2014.371.

298. Sequeira, S.; Soscia, D.; Oztan, B.; Mosier, A.; Jean-Gilles, R.; Castracane, J.; Larsen, M. The Regulation of Focal Adhesion Complex Formation and Salivary Gland Epithelial Cell Organization by Nanofibrous PLGA Scaffolds. *Bone* **2012**, *23*, 1–7, doi:10.1038/jid.2014.371.

299. Zhang, B.X.; Zhang, Z.L.; Lin, A.L.; Wang, H.; Pilia, M.; Ong, J.L.; Dean, D.D.; Chen, X.D.; Yeh, C.K. Silk Fibroin Scaffolds Promote Formation of the Ex Vivo Niche for Salivary Gland Epithelial Cell Growth, Matrix Formation, and Retention of Differentiated Function. *Tissue Eng Part A* **2015**, *21*, 1611–1620, doi:10.1089/ten.tea.2014.0411.

300. Pradhan, S.; Liu, C.; Zhang, C.; Jia, X.; Farach-Carson, M.C.; Witt, R.L. Lumen Formation in Three-Dimensional Cultures of Salivary Acinar Cells. *Otolaryngology - Head and Neck Surgery* **2010**, *142*, 191–195, doi:10.1016/j.otohns.2009.10.039.

301. Pradhan-Bhatt, S.; Harrington, D.A.; Duncan, R.L.; Jia, X.; Witt, R.L.; Farach-Carson, M.C. Implantable Three-Dimensional Salivary Spheroid Assemblies Demonstrate Fluid and Protein Secretory Responses to Neurotransmitters. *Tissue Eng Part A* **2013**, *19*, 1610, doi:10.1089/TEN.TEA.2012.0301.

302. Pradhan-Bhatt, S.; Harrington, D.A.; Duncan, R.L.; Farach-Carson, M.C.; Jia, X.; Witt, R.L. A Novel in Vivo Model for Evaluating Functional Restoration of a Tissue-Engineered Salivary Gland. *Laryngoscope* **2014**, *124*, 456—461, doi:10.1002/lary.24297.

303. Pradhan-Bhatt, S.; Harrington, D.A.; Duncan, R.L.; Jia, X.; Witt, R.L.; Farach-Carson, M.C. Implantable Three-Dimensional Salivary Spheroid Assemblies Demonstrate Fluid and Protein

Secretory Responses to Neurotransmitters. *Tissue Eng Part A* **2013**, *19*, 1610–1620, doi:10.1089/ten.tea.2012.0301.

304. Liu, S.; Zhang, H.; Remy, R.; Deng, F.; Mackay, M.; Fox, J.; Jia, X. Meter-Long Multiblock Copolymer Microfibers via Interfacial Bioorthogonal Polymerization. *Advanced Materials* **2017**, *27*, 2783–2790, doi:doi:10.1002/adma.201500360.

305. Shubin, A.D.; Felong, T.J.; Graunke, D.; Ovitt, C.E.; Benoit, D.S.W. Development of Poly(Ethylene Glycol) Hydrogels for Salivary Gland Tissue Engineering Applications. *Tissue Eng Part A* **2015**, doi:10.1089/ten.tea.2014.0674.

306. Peters, S.B.; Naim, N.; Nelson, D.A.; Mosier, A.P.; Cady, N.C.; Larsen, M. Salivary Gland Morphogenesis and Differentiation. **2014**, *20*, 1632–1642, doi:10.1089/ten.tea.2013.0515.

307. Miyajima, H.; Matsumoto, T.; Sakai, T.; Yamaguchi, S.; An, S.H.; Abe, M.; Wakisaka, S.; Lee, K.Y.; Egusa, H.; Imazato, S. Hydrogel-Based Biomimetic Environment for in Vitro Modulation of Branching Morphogenesis. *Biomaterials* **2011**, *32*, 6754–6763, doi:10.1016/j.biomaterials.2011.05.072.

308. Jorgensen, M.; Ramesh, P.; Toro, M.; Evans, E.; Moskwa, N.; Zhang, X.; Sharfstein, S.T.; Larsen, M.; Xie, Y. Alginate Hydrogel Microtubes for Salivary Gland Cell Organization and Cavitation. *Bioengineering* **2022**, *9*, 38, doi:10.3390/BIOENGINEERING9010038/S1.

309. Nam, K.; Jones, J.P.; Lei, P.; Andreadis, S.T.; Baker, O.J. Laminin-111 Peptides Conjugated to Fibrin Hydrogels Promote Formation of Lumen Containing Parotid Gland Cell Clusters. *Biomacromolecules* **2016**, *17*, 2293–2301, doi:10.1021/ACS.BIOMAC.6B00588.

310. Miyake, Y.; Shimizu, O.; Shiratsuchi, H.; Tamagawa, T.; Tonogi, M. Wound Healing after Applying a Gelatin-Based Hydrogel Sheet to Resected Rat Submandibular Gland. *J Oral Sci* **2020**, *62*, 222–225, doi:10.2334/JOSNUSD.19-0244.

311. Adine, C.; Ng, K.K.; Rungarunlert, S.; Souza, G.R.; Ferreira, J.N. Engineering Innervated Secretory Epithelial Organoids by Magnetic Three-Dimensional Bioprinting for Stimulating Epithelial Growth in Salivary Glands. *Biomaterials* **2018**, *180*, 52–66, doi:10.1016/j.biomaterials.2018.06.011.

312. MacLaren, R.E.; Pearson, R.A.; MacNeil, A.; Douglas, R.H.; Salt, T.E.; Akimoto, M.; Swaroop, A.; Sowden, J.C.; Ali, R.R. Retinal Repair by Transplantation of Photoreceptor Precursors. *Nature* **2006**, doi:10.1038/nature05161.

313. Payne, S.L.; Anandakumaran, P.N.; Varga, B. V.; Morshead, C.M.; Nagy, A.; Shoichet, M.S. In Vitro Maturation of Human IPSC-Derived Neuroepithelial Cells Influences Transplant Survival in the Stroke-Injured Rat Brain. *Tissue Eng Part A* **2018**, doi:10.1089/ten.tea.2016.0515.

314. Hatzimichael, E.; Tuthill, M. Hematopoietic Stem Cell Transplantation. *Stem Cells Cloning* 2010.

315. Cavazzana, M.; Six, E.; Lagresle-Peyrou, C.; André-Schmutz, I.; Hacein-Bey-Abina, S. Gene Therapy for X-Linked Severe Combined Immunodeficiency: Where Do We Stand? *Hum Gene Ther* **2016**, doi:10.1089/hum.2015.137.

316. Voermans, C.; Kooi, M.L.K.; Rodenhuis, S.; Van Der Lelie, H.; Van Der Schoot, C.E.; Gerritsen, W.R. In Vitro Migratory Capacity of CD34+ Cells Is Related to Hematopoietic Recovery after Autologous Stem Cell Transplantation. *Blood* **2001**, doi:10.1182/blood.V97.3.799.

317. Richardson, P.M.; McGuinness, U.M.; Aguayo, A.J. Axons from CNS Neurones Regenerate into PNS Grafts. *Nature* **1980**, doi:10.1038/284264a0.

318. Peled, A.; Petit, I.; Kollet, O.; Magid, M.; Ponomaryov, T.; Byk, T.; Nagler, A.; Ben-Hur, H.; Many, A.; Shultz, L.; et al. Dependence of Human Stem Cell Engraftment and Repopulation of NOD/SCID Mice on CXCR4. *Science (1979)* **1999**, doi:10.1126/science.283.5403.845.

319. Chakrapani, V.Y.; Gnanamani, A.; Giridev, V.R.; Madhusoothanan, M.; Sekaran, G. Electrospinning of Type i Collagen and PCL Nanofibers Using Acetic Acid. *J Appl Polym Sci* **2012**, doi:10.1002/app.36504.

320. Zhang, Z.; Chen, N.; Li, S.; Battig, M.R.; Wang, Y. Programmable Hydrogels for Controlled Cell Catch and Release Using Hybridized Aptamers and Complementary Sequences. *J Am Chem Soc* **2012**, *134*, 15716–15719, doi:10.1021/ja307717w.

321. Park, J.S.; Choi, J.B.; Jo, S.Y.; Lim, Y.M.; Gwon, H.J.; Khil, M.S.; Nho, Y.C. Characterization and Structure Analysis of PLGA/Collagen Nanofibrous Membranes by Electrospinning. *J Appl Polym Sci* **2012**, doi:10.1002/app.36833.

322. Bhattarai, N.; Zhang, M. Controlled Synthesis and Structural Stability of Alginate-Based Nanofibers. *Nanotechnology* **2007**, doi:10.1088/0957-4484/18/45/455601.

323. Sfakis, L.; Sharikova, A.; Tuschel, D.; Costa, F.X.; Larsen, M.; Khmaladze, A.; Castracane, J. Core/Shell Nanofiber Characterization by Raman Scanning Microscopy. *Biomed Opt Express* **2017**, *8*, 1025, doi:10.1364/BOE.8.001025.

324. Jean-Gilles, R.; Soscia, D.; Sequeira, S.; Melfi, M.; Gadre, A.; Castracane, J.; Larsen, M. Novel Modeling Approach to Generate a Polymeric Nanofiber Scaffold for Salivary Gland Cells. *J Nanotechnol Eng Med* **2010**, *1*, doi:10.1115/1.4001744.

325. Sequeira, S.; Soscia, D.; Oztan, B.; Mosier, A.; Jean-Gilles, R.; Castracane, J.; Larsen, M. The Regulation of Focal Adhesion Complex Formation and Salivary Gland Epithelial Cell Organization by Nanofibrous PLGA Scaffolds. *Bone* **2012**, *23*, 1–7, doi:10.1038/jid.2014.371.

326. Soscia, D.A.; Sequeira, S.J.; Schramm, R.A.; Jayarathanam, K.; Cantara, S.I.; Larsen, M.; Castracane, J. Salivary Gland Cell Differentiation and Organization on Micropatterned PLGA Nanofiber Craters. *Biomaterials* **2013**, doi:10.1016/j.biomaterials.2013.05.061.

327. Cantara, S.; Soscia, D.; Sequeira, S.; Jean-Gilles, R.; Castracane, J.; Larsen, M. Selective Functionalization of Nanofiber Scaffolds to Regulate Salivary Gland Epithelial Cell Proliferation and Polarity. *Biomaterials* **2012**, *33*, 8372–8382, doi:doi:10.1016/j.biomaterials.2012.08.021.

328. Lee, K.W.D.; Chan, P.K.; Feng, X. Morphology Development and Characterization of the Phase-Separated Structure Resulting from the Thermal-Induced Phase Separation Phenomenon in Polymer Solutions under a Temperature Gradient. *Chem Eng Sci* **2004**, doi:10.1016/j.ces.2003.12.025.

329. Bischof, J.C.; He, X. Thermal Stability of Proteins. *Ann N Y Acad Sci* 2006.

330. Qian, L.; Zhang, H. Controlled Freezing and Freeze Drying: A Versatile Route for Porous and Micro-/Nano-Structured Materials. *Journal of Chemical Technology & Biotechnology* **2011**, *86*, 172–184, doi:10.1002/JCTB.2495.

331. Peters, S.B.; Naim, N.; Nelson, D.A.; Mosier, A.P.; Cady, N.C.; Larsen, M. Biocompatible Tissue Scaffold Compliance Promotes Salivary Gland Morphogenesis and Differentiation. *Tissue Eng Part A* **2014**, *20*, 1632–1642, doi:10.1089/ten.tea.2013.0515.

332. Taketa, H.; Sathi, G.A.; Farahat, M.; Rahman, K.A.; Sakai, T.; Hirano, Y.; Kuboki, T.; Torii, Y.; Matsumoto, T. Peptide-Modified Substrate for Modulating Gland Tissue Growth and Morphology In Vitro. *Scientific Reports 2015 5:1* **2015**, *5*, 1–9, doi:10.1038/srep11468.

333. Kazi, G.A.S.; Yamanaka, T.; Osamu, Y. Chitosan Coating an Efficient Approach to Improve the Substrate Surface for In Vitro Culture System. *J Electrochem Soc* **2019**, *166*, B3025–B3030, doi:10.1149/2.0051909JES/XML.

334. Hsiao, Y.C.; Chen, C.N.; Chen, Y.T.; Yang, T.L. Controlling Branching Structure Formation of the Salivary Gland by the Degree of Chitosan Deacetylation. *Acta Biomater* **2013**, *9*, 8214–8223, doi:10.1016/J.ACTBIO.2013.06.002.

335. Yang, T.L.; Young, T.H. The Enhancement of Submandibular Gland Branch Formation on Chitosan Membranes. *Biomaterials* **2008**, *29*, 2501–2508, doi:10.1016/J.BIOMATERIALS.2008.02.014.

336. Yang, T.L.; Young, T.H. Chitosan Cooperates with Mesenchyme-Derived Factors Inregulating Salivary Gland Epithelial Morphogenesis. *J Cell Mol Med* **2009**, *13*, 2853–2863, doi:10.1111/J.1582-4934.2008.00425.X.

337. Yang, T.L.; Hsiao, Y.C. Chitosan Facilitates Structure Formation of the Salivary Gland by Regulating the Basement Membrane Components. *Biomaterials* **2015**, *66*, 29–40, doi:10.1016/J.BIOMATERIALS.2015.06.028.

338. Pham, H.M.; Zhang, Y.; Munguia-Lopez, J.G.; Tran, S.D. Egg White Alginate as a Novel Scaffold Biomaterial for 3D Salivary Cell Culturing. *Biomimetics (Basel)* **2021**, *7*, doi:10.3390/BIOMIMETICS7010005.

339. Nam, K.; dos Santos, H.T.; Maslow, F.; Trump, B.G.; Lei, P.; Andreadis, S.T.; Baker, O.J. Laminin-1 Peptides Conjugated to Fibrin Hydrogels Promote Salivary Gland Regeneration in Irradiated Mouse Submandibular Glands. *Front Bioeng Biotechnol* **2021**, *9*, 729180, doi:10.3389/FBIOE.2021.729180/BIBTEX.

340. Lee, J.K.; Link, J.M.; Hu, J.C.Y.; Athanasiou, K.A. The Self-Assembling Process and Applications in Tissue Engineering. **2017**, 1–17.

341. Wei, C.; Larsen, M.; Ph, D.; Hoffman, M.P.; Ph, D.; Yamada, K.M.; Ph, D. Self-Organization and Branching Morphogenesis of Primary Salivary Epithelial Cells. *Tissue Eng* **2007**, *13*, doi:10.1089/ten.2006.0123.

342. Dost, P. Ultrasonographic Biometry in Normal Salivary Glands. *European Archives of Oto-Rhino-Laryngology* **1997**, *254*, 18–19, doi:10.1007/BF02439713.

343. Mandrycky, C.; Wang, Z.; Kim, K.; Kim, D.H. 3D Bioprinting for Engineering Complex Tissues. *Biotechnol Adv* **2016**, *34*, 422–434, doi:10.1016/j.biotechadv.2015.12.011.

344. Shpichka, A.I.; Koroleva, A. V.; Deiwick, A.; Timashev, P.S.; Semenova, E.F.; Moiseeva, I.Y.; Konoplyannikov, M.A.; Chichkov, B.N. EVALUATION OF VASCULOGENIC POTENTIAL OF MODIFIED FIBRIN HYDROGEL. *Tsitologiia* **2016**, *58*, 785–791.

345. Ferreira, J.N.; Hoffman, M.P. Interactions between Developing Nerves and Salivary Glands. *Organogenesis* **2013**, *9*, 152–158, doi:10.4161/org.25224.

346. Patel, V.N.; Hoffman, M.P. Salivary Gland Development: A Template for Regeneration. *Semin Cell Dev Biol* **2014**, *25–26*, 52–60, doi:10.1016/j.semcdb.2013.12.001.

347. Hong, G.; Yang, X.; Zhou, T.; Lieber, C.M. Mesh Electronics: A New Paradigm for Tissue-like Brain Probes. *Curr Opin Neurobiol* **2018**, *50*, 33–41, doi:10.1016/j.conb.2017.11.007.

348. Viveros, R.D.; Zhou, T.; Hong, G.; Fu, T.M.; Lin, H.Y.G.; Lieber, C.M. Advanced One- and Two-Dimensional Mesh Designs for Injectable Electronics. *Nano Lett* **2019**, *19*, 4180–4187, doi:10.1021/acs.nanolett.9b01727.

349. Goldman, E.B.; Zak, A.; Tenne, R.; Kartvelishvily, E.; Levin-Zaidman, S.; Neumann, Y.; Stiubea-Cohen, R.; Palmon, A.; Hovav, A.H.; Aframian, D.J. Biocompatibility of Tungsten Disulfide Inorganic Nanotubes and Fullerene-like Nanoparticles with Salivary Gland Cells. *Tissue Eng Part A* **2015**, *21*, 1013–1023, doi:10.1089/ten.tea.2014.0163.

350. Chen, X.; Wu, P.; Rousseas, M.; Okawa, D.; Gartner, Z.; Zettl, A.; Bertozzi, C.R. Boron Nitride Nanotubes Are Noncytotoxic and Can Be Functionalized for Interaction with Proteins and Cells. *J Am Chem Soc* **2009**, doi:10.1021/ja807334b.

351. Oprych, K.M.; Whitby, R.L.D.; Mikhalovsky, S. V.; Tomlins, P.; Adu, J. Repairing Peripheral Nerves: Is There a Role for Carbon Nanotubes? *Adv Healthc Mater* **2016**, *5*, 1253–1271, doi:10.1002/ADHM.201500864.

352. Owens, C.M.; Marga, F.; Forgacs, G.; Heesch, C.M. Biofabrication and Testing of a Fully Cellular Nerve Graft. *Biofabrication* **2013**, doi:10.1088/1758-5082/5/4/045007.

353. Lorber, B.; Hsiao, W.K.; Hutchings, I.M.; Martin, K.R. Adult Rat Retinal Ganglion Cells and Glia Can Be Printed by Piezoelectric Inkjet Printing. *Biofabrication* **2013**, *6*, 015001, doi:10.1088/1758-5082/6/1/015001.

354. Pateman, C. Development Of Microstereolithography And Photopolymerisable Polymers for Peripheral Nerve Repair. **2014**.

355. Varghese, J.J.; Schmale, I.L.; Wang, Y.; Hansen, M.E.; Newlands, S.D.; Ovitt, C.E.; Benoit, D.S.W. Retroductal Nanoparticle Injection to the Murine Submandibular Gland. **2018**, 1–7, doi:10.3791/57521.

356. Aguado, B.A.; Mulyasasmita, W.; Su, J.; Lampe, K.J.; Heilshorn, S.C. Improving Viability of Stem Cells during Syringe Needle Flow through the Design of Hydrogel Cell Carriers. *Tissue Eng Part A* **2012**, doi:10.1089/ten.tea.2011.0391.

357. Amer, M.H.; Rose, F.R.A.J.; Shakesheff, K.M.; Modo, M.; White, L.J. Translational Considerations in Injectable Cell-Based Therapeutics for Neurological Applications: Concepts, Progress and Challenges. *NPJ Regen Med* **2017**, doi:10.1038/s41536-017-0028-x.

358. Rodell, C.B.; Kaminski, A.L.; Burdick, J.A. Rational Design of Network Properties in Guest-Host Assembled and Shear-Thinning Hyaluronic Acid Hydrogels. *Biomacromolecules* **2013**, doi:10.1021/bm401280z.

359. Frisch, S.M.; Francis, H. Disruption of Epithelial Cell-Matrix Interactions Induces Apoptosis. *Journal of Cell Biology* **1994**, doi:10.1083/jcb.124.4.619.

360. Lee, J.W.; Juliano, R. Mitogenic Signal Transduction by Integrin- and Growth Factor Receptor-Mediated Pathways. *Mol Cells* 2004.

361. Pierschbacher, M.D.; Ruoslahti, E. Cell Attachment Activity of Fibronectin Can Be Duplicated by Small Synthetic Fragments of the Molecule. *Nature* **1984**, doi:10.1038/309030a0.

362. Plow, E.F.; Haas, T.A.; Zhang, L.; Loftus, J.; Smith, J.W. Ligand Binding to Integrins. *Journal of Biological Chemistry* 2000.

363. Hersel, U.; Dahmen, C.; Kessler, H. RGD Modified Polymers: Biomaterials for Stimulated Cell Adhesion and Beyond. *Biomaterials* **2003**, doi:10.1016/S0142-9612(03)00343-0.

364. Ho, S.S.; Murphy, K.C.; Binder, B.Y.K.; Vissers, C.B.; Leach, J.K. Increased Survival and Function of Mesenchymal Stem Cell Spheroids Entrapped in Instructive Alginate Hydrogels. *Stem Cells Transl Med* **2016**, doi:10.5966/sctm.2015-0211.

365. Saliba, J.; Daou, A.; Damiati, S.; Saliba, J.; El-Sabban, M.; Mhanna, R. Development of Microplatforms to Mimic the in Vivo Architecture of CNS and PNS Physiology and Their Diseases. *Genes (Basel)* 2018, *9*.

366. Somaa, F.A.; Wang, T.Y.; Niclis, J.C.; Bruggeman, K.F.; Kauhausen, J.A.; Guo, H.; McDougall, S.; Williams, R.J.; Nisbet, D.R.; Thompson, L.H.; et al. Peptide-Based Scaffolds Support Human Cortical Progenitor Graft Integration to Reduce Atrophy and Promote Functional Repair in a Model of Stroke. *Cell Rep* **2017**, doi:10.1016/j.celrep.2017.07.069.

367. Tam, R.Y.; Fuehrmann, T.; Mitrousis, N.; Shoichet, M.S. Regenerative Therapies for Central Nervous System Diseases: A Biomaterials Approach. *Neuropsychopharmacology* 2014.

368. Wang, C.; Liu, Y.; Fan, Y.; Li, X. The Use of Bioactive Peptides to Modify Materials for Bone Tissue Repair. *Regen Biomater* **2017**, doi:10.1093/rb/rbx011.

369. Lu, Z.F.; Singh, G.; Lesani, P.; Zreiqat, H. Promise and Perspective of Nanomaterials in Antisenescence Tissue Engineering Applications. *ACS Biomater Sci Eng* **2022**, *8*, 3133–3141, doi:10.1021/ACSBIOMATERIALS.1C01298/ASSET/IMAGES/MEDIUM/AB1C01298_0005.GIF.

370. Wissler Gerdes, E.O.; Zhu, Y.; Tchkonia, T.; Kirkland, J.L. Discovery, Development, and Future Application of Senolytics: Theories and Predictions. *FEBS J* **2020**, *287*, 2418–2427, doi:10.1111/FEBS.15264.

371. Fontoura, J.C.; Viezzer, C.; dos Santos, F.G.; Ligabue, R.A.; Weinlich, R.; Puga, R.D.; Antonow, D.; Severino, P.; Bonorino, C. Comparison of 2D and 3D Cell Culture Models for Cell Growth, Gene Expression and Drug Resistance. *Materials Science and Engineering: C* **2020**, *107*, 110264, doi:10.1016/J.MSEC.2019.110264.

372. Baker, B.M.; Chen, C.S. Deconstructing the Third Dimension-How 3D Culture Microenvironments Alter Cellular Cues. *J Cell Sci* **2012**, *125*, 3015–3024, doi:10.1242/JCS.079509.

373. Santos, J.M.; Camões, S.P.; Filipe, E.; Cipriano, M.; Barcia, R.N.; Filipe, M.; Teixeira, M.; Simões, S.; Gaspar, M.; Mosqueira, D.; et al. Three-Dimensional Spheroid Cell Culture of Umbilical Cord Tissue-Derived Mesenchymal Stromal Cells Leads to Enhanced Paracrine Induction of Wound Healing. *Stem Cell Res Ther* **2015**, *6*, 1–19, doi:10.1186/S13287-015-0082-5/FIGURES/7.

374. Kabiri, M.; Kul, B.; Lott, W.B.; Futrega, K.; Ghanavi, P.; Upton, Z.; Doran, M.R. 3D Mesenchymal Stem/Stromal Cell Osteogenesis and Autocrine Signalling. *Biochem Biophys Res Commun* **2012**, *419*, 142–147, doi:10.1016/J.BBRC.2012.01.017.

375. Song, Y.; Uchida, H.; Sharipol, A.; Piraino, L.; Mereness, J.A.; Ingalls, M.H.; Rebhahn, J.; Newlands, S.D.; DeLouise, L.A.; Ovitt, C.E.; et al. Development of a Functional Salivary Gland Tissue Chip with Potential for High-Content Drug Screening. *Communications Biology 2021 4:1* **2021**, *4*, 1–15, doi:10.1038/s42003-021-01876-x.

376. Geckil, H.; Xu, F.; Zhang, X.; Moon, S.; Demirci, U. Engineering Hydrogels as Extracellular Matrix Mimics. *Nanomedicine* **2010**, *5*, 469–484, doi:10.2217/NNM.10.12.

377. Jain, R.; Roy, S. Designing a Bioactive Scaffold from Coassembled Collagen–Laminin Short Peptide Hydrogels for Controlling Cell Behaviour. *RSC Adv* **2019**, *9*, 38745–38759, doi:10.1039/C9RA07454F.

378. Ozdemir, T.; Fowler, E.W.; Liu, S.; Harrington, D.A.; Witt, R.L.; Farach-Carson, M.C.; Pradhan-Bhatt, S.; Jia, X. Tuning Hydrogel Properties to Promote the Assembly of Salivary Gland Spheroids in 3D. *ACS Biomater Sci Eng* **2016**, *2*, 2217–2230, doi:10.1021/ACSBIOMATERIALS.6B00419/ASSET/IMAGES/LARGE/AB-2016-00419P_0009.JPEG.

379. Rose, S.C.; Larsen, M.; Xie, Y.; Sharfstein, S.T. Salivary Gland Bioengineering. *Bioengineering 2024, Vol. 11, Page 28* **2023**, *11*, 28, doi:10.3390/BIOENGINEERING11010028.

380. Sasportas, L.S.; Hosford, D.N.; Sodini, M.A.; Waters, D.J.; Zambricki, E.A.; Barral, J.K.; Graves, E.E.; Brinton, T.J.; Yock, P.G.; Le, Q.T.; et al. Cost-Effectiveness Landscape Analysis of Treatments Addressing Xerostomia in Patients Receiving Head and Neck Radiation Therapy. *Oral Surg Oral Med Oral Pathol Oral Radiol* **2013**, *116*, doi:10.1016/J.OOOO.2013.02.017.

381. Wolff, A.; Joshi, R.K.; Ekström, J.; Aframian, D.; Pedersen, A.M.L.; Proctor, G.; Narayana, N.; Villa, A.; Sia, Y.W.; Aliko, A.; et al. A Guide to Medications Inducing Salivary Gland Dysfunction,

Xerostomia, and Subjective Sialorrhea: A Systematic Review Sponsored by the World Workshop on Oral Medicine VI. *Drugs in R&D 2016 17:1* **2016**, *17*, 1–28, doi:10.1007/S40268-016-0153-9.

382. Stewart, C.R.; Obi, N.; Epane, E.C.; Akbari, A.A.; Halpern, L.; Southerland, J.H.; Gangula, P.R. The Effects of Diabetes on Salivary Gland Protein Expression of Tetrahydrobiopterin and Nitric Oxide Synthesis and Function. *J Periodontol* **2016**, *87*, 735, doi:10.1902/JOP.2016.150639.

383. Jensen, S.B.; Pedersen, A.M.L.; Vissink, A.; Andersen, E.; Brown, C.G.; Davies, A.N.; Dutilh, J.; Fulton, J.S.; Jankovic, L.; Lopes, N.N.F.; et al. A Systematic Review of Salivary Gland Hypofunction and Xerostomia Induced by Cancer Therapies: Prevalence, Severity and Impact on Quality of Life. *Support Care Cancer* **2010**, *18*, 1039–1060, doi:10.1007/S00520-010-0827-8.

384. Turner, M.D.; Ship, J.A. Dry Mouth and Its Effects on the Oral Health of Elderly People. *J Am Dent Assoc* **2007**, *138 Suppl*, S15–S20, doi:10.14219/JADA.ARCHIVE.2007.0358.

385. Stewart, B.W.; Wild, C.P. *World Cancer Report 2014,Geneva, Switzerland: World Health Organization, International Agency for Research on Cancer, WHO Press, 2015*; 2015; Vol. XV; ISBN 978-92-832-0429-9.

386. Coppes, R. *First in Man Clinical Trial on Salivary Gland Stem Cell Transplantation to Ameliorate Radiotherapy Induced Xerostomia*; 2021;

387. Polaris Market Research Xerostomia (Dry Mouth) Therapeutics Market - Industry Report, 2023-2032 Available online: https://www.polarismarketresearch.com/industry-analysis/xerostomia-therapeutics-market (accessed on 16 June 2024).

388. Weng, P.L.; Aure, M.H.; Maruyama, T.; Ovitt, C.E. Limited Regeneration of Adult Salivary Glands after Severe Injury Involves Cellular Plasticity. *Cell Rep* **2018**, *24*, 1464-1470.e3, doi:10.1016/J.CELREP.2018.07.016.

389. Yoo, C.; Vines, J.B.; Alexander, G.; Murdock, K.; Hwang, P.; Jun, H.W. Adult Stem Cells and Tissue Engineering Strategies for Salivary Gland Regeneration: A Review. *Biomater Res* **2014**, *18*, doi:10.1186/2055-7124-18-9.

390. Konkel, J.E.; O'Boyle, C.; Krishnan, S. Distal Consequences of Oral Inflammation. *Front Immunol* **2019**, *10*, doi:10.3389/FIMMU.2019.01403.

391. Jorgensen, M.; Ramesh, P.; Toro, M.; Evans, E.; Moskwa, N.; Zhang, X.; Sharfstein, S.T.; Larsen, M.; Xie, Y. Alginate Hydrogel Microtubes for Salivary Gland Cell Organization and Cavitation. *Bioengineering* **2022**, *9*, 38, doi:10.3390/BIOENGINEERING9010038/S1.

392. Jainchill, J.L.; Aaronson, S.A.; Todaro, G.J. Murine Sarcoma and Leukemia Viruses: Assay Using Clonal Lines of Contact-Inhibited Mouse Cells. *J Virol* **1969**, *4*, 549, doi:10.1128/JVI.4.5.549-553.1969.

393. Barka, T.; Gresik, E.S.; Miyazaki, Y. Differentiation of a Mouse Submandibular Gland-Derived Cell Line (SCA) Grown on Matrigel. *Exp Cell Res* **2005**, *308*, 394–406, doi:10.1016/J.YEXCR.2005.04.025.

394. Barka, T.; Van Der Noen, H.; Michelakis, A.M.; Schenkein, I. Epidermal Growth Factor, Renin, and Peptidase in Cultured Tumor Cells of Submandibular Gland Origin. *Lab Invest* **1980**, *42*, 656–662.

395. Daley, W.P.; Gulfo, K.M.; Sequeira, S.J.; Larsen, M. Identification of a Mechanochemical Checkpoint and Negative Feedback Loop Regulating Branching Morphogenesis. *Dev Biol* **2009**, doi:10.1016/j.ydbio.2009.09.037.

396. Dmytrenko, G.; Castro, M.E.; Sales, M.E. Denatonium and Naringenin Promote SCA-9 Tumor Growth and Angiogenesis: Participation of Arginase. *Nutr Cancer* **2017**, *69*, 780–790, doi:10.1080/01635581.2017.1328605.

397. Barisam, M.; Saidi, M.S.; Kashaninejad, N.; Nguyen, N.T. Prediction of Necrotic Core and Hypoxic Zone of Multicellular Spheroids in a Microbioreactor with a U-Shaped Barrier. *Micromachines 2018, Vol. 9, Page 94* **2018**, *9*, 94, doi:10.3390/MI9030094.

398. Adler, E.; Hoon, M.A.; Mueller, K.L.; Chandrashekar, J.; Ryba, N.J.P.; Zuker, C.S. A Novel Family of Mammalian Taste Receptors. *Cell* **2000**, *100*, 693–702, doi:10.1016/S0092-8674(00)80705-9.

399. Kertesz, Z.; Harrington, E.O.; Braza, J.; Guarino, B.D.; Chichger, H. Agonists for Bitter Taste Receptors T2R10 and T2R38 Attenuate LPS-Induced Permeability of the Pulmonary Endothelium in Vitro. *Front Physiol* **2022**, *13*, 794370, doi:10.3389/FPHYS.2022.794370.

400. Anderson, G.; Ebadi, M.; Vo, K.; Novak, J.; Govindarajan, A.; Amini, A. An Updated Review on Head and Neck Cancer Treatment with Radiation Therapy. *Cancers (Basel)* **2021**, *13*, doi:10.3390/CANCERS13194912.

401. Nutting, C.M.; Morden, J.P.; Harrington, K.J.; Urbano, T.G.; Bhide, S.A.; Clark, C.; Miles, E.A.; Miah, A.B.; Newbold, K.; Tanay, M.A.; et al. Parotid-Sparing Intensity Modulated versus Conventional Radiotherapy in Head and Neck Cancer (PARSPORT): A Phase 3 Multicentre Randomised Controlled Trial. *Lancet Oncol* **2011**, *12*, 127–136, doi:10.1016/S1470-2045(10)70290-4.

402. Griffin, K.H.; Fok, S.W.; Kent Leach, J. Strategies to Capitalize on Cell Spheroid Therapeutic Potential for Tissue Repair and Disease Modeling. *npj Regenerative Medicine 2022 7:1* **2022**, *7*, 1–13, doi:10.1038/s41536-022-00266-z.

403. Arnold, J.T.; Kaufman, D.G.; Seppälä, M.; Lessey, B.A. Endometrial Stromal Cells Regulate Epithelial Cell Growth in Vitro: A New Co-Culture Model. *Human Reproduction* **2001**, *16*, 836–845, doi:10.1093/HUMREP/16.5.836.

404. Sfakis, L.; Kamaldinov, T.; Khmaladze, A.; Hosseini, Z.F.; Nelson, D.A.; Larsen, M.; Castracane, J. Mesenchymal Cells Affect Salivary Epithelial Cell Morphology on PGS/PLGA Core/Shell Nanofibers. *Int J Mol Sci* **2018**, *19*, doi:10.3390/IJMS19041031.

405. Tanaka, J.; Mishima, K. In Vitro Three-Dimensional Culture Systems of Salivary Glands. *Pathol Int* **2020**, *70*, 493–501, doi:10.1111/PIN.12947.

406. Lindberg, G.C.J.; Cui, X.; Durham, M.; Veenendaal, L.; Schon, B.S.; Hooper, G.J.; Lim, K.S.; Woodfield, T.B.F. Probing Multicellular Tissue Fusion of Cocultured Spheroids—A 3D-Bioassembly Model. *Advanced Science* **2021**, *8*, 2103320, doi:10.1002/ADVS.202103320.

407. Ramesh, P. Biomimetic Scaffolds Targeting Remediation of Fibrosis and Regeneration of the Salivary Gland, SUNY Polytechnic University: Albany, 2022.

408. Li, H.; Madnick, S.; Zhao, H.; Hall, S.; Amin, A.; Dent, M.P.; Boekelheide, K. A Novel Co-Culture Model of Human Prostate Epithelial and Stromal Cells for Androgenic and Antiandrogenic Screening. *Toxicology in Vitro* **2023**, *91*, 105624, doi:10.1016/J.TIV.2023.105624.

409. Rock, K.L.; Kono, H. The Inflammatory Response to Cell Death. *Annual Review of Pathology: Mechanisms of Disease* **2008**, *3*, 99–126, doi:10.1146/ANNUREV.PATHMECHDIS.3.121806.151456/CITE/REFWORKS.

410. Altrieth, A.L.; O'Keefe, K.J.; Gellatly, V.A.; Tavarez, J.R.; Feminella, S.M.; Moskwa, N.L.; Cordi, C. V.; Turrieta, J.C.; Nelson, D.A.; Larsen, M. Identifying Fibrogenic Cells Following Salivary Gland Obstructive Injury. *Front Cell Dev Biol* **2023**, *11*, 1190386, doi:10.3389/FCELL.2023.1190386/BIBTEX.

411. Vanlangenakker, N.; Berghe, T.; Krysko, D.; Festjens, N.; Vandenabeele, P. Molecular Mechanisms and Pathophysiology of Necrotic Cell Death. *Cur Mol Med* **2008**, *8*, 207–220, doi:10.2174/156652408784221306.

412. Berghe, T. Vanden; Vanlangenakker, N.; Parthoens, E.; Deckers, W.; Devos, M.; Festjens, N.; Guerin, C.J.; Brunk, U.T.; Declercq, W.; Vandenabeele, P. Necroptosis, Necrosis and Secondary Necrosis Converge on Similar Cellular Disintegration Features. *Cell Death & Differentiation 2010 17:6* **2009**, *17*, 922–930, doi:10.1038/cdd.2009.184.

413. Takahara, T.; Nakayama, Y.; Itoh, H.; Miyabayashi, C.; Watanabe, A.; Sasaki, H.; Inoue, K.; Muragaki, Y.; Ooshima, A. Extracellular Matrix Formation in Piecemeal Necrosis: Immunoelectron Microscopic Study. *Liver* **1992**, *12*, 368–380, doi:10.1111/J.1600-0676.1992.TB00591.X.

414. Trump, B.F.; Berezesky, I.K.; Chang, S.H.; Phelps, P.C. The Pathways of Cell Death: Oncosis, Apoptosis, and Necrosis. *http://dx.doi.org/10.1177/019262339702500116* **1997**, *25*, 82–88, doi:10.1177/019262339702500116.

415. Pinto, B.; Henriques, A.C.; Silva, P.M.A.; Bousbaa, H. Three-Dimensional Spheroids as In Vitro Preclinical Models for Cancer Research. *Pharmaceutics* **2020**, *12*, 1–38, doi:10.3390/PHARMACEUTICS12121186.

416. Lee, S. Il; Yeo, S. Il; Kim, B.B.; Ko, Y.; Park, J.B. Formation of Size-Controllable Spheroids Using Gingiva-Derived Stem Cells and Concave Microwells: Morphology and Viability Tests. *Biomed Rep* **2016**, *4*, 97, doi:10.3892/BR.2015.539.

417. Valstar, M.H.; de Bakker, B.S.; Steenbakkers, R.J.H.M.; de Jong, K.H.; Smit, L.A.; Klein Nulent, T.J.W.; van Es, R.J.J.; Hofland, I.; de Keizer, B.; Jasperse, B.; et al. The Tubarial Salivary Glands: A Potential New Organ at Risk for Radiotherapy. *Radiotherapy and Oncology* **2021**, *154*, 292–298, doi:10.1016/j.radonc.2020.09.034.

418. Leehan, K.M.; Pezant, N.P.; Rasmussen, A.; Grundahl, K.; Moore, J.S.; Radfar, L.; Lewis, D.M.; Stone, D.U.; Lessard, C.J.; Rhodus, N.L.; et al. Minor Salivary Gland Fibrosis in Sjögren's Syndrome

Is Elevated, Associated with Focus Score and Not Solely a Consequence of Aging. *Clin Exp Rheumatol* **2018**, *36*, 80.

419. Luitje, M.E.; Israel, A.K.; Cummings, M.A.; Giampoli, E.J.; Allen, P.D.; Newlands, S.D.; Ovitt, C.E. Long-Term Maintenance of Acinar Cells in Human Submandibular Glands After Radiation Therapy. *Int J Radiat Oncol Biol Phys* **2021**, *109*, 1028, doi:10.1016/J.IJROBP.2020.10.037.

420. Gao, Z.; Yin, J.; Zhang, J.; Ward, R.E.; Martin, R.J.; Lefevre, M.; Cefalu, W.T.; Ye, J. Butyrate Improves Insulin Sensitivity and Increases Energy Expenditure in Mice. *Diabetes* **2009**, *58*, 1509–1517, doi:10.2337/db08-1637.

421. Zhang, X.; Yun, J.S.; Han, D.; Yook, J.I.; Kim, H.S.; Cho, E.S. TGF-β Pathway in Salivary Gland Fibrosis. *International Journal of Molecular Sciences 2020, Vol. 21, Page 9138* **2020**, *21*, 9138, doi:10.3390/IJMS21239138.

422. Altrieth, A.L.; O'Keefe, K.J.; Gellatly, V.A.; Tavarez, J.R.; Feminella, S.M.; Moskwa, N.L.; Cordi, C. V.; Turrieta, J.C.; Nelson, D.A.; Larsen, M. Identifying Fibrogenic Cells Following Salivary Gland Obstructive Injury. *Front Cell Dev Biol* **2023**, *11*, 1190386, doi:10.3389/FCELL.2023.1190386/BIBTEX.

423. Asam, S.; Neag, G.; Berardicurti, O.; Gardner, D.; Barone, F. The Role of Stroma and Epithelial Cells in Primary Sjögren's Syndrome. *Rheumatology (Oxford)* **2021**, *60*, 3503–3512, doi:10.1093/RHEUMATOLOGY/KEZ050.

424. Stoopler, E.T.; Villa, A.; Bindakhil, M.; Díaz, D.L.O.; Sollecito, T.P. Common Oral Conditions: A Review. *JAMA* **2024**, *331*, 1045–1054, doi:10.1001/JAMA.2024.0953.

425. Hall, E.J.; Giaccia, A.J. *Radiobiology for the Radiologist*; Wolters Kluwer, 2018; ISBN 9781496335418.

426. Santivasi, W.L.; Xia, F. Ionizing Radiation-Induced DNA Damage, Response, and Repair. *https://home.liebertpub.com/ars* **2014**, *21*, 251–259, doi:10.1089/ARS.2013.5668.

427. Konings, A.W.T.; Coppes, R.P.; Vissink, A. On the Mechanism of Salivary Gland Radiosensitivity. *International Journal of Radiation Oncology*Biology*Physics* **2005**, *62*, 1187–1194, doi:10.1016/J.IJROBP.2004.12.051.

428. Stephens, L.C.; Schultheiss, T.E.; Price, R.E.; Kian Ang, " K; Peters, L.J. Radiation Apoptosis of Serous Acinar Cells of Salivary and Lacrimal Glands. **1991**, doi:10.1002/1097-0142.

429. Saarilahti, K.; Kouri, M.; Collan, J.; Hämäläinen, T.; Atula, T.; Joensuu, H.; Tenhunen, M. Intensity Modulated Radiotherapy for Head and Neck Cancer: Evidence for Preserved Salivary Gland Function. *Radiotherapy and Oncology* **2005**, *74*, 251–258, doi:10.1016/J.RADONC.2004.11.004.

430. Wirsdörfer, F.; Jendrossek, V. The Role of Lymphocytes in Radiotherapy-Induced Adverse Late Effects in the Lung. *Front Immunol* **2016**, *7*, 591, doi:10.3389/FIMMU.2016.00591.

431. Herranz, N.; Gil, J. Mechanisms and Functions of Cellular Senescence. *Journal of Clinical Investigation* **2018**, *128*, 1238–1246, doi:10.1172/JCI95148.

432. Coppé, J.P.; Desprez, P.Y.; Krtolica, A.; Campisi, J. The Senescence-Associated Secretory Phenotype: The Dark Side of Tumor Suppression. *Annual Review of Pathology: Mechanisms of Disease* **2010**, *5*, 99–118, doi:10.1146/ANNUREV-PATHOL-121808-102144/CITE/REFWORKS.

433. Rose, S.C.; Larsen, M.; Xie, Y.; Sharfstein, S.T. Salivary Gland Bioengineering. *Bioengineering 2024, Vol. 11, Page 28* **2023**, *11*, 28, doi:10.3390/BIOENGINEERING11010028.

434. Piraino, L.R.; Benoit, D.S.W.; Delouise, L.A. Salivary Gland Tissue Engineering Approaches: State of the Art and Future Directions. *Cells 2021, Vol. 10, Page 1723* **2021**, *10*, 1723, doi:10.3390/CELLS10071723.

435. Zhao, C.; Meng, C.; Cui, N.; Sha, J.; Sun, L.; Zhu, D. Organoid Models for Salivary Gland Biology and Regenerative Medicine. *Stem Cells Int* **2021**, *2021*, doi:10.1155/2021/9922597.

436. Phan, T. V.; Oo, Y.; Ahmed, K.; Rodboon, T.; Rosa, V.; Yodmuang, S.; Ferreira, J.N. Salivary Gland Regeneration: From Salivary Gland Stem Cells to Three-Dimensional Bioprinting. *SLAS Technol* **2023**, *28*, 199–209, doi:10.1016/J.SLAST.2023.03.004.

437. Klangprapan, J.; Souza, G.R.; Ferreira, J.N. Bioprinting Salivary Gland Models and Their Regenerative Applications. *BDJ Open 2024 10:1* **2024**, *10*, 1–9, doi:10.1038/s41405-024-00219-2.

438. Soscia, D.A.; Sequeira, S.J.; Schramm, R.A.; Jayarathanam, K.; Cantara, S.I.; Larsen, M.; Castracane, J. Salivary Gland Cell Differentiation and Organization on Micropatterned PLGA Nanofiber Craters. *Biomaterials* **2013**, *34*, 6773–6784, doi:10.1016/J.BIOMATERIALS.2013.05.061.

439. Shin, H.S.; Hong, H.J.; Koh, W.G.; Lim, J.Y. Organotypic 3D Culture in Nanoscaffold Microwells Supports Salivary Gland Stem-Cell-Based Organization. *ACS Biomater Sci Eng* **2018**, *4*, 4311–4320, doi:10.1021/ACSBIOMATERIALS.8B00894/ASSET/IMAGES/LARGE/AB-2018-008946_0007.JPEG.

440. Shin, H.S.; Kook, Y.M.; Hong, H.J.; Kim, Y.M.; Koh, W.G.; Lim, J.Y. Functional Spheroid Organization of Human Salivary Gland Cells Cultured on Hydrogel-Micropatterned Nanofibrous Microwells. *Acta Biomater* **2016**, *45*, 121–132, doi:10.1016/J.ACTBIO.2016.08.058.

441. Ramesh, P.; Moskwa, N.; Hanchon, Z.; Koplas, A.; Nelson, D.A.; Mills, K.L.; Castracane, J.; Larsen, M.; Sharfstein, S.T.; Xie, Y. Engineering Cryoelectrospun Elastin-Alginate Scaffolds to Serve as Stromal Extracellular Matrices. *Biofabrication* **2022**, *14*, 035010, doi:10.1088/1758-5090/AC6B34.

442. Kim, D.; Yoon, Y.J.; Choi, D.; Kim, J.; Lim, J.Y. 3D Organoid Culture From Adult Salivary Gland Tissues as an Ex Vivo Modeling of Salivary Gland Morphogenesis. *Front Cell Dev Biol* **2021**, *9*, doi:10.3389/FCELL.2021.698292/FULL.

443. Yoon, Y.J.; Kim, D.; Tak, K.Y.; Hwang, S.; Kim, J.; Sim, N.S.; Cho, J.M.; Choi, D.; Ji, Y.; Hur, J.K.; et al. Salivary Gland Organoid Culture Maintains Distinct Glandular Properties of Murine and Human Major Salivary Glands. *Nature Communications 2022 13:1* **2022**, *13*, 1–16, doi:10.1038/s41467-022-30934-z.

444. Koslow, M.; O'Keefe, K.J.; Hosseini, Z.F.; Nelson, D.A.; Larsen, M. ROCK Inhibitor Increases Proacinar Cells in Adult Salivary Gland Organoids. *Stem Cell Res* **2019**, *41*, doi:10.1016/J.SCR.2019.101608.

445. Hosseini, Z.F.; Nelson, D.A.; Moskwa, N.; Larsen, M. Generating Embryonic Salivary Gland Organoids. *Curr Protoc Cell Biol* **2019**, *83*, doi:10.1002/CPCB.76.

446. Maimets, M.; Rocchi, C.; Bron, R.; Pringle, S.; Kuipers, J.; Giepmans, B.N.G.; Vries, R.G.J.; Clevers, H.; De Haan, G.; Van Os, R.; et al. Long-Term In Vitro Expansion of Salivary Gland Stem Cells Driven by Wnt Signals. *Stem Cell Reports* **2016**, *6*, 150–162, doi:10.1016/J.STEMCR.2015.11.009.

447. Joraku, A.; Sullivan, C.A.; Yoo, J.; Atala, A. In-Vitro Reconstitution of Three-Dimensional Human Salivary Gland Tissue Structures. *Differentiation* **2007**, *75*, 318–324, doi:10.1111/J.1432-0436.2006.00138.X.

448. Pringle, S.; Maimets, M.; Van Der Zwaag, M.; Stokman, M.A.; Van Gosliga, D.; Zwart, E.; Witjes, M.J.H.; De Haan, G.; Van Os, R.; Coppes, R.P. Human Salivary Gland Stem Cells Functionally Restore Radiation Damaged Salivary Glands. *Stem Cells* **2016**, *34*, 640–652, doi:10.1002/STEM.2278.

449. Nam, K.; Jones, J.P.; Lei, P.; Andreadis, S.T.; Baker, O.J. Laminin-111 Peptides Conjugated to Fibrin Hydrogels Promote Formation of Lumen Containing Parotid Gland Cell Clusters. *Biomacromolecules* **2016**, *17*, 2293–2301, doi:10.1021/ACS.BIOMAC.6B00588.

450. Phan, T. V.; Oo, Y.; Rodboon, T.; Nguyen, T.T.; Sariya, L.; Chaisuparat, R.; Phoolcharoen, W.; Yodmuang, S.; Ferreira, J.N. Plant Molecular Farming-Derived Epidermal Growth Factor Revolutionizes Hydrogels for Improving Glandular Epithelial Organoid Biofabrication. *SLAS Technol* **2023**, *28*, 278–291, doi:10.1016/J.SLAST.2023.03.002.

451. Jorgensen, M.; Ramesh, P.; Toro, M.; Evans, E.; Moskwa, N.; Zhang, X.; Sharfstein, S.T.; Larsen, M.; Xie, Y. Alginate Hydrogel Microtubes for Salivary Gland Cell Organization and Cavitation. *Bioengineering (Basel)* **2022**, *9*, doi:10.3390/BIOENGINEERING9010038.

452. Yin, Y.; Vázquez-Rosado, E.J.; Wu, D.; Viswananthan, V.; Farach, A.; Farach-Carson, M.C.; Harrington, D.A. Microfluidic Coaxial 3D Bioprinting of Cell-Laden Microfibers and Microtubes for Salivary Gland Tissue Engineering. *Biomaterials advances* **2023**, *154*, doi:10.1016/J.BIOADV.2023.213588.

453. Shubin, A.D.; Felong, T.J.; Graunke, D.; Ovitt, C.E.; Benoit, D.S.W. Development of Poly(Ethylene Glycol) Hydrogels for Salivary Gland Tissue Engineering Applications. *https://home.liebertpub.com/tea* **2015**, *21*, 1733–1751, doi:10.1089/TEN.TEA.2014.0674.

454. Mereness, J.A.; Piraino, L.; Chen, C.Y.; Moyston, T.; Song, Y.; Shubin, A.; DeLouise, L.A.; Ovitt, C.E.; Benoit, D.S.W. Slow Hydrogel Matrix Degradation Enhances Salivary Gland Mimetic Phenotype. *Acta Biomater* **2023**, *166*, 187–200, doi:10.1016/J.ACTBIO.2023.05.005.

455. Ahmed, K.; Rodboon, T.; Oo, Y.; Phan, T.; Chaisuparat, R.; Yodmuang, S.; Rosa, V.; Ferreira, J.N. Biofabrication, Biochemical Profiling, and in Vitro Applications of Salivary Gland Decellularized Matrices via Magnetic Bioassembly Platforms. *Cell Tissue Res* **2023**, *392*, 499–516, doi:10.1007/S00441-022-03728-4.

456. Ferreira, J.N.; Hasan, R.; Urkasemsin, G.; Ng, K.K.; Adine, C.; Muthumariappan, S.; Souza, G.R. A Magnetic Three-Dimensional Levitated Primary Cell Culture System for the Development of

Secretory Salivary Gland-like Organoids. *J Tissue Eng Regen Med* **2019**, *13*, 495–508, doi:10.1002/TERM.2809.

457. Adine, C.; Ng, K.K.; Rungarunlert, S.; Souza, G.R.; Ferreira, J.N. Engineering Innervated Secretory Epithelial Organoids by Magnetic Three-Dimensional Bioprinting for Stimulating Epithelial Growth in Salivary Glands. *Biomaterials* **2018**, *180*, 52–66, doi:10.1016/J.BIOMATERIALS.2018.06.011.

458. Wallace, D.I.; Guo, X. Properties of Tumor Spheroid Growth Exhibited by Simple Mathematical Models. *Front Oncol* **2013**, *3*, doi:10.3389/FONC.2013.00051.

459. Barisam, M.; Saidi, M.S.; Kashaninejad, N.; Nguyen, N.T. Prediction of Necrotic Core and Hypoxic Zone of Multicellular Spheroids in a Microbioreactor with a U-Shaped Barrier. *Micromachines 2018, Vol. 9, Page 94* **2018**, *9*, 94, doi:10.3390/MI9030094.

460. Sacchi, M.; Bansal, R.; Rouwkema, J. Bioengineered 3D Models to Recapitulate Tissue Fibrosis. *Trends Biotechnol* **2020**, 1–14, doi:10.1016/j.tibtech.2019.12.010.

461. Jainchill, J.L.; Aaronson, S.A.; Todaro, G.J. Murine Sarcoma and Leukemia Viruses: Assay Using Clonal Lines of Contact-Inhibited Mouse Cells. *J Virol* **1969**, *4*, 549–553, doi:10.1128/JVI.4.5.549-553.1969.

462. Nichols, W.W.; Murphy, D.G.; Cristofalo, V.J.; Toji, L.H.; Greene, A.E.; Dwight, S.A. Characterization of a New Human Diploid Cell Strain, IMR-90. *Science* **1977**, *196*, 60–63, doi:10.1126/SCIENCE.841339.

463. Sherwood, S.W.; Rush, D.; Ellsworth, J.L.; Schimke, R.T. Defining Cellular Senescence in IMR-90 Cells: A Flow Cytometric Analysis. *Proc Natl Acad Sci U S A* **1988**, *85*, 9086, doi:10.1073/PNAS.85.23.9086.

464. Neri, F.; Basisty, N.; Desprez, P.Y.; Campisi, J.; Schilling, B. Quantitative Proteomic Analysis of the Senescence-Associated Secretory Phenotype by Data-Independent Acquisition. *Curr Protoc* **2021**, *1*, e32, doi:10.1002/CPZ1.32.

465. Rodier, F.; Campisi, J. Four Faces of Cellular Senescence. *Journal of Cell Biology* **2011**, *192*, 547–556, doi:10.1083/JCB.201009094.

466. Levi, N.; Papismadov, N.; Solomonov, I.; Sagi, I.; Krizhanovsky, V. The ECM Path of Senescence in Aging: Components and Modifiers. *FEBS J* **2020**, *287*, 2636–2646, doi:10.1111/FEBS.15282.

467. Leask, A.; Abraham, D.J. TGF-β Signaling and the Fibrotic Response. *The FASEB Journal* **2004**, *18*, 816–827, doi:10.1096/FJ.03-1273REV.

468. Wynn, T.A. Cellular and Molecular Mechanisms of Fibrosis. *J Pathol* **2008**, *214*, 199–210, doi:10.1002/PATH.2277.

469. Jun, J. Il; Lau, L.F. The Matricellular Protein CCN1 Induces Fibroblast Senescence and Restricts Fibrosis in Cutaneous Wound Healing. *Nature Cell Biology 2010 12:7* **2010**, *12*, 676–685, doi:10.1038/ncb2070.

470. Hinz, B. Myofibroblasts. *Exp Eye Res* **2016**, *142*, 56–70, doi:10.1016/J.EXER.2015.07.009.

471. Ramesh, P. Biomimetic Scaffolds Targeting Remediation of Fibrosis and Regeneration of the Salivary Gland. **2022**.

472. Lawko, N.; Plaskasovitis, C.; Stokes, C.; Abelseth, L.; Fraser, I.; Sharma, R.; Kirsch, R.; Hasan, M.; Abelseth, E.; Willerth, S.M. 3D Tissue Models as an Effective Tool for Studying Viruses and Vaccine Development. *Front Mater* **2021**, *8*, doi:10.3389/FMATS.2021.631373.

473. Rose, S. Electronic Mesh Available online: https://app.biorender.com/illustrations/6512ced1cee7246df2c27068 (accessed on 14 November 2023).

CV

Stephen Christopher Rose
5092 Route 28, Cooperstown, NY 13326
518-833-4982
scrose@albany.edu

PROFESSIONAL SUMMARY

Bioengineering and Nanotechnology Ph.D. candidate with extensive management, marketing, and business strategy experience. Self-starter with a passion for improving health span through bioengineering and nanotechnology applications.

CORE COMPETENCIES

Skilled in experimental design and data analysis
Proficient in laboratory techniques and procedures
Excellent report writing and preparation skills.
Experienced and influential leader in military, business, and cooperative organizations.

WORK EXPERIENCE

Life Extension Advocacy Foundation | London, England | March 2022-Present

Wrote white papers on various longevity topics.
Curated Rejuvenation Roadmap, a database of aging studies and age-related pharmaceuticals.

SUNY CNSE | Albany, NY 12207 | April 2018-Present

Developing 3D in vitro model of fibrosis for.
Conducted mammalian stem cell culture and bioreactor development.

Olympus Training LLC | White Plains, NY 10601 | April 2009 - 2020

Owned and managed a personal training studio.
Developed and implemented training programs, maintained client motivation.
Twice featured in Westchester Magazine.

New York Sports Club | White Plains, NY | September 2005 – August 2012

NASM certified in corrective exercise, sports performance enhancement, and special populations.
Trained the highest number of monthly sessions and generated the most sales for four years.

North Raleigh and Central YMCA | Raleigh, NC | June 1997 - July 1999

Conducted fitness appraisals and risk factor analysis, prescribed fitness programs.
Introduced the use of cognitive-behavioral techniques.

Ramada Inn Crabtree| Raleigh, NC | September 1993- September 1996
Reduced waste by 20% and established restaurant as a profit center rather than a loss leader.
Twice nominated for the best food & beverage operation nationwide as PM Operations Manager.

Rhulen/Markel | Monticello, NY | May 1990 – November 1992
Claims Adjudication Officer.

PROJECTS & RELATED LABORATORY EXPERIENCE

POC Stand-Alone Pseudomonas Aeruginosa Viability Detector, December 2018: CAD, SELEX, LAMP PCR, DNA sequencing, cyclic voltammetry, extraction, and quantification.

Airway-Administered Cyclodextrin Loaded Liposome Targeted to Macrophage Foam Cells, May 2016: Nanoparticle preparation.

POC Breast Milk Safety Testing Device, May 2015: ELISA and Immunofluorescence.

Glucosepane-Targeted DNA Aptamer for Atherosclerosis Treatment, May 2017: SELEX, phosphorothioate modification.

National Institutes of Health Stem Cell Workshop, March 3-7, 2014: Field Review and Laboratory Basics.

MILITARY EXPERIENCE

USMCR / NYSARNG Armor Crewman/ Machinist | 1985-1991

EDUCATION

Ph.D, Candidate Nanoscale Engineering | SUNY Polytechnic, Albany, NY | Anticipated December 2023

Post-Graduate Work (30 cr) Bioengineering & Nanotechnology | Harvard University, Cambridge, MA| 2014-2018

M.S., Management - Marketing & Operations Research | Clarkson University, Potsdam, NY | December 1991

B.S., Business Economics/Premedical | State University College at Oneonta, Oneonta, NY | August 1989

Publications

Stephen Christopher Rose
Apt 1B, 31 Wellington Avenue, Albany, NY 12203
518-833-4982
srose@sunypoly.edu

PROFESSIONAL SUMMARY

Bioengineering and Nanotechnology Ph.D candidate with extensive management, marketing, and business strategy experience. Self-starter with a passion for improving healthspan through bioengineering and nanotechnology applications.

CORE COMPETENCIES

Skilled in experimental design and data analysis
Proficient in laboratory techniques and procedures

Excellent report writing and preparation skills.
Experienced and effective leader in military, business, and cooperative organizations.

WORK EXPERIENCE

Life Extension Advocacy Foundation | London, England | March 2022-Present

Wrote white papers on various longevity topics.
Curated Rejuvenation Roadmap, a database of aging studies and age-related pharmaceuticals.

SUNY CNSE | Albany, NY 12207 | April 2018-Present

Developing 3D in vitro model of fibrosis for.
Conducted mammalian stem cell culture and bioreactor development.

Olympus Training LLC | White Plains, NY 10601 | April 2009 - 2020

Owner/Manager. Personal training, group fitness, and wellness studio.
Developed and implemented training programs, maintained client motivation.
Twice featured in Westchester Magazine.

New York Sports Club | White Plains, NY | September 2005 – August 2012
Master Trainer. NASM certified in corrective exercise, sports performance enhancement, and special populations. Trained the highest number of monthly sessions and generated the most sales for four years.

North Raleigh and Central YMCA | Raleigh, NC | June 1997 - July 1999
Fitness Specialist. Conducted fitness appraisals and risk factor analysis, prescribed fitness programs. Introduced the use of cognitive-behavioral techniques.

Ramada Inn Crabtree| Raleigh, NC | September 1993- September 1996
Operations Manager. Reduced waste by 20% and established restaurant as a profit center rather than a loss leader. Twice nominated for the best food & beverage operation nationwide as PM Operations Manager.

Rhulen/Markel | Monticello, NY | May 1990 – November 1992
Claims Adjudication Officer.

PROJECTS & RELATED LABORATORY EXPERIENCE

POC Stand-Alone Pseudomonas Aeruginosa Viability Detector, December 2018: CAD, SELEX, LAMP PCR, DNA sequencing, cyclic voltammetry, extraction, and quantification.

Airway-Administered Cyclodextrin Loaded Liposome Targeted to Macrophage Foam Cells, May 2016: Nanoparticle preparation.

POC Breast Milk Safety Testing Device, May 2015: ELISA and Immunofluorescence.

Glucosepane-Targeted DNA Aptamer for Atherosclerosis Treatment, May 2017: SELEX, phosphorothioate modification.

National Institutes of Health Stem Cell Workshop, March 3-7, 2014: Field Review and Laboratory Basics.

MILITARY EXPERIENCE

USMCR / NYSARNG Armor Crewman/ Machinist | 1985-1991

EDUCATION

Ph.D, Candidate Nanoscale Engineering | SUNY Albany, Albany, NY | Anticipated December 2023

Post-Graduate Work (30 cr) Bioengineering & Nanotechnology | Harvard University, Cambridge, MA| 2014-2018

M.S., Management - Marketing & Operations Research | Clarkson University, Potsdam, NY | December 1991

B.S., Business Economics/Premedical | State University College at Oneonta, Oneonta, NY | August 1989

Journal Papers:

1. **Rose, S., Larsen, M., Xie, Y., Sharfstein, S. (2024). Salivary Gland Bioengineering. Bioengineering, 11(1), 28**
2. **Haines, D. D., Trushin, M. V., Rose, S., Bernard, I. A. S., & Mahmoud, F. F. (2018). Parkinson's Disease: Alpha Synuclein, Heme Oxygenase and Biotherapeutic Countermeasures. Current Pharmaceutical Design, 24(20), 2317–2321**

Other Publications:

1. Rose, S. C. (September 2023). Improving Sleep Quality for Better Health
2. Rose, S. C. (September 2023). Why People Use Centrophenoxine as a Nootropic
3. Rose, S. C. (July 2023). Biotin: Side Effects and Benefits You Should Know About
4. Rose, S. C. (July 2023). L-Carnitine: Benefits, Uses, and Side Effects
5. Rose, S. C. (May 2023). Apple Cider Vinegar: Benefits, Myths, and Side Effects
6. Rose, S. C. (April 2023). Intermittent Fasting and Time-Restricted Feeding
7. Rose, S. C. (June 2023). How Metabolic Syndrome Makes Aging Worse
8. Rose, S. C. (February 2023). Urea Is a Blood Biomarker of Aging
9. Rose, S. C. (February 2023). Red Blood Cells as Biomarkers of Aging
10. Rose, S. C. (January 2023). The Relationship Between ApoE and Alzheimer's
11. Rose, S. C. (November 2022). Blood Glucose Is a Biomarker of Aging
12. Rose, S. C. (November 2022). Vitamin K2 Uses and Possible Side Effects
13. Rose, S. C. (October 2022). What Alkaline Phosphatase Is and Does
14. Rose, S. C. (October 2022). Albumin as a Blood Biomarker of Aging

15. Rose, S. C. (September 2022). Hyaluronic Acid: Benefits, Side Effects, and Research
16. Rose, S. C. (September 2022). Butyrate: Health Benefits and Side Effects
17. Rose, S. C. (July 2022). Alpha-Lipoic Acid: Benefits, Side Effects, and Research
18. Rose, S. C. (July 2022). Resveratrol: Benefits, Side Effects, and Research
19. Rose, S. C. (July 2022). Metformin: Benefits, Side Effects, and Research
20. Rose, S. C. (July 2022). Chondroitin Sulfate: Benefits, Side Effects, and Research
21. Rose, S. C. (April 2022). Low-Dose Naltrexone: Benefits and Side Effects
22. Rose, S. C. (March 2022). What Is Glutathione? A Summary of Glutathione

Book Reviews

1. Rose, S. C. (April 2024) Review of “Jellyfish Age Backwards: Nature’s Secrets to Longevity” by Nicklas Brendborg
2. Rose, S. C. (July 2023). Review of "The Rising Tide of Stem Cell Therapies" by Niel Riordan
3. Rose, S. C. (June 2023). Review of "Why We Sleep" by Dr. Matthew Walker
4. Rose, S. C. (June 2023). Review of "Microbial Burden: A Major Cause of Aging and Age-Related Disease and What We Can Do to Fight Back!" by Dr. Michael Lustgarten
5. Rose, S. C. (May 2023). Review of "OUTLIVE The Science and Art of Longevity" by Dr. Peter Attia
6. Rose, S. C. (March 2023). Review of "Age Later" by Dr. Nir Barzilai
7. Rose, S. C. (February 2023). Review of "Lifespan: Why We Age and Why We Don’t Have to" by Dr. David Sinclair
8. Rose, S. C. Review of "Younger You" by Dr. Kara Fitzgerald

Honors and awards

John J. Sullivan Professional Development Award, SUNY Polytechnic Institute, March 2023

Presentations

Rose, S. C. (March 19–23, 2023). **Toward an in vitro 3D model of radiation-induced salivary gland fibrosis**.Poster presented at the Keystone Symposia: Fibrosis Pathogenesis and Resolution: From Mechanisms to Therapies, Fairmont Banff Springs, Banff, Alberta, Canada.